SYNTHESIS, CHARACTERIZATION AND CATALYTIC ASPECTS OF DIOXIDOMOLYBDENUM(VI) COMPLEXES

Ph.D. THESIS

by

SARITA DHAKA

DEPARTMENT OF CHEMISTRY
INDIAN INSTITUTE OF TECHNOLOGY ROORKEE
ROORKEE-247 667 (INDIA)

MAY, 2015

SYNTHESIS, CHARACTERIZATION AND CATALYTIC ASPECTS OF DIOXIDOMOLYBDENUM(VI) COMPLEXES

A THESIS

Submitted in partial fulfilment of the requirements for the award of the degree

of

DOCTOR OF PHILOSOPHY

in

CHEMISTRY

by

SARITA DHAKA

DEPARTMENT OF CHEMISTRY
INDIAN INSTITUTE OF TECHNOLOGY ROORKEE
ROORKEE-247 667 (INDIA)

MAY, 2015

INDIAN INSTITUTE OF TECHNOLOGY ROORKEE
ROORKEE

CANDIDATE'S DECLARATION

I hereby certify that the work which is being presented in the thesis entitled **"SYNTHESIS, CHARACTERIZATION AND CATALYTIC ASPECTS OF DIOXIDOMOLYBDENUM(VI) COMPLEXES"** in partial fulfilment of the requirements for the award of the Degree of Doctor of Philosophy and submitted in the Department of Chemistry of the Indian Institute of Technology Roorkee, Roorkee is an authentic record of my own work carried out during a period from July, 2011 to May, 2015 under the supervision of Professor Mannar R. Maurya, Department of Chemistry, Indian Institute of Technology Roorkee, Roorkee.

The matter presented in this thesis has not been submitted by me for the award of any other degree of this or any other Institute.

(SARITA DHAKA)

This is to certify that the above statement made by the candidate is correct to the best of my knowledge.

Date: **(Mannar R. Maurya)**
Supervisor

The Ph.D. Viva Voice Examination of **Sarita Dhaka**, Research Scholar, has been held on ……

Chairman, SRC Signature of External Examiner

This is to certify that the student has made all the corrections in the thesis.

Signature of the Supervisor Head of the Department

Dedicated To

My Beloved Son
Vihan Dhaka

ACKNOWLEDGEMENTS

The secular and objective spirit of scientific philosophy has been the greatest attraction for me and I thank Almighty God to direct me on this path of scientific research. This journey would not have been possible without the support and assistance of a number of people over the past several years.

At the outset, I wish to express my deepest sense of gratitude and reverence to my supervisor Professor M.R. Maurya (Chemistry Department, IIT Roorkee) for his constant guidance and support. I am deeply indebted to my guide for his generous behavior, enthusiastic supervision as well as for providing necessary information from the preliminary to the concluding level. My thanks also goes to Mrs. Usha Maurya, for caring, kindness and generosity. I seek their pious blessing ever in my life.

I am sincerely thankful to Prof. Anil Kumar (Head of the Department) for providing the basic facilities. I would like to thank Prof. S. N. Tandon and Dr. (Mrs.) Uma Tandon for her affection and encouragement shown towards me. They were always available whenever I needed their advice.

This thesis could not have been completed without the endless blessings of my Parents (Shri Tirmal Singh and Smt. Vimla Devi) and In-laws (Shri Ompal Singh and Smt. Munesh Devi). A special mention of my sisters Mrs. Lata, Mrs Sushma, Mrs Anju, Mrs. Renu, brother in-law Ashok and my loving younger brothers Mohit and Vinay for their love and care.

My utmost appreciation goes to my husband Dr. Rahul Kumar Dhaka for his unconditional love, motivation, support and patience. I would have never been able to complete this academic endeavour without his support.

Heartiest thanks are due to my dearest friends R.K. Siwatch (IIT Delhi) and Dr. Amit Kumar Rawat (University of Delhi) for their timely help. I am thankful to Mr. Madanpal, Mr. Abdul Haque and D. C. Meena for the technical assistance. I express my

sincere thanks to the official staff in the Department, especially to Mr. K.C. Tiwari for expediting the official formal correspondences. Thanks are due to for his timely help.

I would like to mention my sincere thanks to my seniors Dr. Manisha Bisht, Dr. Priyanka Saini, Dr. Chanchal Haldar, Dr. Nikita Chaudhary, and colleagues Naveen kumar, Neeraj Saini, Bhawna Uprety, Lata Rana, Bithika Sarkar and Naveen Rawat for giving me an excellent company. I am thankful to Dr. Sudhir Gupta, Himanshu Gupta and Dr. Surbhi Arya for their constant cooperation.

This thesis would not have been feasible without the financial support of the Department of Science and Technology (New Delhi) and University Grant Commission.

Indian Institute of Technology Roorkee **(SARITA DHAKA)**
Roorkee, UK, INDIA
May, 2015

ABSTRACT

Chemical reactions generally proceed through the breaking and formation of bonds between atoms in molecules to produce new compounds. In a general sense, anything that increases the rate of any process is often called “catalyst”, a term derived from Greek καταλϑϱιυ, meaning “to annul”, or “to untie”, or “to pick up”. The catalyst decreases the activation energy of a reaction by altering the reaction path but it itself remains unchanged. The word “catalysis” was probably used first time in the sixteenth century by the chemist A. Libavious. These days catalysts are playing a vital role in petrochemicals, fine chemicals, pharmaceuticals, fertilizers and food industries. The biochemically significant processes are also based on catalysts.

Sometimes chemists surprise the nature, which is a foundation of motivation, by mimicking its complex reactions like most popular mimetic approach of molybdenum compounds. Initially Bortels highlighted the biological importance of molybdenum compounds in 1930. Oxyanion molybdate is the soluble biological active form of molybdenum. On one hand molybdenum is a minor constituent of the earth's crust and on the other hand it is widely bioavailable due to the high solubility of molybdate salts in water, the most abundant transition metal in seawater. Molybdenum is the single 4d transition metal, present in biological a system which outlines the part of the lively site of molybdoenzymes that accomplish the key transformations in the metabolism of nitrogen, sulfur and carbon compounds. On the basis of amino acid sequences, spectroscopic properties, active site structures and catalyzed reactions molybdenum containing enzymes can be distributed in many classes. R. Hille gave a classification of molybdoenzymes with the help of rapidly growing number of X-ray crystal structures, which is based on structural homology of the active sites. Two different types of molybdoenzymes are acknowledged: Molybdenum nitrogenase which catalyzes the reduction of atmospheric dinitrogen to ammonia and another types of molybdoenzymes are oxidoreductases such as aldehyde oxidase, xanthine oxidase, sulfite oxidase, nitrate reductase and xanthine dehydrogenase that transfer an oxido group or two electrons to from the substrate. The

enormous majority of these molybdoenzymes acquire at least one Mo=O unit in their active sites and are frequently named as oxidomolybdenum enzymes.

Upon going through the literature, it is evident that molybdenum Schiff base complexes have provided opportunities to develop catalytic system for various industrial processes. Particularly, oxidation reactions catalyzed by these specialized complexes are well documented. However, in most cases optimization of the reaction conditions to effect maximum efficiency of the catalysts have not been set out. It was, therefore, reasonable to undertake systematic study on the synthesis and characterization of new molybdenum catalysts and to explore their catalytic potential for the oxidation of organic substrates under optimized reaction conditions.

First chapter is the introductory one and describes a variety of molybdenum complexes that have been used as homogeneous catalysts in different types of organic transformations. Literature on the catalytic applications of various dioxidomolybdenum(VI) complexes has also been reviewed.

In **Second Chapter**, the dioxidomolybdenum(VI) complexes [$Mo^{VI}O_2$(Hsal-dahp)(H_2O)] (**2.1**), [$Mo^{VI}O_2$(Hclsal-dahp)(H_2O)] (**2.2**) and [$Mo^{VI}O_2$(Hbrsal-dahp)(H_2O)] (**2.3**) have been prepared by the reaction of [$Mo^{VI}O_2(acac)_2$] (Hacac = acetylacetone) with tribasic pentadentate Schiff bases H_3sal-dahp (**2.I**), H_3clsal-dahp(**2.II**) and H_3brsal-dahp(**2.III**) (sal = salicylaldehyde, clsal = 5-chlorosalicylaldehyde, brsal = 5-bromosalicylaldehyde, dahp = 1,3-diamino-2-hydroxypropane) in methanol at reflux condition. Reactions of these complexes with pyridine result in the formation of [$Mo^{VI}O_2$(Hsal-dahp)(py)] (**2.4**), [$Mo^{VI}O_2$(Hclsal-dahp)(py)] (**2.5**) and [$Mo^{VI}O_2$(Hbrsal-dahp)(py)] (**2.6**). These complexes have been used as catalysts for the oxidation of methyl phenyl sulfide, benzoin and oxidative bromination of styrene efficiently using H_2O_2 as green oxidant. Oxidation of methyl phenyl sulphide under the optimized reaction conditions gave ca. 98 % conversion with two major products methyl phenyl sulfoxide and methyl phenyl sulfone in the ca. 66.8 % and 33.2 % selectivity, respectively. The oxidation of benzoin, catalyzed by $Mo^{VI}O_2$ complexes was carried out in refluxing methanol which gave 95% conversion in 4 h of reaction time and the selectivity of the

reaction products varied in the order: benzoic acid (40) > methyl benzoate (32 %), > benzil (15%) > benzaldehyde-dimethylacetal (13 %). The oxidative bromination of styrene using molybdenum complexes as catalyst precursors gave 98% conversion and the selectivity of different major products followed the order: phenylethane-1,2-diol (67%) > 1,2-dibromo-1-phenylethane (21%) > 2-bromo-1-phenylethane-1-ol (3%).

Third Chapter describes the synthesis of $[Mo^{VI}O_2\{Hdfmp(sbdt)_2\}(H_2O)]$ **(3.1),** $[Mo^{VI}O_2\{Hdfmp(smdt)_2\}(H_2O)]$ **(3.2)** and $[Mo^{VI}O_2\{Hdfmp(tsc)_2\}(H_2O)]$ **(3.3)** by the reaction of $[Mo^{VI}O_2(acac)_2]$ with the tribasic pentadenate O, N and S donor ligands $H_3dfmp(sbdt)_2$ (**3.I**), $H_3dfmp(smdt)_2$ (**3.II**) and $H_3dfmp(tsc)_2$ (**3.III**) derived from 2,6-diformyl-4-methylphenol and *S*-benzyldithiocarbazate, *S*-methyldithiocarbazate, and thiosemicarbazide. These complexes were characterized using spectroscopic studies (IR, UV/Vis and NMR), elemental analyses, thermal studies and single crystal study which reveal that only one set of azomethine nitrogen, enthiolate sulfur and phenolate oxygen atoms of the ligands are coordinated to the molybdenum. Oxidations of styrene and cyclohexene have been investigated using these complexes as catalyst precursors in the presence of H_2O_2 as oxidant in the presence of $NaHCO_3$. Under the optimized reaction conditions, a maximum of 96 % conversion of styrene has been obtained with **3.1**, 98 % conversion with **3.2** and 97 % conversion with **3.3** in 2 h of reaction time. The selectivity of the products is similar for the catalyst precursors (i.e. complexes **3.1** to **3.3**) and follows the order: styrene oxide > phenyl acetaldehyde. With cyclohexene, a maximum conversion of 96% has been achieved with **3.1**, 94 % with **3.2** and 96 % conversion with **3.3**, also in 2.5 h of reaction time and cyclohexene oxide is formed as a product with 100 % selectivity. UV-Vis experiment with all complexes confirm the plausible formation of $Mo^{VI}O(O_2)L$ as intermediates in the catalytic oxidations.

New dioxidomolybdenum(VI) complexes, $[Mo^{VI}O_2\{Hdfmp(bhz)_2\}(MeOH)]$ (**4.1**), $[Mo^{VI}O_2\{Hdfmp(inh)_2\}(MeOH)]$ (**4.2**) and $[Mo^{VI}O_2\{Hdfmp(nah)_2\}(MeOH)]$ (**4.3**) of ligand $H_3dfmp(L)_2$ obtained by the condensation of 2,6-diformyl-4-methylphenol (dfmp) and hydrazides (L) [L = benzoylhydrazide (bhz), isonicotinoylhydrazide (inh), and nicotinoylhydrazide (nah)], respectively. Studies on these complexes are described in

Fourth Chapter. All complexes are characterized by various physico-chemical studies. Oxidation of secondary alcohols: 1-phenyl ethanol, 2-propanol and 2-butanol, catalyzed by these molybdenum complexes, using conventional liquid phase and microwave-assisted methods in the presence of 30 % H_2O_2 as an oxidant have been tested. The effects of various factors, such as temperature and amounts of catalyst, H_2O_2 and solvent have been investigated. These alcohols under the optimized reaction conditions gave high yields of the respective ketone. Addition of an N-based additive reduces the reaction time considerably. Amongst the two methods studied, the microwave technique proves to be a time efficient system.

In **Fifth Chapter** the synthesis of dioxidomolybdenum(VI) complexes, [$Mo^{VI}O_2$(fhmc-bhz)(MeOH)] (**5.1**), [$Mo^{VI}O_2$(fhmc-inh)(MeOH)] (**5.2**) [$Mo^{VI}O_2$(fhmc-nah)(MeOH)] (**5.3**) and [$Mo^{VI}O_2$(fhmc-fah)(MeOH)] (**5.4**) have been described. These complexes are obtained by the reaction of [$Mo^{VI}O_2(acac)_2$] and potential ONO tridentate ligands H_2fhmc-bhz (**5.I**), H_2fhmc-inh (**5.II**), H_2fhmc-nah (**5.III**), and H_2fhmc-fah (**5.IV**), derived from condensation of equimolar amount of 8-formyl-7-hydroxy-4-methylcoumarin (fhmc) and hydrazides [benzoylhydrazide (bhz), isonicotinoylhydrazide (inh), nicotinoylhydrazide (nah) and furoic acid hydrazide (fah)] in methanol. The structures of the obtained ligands and their respective metal complexes were elucidated by elemental analyses, spectroscopic techniques (IR, electronic, ^{1}H and ^{13}C NMR) and thermogravmetric analyses. These metal complexes have been tested against oxidative bromination of monoterpene (thymol) by using H_2O_2 as an oxidant. Therefore, they act as functional models of vanadium dependent haloperoxidases. A maximum of 94% conversion has been achieved where selectivity of different major products follows the order: 2,4-dibromothymol (84.6%) > 2-bromothymol (8.4%) > 4-bromothymol (7%). The effects of various factors, such as amounts of catalyst, oxidant, KBr, $HClO_4$ and different solvents have been considered to optimize the reaction conditions for the maximum brominated products.

Finally, summary and over all conclusions based on the achievements are presented.

CONTENTS

CHAPTER 4

Oxidation of secondary alcohols by conventional and microwave-assisted methods using molybdenum complexes of ONO donor ligands

LIST OF FIGURES

Figure 2.10(a). Plots showing percentage conversion of styrene and the selectivity of the formation of different reaction products as a function of time. Reaction conditions: styrene (1.04 g, 10 mmol), [$Mo^{VI}O_2$(Hsal-dahp)(H_2O)] (**2.1**) (0.001g), 30 % aqueous H_2O_2 (2.27g, 20 mmol), KBr (2.38 g, 20 mmol) and 70 % aqueous $HClO_4$ (2.86 g, 20 mmol).

Figure 2.10(b). Plots showing percentage conversion of styrene and the selectivity of the formation of different reaction products as a function of time. Reaction conditions: styrene (1.04 g,10mmol), [$Mo^{VI}O_2$(Hsal-dahp)(H_2O)] (**2.1**) (0.001g), 30 % aqueous H_2O_2 (2.27 g, 20 mmol), KBr (2.38 g, 20 mmol) and 70 % aqueous $HClO_4$ (4.29 g, 30 mmol).

Figure 2.10(c). Plots showing percentage conversion of styrene and the selectivity of the formation of different reaction products as a function of time. Reaction conditions are similar to Fig. 2.10(b) taking [$Mo^{VI}O_2$(Hclsal-dahp)(H_2O)] (**2.2**) as catalyst.

Figure 2.10(d). Plots showing percentage conversion of styrene and the selectivity of the formation of different reaction products as a function of time under reaction conditions similar to (b) taking [$Mo^{VI}O_2$(Hbrsal-dahp)(H_2O)] (**2.3**) as catalyst.

Figure 2.11(a). Effect of catalyst amount on the oxidation of methyl phenyl sulfide. Reaction conditions: methyl phenyl sulfide (1.24 g, 10 mmol), 30 % H_2O_2 (2.27 g, 20 mmol) and acetonitrile (5 mL).

Figure 2.11(b). Effect of oxidant amount on the oxidation of methyl phenyl sulfide. Reaction conditions: methyl phenyl sulfide (1.24 g, 10 mmol), catalyst (0.0015 g) and acetonitrile (5 mL)**.**

Figure 2.11(c). Effect of solvent amount on the oxidation of methyl phenyl sulfide. Reaction conditions: methyl phenyl sulfide (1.24 g, 10 mmol), catalyst (0.0015 g) and 30 % H_2O_2 (2.27 g, 20 mmol).

Figure 2.11(d). Plot showing percentage conversion of methyl phenyl sulfide and the selectivity of the formation of methyl phenyl sulfoxide and methyl phenyl sulfone as a function of time under optimized conditions using [MoO_2(sal-dahp)(H_2O)] (**2.1**) as catalyst.

Figure 2.12. Effect of different catalysts on oxidation of methyl phenyl sulfide.

Figure 3.9(a). Effect of catalyst amount on the oxidation of styrene. Reaction conditions: styrene (0.520 g, 5 mmol), 30 % H_2O_2 (2.27 g, 20 mmol), $NaHCO_3$ (0.168 g, 2 mmol), temperature (60 ^oC and acetonitrile (5 ml).

Figure 3.9(b). Effect of oxidant amount on the oxidation of styrene. Reaction conditions: styrene (0.520 g, 5 mmol), catalyst (0.0005 g), $NaHCO_3$ (0.168 g, 2 mmol), temperature (60 ^oC) and acetonitrile (5 ml).

Figure 3.9(c). Effect of $NaHCO_3$ amount on the oxidation of styrene. Reaction conditions: styrene (0.520 g, 5 mmol), catalyst (0.0005 g), 30 % H_2O_2 (2.27 g, 20 mmol), temperature (60 ^oC) and acetonitrile (5 ml).

Figure 3.9(d). Effect of solvent amount on the oxidation of styrene. Reaction conditions: styrene (0.520 g, 5 mmol), 30 % H_2O_2 (2.27 g, 20 mmol), $NaHCO_3$ (0.168 g, 2 mmol), catalyst (0.0005 g) and temperature (60 ^oC).

Figure 3.9(e). Effect of temperature on the oxidation of styrene. Reaction conditions: styrene (0.520 g, 5 mmol), 30 % H_2O_2 (2.27 g, 20 mmol), $NaHCO_3$ (0.168 g, 2 mmol), catalyst (0.0005 g) and acetonitrile (5 ml).

Figure 3.9(f). Plot showing conversion of oxidation of styrene using different metal complexes.

Figure 3.10. Profiles showing conversion and selectivity of products as a function of time.

Figure 3.11(a). Effect of catalyst amount on the oxidation of cyclohexene. Reaction conditions: cyclohexene (0.410 g, 5 mmol), 30 % H_2O_2 (2.27 g, 20 mmol), $NaHCO_3$ (0.168 g, 2 mmol), temperature (60 ^oC) and acetonitrile (5 ml).

Figure 3.11(b). Effect of oxidant amount on the oxidation of cyclohexene. Reaction conditions: cyclohexene (0.410 g, 5 mmol), catalyst (0.0005 g), $NaHCO_3$ (0.168 g, 2 mmol), temperature (60 ^oC) and acetonitrile (5 ml).

Figure 3.11(c). Effect of $NaHCO_3$ amount on the oxidation of cyclohexene. Reaction conditions: cyclohexene (0.410 g, 5 mmol), catalyst (0.0005 g), 30 % H_2O_2 (2.27 g, 20 mmol), temperature (60 ^oC) and acetonitrile (5 ml).

Figure 3.11(d). Effect of solvent amount on the oxidation of cyclohexene. Reaction conditions: cyclohexene (0.410 g, 5 mmol), 30 % H_2O_2 (2.27 g, 20 mmol), $NaHCO_3$ (0.168 g, 2 mmol), catalyst (0.0005 g) and temperature (60 ^oC)

Figure 3.11(e). Effect of temperature on the oxidation of cyclohexene. Reaction conditions: cyclohexene (0.410 g, 5 mmol), 30 % H_2O_2 (2.27 g, 20 mmol), $NaHCO_3$ (0.168 g, 2mmol), catalyst (0.0005 g) and acetonitrile (5 ml).

Figure 3.11(f). Plot showing conversion of cyclohexene using different metal complexes.

Figure 3.12(a). The spectra were recorded after successive addition of one drop portion of 30% H_2O_2 (0.825 g, 7.3 mmol) dissolved in 5 mL of MeOH (final concentration of H_2O_2 = 1.46 M) to 20 mL of 2×10^{-5} M solution of $[Mo^{VI}O_2\{Hdfmp(smdt)_2\}(H_2O)]$ (**3.2**).

Figure 3.12(b). The spectra were recorded after successive addition of one drop portion of 30% H_2O_2 (0.565 g, 5 mmol) dissolved in 5 mL of MeOH (final concentration of H_2O_2 = 0.97 M) to 20 mL of 10^{-4} M solution of $[Mo^{VI}O_2\{Hdfmp(smdt)_2\}(H_2O)]$ (**3.2**).

Figure 3.12(c). The spectra were recorded after successive addition of one drop portion of 30% H_2O_2 (0.715 g, 6.3 mmol) dissolved in 5 mL of MeOH (final concentration of H_2O_2 = 1.25 M) to 20 of mL of 1.2×10^{-4} M solution of $[Mo^{VI}O_2\{Hdfmp(sbdt)_2\}(H_2O)]$ (**3.1**).

Figure 3.12(d). The spectra were recorded after successive addition of one drop portion of 30% H_2O_2 (0.450 g, 4.0 mmol) dissolved in 5 mL of MeOH (final concentration of H_2O_2 = 0.79 M) to 20 mL of 1.7×10^{-4} M solution of $[Mo^{VI}O_2\{Hdfmp(tsc)_2\}(H_2O)]$ (**3.3**).

Figure 3.13(a). The spectra were recorded after successive addition of one drop portion of mixture of $NaHCO_3$ (0.025g, 0.30 mmol) and 30% H_2O_2 (0.146 g, 1.3 mmol) dissolved in 5 mL of MeOH to 20 mL of 2×10^{-5} M solution of $[Mo^{VI}O_2\{Hdfmp(smdt)_2\}(H_2O)]$ (**3.2**).

Figure 3.13(b). The spectra were recorded after successive addition of one drop portion of mixture of $NaHCO_3$ (0.020 g, 0.24 mmol) and 30% H_2O_2 (0.073 g, 0.65 mmol) dissolved in 5 mL of MeOH to 20 mL of 10^{-4} M solution of $[Mo^{VI}O_2\{Hdfmp(smdt)_2\}(H_2O)]$ (**3.2**).

Figure 4.1. ORTEP plot of complex **4.1a**.

Figure 4.2. ORTEP plot of complex **4.3**·DMSO.

Figure 4.3. Intermolecular π-π interactions in **4.1a**.

Figure 4.4. ^{1}H NMR spectra of $H_3dfmp(bhz)_2$ (**4.I**), and $[Mo^{VI}O_2\{Hdfmp(bhz)_2\}(MeOH)]$ (**4.1**).

Figure 4.5. ^{13}C NMR spectra of $H_3dfmp(bhz)_2$ (**4.I**) and complex $Mo^{VI}O_2\{Hdfmp(bhz)_2\}(MeOH)]$ (**4.1**).

Figure 4.6(a). Effect of catalyst amount on the oxidation of 5 mmol of 1-phenyl ethanol. Other reaction conditions: 30 % H_2O_2 (1.70g, 15 mmol), temperature (80 ^{o}C) and acetonitrile (5 ml).

Figure 4.6(b). Effect of oxidant amount on the oxidation of 5 mmol of 1-phenyl ethanol. Other reaction conditions: catalyst (0.002 g), temperature (80 ^{o}C) and acetonitrile (5 ml).

Figure 4.6(c). Effect of solvent amount on the oxidation of 5 mmol of 1-phenyl ethanol. Other reaction conditions: catalyst (0.002 g), 30 % H_2O_2 (1.70 g, 15 mmol) and temperature (80 ^{o}C)

Figure 4.6(d). Effect of temperature variation on the oxidation of 5 mmol of 1-phenyl ethanol. Other reaction conditions: catalyst (0.002 g), 30 % H_2O_2 (1.70 g, 15 mmol) and acetonitrile (5 ml).

Figure 4.7(a). The spectra were recorded after successive addition of one drop portion of H_2O_2 [30% H_2O_2 (0.715 g, 6.3 mmol) dissolved in 5 mL of MeOH; final concentration of H_2O_2 = 1.26 M)] to 20 mL of 2.6×10^{-5} M solution of $[Mo^{VI}O_2\{Hdfmp(bhz)_2\}(MeOH)]$ (**4.1**).

Figure 4.7(b). The spectra were recorded after successive addition of one drop portion of H_2O_2 [30% H_2O_2 (0.910 g, 8.0 mmol) dissolved in 5 mL of MeOH; final concentration of H_2O_2 = 1.60 M)] to 20 mL of 3.2×10^{-5} M solution of $[Mo^{VI}O_2\{Hdfmp(inh)_2\}(MeOH)]$ (**4.2**).

Figure 4.7(c). The spectra were recorded after successive addition of one drop portion of H_2O_2 [30% H_2O_2 (0.845 g, 7.5 mmol) dissolved in 5 mL of MeOH; final concentration of H_2O_2 = 1.48 M] to 20 of mL of 2.4×10^{-5} M solution of $[Mo^{VI}O_2\{Hdfmp(nah)_2\}(MeOH)]$ (**4.3**).

LIST OF TABLES

CHAPTER 1

General introduction and literature survey

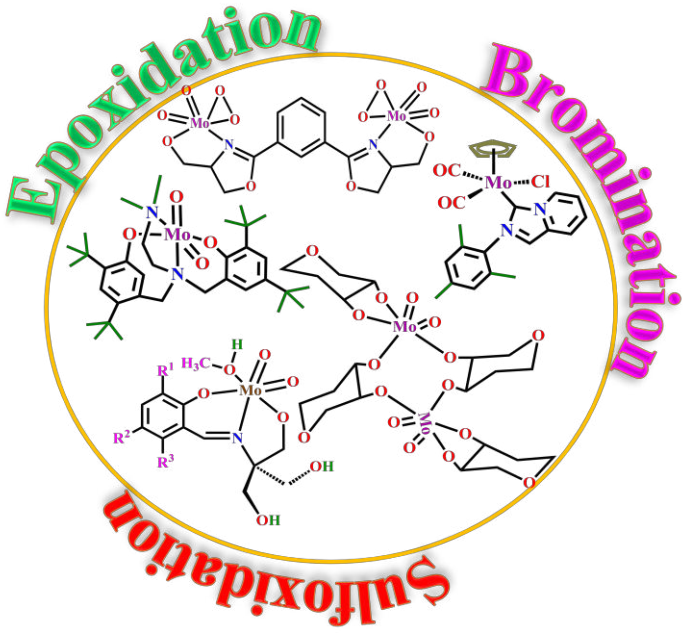

1.1. Historical

Chemical reactions generally proceed through the breaking and formation of bonds between atoms in molecules to produce new compounds. In general, any substance that increases the rate of any chemical reaction is often called "catalyst". The catalyst decreases the activation energy of a reaction by altering the reaction path but it itself remains unchanged. The word "catalysis" was probably used first time in the sixteenth century by the chemist A. Libavious in his book Alchemia [1]. In 1793, Clement and Desormes used the nitre (KNO_3) as a catalyst for the synthesis of sulfuric acid in the presence of air. In 1835 Jöns Jakob Berzelius used the term catalysis for some compounds / chemicals which can fasten the reaction. Synthesis of sulfuric acid by burning sulfur with nitric acid in humid air is one of the examples for the catalysis in the middle age. This was followed by the discovery of ammonia synthesis by Nernst and Haber. Horiuti and Polanyi, in 1930s, suggested a catalytic reaction mechanism for ethylene hydrogenation [2]. Langmuir in the same period derived the Langmuir adsorption isotherm, suggesting the heterogeneous surface [3] which has different sites and these different sites have different rates for reaction. Langmuir used the heterogeneous nickel surface for the nickel carbonyl formation. The first significant use of solid catalyst was made in the cracking of hydrocarbons during 1935–1940 in the petroleum industry [4, 5]. The catalytic naphtha reforming, dehydrogenation of cyclohexene to benzene and isomerisation of straight chain alkenes were developed in 1950. Ziegler and Natta in 1955 discovered the use of $AlCl_3$ as a catalyst for the production of polypropylene at low pressure [6]. Around 1960, hydro treating catalyst was introduced in catalyst technology at refineries for the removal of sulfur, nitrogen and metals from petroleum products [7, 8]. In the Wacker process in 1960, catalyst $[PdCl_4]^{2-}$ enabled the reduction of temperature from 500 to 100 °C at 7 atm during the formation of acetaldehyde from ethylene [9, 10]. In 1960, Weisz and Frilette used the unique property of zeolites in shape selective catalysis for cracking of n–alkanes to exclusively straight chain products [11, 12]. In early 1970's, catalytic reaction was classified by Boudart in two groups: (i) structure sensitive and (ii) structure insensitive [13]. According to

Boudart, the rate of reaction of structure sensitive reactions changes as a function of particle size, while on increasing the particle size the structure insensitive reactions keep reaction rate unchanged [14]. Haensel in same period proposed the concept of bifunctional catalysis to obtain a desired product using two catalysts, in the dual catalytic system initially one catalyst produces one reaction intermediate and afterwards this shifts to other catalyst for the formation of other reaction intermediate or products and finally reaction products separate out from the catalyst. Noble metal catalysts were developed in the late 1970 and early 1980's for the control of CO, hydrocarbon and NO emission from automobiles [15, 16]. During 1980–1990, the vanadia, titania and zeolite catalysts were developed for the selective reduction of nitrogen oxides with ammonia or light hydrocarbons [17, 18]. Catalysts for the removal of volatile hazardous organic hydrocarbons such as chlorohydrocarbons were also developed during this period [19, 20]. These day's catalysts are playing a vital role in petrochemicals, fine chemicals, pharmaceuticals, fertilizers and food industries. The biochemically significant processes are also based on catalysts.

Catalysis is relevant to many aspects of environmental science, e.g. the catalytic converter in automobiles and the dynamics of the ozone hole. To avoid the production of waste, catalytic reactions are normally preferred in environment friendly conditions [21] as opposed to stoichiometric reactions where all reagents are consumed resulting in the generation of generally hazardous side product(s) in addition to expected product(s). Metal complexes e.g. of vanadium, molybdenum, iron, palladium, platinum, ruthenium etc. have been used as catalysts for many catalytic reactions [22–27].

1.2. Molybdenum compounds – Natural sources

Molybdenum (originated from the Greek word "*molybdos"* means "lead–like") is not found free in environment. It was first observed to be present in the form of molybdenite (MoS_2) by Scheele in 1778–79 and afterward isolated from molybdenite by Hjelm in 1782, who called it molybdenum. Though, main source of molybdenum is molybdenite (MoS_2), other minerals such as wulfenite ($PbMoO_4$) and powellite

($CaMoO_4$) contains considerable amount of molybdenum. This way 0.01% to 0.5% molybdenum is present in earth's crust.

Sometimes chemists surprise the nature, which is a foundation of motivation, by mimicking its complex reactions like most popular mimetic approach of molybdenum compounds. Initially Bortels highlighted the biological importance of molybdenum compounds in 1930 [28]. Molybdenum is the most abundant transition metal in see water and mostly present as oxyanion [29]. Molybdenum is the single 4d transition metal, present in biological system as an active site of molybdoenzymes that show the key transformations in the metabolism of nitrogen, sulfur and carbon compounds. Based on the structural homology of the active sites, R. Hille gave a classification of molybdoenzymes with the help of single crystal X–ray studies [30]. Two different types of molybdoenzymes are acknowledged: Molybdenum nitrogenase has a single molybdenum–iron–sulfur cluster, the $[Fe_4S_3]$–$(bridging–S)_3$–$[MoFe_3S_3]$ center called FeMo cofactor [31]. Nitrogenase catalyzes the reduction of atmospheric dinitrogen to ammonia. Other types of molybdoenzymes are oxidoreductases such as aldehyde oxidase, xanthine oxidase, sulfite oxidase, nitrate reductase and xanthine dehydrogenase. These enzymes transfer an oxido group or two electrons to from the substrate (Fig. 1.1) [30]. Oxidoreductases have a molybdenum cofactor (Moco) in which molybdenum is coordinated to a dithiolene group on the 6–alkyl side chain of a pterin called molybdopterin (MPT) [32]. Most of these molybdoenzymes contain at least one Mo=O unit in their active sites and because of this they are generally named as oxidomolybdenum enzymes.

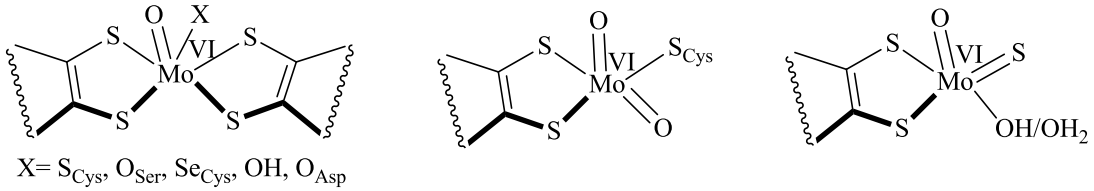

1 **2** **3**

Figure 1.1. Three main families of mononuclear molybdo enzymes (after Hille classification).

Molybdenum extends co–ordination numbers ranging from 4 to 8 and demonstrates diverse stereochemistry. Molybdoenzymes contain molybdenum–oxygen bonds which act as an inspiration to researchers to work with molybdenum complexes in oxygen atmospheres. It can figure out various compounds with inorganic and organic ligands, particularly with oxygen, sulphur, fluorine and chlorine donor atoms.

1.3. Different types of oxidomolybdenum compounds for catalytic organic transformations

There are two types of oxidomolybdenum compounds reported for catalytic organic transformations (i) dioxido molybdenum compounds and (ii) oxidoperoxido and oxidodiperoxido molybdenum compounds.

Molybdenum trioxide (MoO_3), the simplest source of oxidomolybdenum compounds which is applied as catalyst for a variety of organic transformations, is usually obtained during the roasting of the molybdenite (MoS_2) ore [33]. Molybdenum trioxide is also resulted from the reaction of ammonium molybdate with concentrated nitric acid in hydrated form (H_2MoO_4) which on further dehydration gives MoO_3 [34]. In addition, this is one of the most suitable molybdenum precursor for the preparation of a range of molybdenum complexes like $Mo^{VI}O_2C1_2(DMSO)_2$, $Mo^{VI}O_2C1_2(DMF)_2$, $Mo^{VI}O_2C1_2(OPPh_3)_2$ and $Mo^{VI}O_2C1_2(HMPA)_2$ [35,36].

Another significant group of molybdenum compounds are $[Mo^{VI}O_2C1_2(L)_n]$ (where L neutral monodentate/ bidentate organic ligands) which are highly useful as catalysts for

different kinds of organic reactions [37]. Numerous organic molecules having oxygen and nitrogen functionalities are capable to form dioxidomolybdenum(VI) complexes through ligand exchange reaction with $Mo^{VI}O_2C1_2(THF)_2$ [36,38].

Another suitable precursor is $[Mo^{VI}O_2(acac)_2]$ (acac = acetylacetonate) which has widely been used to develop molybdenum chemistry. Using $[Mo^{VI}O_2(acac)_2]$ as starting precursor, complexes with general formula $[Mo^{VI}O_2(\mathbf{L})_n]$ (where L = dianionic tridentate ligands) can be simply prepared by ligand exchange reaction method in appropriate solvent [39].

Coordination chemistry of dioxidomolybdenum(VI) complexes finds special place in the literature due to the following reasons:

(i) Molybdenum complexes have most immense applications in the field of catalysis like chemical and petrochemical routes in various industries like ammoxidation of propene [40], epoxidation of olefin [41–45], olefin metathesis [46], isomerization of allylic alcohols [47], oxidation of sulfides [48, 49], oxidative bromination of organic substrates etc. [50].

(ii) Molybdenum (VI) is relatively harmless to the environment over other transition metals [51], and

(iii) Schiff base complexes of molybdenum(VI) are of noteworthy concern and attention due to their biological activity like anticancer [52], antibacterial [53, 54], antifungal [55] and antitumor [56] properties.

The coordination environments around the central metal (molybdenum) ion play a key role in that the properties of the complexes can be altered with the modification in the coordination environment. Thus chemistry of dioxidomolybdenum(VI) complexes with various types of ligands has been of considerable importance in this regard.

Lee and his group accounted [57] the synthesis of a series of *cis*–$[Mo^{VI}O_2]^{2+}$ complexes of general formula $MoO_2(L)Cl$ (Fig. 1.2 (**4**)), through the reaction of

MoO_2Cl_2(DME) (DME = 1,2–dimethoxyethane) with 2–N–(2–pyridylmethyl)aminophenol (HL^1) or its N–alkyl derivatives (HL^n) (n = 2–5) in the presence of triethylamine. The *cis*–$[Mo^{VI}O_2]^{2+}$- alkyl complexes (Fig. 1.2 (**5**)) were obtained by the reaction of $MoO_2(L^1)Cl$ or $[MoO_2(L^1)]_2O$ with the Grignard reagent Me_3SiCH_2MgCl. They have also checked the catalytic properties of these complexes towards epoxidation of styrene with tert–butyl hydroperoxide (TBHP).

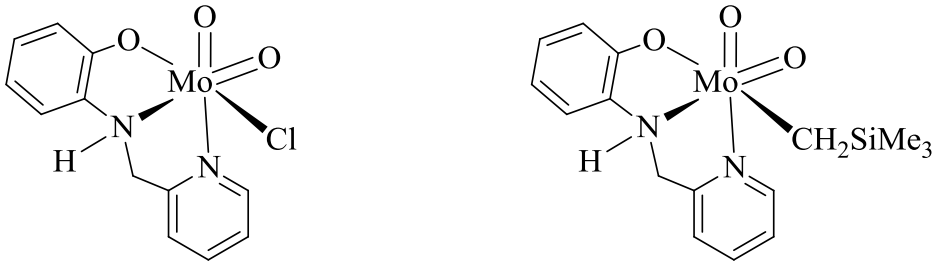

4 **5**

Figure 1.2. Alkyl complexes of dioxidomolybdenum(VI).

A series of *cis*–$[Mo^{VI}O_2]^{2+}$ complexes with aminobis(phenolate) derived tridentate ligand has been reported by Lehtonen and Sillanpää in 2005 [58]. These ligands form monomeric complexes in which a solvent methanol occupies the sixth coordination site (Fig. 1.3 (**6**)). In the absence of methanol, the monomeric complexes get dimerized through oxygen bridges (Fig. 1.3 (**7**)). They have also reported the catalytic properties of these complexes towards oxidation of benzoin, triphenylphosphine and polymerization of norbornene.

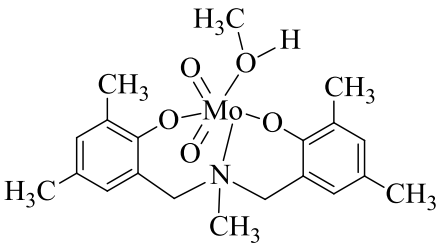

6

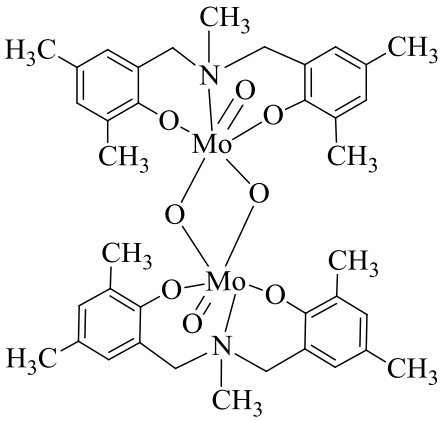

7

Figure 1.3. Dioxidomolybdenum(VI) complexes with tridentate ligand derived from aminobis(phenolate).

A new series of dioxidomolybdenum(VI) complexes were prepared using $[Mo^{VI}O_2(acac)_2]$ and HL_1 and HL_2 (where HL_1 and HL_2 are obtained from the condensation of salicylaldehyde or *o*–hydroxyacetophenone and 4,6–dimethyl–2–hydrazino pyrimidine). The ligand (HL_1) produced the regular ligand exchange product $[Mo^{VI}O_2(L_1)Cl]$ (**8**) whereas HL_2 resulted two different types of dichloro dioxidomolybdenum(VI) complexes $[Mo^{VI}O_2(L_3)Cl_2]$ (**9**) and $[Mo^{VI}{}_2O_5(L_3)Cl_2]$ (**10**) [where L_3 is a neutral bidentate ligand, 2–(3, 5–dimethyl–1–pyrazolyl) 4,6–dimethyl pyrimidine] (Fig. 1.4). X–ray crystallography reveals that a metal mediated C=N bond cleavage occurs in ligands during complex formation [59]. Though these complexes should show potential catalytic activity but their catalytic activity has not been reported.

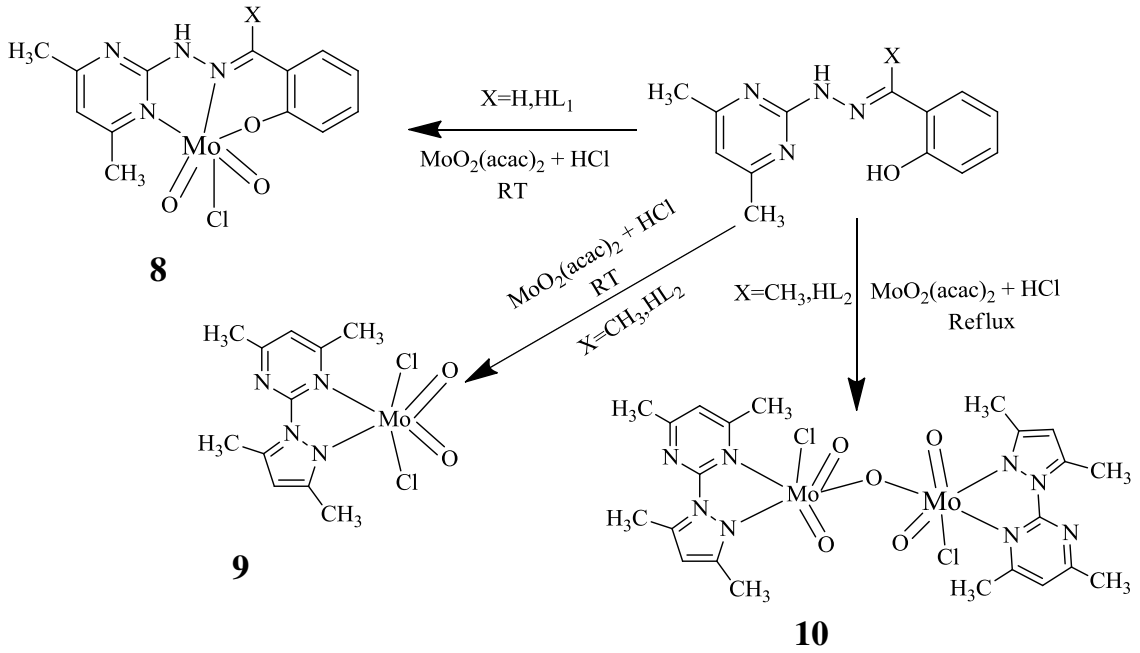

Figure 1.4. Synthetic route for the formation of molybdenum(VI) complexes with the ligands, HL_1 and HL_2.

Wong *et al.* have reported a series of dioxidomolybdenum(VI) complexes using new N_2O_2 type tripodal tetradentate ligands obtained from di– or tetra–*tert*–butyl substituted 2–[bis(2–hydroxybenzyl)aminomethyl]pyridine/ benzimidazole and 8–[bis(3,5–di–*tert*–butyl–2–hydroxybenzyl)]aminoquinoline (Fig. 1.5). The complexes of the type $[Mo^{VI}O_2(L)]$ were prepared by the reaction of $[Mo^{VI}O_2(acac)_2]$ or $[Mo^{VI}O_2Cl_2(dme)]$ (dme = 1,2–dimethoxyethane) with these ligands [60].

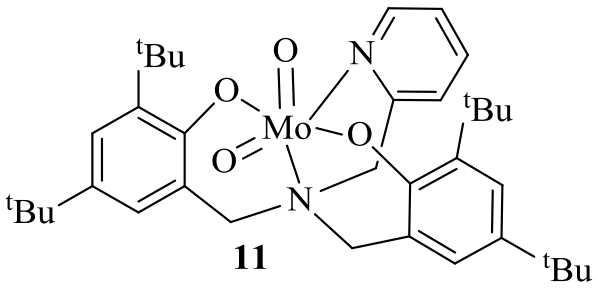

Figure 1.5. Dioxidomolybdenum(VI) complexes of new N_2O_2 type tripodal tetradentate ligands.

A series *cis*–$[Mo^{VI}O_2]^{2+}$ complexes (Fig. 1.6) of chiral Schiff–base ligands, derived from the condensation of salicylaldehyde or substituted salicylaldehydes and various amino alcohols has been prepared by Chakravarthy et al. [61]. A labile solvent molecule completed the sixth coordination site of octahedral geometry of the *cis*–$[Mo^{VI}O_2]^{2+}$ center. These complexes have also been tested for the catalytic enantioselective sulfoxidation reactions using H_2O_2 as a green oxidant.

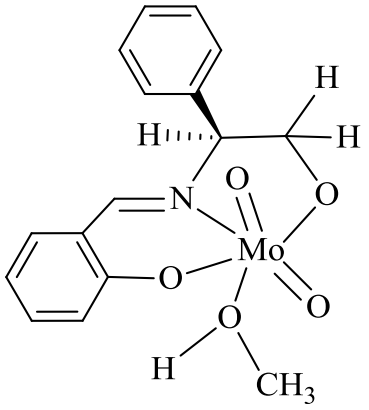

12

Figure 1.6. *cis*–$[Mo^{VI}O_2]^{2+}$ complexes of chiral ligands.

Neves and coworkers have reported molybdenum complexes $[Mo^{VI}O_2Cl\{HC(3,5–Me_2pz)_3\}]BF_4$ (**13**) with the ligand [$HC(3,5–Me_2pz)_3$ = tris(3,5–dimethyl–1–pyrazolyl)methane] and tested as a catalyst for the epoxidation of olefins at 55 ^oC using tert–butyl hydroperoxide (TBHP) as the oxidant. Transformation of **13** into the trioxidomolybdenum(VI) complex $[\{HC(3,5–Me_2pz)_3\}MoO_3]$ (**16**) occurred on increasing amounts of water in the reaction mixture (without affecting product selectivity). Treatment of **13** in dichloromethane with excess TBHP led to the isolation of the symmetrical $[Mo_2O_4(\mu_2–O)\{HC(3,5–Me_2pz)_3\}_2](BF_4)_2$ (**14**) and unsymmetrical $[Mo_2O_3(O_2)_2(\mu_2–O)(H_2O)\{HC(3,5–Me_2pz)_3\}]$ (**15**) oxido–bridged dimmers (Fig. 1.7) [62].

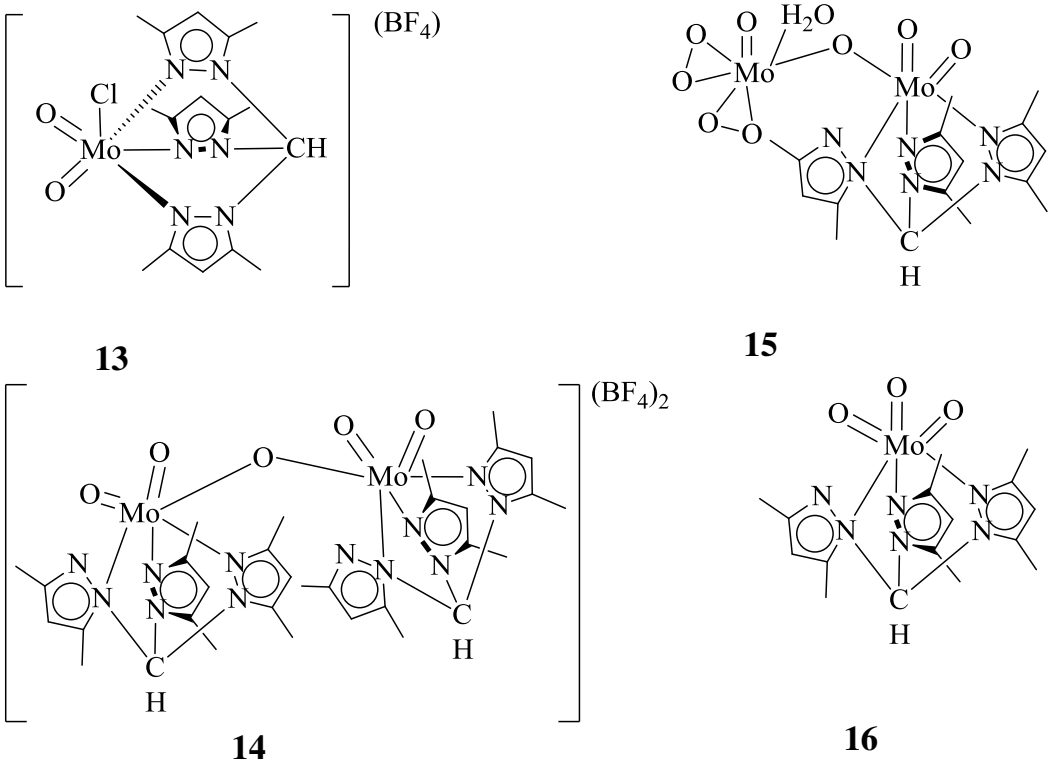

Figure 1.7. Different types of molybdenum(VI) complexes with pyrazolyl containing ligands.

The dioxidomolybdenum(VI) $[MoO_2L_1]$ (**17**) having a diamine bis(phenolate) ligand was prepared from $[Mo^{VI}O_2Cl_2]$ in good yields (Fig. 1.8). Its catalytic potential in the epoxidation of *cis*–cyclooctene using H_2O_2 as well as TBHP as oxidant has also been evaluated [63].

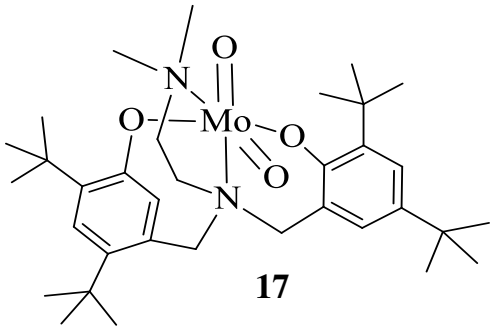

Figure 1.8. Dioxidomolybdenum complexes $[Mo^{VI}O_2L_1]$ of a diamine bis(phenolate) ligand.

Judmaier and coworkers developed a series of new $[Mo^{VI}O_2(L^X)_2]$ complexes of Schiff base ligands with the unusual η^2 coordinated $[Mo^{VI}O_2(\eta^2\text{–}tBu_2pz)_2]$ complex as starting material (Fig. 1.9). All ligands are coordinated to the metal ion in a bidentate manner through O and N atoms and the third donor atom (R = OMe or NMe_2) of the side chain does not participate in coordination and behaves like a pendant. All the complexes have also been tested as catalyst towards the epoxidation of various alkenes using TBHP as oxidant [64].

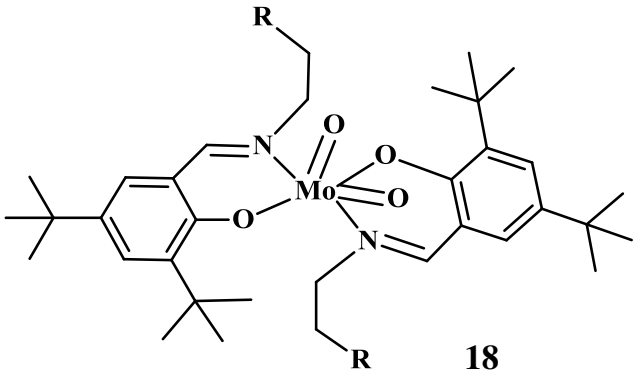

18

Figure 1.9. New $[Mo^{VI}O_2(L^X)_2]$ type complexes prepared from Schiff base ligands. R = OMe or NMe_2.

Chakraborty *et al.* have reported *cis*–$[Mo^{VI}O_2]^{2+}$ complexes of the type $[Mo^{VI}O_2L]$ and $[Mo^{VI}O_2L\text{–}B]$ (Fig. 1.10 (**19, 20**)) with new diprotic tridentate ONS chelating ligands. These complexes have potential to behave as models for the active site of an oxidoreductase molybdoenzyme like xanthineoxidase. MoO_2L–B type complex prepared on the treatment of MoO_2L with neutral monodentate Lewis bases such as 2–picoline, 2–methylimidazole or 1–allylimidazole, utilizing the vacant sixth coordination site [65].

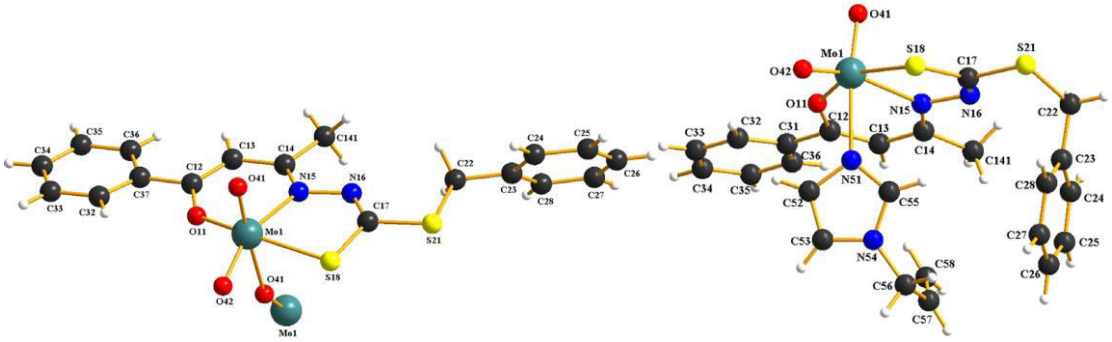

19 **20**

Figure 1.10. *cis*–$[Mo^{VI}O_2]^{2+}$ complexes with diprotic tridentate ONS chelating ligands which behave as models for the xanthine oxidase. (Reproduced from the reference [65]).

Kurapati *et. al.* have reported a series of cis–dioxidomolybdenum(VI) complexes of common formula cis–$[Mo^{VI}O_2(HL^n)]$ (Fig. 1.11) with 2,2'–(2–hydroxy–3,5–R_1,R_2–benzylazanediyl) diethanols in methanol. In these complexes, the metal centre is in a distorted octahedral NO_5 coordination sphere assembled by the single edge shared 5,5,6–membered chelate rings forming NO_3–donor (HL^n) and two *cis* oriented oxido groups. All these complexes have been evaluated as catalysts for the oxidative bromination of styrene and salicylaldehyde and in benzoin oxidation reaction [66].

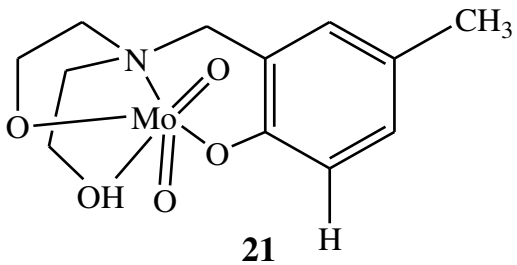

21

Figure 1.11. *Cis*–dioxidomolybdenum(VI) complexes of NO_5 donor ligand.

Alkoxo–rich Schiff–bases of potentially tri–, tetra– and penta–dentate binding capacity and their molybdenum(VI) complexes have been synthesized by Rao and his co–workers and characterized using several analytical and spectral techniques such as multinuclear NMR and single–crystal X–ray diffraction studies (Fig. 1.12 (**22**)) [67]. In the same year, they have reported *cis*–dioxidomolybdenum(VI) complexes of monosaccharides (D–glucose, D–fructose, D–galactose, D–mannose, D–ribose and D–xylose) and characterized by several analytical and spectral methods which reveals the presence of dimeric structures, formed through the *cis*–$Mo^{VI}O_2$ moieties and the bridging saccharide units (Fig. 1.12 (**23**)) [68]. Molybdenum complexes of Schiff bases, derived from saccharide moiety were further prepared by this group [69]. The catalytic potential of these complexes has not been reported, though, they should show potential catalytic activity.

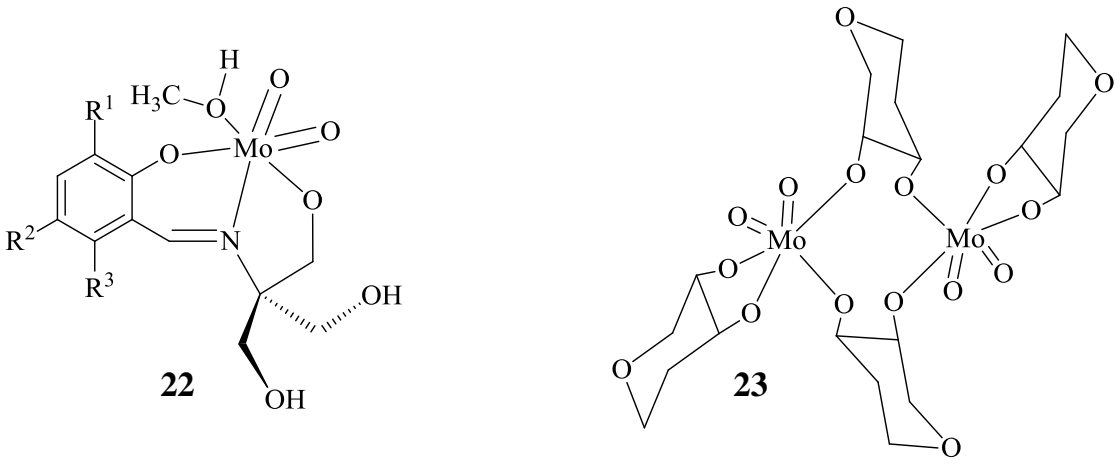

Figure 1.12. *Cis*–dioxidomolybdenum(VI) complexes of alkoxo–rich Schiff–base and monosaccharides.

1.4. Dioxidomolybdenum(VI) compounds as catalysts for various organic reactions

Dioxidodimolybdenum(VI) compounds have been used as valuable catalysts for different kind of redox reactions [70]. These compounds play a vital role in various catalytic organic transformations [37]. Some important catalytic reactions are given here.

1.4.1. Epoxidation Reactions

In organic chemistry, epoxidation is one of the most elementary reactions. Molybdenum complexes are found very suitable catalyst precursors for such reactions with alkyl hydroperoxide as an oxidant. Halcon and ARCO have set up epoxidation reactions using molybdenum based catalysts [71, 72]. Subsequently, researchers got engaged and used molybdenum catalysts for epoxidation reactions. Epoxidation of alkenes was reported using molybdenum hexacarbonyl as a catalyst. In the presence of hydroperoxide, molybdenum hexacarbonyl forms active oxidomolybdenum(VI) species which is considered as a key intermediate responsible for catalytic reactions (Fig. 1.13). Several olefins and allylic compounds were effectively oxidized using molybdenum complexes as catalysts [73].

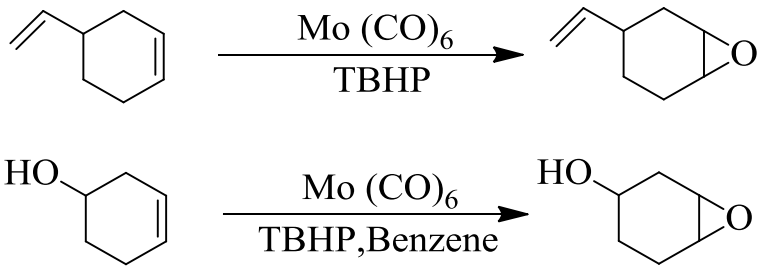

Figure 1.13. Epoxidation reactions using TBHP as an oxidant.

Barlan *et al.* have been studied asymmetric epoxidation reactions with chiral ligands of a range of substrates. In most of the cases low enantioselectivity was noted

because of the weak coordination of the chiral ligands. They also prepared molybdenum complexes by the reaction of chiral bis–hydroxamic acid and $[Mo^{VI}O_2(acac)_2]$ and used them for asymmetric epoxidation of various alkenes [74]. As high as 96% enantioselectivity was achieved with these catalytic systems (Fig. 1.14).

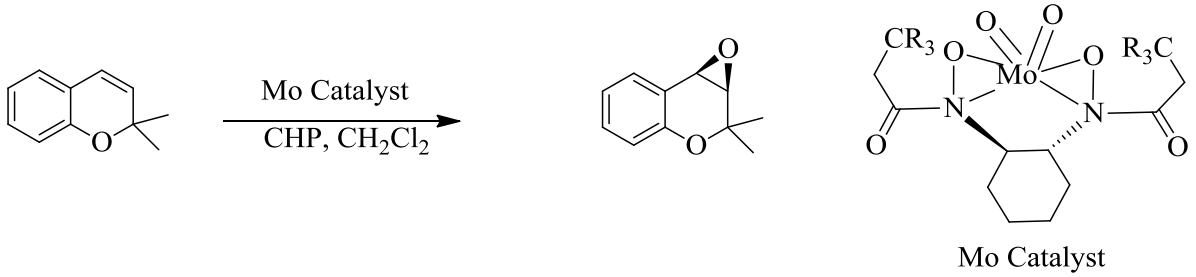

Figure 1.14. Asymmetric epoxidation reaction with Mo catalyst.

Two novel cyclopentadienyl molybdenum complexes $[CpMo(CO)_2(ImPyMes)Cl]$ (ImPyMes = 2–mesitylimidazo[1,5–a]pyridine–3–ylidene) and $[CpMo(CO)_2(ImPyMes)(NCCH_3)]BF_4$ were employed as pre–catalysts in the olefin epoxidation reaction using tert–butylhydroperoxide (TBHP) as an oxidant in chloroform at 55 ^oC with excellent TOF (Fig. 1.15) [75].

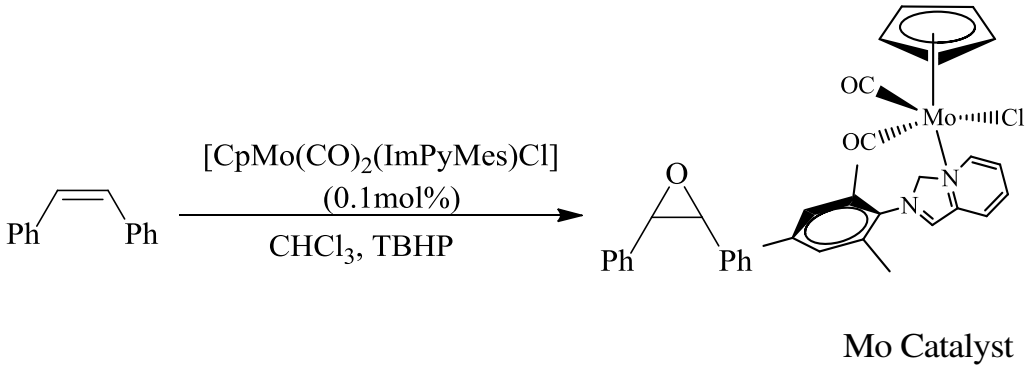

Figure 1.15. Epoxidation reaction with Mo catalyst.

Javadi and his group reported a novel bis(oxazoline) ligand derived from 1,3–dicyanobenzene and used as a ligand for the preparation of a new binuclear molybdenyl complex. This catalytic system was proficiently used for the oxidation of alkenes in the

presence of TBHP. For the substrate *cis*–octene, it gives epoxide with 100% yield (Fig. 1.16) [76].

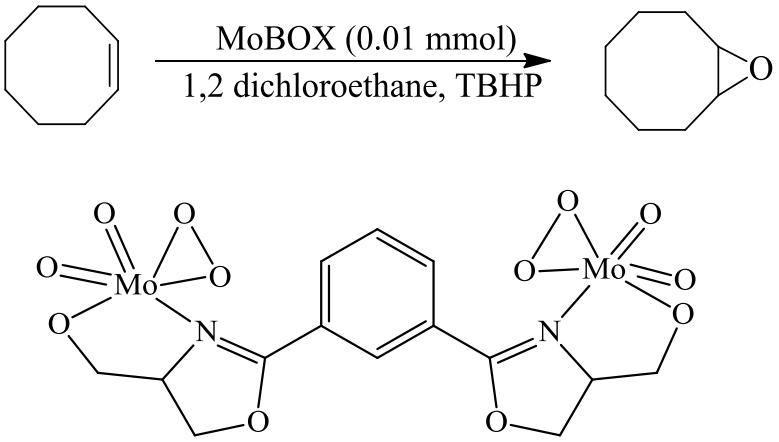

Figure 1.16. Epoxidation reaction with binuclear molybdenum complexes.

Mösch–Zanetti and coworker prepared air–stable chiral dioxidomolybdenum(VI) complexes of the type $[Mo^{VI}O_2(L)]$ by the reaction of $[Mo^{VI}O_2Cl_2]$ with the bis(phenol) ligands 1,4–bis(2–hydroxy–benzyl)–(*S*,*S*)–2,2′–bipyrrolidine and 1,4–bis(2–hydroxy–3,5–di–*tert*–butylbenzyl)–(*S*,*S*)–2,2′–bipyrrolidine. These complexes are efficient epoxidation catalysts for various internal and terminal alkenes and give epoxides in moderate to good yields along with high selectivity (Fig. 1.17) [77].

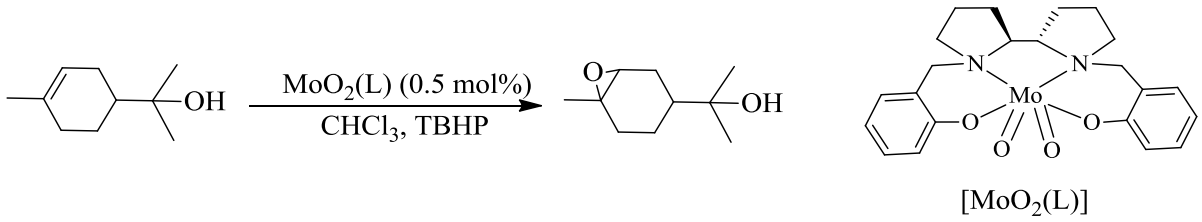

Figure 1.17. Epoxidation reaction with Mo–L catalyst.

1.4.2. Oxidation of alcohols

$[Mo^{VI}O_2(acac)_2]$ was also developed as a potential catalyst precursor in the presence of sodium peroxidocarbonate (SPC) for the oxidation of a variety of primary and secondary alcohols to the corresponding aldehydes and ketones, respectively in CH_3CN (Fig. 1.18) [78].

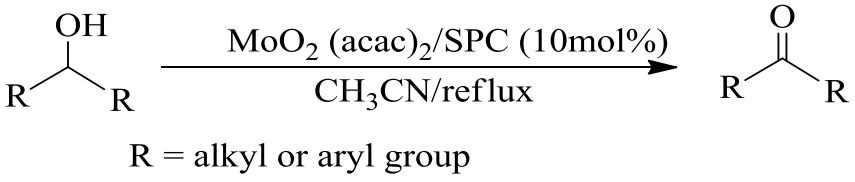

Figure 1.18. Oxidation of alcohols by $[Mo^{VI}O_2(acac)_2]$ as catalyst precursor.

Chand *et al.,* examined *cis*–$[Mo^{VI}O_2]^{2+}$ complexes of general formula $[Mo^{VI}O_2Cl_2(\mathbf{L})_2]$ (where **L =** DMSO, DMF and THF) as catalysts for aerobic oxidation of activated benzyl alcohols and other secondary alcohols. Among complexes tested, DMSO adduct was observed to be most dynamic catalyst. These reactions were carried out simply in open air without using any other external oxidant. The activity of catalysts was maintained when the reaction was carried out by passing oxygen through the reaction mixture (Fig. 1.19) [79, 80].

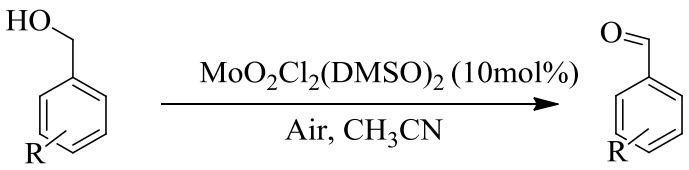

R = electron donating substituents

Figure 1.19. Oxidation product of various benzyl alcohols using $[Mo^{VI}O_2Cl_2(DMSO)_2]$ as catalyst.

Biradar and group have reported selective oxidation of various aromatic alcohols to aldehydes with very high conversion (90%) and selectivity (90%) using cyclopentadienyl molybdenum acetylide complex, $CpMo(CO)_3(C{\equiv}CPh)$ as efficient catalyst using hydrogen peroxide as an environmentally benign oxidant (Fig. 1.20) [81].

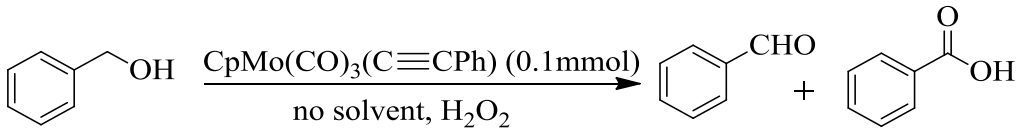

Figure 1.20. Oxidation of benzyl alcohols by catalyst $CpMo(CO)_3(C{\equiv}CPh)$.

Oxidation of alcohols has also been reported by Gharah *et. al.* keeping in mind the cost-effectiveness of the catalyst and environment pollution. Catalyst $PPh_4[MoO(O_2)_2(HPEOH)]$ (HPEOH is 1-(2'-hydroxyphenyl) ethanone oxime) exhibited good catalytic potential towards alcohols, amines and sulfides (Fig. 1.21) [82].

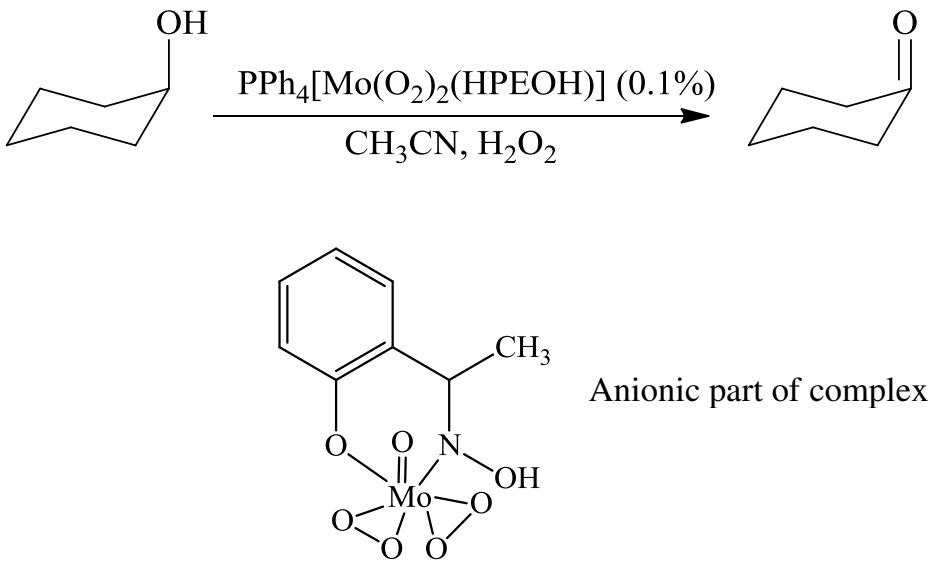

Figure 1.21. Oxidation of alcohols by catalyst $PPh_4[MoO(O_2)_2(HPEOH)]$.

1.4.3. Oxidation of sulfides

Group of Chand found $Mo^{VI}O_2Cl_2$ an effective catalyst for the oxidation of various organic sulfides having additional functional groups like alkene, aldehyde, imine, alcohol, oxime etc. (Fig. 1.22) which are liable to oxidize or deprotect. The catalyst is also selective for the oxidation of symmetrical disulfides into the corresponding monosulfoxides (Fig. 1.23) [83].

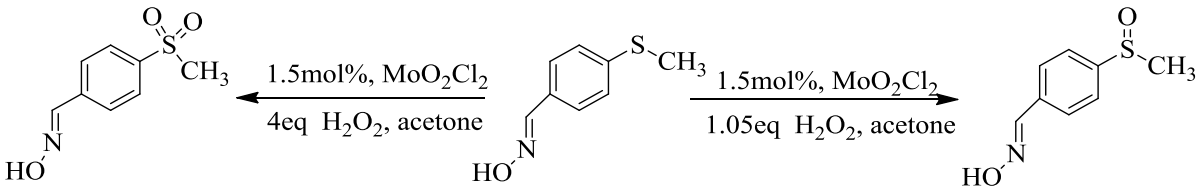

Figure 1.22. Oxidation of 4-(methylthio)benzaldehydeoxime using $Mo^{VI}O_2Cl_2$ as catalyst.

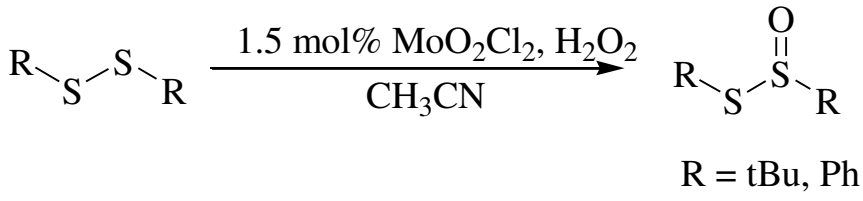

Figure 1.23. Oxidation of disulfides using $Mo^{VI}O_2C1_2$ as catalyst.

A novel organometallic dioxidomolybdenum(VI) complex for chemo–selective sulfoxidation reactions was employed by Gamelas and co–workers. Using TBHP as oxidant, catalyst [$CpMoO_2Cl$[(2 mol%) resulted in the oxidation of organic sulfides (dialkyl, arylalkyl and benzothiophenic) to the corresponding sulfones at 35 °C in good to excellent yields (Fig. 1.24) [84].

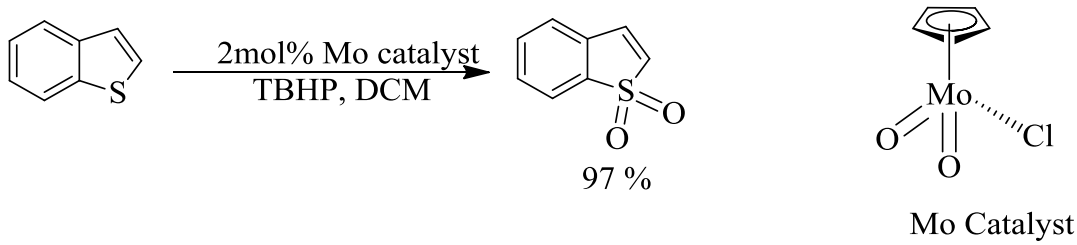

Figure 1.24. Oxidation of benzothiophene by [$CpMoO_2Cl$] catalyst.

Wen Shuai Zhu research group have prepared peroxido–molybdenum amino acid complexes (PMAACs) and checked their catalytic activity for the oxidation of dibenzothiophene (DBT) which have further been used in extraction and catalytic oxidative desulfurization system (ECODS) using different ionic liquids (like $BmimPF_6$: 1-butyl-3-mehtylimidazolium hexafluorophosphate). PMAACs were effective wide–ranging catalysts and exhibited high desulfurization efficiency (Fig. 1.25) [85].

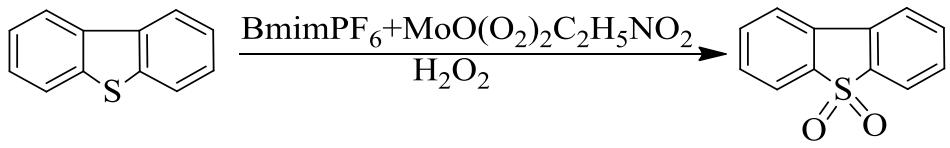

Figure 1.25. Oxidation of dibenzothiophene by Mo catalyst with ionic liquids.

1.4.4. Oxidative bromination of organic substrate

A simple transformation of β-hydroxy carbonyl compounds into α-brominated 1,3-dicarbonyl compounds *via* 1,3-dicarbonyl compounds has been reported using catalyst MoO_2Cl_2 in the presence of N-bromosuccinimide as a co-oxidant (Fig. 1.26). The reaction also proceeds in the same way for most of the different aryl substituted β–hydroxy esters and β–hydroxyketones [86].

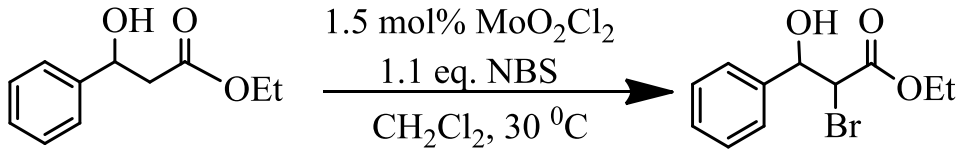

Figure 1.26. Oxidative bromination reaction with MoO_2Cl_2 catalyst.

Sagarika *et al*., employed dioxidomolybdenum(VI) complexes which are functional mimics of haloperoxidases, and successfully perform oxidative bromination of salicylaldehyde in aqueous solution at room temperature. Using these complexes as catalyst precursors and H_2O_2 as oxidant, substrate gave mainly three products, namely 5-bromosalicylaldehyde, 3,5-dibromosalicylaldehyde and 2,4,6-tribromophenol in the presence of KBr and $HClO_4$ (Fig. 1.27) [87].

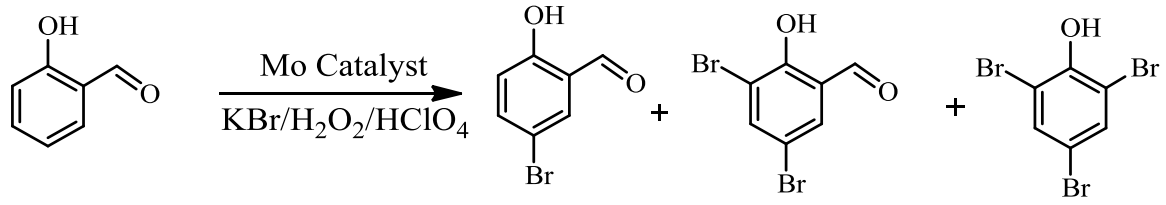

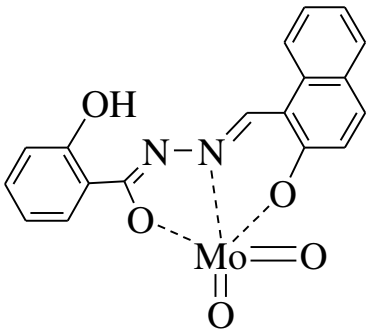

Mo catalyst

Figure 1.27. Different brominated products of salicylaldehyde.

1.4.5. Oxidation of benzoin

Dinda and co-workers examined *cis*–$[Mo^{VI}O_2]^{2+}$ complexes Schiff bases for the oxidation of benzoin. At least four different oxidation products were obtained with green oxidant H_2O_2 in refluxing methanol (Fig. 1.28) [87].

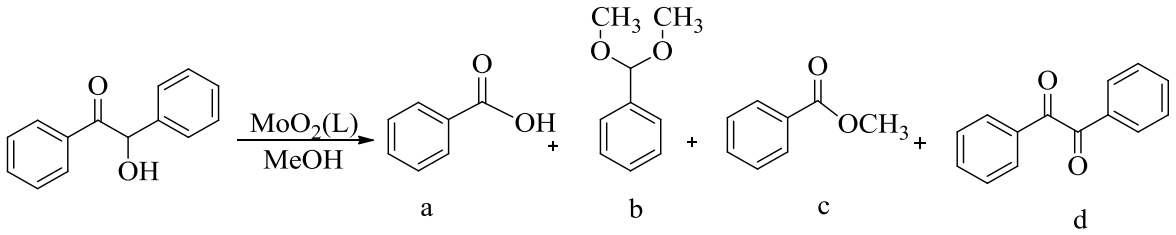

Figure 1.28. Various oxidation products of benzoin; (a) benzoic acid, (b) benzaldehyde–dimethylacetal, (c) methylbenzoate and (d) benzil.

Another group reported a series of *cis*–$[Mo^{VI}O_2]^{2+}$ complexes of general formula *cis*–$[MoO_2(HL^n)]$. All the complexes have also been evaluated for their catalytic oxidation of benzoin (Fig. 1.29) [66].

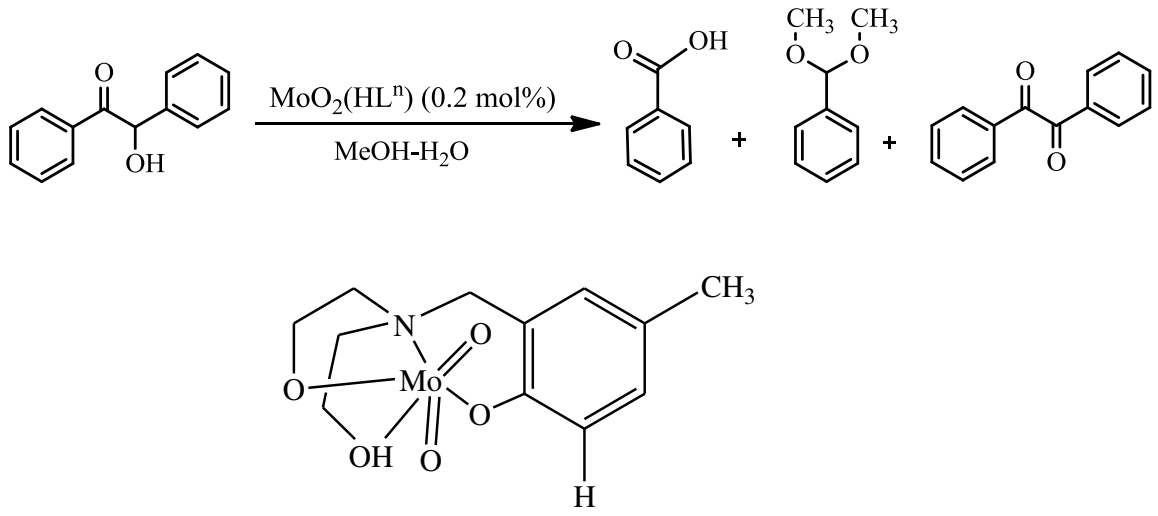

Figure 1.29. Various oxidation products of benzoin.

1.5. Miscellaneous applications

Zhu and co–workers have reported remarkable application of oxidomolybdenum complexes for asymmetric pinacol coupling reactions where aldehyde has been converted into the corresponding 1, 2–diol. Similar reaction has also been catalyzed by *cis*–$[Mo^{VI}O_2]^{2+}$ complex of salan based chiral ligand in the presence of zinc as co–reductant (Fig. 1.30) [88].

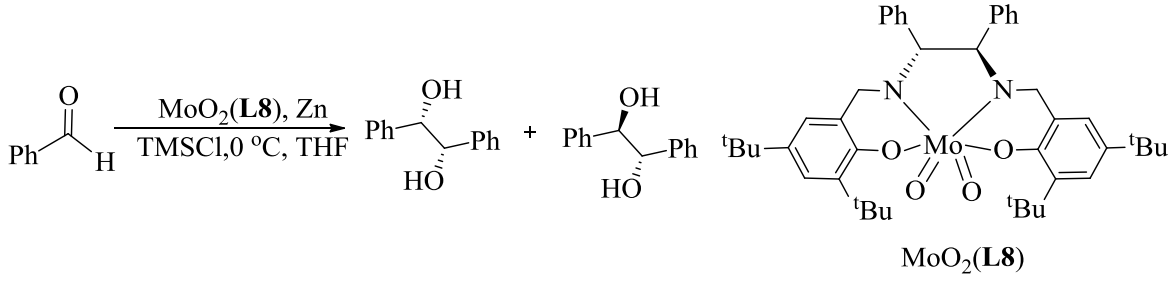

Figure 1.30. Asymmetric pinacol coupling of benzaldehyde using molybdenum(VI) catalyst.

Molybdenum(VI) complexes in DMSO solvent provides a gentle and proficient system for selective oxidation of various aromatic and non-aromatic thiols to the

corresponding disulfides in excellent yields. The reactivity of thiols follows the order: ArSH > $ArCH_2SH$ > AlkSH. This method is important due to its simplicity, general applicability and excellent yields (Fig. 1.31) [89].

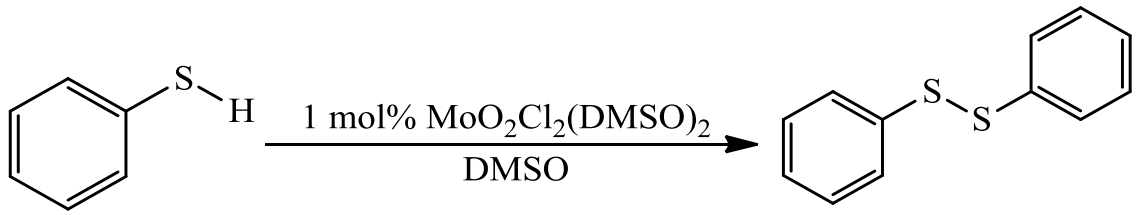

Figure 1.31. Oxidation of thiols with $Mo^{VI}O_2C1_2$ catalyst.

A single step conversion of epoxides into the corresponding α–methoxy ketones has been catalyzed by MoO_2Cl_2/oxone in refluxing methanol (Fig. 1.32). The corresponding methoxy ketone in good yield has also been obtained from epoxycyclohexane, allyloxymethyl, propenyloxymethyl and benzylomethyl and long chain oxirane [90].

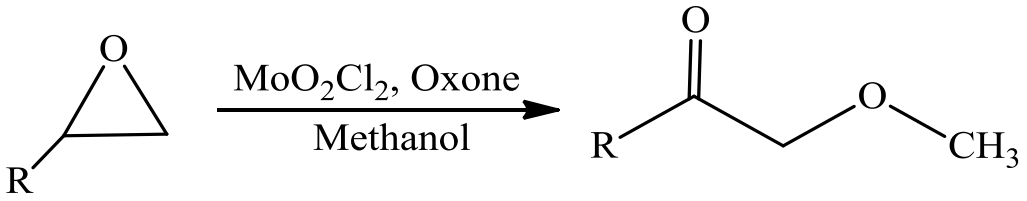

Figure 1.32. Oxidation of epoxides into α–methoxy ketones using $Mo^{VI}O_2C1_2$ catalyst.

Royo and coworkers have used *cis*–$[Mo^{VI}O_2]^{2+}$ complexes as catalysts for the hydrosilylation of 4–(trifluoromethyl) benzaldehyde with dimethylphenylsilane using 5 mol% catalyst loadings (Fig. 1.33) [91].

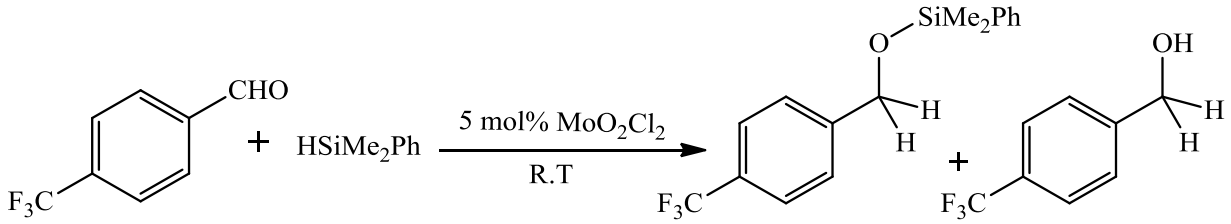

Figure 1.33. Hydrosilylation of 4–(trifluoromethyl) benzaldehyde with dimethylphenylsilane using catalyst MoO_2C1_2.

Under mild conditions, group of Marta Abrantes have used new hybrid material, $\{[MoO_3(bipy)][MoO_3(H_2O)]\}_n$ (bipy = 2,2'–bipyridine) as a water–tolerant catalyst for the oxidation of secondary amines using either urea hydrogen peroxide (UHP) or tert–butylhydroperoxide (TBHP) as oxidant. The optimized reaction conditions for this reaction were concluded as: catalyst (2 mol %), TBHP (3-4 equivalent), solvent (CH_2Cl_2) and temp. (40 ^{0}C). Depending upon the nature of the cyclic or acyclic amine used, the corresponding nitrones were obtained. (Fig. 1.34) [92].

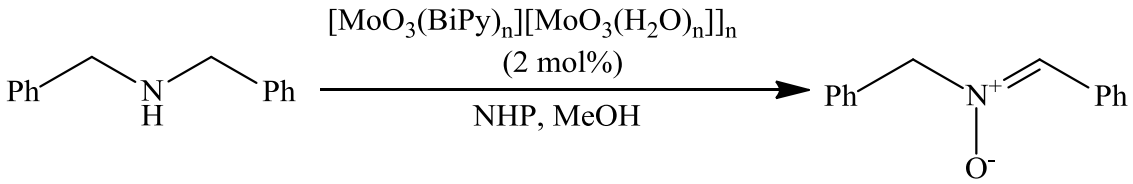

Figure 1.34. Oxidation of secondary amine.

Selective N–oxidation of primary amines into the corresponding nitroso derivatives using $CpMo(CO)_3(C{\equiv}CPh)$ as catalyst has been reported by Biradar and co–workers. A quantitative conversion with 99% selectivity towards nitroso compounds was obtained in the presence of 30% H_2O_2 as an oxidant (Fig. 1.35) [93].

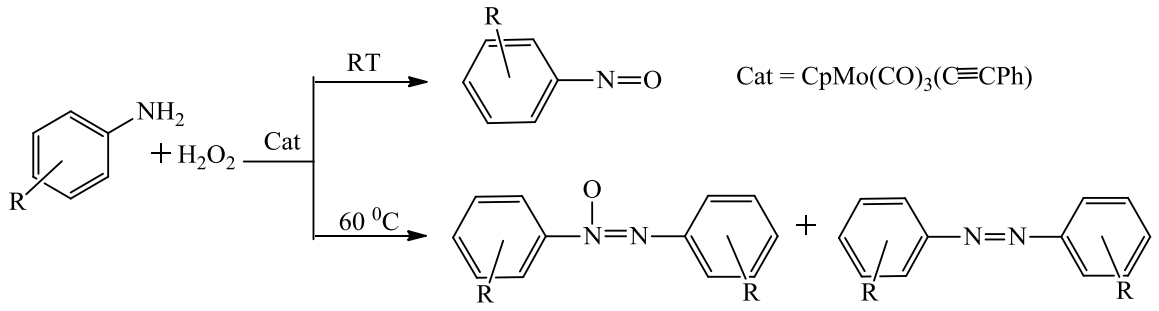

R = –OH, –CH_3, –OCH_3, –Cl, –F

Figure 1.35. Oxidation of primary aromatic amines.

Das *et al.* have employed the molybdenum(VI) peroxido complex, synthesized from the reaction of MoO_3 with H_2O_2 and 3,5–dimethylpyrazole (dmpz), selectively oxidizes benzylic C–H bonds of alkylbenzenes to the corresponding alcohols and ketones in moderate to good yields in the presence of H_2O_2 in acetonitrile under reflux (ca. 80 °C) (Fig. 1.36) [94].

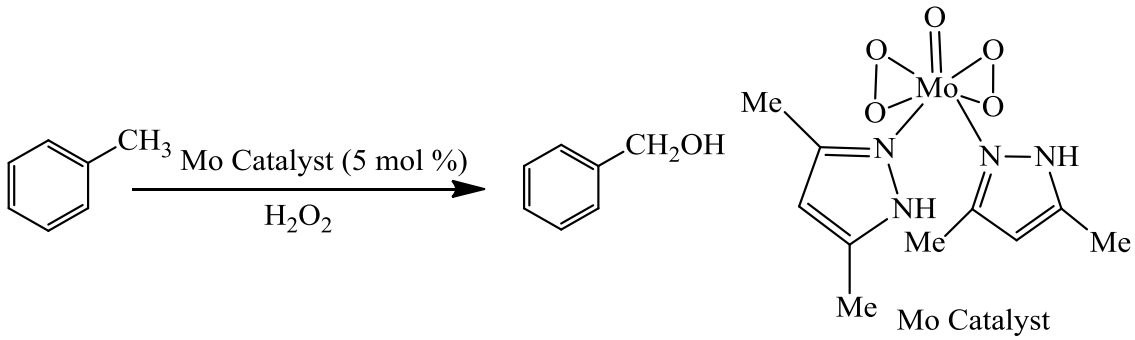

Figure 1.36. Oxidation of alkylbenzenes.

1.6. Objectives of the present thesis

The discovery of molybdenum dependent enzymes and their importance in various biological catalytic processes has stimulated research on the catalytic aspects of molybdenum complexes. Catalysts have played a vital role in organic conversions and have major impact on the quality of human life as well as on economic progress. In recent years many model molybdenum complexes have shown good catalytic activity towards various organic transformations. It is also evident from the review of the literature that molybdenum Schiff base complexes have provided opportunities to develop catalytic system for various industrial processes. Particularly, oxidation reactions catalyzed by these specialized complexes are well documented. However, in most cases optimization of the reaction conditions to effect maximum efficiency of the catalysts have not been set out. It was, therefore, reasonable to undertake systematic study on the synthesis and characterization of new molybdenum catalysts and to explore their catalytic potential for the oxidation of organic substrates under optimized reaction conditions.

Present study is aimed to describe the synthesis of dioxidomolybdenum(VI) complexes of the following ligands:

(i) Tribasic pentadentate N_2O_3 donor Schiff bases derived from salicylaldehyde, substituted salicylaldehyde and 1, 3–diamino–2–hydroxypropane.

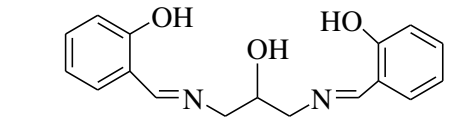

H_3sal-dahp (**2.I**)

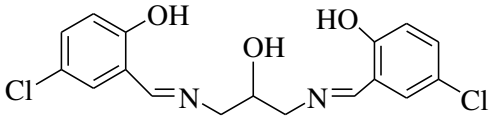

H_3clsal-dahp (**2.II**)

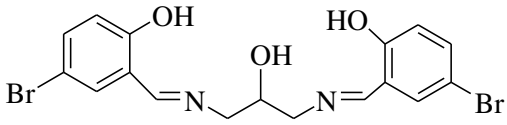

H_3brsal-dahp (**2.III**)

(ii) ONS donor ligands **3.I**, **3.II** and **3.III** derived from the condensation of 2,6–diformyl–4–methylphenol (dfmp) with *S*–benzyldithiocarbazate (sbdt), S–methyldithiocarbazate (smdt) and thiosemicarbazide (tsc):

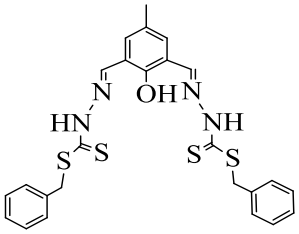

H_3dfmp-(sbdt)$_2$ (**3.I**)

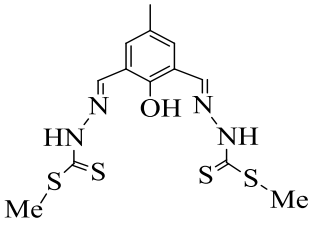

H_3dfmp-(smdt)$_2$ (**3.II**)

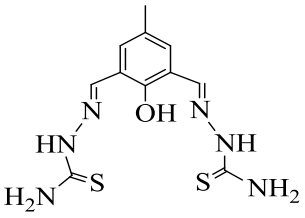

H_3dfmp-(tsc)$_2$ (**3.III**)

(iii) ONO donor ligands **4.I**, **4.II** and **4.III** derived from 2,6–diformyl–4–methylphenol (dfmp) and isonicotinoylhydrazide (inh), nicotinoylhydrazide (nah) and benzoylhydrazide (bhz):

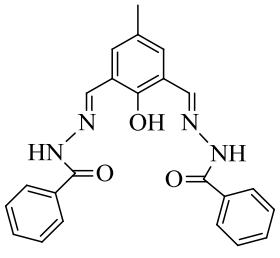

H_3dfmp(bhz)$_2$ (**4.I**)

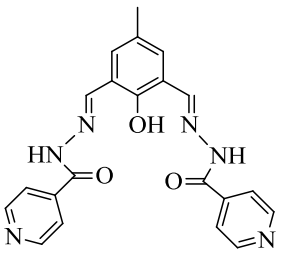

H_3dfmp(inh)$_2$ (**4.II**)

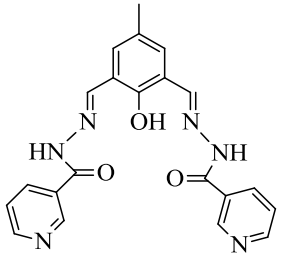

H_3dfmp(nah)$_2$ (**4.III**)

(iv) Dibasic tridentate ONO type ligands obtained by the condensation of equimolar amount of 8–formyl–7–hydroxy–4–methylcoumarin (fhmc) and hydrazides [benzoylhydrazide (bhz), isonicotinoylhydrazide (inh), nicotinoylhydrazide (nah) and furoylhydrazide (fah)]:

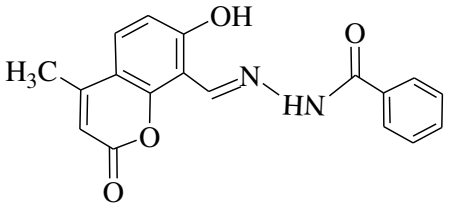

H_2fhmc-bhz (**5.I**)

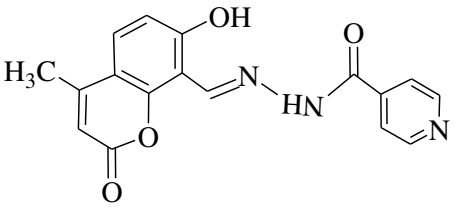

H_2fhmc-inh (**5.II**)

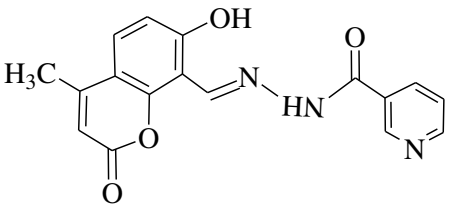

H_2fhmc-nah (**5.III**)

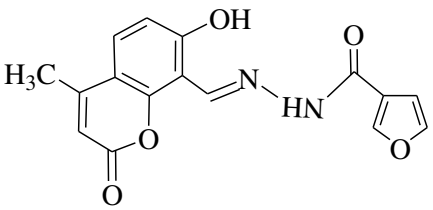

H_2fhmc-fah (**5.IV**)

The synthesized complexes have been characterized by chemical, spectral (IR and electronic and NMR), thermal studies and single crystal X–ray diffraction study. Catalytic potential of these complexes have been explored for the following reactions**:**

(a) Oxidative bromination of styrene

(b) Oxidation of methyl phenyl sulfide

(c) Oxidation of benzoin

(d) Oxidation of cyclohexene

(e) Oxidation of styrene

(f) Oxidation of secondary alcohols

(g) Oxidative bromination of thymol

Reaction conditions for the catalytic reactions have been optimized considering various parameters to obtain optimum performance of the catalysts.

CHAPTER 2

Synthesis, characterization and catalytic activity of dioxidomolybdenum(VI) complexes of tribasic pentadentate ligands

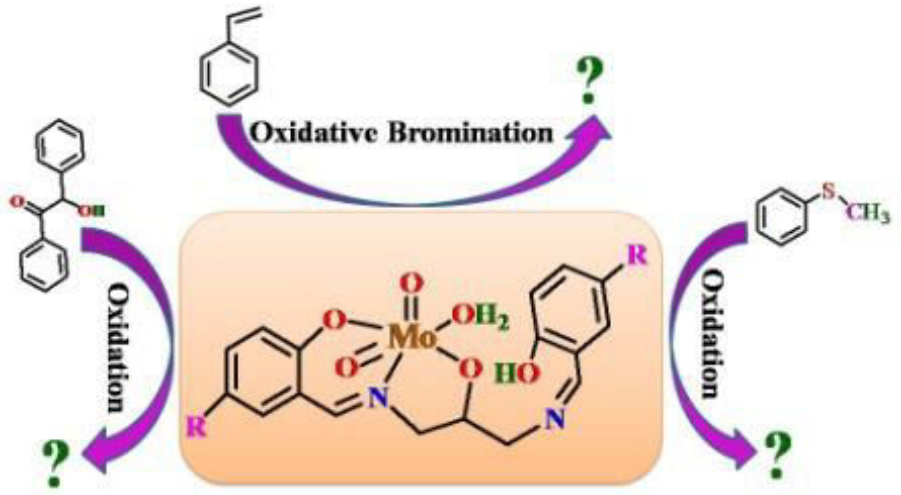

The matter of this chapter is published in the journal "Polyhedron"

2.1. Introduction

The significant enzymatic role of molybdenum in biochemical reactions, especially in the oxidation of aldehydes, purines and sulfides [95, 96] attracted the researchers to use high–valent molybdenum complexes with cis–$[Mo^{VI}O_2]$ functionality as biomimetic catalysts in the oxygenation of organic compounds [97–99]. The oxygen atom transfer properties of these complexes play a significant role in investigating the functioning mechanism of molybdenum-based oxotransfer enzymes that also contain, in many cases, a cis–$[Mo^{VI}O_2]$ moiety in the active site [100–106]. The tendency of molybdenum to form stable complexes with oxygen, nitrogen and sulfur donor containing ligands led to the development of high–valent molybdenum Schiff base complexes which are effective catalysts both in homogeneous and heterogeneous reactions. The performance of these complexes varied noticeably with the nature of ligands and the available coordination sites [64, 107–120].

Ligands derived from 1, 3–diamino–2–hydroxypropane and salicylaldehyde, substituted salicylaldehyde (H_3xsal–dahp, Scheme 2.1) or *o*–hydroxyacetophenone were tribasic pentadenate with good flexibility. However, participation or non–participation of alcoholic hydroxyl group and of second Schiff base moiety may result in interesting tridentate, tetradentate and pentadentate coordinating behavior of these ligands [121, 122]. In fact, dibasic tetradentate and tribasic pentadentate behaviors of these ligands have been confirmed in oxidovanadium(IV) and oxidovanadium(V) complexes, respectively. Further, vanadium complex $[V^{IV}O$(Hsal–dahp)] in which alcoholic oxygen of the amine residue does not participate in coordination, undergoes decomposition under aerobic atmosphere at reflux temperature in methanol producing new dioxidovanadium(V) complex where hydrolysis of azomethine nitrogen occurs giving free amino group along with the loss of salicylaldehyde moiety; here the alcoholic oxygen also coordinates after proton replacement and the new ligand behaves as dibasic tridentate ONO system [121].

Recent review by Chakravarthy and Chand accounts the synthetic strategies of several cis–$[Mo^{VI}O_2]^{2+}$ complexes of dianionic tridentate ONO ligands [39]. Catalytic

applications of molybdenum complexes in organic transformations [37, 64, 107–120, 123–127] and oxidation of sulfides [37, 61, 128] have also been explored while oxidative bromination of organic substrates, a reaction normally promoted by vanadium haloperoxidase enzymes [129–131] has rarely been studied [50, 124].

The interesting behavior of H_3xsal–dahp [121, 122] and a wide catalytic applications of molybdenum complexes prompted us to undertake synthesis and characterization of new dioxidomolybdenum(VI) complexes of H_3xsal–dahp. Their catalytic potentials are demonstrated by studying the oxidative bromination of styrene and oxidation of methyl phenyl sulfide. In addition, oxidation of benzoin by peroxide has also been reported.

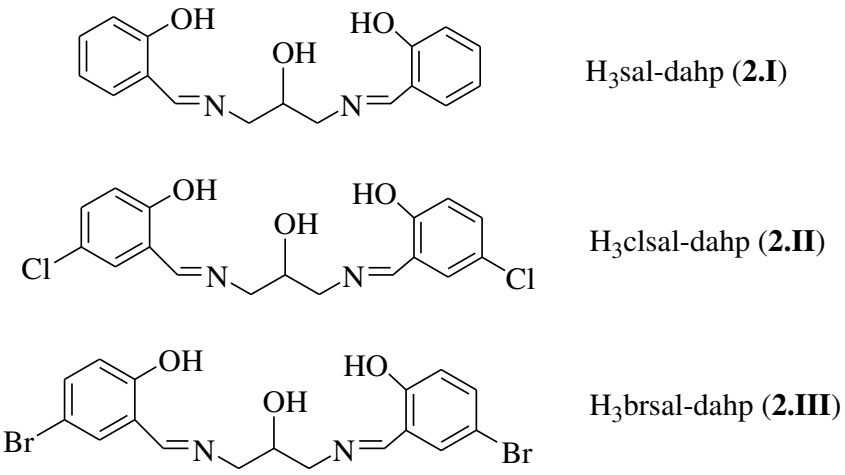

Scheme 2.1. Structure of ligands designated by **2.I**, **2.II** and **2.III** used in this work.

2.2. Experimental section

2.2.1. Materials and methods

Ammonium molybdate (Loba Chemie, India), 1, 3–diamino–2–hydroxypropane (Hdahp), acetylacetone (Hacac) (Aldrich, U.S.A.), salicylaldehyde (Sisco Research, India), methyl phenyl sulfide (Alfa Aesar, U.S.A.), styrene (Acros Organics, U.S.A.), benzoin (S.D. Fine, India), 70 % aqueous $HClO_4$ and 30% aqueous H_2O_2 (Qualigens,

India) were used as obtained. All other chemicals and solvents used were of AR grade. $[Mo^{VI}O_2(acac)_2]$ was prepared according to the method reported in the literature [132].

2.2.2. Instrumentation and Characterization Procedures

Elemental analyses of the ligands and complexes were obtained by an Elementar model Vario–EL–III. IR spectra were recorded as KBr pellets on a Nicolet 1100 FT–IR spectrometer after grinding the sample with KBr. Electronic spectra of ligand and complexes were recorded in methanol or DMSO using Shimadzu 1601 UV–vis spectrophotometer. ^{1}H NMR spectra were recorded on a Bruker Avance 500 MHz spectrometer with the common parameter settings in DMSO–D_6. The δ values are quoted relative to TMS as internal standard. Thermogravimetric analyses of the complexes were carried out using Perkin Elmer (Pyris Diamond) instrument in air with a heating rate of 10 ^{o}C/ min. A Shimadzu Nicolet gas chromatograph with a HP–1 capillary column (30 m × 0.25 mm × 0.25 μm) was used to analyze the reaction products. The identity of the products was confirmed using a GC–MS model Perkin–Elmer, Clarus 500 by comparing the fragments of each product with the library available. The percent conversion of substrate and selectivity of products were calculated from GC data using the formula presented elsewhere [133].

2.2.3. Preparations

2.2.3.1. Preparations of H_3sal–dahp (2.I), H_3clsal–dahp (2.II) and H_3brsal–dahp (2.III)

Ligand H_3sal–dahp was prepared as reported previously [121]. Salicyaldehyde (2.44 g, 20 mmol) was dissolved in 50 ml of methanol. A solution of 1,3–diamino–2–hydroxypropane (0.90 g, 10 mmol) dissolved in 10 ml methanol was added drop wise to the above solution and the reaction mixture was stirred for 2 h. On standing the yellow solid slowly separated out which was filtered, washed with minimum of methanol and dried in a vacuum desiccator over silica gel. Yield 5.36 g (90%). Anal. Calc. for $C_{17}H_{18}N_2O_3$ (298.34): C, 68.41; H, 6.13; N, 9.48. Found: C, 68.05; H, 6.02; N, 9.50%.
Other ligands were prepared following essentially same procedure.

Data for H_3clsal–dahp (**2.II**): Yield: 3.27 g (89%). Anal. Calc. for $C_{17}H_{16}N_2O_3Cl_2$ (367.23): C, 55.69; H, 4.43; N, 7.63. Found: C, 55.60; H, 4.26; N, 7.58 %.

Data for H_3brsal–dahp (2.III): Yield: 4.10 g (90%). Anal. Calc. for $C_{17}H_{16}N_2O_3Br_2$ (456.13): C, 44.76; H, 3.54; N, 6.14. Found: C, 44.69; H, 3.36; N, 6.07%.

2.2.3.2. Preparation of [$Mo^{VI}O_2$(Hsal–dahp)(H_2O)] (2.1)

A stirred solution of H_3sal–dahp (0.60 g, 2 mmol) in methanol (10 mL) was treated with [$Mo^{VI}O_2(acac)_2$] (0.66 g, 2 mmol) dissolved in methanol (10 mL) and the obtained reaction mixture was stirred where an yellow solid starts to form immediately. After 1 h of stirring, the separated solid was filtered, washed with methanol and dried in a vacuum desiccator over silica gel. Yield: 0.643 g (75%). Anal. Calc. for $C_{17}H_{18}N_2O_6Mo$ (444): C, 45.94; H, 4.09; N, 6.31. Found: C, 45.86; H, 4.05; N, 6.27 %.

2.2.3.3. Preparation of [$Mo^{VI}O_2$(Hclsal–dahp)(H_2O)] (2.2)

Complex **2.2** was prepared from [$Mo^{VI}O_2(acac)_2$] (0.66 g, 2 mmol) and H_3clsal–dahp (0.73 g, 2 mmol) by the method outlined for **2.1**. The separated solid was filtered, washed with methanol and dried in a vacuum desiccator over silica gel. Yield: 0.745 g (75%). Anal. Calc. for $C_{17}H_{16}N_2O_6Cl_2Mo$ (512): C, 39.85; H, 3.15; N, 5.47. Found: C, 39.68; H, 3.21; N, 5.38 %.

2.2.3.4. Preparation of [$Mo^{VI}O_2$(Hbrsal–dahp)(H_2O)] (2.3)

This complex was prepared by the procedure outlined for [$Mo^{VI}O_2$(Hsal–dahp)(H_2O)] (**2.1**) using [$Mo^{VI}O_2(acac)_2$] (0.66 g, 2 mmol) and H_3brsal–dahp (0.912 g, 2 mmol). The separated solid was filtered, washed with methanol and dried in a vacuum desiccator over silica gel. Yield: 1.075 g (92%). Anal. Calc. for $C_{17}H_{16}N_2O_6Br_2Mo$ (599.8): C, 34.01; H, 2.69; N, 4.67. Found: C, 33.92; H, 2.62; N, 4.53 %. Crystals of [$Mo^{VI}O_2$(Hbrsal–dahp)(DMSO)] (**2.3a**) were grown by slow evaporation of a solution of **2.3** in DMSO.

2.2.3.5. Preparations of [$Mo^{VI}O_2$(Hsal–dahp)(py)] (2.4), [$Mo^{VI}O_2$(Hclsal–dahp)(py)] (2.5) and [$Mo^{VI}O_2$(Hbrsal–dahp)(py)] (2.6)

Complexes [$Mo^{VI}O_2$(Hsal–dahp)(H_2O)] (**2.1**), [$Mo^{VI}O_2$(Hclsal–dahp)(H_2O)] (**2.2**) and [$Mo^{VI}O_2$(Hbrsal–dahp)(H_2O)] (**2.3**) (1 mmol each) were dissolved in minimum of pyridine and evaporated slowly under vacuum where yellow solid in each case slowly precipitated. These were filtered, washed with methanol and dried in vacuum desiccator over silica gel. Nearly quantitative yield was obtained in all cases.

Data for [$Mo^{VI}O_2$(Hsal–dahp)(py)] (2.4): Anal. Calc. for $C_{22}H_{21}N_3O_5Mo$ (503): C, 56.06; H, 4.49; N, 8.91. Found: C, 56.52; H, 4.78; N, 9.03 %.

Data for [$Mo^{VI}O_2$(Hclsal–dahp)(py)] (2.5): Anal. Calc. for $C_{22}H_{19}N_3O_5Cl_2Mo$ (572.26): C, 48.94; H, 3.54; N, 7.78. Found: C, 48.56; H, 3.62; N, 7.59 %.

Data for [$Mo^{VI}O_2$(Hbrsal–dahp)(py)] (2.6): Anal. Calc. for $C_{22}H_{19}N_3O_5Br_2Mo$ (661.16): C, 42.09; H, 3.04; N, 6.68. Found: C, 42.41; H, 3.12; N, 6.80 %.

2.2.3.6. Preparation of $[Mo^{VI}O_2(Hclsal–hdap)(DMSO)]_4[Mo_8O_{26}]\cdot 6DMSO$ (2.7)

Salicylaldehyde (0.244 g, 2 mmol) and 1,3–diamino–2–hydroxypropane (0.090 g, 1 mmol) were taken in methanol (20 mL) and reflux for 2 h. A solution of [$Mo^{VI}O_2(acac)_2$] (0.33 g, 1 mmol) in DMSO (10 mL) was added to the above solution and the reaction mixture was heated at 80 ^oC for 1 h and then kept at room temperature for slow evaporation. After few days, the obtained yellow crystals were filtered and dried in air. No satisfactory elemental analyses could be obtained.

2.2.4. X–Ray crystal structure determination

Three–dimensional room temperature X–ray data were collected on a Bruker Kappa Apex CCD diffractometer at low temperature for **2.3a** and **2.7** by the ϕ–ω scan method. Reflections were measured from a hemisphere of data collected from frames each of them covering 0.3º in ω. Of the 31885 for **2.3a** and 81546 for **2.7** reflections measured, all were corrected for Lorentz and polarization effects and for absorption by multi–scan methods based on symmetry–equivalent and repeated reflections, 3724 and

10219, respectively, independent reflections exceeded the significance level ($|F|/\sigma|F|$) > 4.0. Complex scattering factors were taken from the program package SHELXTL [134]. The structures were solved by direct methods and refined by full matrix least–squares on F^2. Hydrogen atoms were included in calculation positions and refined in the riding mode. Refinements were done with allowance for thermal anisotropy of all non–hydrogen atoms. Further details of the crystal structure determination are given in Table 2.1.

Table 2.1.

Crystal data and structure refinement parameters for $[Mo^{VI}O_2(Hbrsal–dahp)(DMSO)]$ (**2.3a**) and for $[Mo^{VI}O_2(clsal–hdap)(DMSO)]_4[Mo_8O_{26}]\cdot 6DMSO$ (**2.7**).

	2.3a	**2.7**
Formula	$C_{19}H_{20}Br_2MoN_2O_6S$	$C_{60}H_{108}Cl_4\ Mo_{12}N_8O_{52}S_{10}$
Formula mass	660.19	3387.22
T, *K*	100(2)	100(2)
Wavelength, Å	0.71073	0.71073
Crystal system	Triclinic	Triclinic
Space group	P $\bar{1}$	P $\bar{1}$
a/Å	6.4781(11)	11.1756(3)
b/Å	12.819(2)	15.9726(5)
c/Å	14.330(3)	16.6625(5)
α/º	82.617(8)	109.950(2)
β/º	83.191(9)	102.650(2)
γ/º	75.476(8)	98.962(2)
V/Å^3	1137.7(3)	2640.40(13)

Z	2	1
F_{000}	648	1672
D_{calc}/g cm^{-3}	1.927	2.130
μ/mm^{-1}	4.218	1.766
θ/ (°)	1.44 to 28.02	1.36 – 28.80
R_{int}	0.1230	0.0638
Crystal size/ mm^3	0.47 × 0.05 × 0.05	0.160 × 0.145 × 0.050
Goodness–of–fit on F^2	1.131	1.077
R_1 [a]	0.0683	0.0482
wR_2 (all data)[b]	0.1751	0.1497
Largest differences peak and hole (eÅ^{-3})	1.589 and –1.466	3.682 and –2.084

[a] $R_1 = \Sigma \left| \left| F_o \right| - \left| F_c \right| \right| / \Sigma \left| F_o \right|$. [b] $wR_2 = \{\Sigma[w(\left| \left| F_o \right|^2 - \left| F_c \right|^2 \right|)^2] / \Sigma[w(F_o^4)]\}^{1/2}$

2.2.5. Catalytic activity studies

Complexes [$Mo^{VI}O_2$(Hsal–dahp)(H_2O)] (**2.1**), [$Mo^{VI}O_2$(Hclsal–dahp)(H_2O)] (**2.2**) and [$Mo^{VI}O_2$(Hbrsal–dahp)(H_2O)] (**2.3**) were used as catalyst for the oxidative bromination of styrene, oxidation of methyl phenyl sulfide and benzoin. All reactions were carried out in a 50 mL two neck glass reaction flask fitted with a water circulated condenser.

2.2.5.1. Oxidative bromination of styrene

Styrene (1.04 g, 10 mmol), 30% aqueous H_2O_2 (2.27 g, 20 mmol), 70% $HClO_4$ (4.29 g, 30 mmol) and KBr (2.38 g, 20 mmol) were taken in a mixture of dichloromethane–water (40 mL, V/V) at room temperature. After adding catalyst (0.001g) to the above reaction mixture, it was stirred and the obtained oxidized products were analyzed quantitatively by gas chromatography by withdrawing small aliquots of the reaction mixture present in CH_2Cl_2 layer at every 15 min interval. The identities of

the products were confirmed by GC–MS and their quantifications were made on the basis of the relative peak area of the respective product.

2.2.5.2. Oxidation of methyl phenyl sulfide

Methyl phenyl sulfide (1.24 g, 10 mmol), 30% aqueous H_2O_2 (2.27 g, 20 mmol) and catalyst (0.0015 g) were mixed in acetonitrile (5 mL) and stirred at room temperature. The reaction was monitored by withdrawing small aliquots of the reaction mixture at every 30 min and analyzing them quantitatively by gas chromatography. The identities of the products were confirmed by GC–MS. The effects of various parameters, such as amounts of oxidant, catalyst and solvent were studied to see their effect on the conversion and selectivity of the reaction products.

2.2.5.3. Oxidation of Benzoin

Benzoin (1.06 g, 5 mmol), 30% aqueous H_2O_2 (1.69 g, 15 mmol) and catalyst (0.0005 g) were mixed in methanol (10 mL) and the reaction was carried out at reflux temperature of methanol. The reaction was monitored by withdrawing small aliquots of the reaction mixture at every 60 min and analyzing them quantitatively by gas chromatography. The identities of the products were confirmed by GC–MS. The effects of various parameters, such as amounts of oxidant, catalyst and solvent were studied to see their effect on the conversion and selectivity of the reaction products.

2.3. Results and discussion

2.3.1. Synthesis and characterization of complexes

The reaction between equimolar amounts of $[Mo^{VI}O_2(acac)_2]$ (Hacac = acetylacetone) and ligands H_3sal–dahp (**2.I**), H_3clsal–dahp (**2.II**) and H_3brsal–dahp (**2.III**) in refluxing methanol leads to the formation of dioxidomolybdenum(VI) complexes $[Mo^{VI}O_2(Hsal–dahp)(H_2O)]$ (**2.1**), $[Mo^{VI}O_2(Hclsal–dahp)(H_2O)]$ (**2.2**) and $[Mo^{VI}O_2(Hbrsal–dahp)(H_2O)]$ (**2.3**), respectively [Eq. (2.1) taking H_3sal–dahp (**2.I**) as a representative].

$$[Mo^{VI}O_2(acac)_2] + H_3sal–dahp + H_2O \rightarrow [Mo^{VI}O_2(Hsal–dahp)(H_2O)] + 2Hacac \quad (2.1)$$

All these complexes possibly exist as monomer [135, 136] and are soluble in DMSO and DMF only. Complexes **2.1**–**2.3** also dissolve in pyridine giving $[Mo^{VI}O_2(Hsal–dahp)(py)]$ (**2.4**), $[Mo^{VI}O_2(Hclsal–dahp)(py)]$ (**2.5**) and $[Mo^{VI}O_2(Hbrsal–dahp)(py)]$ (**2.6**) [Eq. (2.2) considering $[Mo^{VI}O_2(Hsal–dahp)(H_2O)]$ (**2.1**) as a representative] where pyridine occupies the sixth coordination position in these complexes. Pyridine containing complexes are soluble in methanol, DMSO and DMF. Complex $[Mo^{VI}O_2(Hclsal–hdap)(DMSO)]_4[Mo_8O_{26}]\cdot 6DMSO$ (**2.7**), obtained by the reaction of $[Mo^{VI}O_2(acac)_2]$ dissolved in DMSO and in–situ generated H_3clsal–dahp in methanol, is of interest as one of the salicylaldehyde moieties is lost and the azomethine group converted into amine upon hydrolysis followed by protonation. Part of the complex is also decomposed to give molybdenum polyhedron as a side product. Scheme 2.2 provides idealized structures of the complexes which are based on the spectroscopic (IR, UV/Vis, ^{1}H and ^{13}C NMR) data, elemental analyses and X–ray diffraction studies of **2.3a** and **2.7**.

$[Mo^{VI}O_2(Hsal–dahp)(H_2O)] + py \rightarrow$

$[Mo^{VI}O_2(Hsal–dahp)(py)] + H_2O$ (2.2)

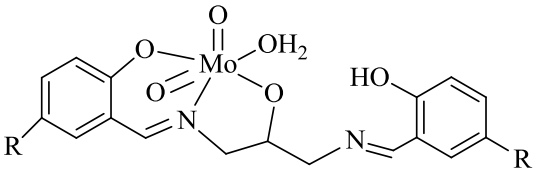

R = H: $[Mo^{VI}O_2(Hsal\text{-}dahp)(H_2O)]$ **(2.1)**
R = Cl: $[Mo^{VI}O_2(Hclsal\text{-}dahp)(H_2O)]$ **(2.2)**
R = Br: $[Mo^{VI}O_2(Hbrsal\text{-}dahp)(H_2O)]$ **(2.3)**

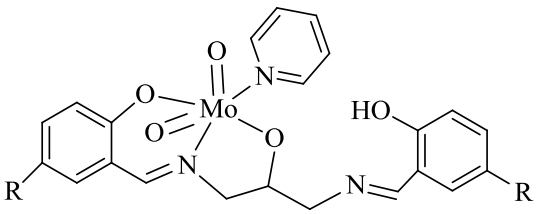

R = H: $[Mo^{VI}O_2(Hsal\text{-}dahp)(py)]$ **(2.4)**
R = Cl: $[Mo^{VI}O_2(Hclsal\text{-}dahp)(py)]$ **(2.5)**
R = Br: $[Mo^{VI}O_2(Hbrsal\text{-}dahp)(py)]$ **(2.6)**

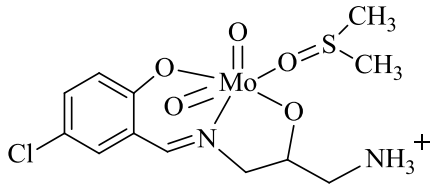

$[Mo^{VI}O_2(Hclsal\text{-}hdap)(DMSO)]^+$ (Cation part of **(2.7)**

Scheme 2.2. Proposed structures of complexes reported in this contribution.

2.3.2. Thermal studies

The dioxidomolybdenum(VI) complexes **2.1**, **2.2** and **2.3** lose mass equal to one water molecule [4.3 % (Calcd: 4.1 %) for **2.1**, 3.6 % (Calcd: 3.5 %) for **2.2** and 3.2 % (Calcd: 3.0 %) for **2.3**] in the temperature range 100–265 °C, indicative of the covalently but not strongly bonded water. When water is coordinated in the trans position to one of the doubly bonded oxygen atoms (see structure of **2.3a**), its week bonding is expected. (cf. Scheme 2.2). The anhydrous complexes decompose exothermically in two/ three but overlapping steps on further increasing the temperature and form MoO_3 at ca. 600 ^oC for **2.1**, ca. 500 ^oC for **2.2** and at ca. 450 ^oC for **2.3** as the final product. Pyridine coordinated complexes are stable up to ca. 150 ^oC. The mass loss equivalent to one pyridine takes place between 150–200 ^oC in a first step. Above this temperature continuous exothermic decomposition of complexes occurs until the formation of respective metal trioxide, MoO_3 at ca. 600 ^oC (for **2.4**), ca. 480 ^oC (for **2.5**) and at ca. 450 ^oC (for **2.6**). Decomposition of ligands in these complexes in overlapping multiple steps did not allow the estimation of intermediates.

2.3.3. Structure descriptions

The ORTEP diagram along with atom–labeling scheme for $[Mo^{VI}O_2$(Hbrsal–dahp)(DMSO)] (**2.3a**) is shown in Fig. 2.1 while ORTEP diagrams for the cation $[Mo^{VI}O_2$(Hclsal–hdap)(DMSO)$]^+$ and anion $[Mo_8O_{26}]^{4-}$ of $[Mo^{VI}O_2$(Hclsal–hdap)(DMSO)$]_4[Mo_8O_{26}]\cdot$6DMSO (**2.7**) are shown in Figs. 2.2 and 2.3, respectively. Selected bond distances and angles are given in Table 2.2. The complexes adopt a six–coordinated structure in a distorted octahedral geometry. In these complexes, phenolic oxygen, alcoholic oxygen and azomethine nitrogen of the ligands coordinate to the molybdenum. One DMSO molecule and two oxo groups complete the coordination sphere. In the complex **2.3a**, other phenolic oxygen and azomethine nitrogen remain non–coordinated while in $[Mo^{VI}O_2$(Hclsal–hdap)(DMSO)$]^+$ of complex **2.7**, non–coordinated moiety hydrolyzes at azomethine nitrogen giving free amine group which exists as protonated.

The asymmetric unit of **2.7** contains two complexes $[Mo^{VI}O_2(Hclsal–hdap)(DMSO)]^+$, half $[Mo_8O_{26}]^{4–}$ anion, and three molecules of free DMSO. The whole formula is thus written as $[Mo^{VI}O_2(Hclsal–hdap)(DMSO)]_4[Mo_8O_{26}]\cdot 6DMSO$ (see Fig.2.4). One DMSO molecule coordinated to Mo atom, of one of the complexes presents in the asymmetric unit, shows a disorder on sulphur and carbon atoms. Two atomic sites have been observed for this DMSO molecule [site occupancy factor for C (1A), C (2A), S (1A) is 0.38347]. One coordinated oxygen atom of oxo group presents a disorder in the same complex. Two atomic sites have been observed for this oxygen atom [site occupancy factor for O (3C) is 0.36016]. The molecular geometry of $[Mo_8O_{26}]^{4–}$ anions correspond to β isomers with C_{2h} symmetry. In this form, all Mo atoms are six–coordinated but are not equivalents [137]. The oxygen sites can be included in four categories, terminal (O_t), two–coordinate (O_{2c}), three coordinate (O_{3c}) and five–coordinate (O_{5c}). Bond distances are given in Table 2.3 and are in agreement with those observed for other compounds containing the β–octamolybdate anion [137]. The O (15) constitutes a special case because it has two different distances to metal centre. It can be considered as a pseudo–terminal oxygen atom [138].

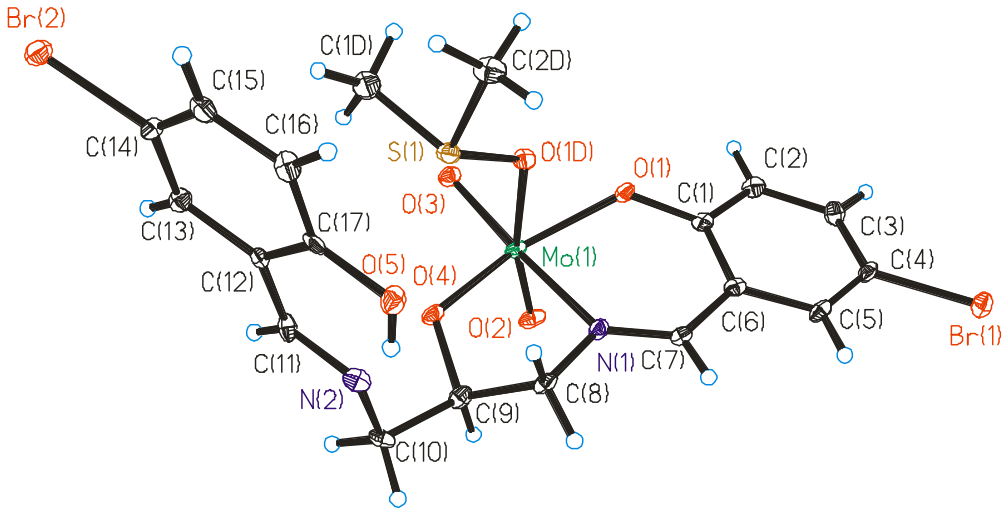

Figure 2.1. ORTEP plot of the complex $[Mo^{VI}O_2(Hbrsal–dahp)(DMSO)]$ (**2.3a**). All the non–hydrogen atoms are presented by their 30% probability ellipsoids.

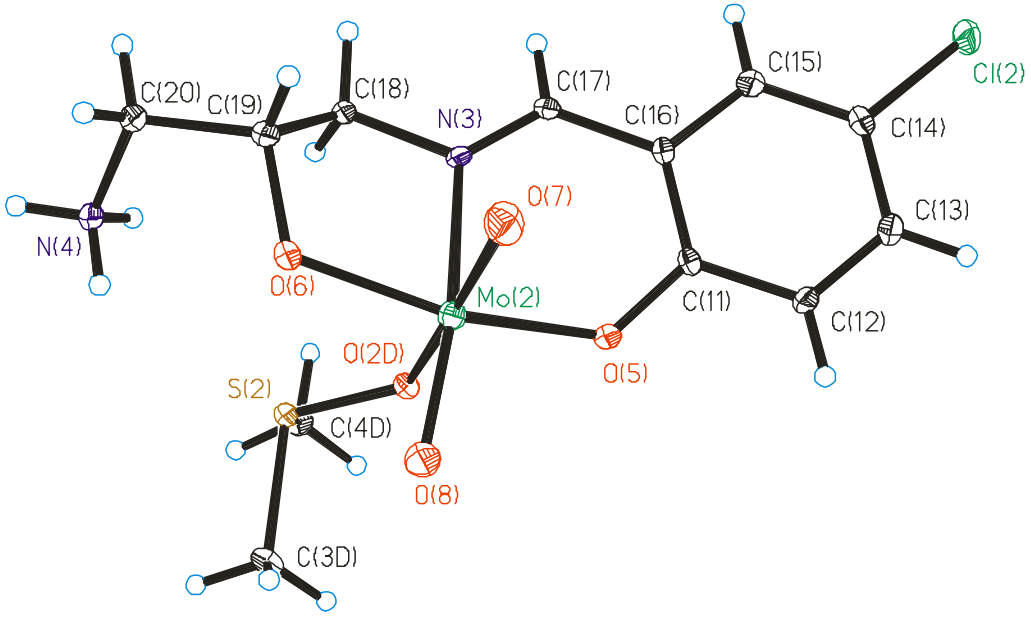

Figure 2.2. ORTEP plot of cation $[Mo^{VI}O_2(Hclsal–hdap)(DMSO)]^+$ in the compound $[Mo^{VI}O_2(Hclsal–hdap)(DMSO)]_4[Mo_8O_{26}]\cdot 6DMSO$ (**2.7**). All the non–hydrogen atoms are presented by their 30% probability ellipsoids.

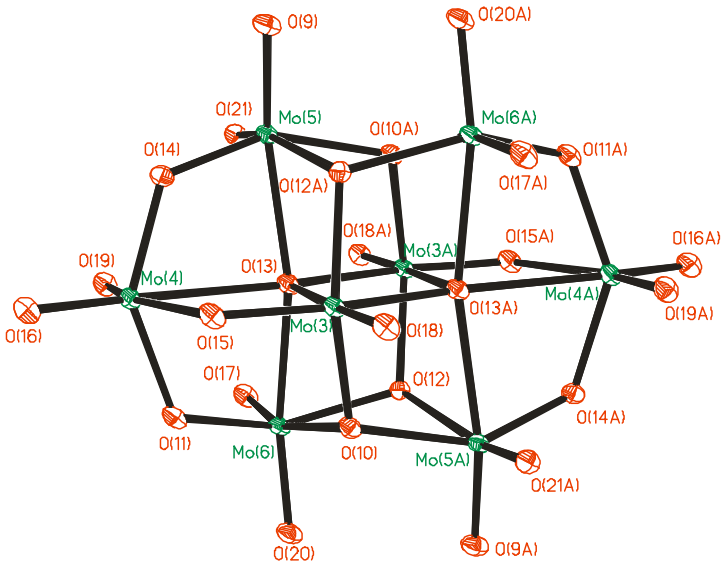

Figure 2.3. Structural and atom–labeling schemes for β–$[Mo_8O_{26}]^{4-}$ anion in the compound $[Mo^{VI}O_2(Hclsal–hdap)(DMSO)]_4[Mo_8O_{26}]\cdot 6DMSO$ (**2.7**).

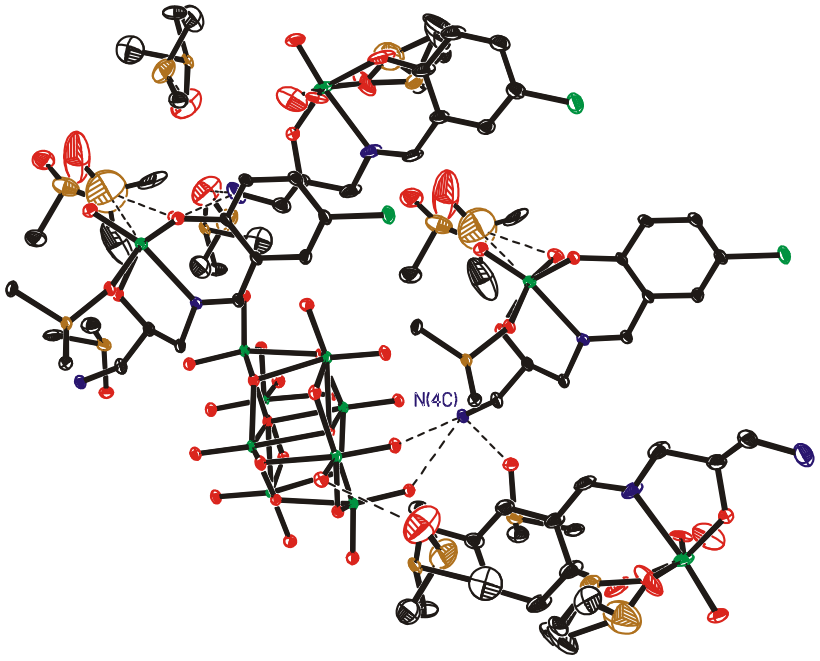

Figure 2.4. Crystal packing of $[Mo^{VI}O_2(Hclsal–hdap)(DMSO)]_4[Mo_8O_{26}]\cdot 6DMSO$ (**2.7**) along with hydrogen bonding scheme.

Table 2.2.

Bond lengths [Å] and angles [°] for [$Mo^{VI}O_2$(Hbrsal–dahp)(DMSO)] (**2.3a**) and for [$Mo^{VI}O_2$(Hclsal–hdap)(DMSO)]$_4$[Mo_8O_{26}]·6DMSO (**2.7**).

Bond lengths	**2.7**		**2.3a**
Mo(1)–O(1)	1.947(6)		1.971(6)
Mo(1)–O(2)	1.922(4)		1.714(7)
Mo(1)–O(3C)	1.651(13)		Mo(1)–O(3)1.714(6)
Mo(1)–O(3D)	1.713(13)		
Mo(1)–O(4)	1.683(5)		1.935(7)
Mo(1)–O(1D)	2.283(7)		2.303(6)
Mo(2)–O(5)	1.943(4)		
Mo(2)–O(6)	1.930(4)		
Mo(2)–O(7)	1.724(4)		
Mo(2)–O(8)	1.707(4)		
Mo(2)–O(2D)	2.270(4)		
Mo(1)–N(1)	2.268(6)		2.272(7)
Mo(2)–N(3)	2.270(5)		
Bond angles	**2.7**		**2.3a**
O(3C)–Mo(1)–O(4)	114.2(9)		
O(4)–Mo(1)–O(3D)	100.1(11)	O(3)–Mo(1)–O(4)	98.5(3)
O(3C)–Mo(1)–O(2)	110.6(10)	O(3)–Mo(1)–O(2)	105.8(3)
O(4)–Mo(1)–O(2)	99.1(2)	O(4)–Mo(1)–O(2)	98.7(3)
O(3D)–Mo(1)–O(2)	94.4(10)		
O(3C)–Mo(1)–O(1)	81.8(13)	O(3)–Mo(1)–O(1)	100.8(3)

O(4)–Mo(1)–O(1)	99.0(2)	O(4)–Mo(1)–O(1)	152.9(3)
O(3D)–Mo(1)–O(1)	104.4(13)		
O(2)–Mo(1)–O(1)	151.0(3)	O(2)–Mo(1)–O(1)	94.1(3)
O(3C)–Mo(1)–N(1)	83.8(9)	O(3)–Mo(1)–N(1)	162.6(3)
O(4)–Mo(1)–N(1)	161.9(3)	O(4)–Mo(1)–N(1)	75.3(3)
O(3D)–Mo(1)–N(1)	97.4(11)		
O(2)–Mo(1)–N(1)	74.94(19)	O(2)–Mo(1)–N(1)	91.2(3)
O(1)–Mo(1)–N(1)	80.8(2)	O(1)–Mo(1)–N(1)	80.7(3)
O(3C)–Mo(1)–O(1D)	154.2(13)	O(3)–Mo(1)–O(1D)	86.3(3)
O(4)–Mo(1)–O(1D)	85.9(3)	O(4)–Mo(1)–O(1D)	84.7(2)
O(3D)–Mo(1)–O(1D)	172.4(6)		
O(2)–Mo(1)–O(1D)	80.0(2)	O(2)–Mo(1)–O(1D)	166.6(3)
O(1)–Mo(1)–O(1D)	79.0(4)	O(1)–Mo(1)–O(1D)	77.9(2)
N(1)–Mo(1)–O(1D)	76.2(3)	N(1)–Mo(1)–O(1D)	77.1(3)
O(8)–Mo(2)–O(7)	106.5(2)		
O(8)–Mo(2)–O(6)	98.31(18)		
O(7)–Mo(2)–O(6)	96.92(19)		
O(8)–Mo(2)–O(5)	101.55(18)		
O(7)–Mo(2)–O(5)	95.48(19)		
O(6)–Mo(2)–O(5)	152.49(17)		
O(8)–Mo(2)–O(2D)	86.80(18)		
O(7)–Mo(2)–O(2D)	166.41(18)		
O(6)–Mo(2)–O(2D)	83.48(15)		
O(5)–Mo(2)–O(2D)	78.84(15)		
O(8)–Mo(2)–N(3)	163.27(19)		

O(7)–Mo(2)–N(3)	89.72(19)
O(6)–Mo(2)–N(3)	75.24(16)
O(5)–Mo(2)–N(3)	80.37(15)
O(2D)–Mo(2)–N(3)	77.21(15)

Table 2.3.

Mo–O bond distances for the β isomer of $[Mo_8O_{26}]^{4-}$.

Mo–O_t		
	Mo(5)–O(9)	1.703(4)
	Mo(4)–O(16)	1.688(4)
	Mo(6)–O(17)	1.707(4)
	Mo(3)–O(18)	1.693(4)
	Mo(4)–O(19)	1.708(4)
	Mo(6)–O(20)	1.697(4)
	Mo(5)–O(21)	1.713(4)
Mo–O_{2c}		
	Mo(4)–O(11)	1.927(4)
	Mo(6)–O(11)	1.895(4)
	Mo(4)–O(14)	1.935(3)
	Mo(5)–O(14)	1.883(4)
	Mo(3)–O(15)	1.744(4)
	Mo(4)–O(15)	2.291(4)
Mo–O_{3c}		

	Mo(3)–O(10)	1.958(4)
	Mo(5)–O(10)#1	1.994(4)
	Mo(6)–O(10)	2.318(3)
	Mo(3)–O(12)#1	1.942(3)
	Mo(5)–O(12)#1	2.322(3)
	Mo(6)–O(12)	2.013(3)
$Mo–O_{5c}$		
	Mo(3)–O(13)	2.331(3)
	Mo(3)–O(13)#1	2.145(4)
	Mo(4)–O(13)	2.461(4)
	Mo(5)–O(13)	2.323(4)
	Mo(6)–O(13)	2.333(4)

Symmetry transformations used to generate equivalent atoms: #1 –x+1,–y,–z+1

2.3.4. IR Spectral studies

Fig. 2.5 presents IR spectra of H_3sal–dahp (**2.I**) and [$Mo^{VI}O_2$(Hsal–dahp)(H_2O)] (**2.1**). The IR spectra of ligands (Table 2.4) exhibit a sharp band due to ν(C=N) (azomethine) stretch at 1633–1638 cm^{-1}. This band changes its position only slightly in respective complexes but the appearance of a new band at considerably lower wave number indicates the coordination of only one of the azomethine nitrogens to the molybdenum. The presence of several medium intensity bands between 2800 and 2500 cm^{-1} in the ligands as well as in complexes suggests the existence of C–H stretching due to $–CH_2$. The coordination of pyridine is characterized by the appearance of the ring breathing mode, the totally symmetric ring stretching mode, the in–plane antisymmetric ring stretching mode and the in–plane totally symmetric ring breathing mode at ca. 1000, 1600, 1440 and 1040 cm^{-1}, respectively [139]. In addition, these complexes display two

sharp bands at 914–928 and 889–903 cm^{-1} due to the ν_{asym}(O=Mo=O) and ν_{sym}(O=Mo=O) modes, respectively. These data indicate the presence of a cis–[$Mo^{VI}O_2$] structure [136].

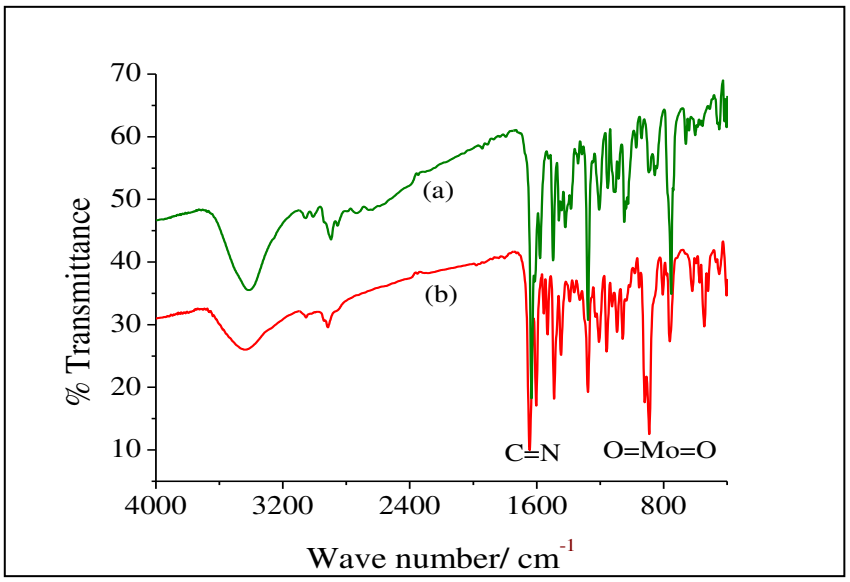

Figure 2.5. IR spectra of H_3sal–dahp (**2.I**) (a) and [$Mo^{VI}O_2$(Hsal–dahp)(H_2O)] (**2.1**) (b).

Table 2.4.

IR spectral data [in cm^{-1}] of compounds.

Compounds	ν(C=$N_{azomethine}$/ N_{ring})	ν_{asym}(O=Mo=O)	ν_{sym}(O=Mo=O)
H_3sal–dahp (**2.I**)	1633		
H_3clsal–dahp (**2.II**)	1638		
H_3brsal–dahp (**2.III**)	1638		
[$Mo^{VI}O_2$(sal–dahp)(H_2O)] (**2.1**)	1644, 1603	918	890
[$Mo^{VI}O_2$(clsal–dahp)(H_2O)] (**2.2**)	1650, 1598	918	892
[$Mo^{VI}O_2$(brsal–dahp)(H_2O)] (**2.3**)	1649, 1598	914	889
[$Mo^{VI}O_2$(sal–dahp)(py)] (**2.4**)	1650, 1597	928	903
[$Mo^{VI}O_2$(clsal–dahp)(py)] (**2.5**)	1652, 1639	917	903
[$Mo^{VI}O_2$(brsal–dahp)(py)] (**2.6**)	1654, 1638	921	902

2.3.5. Electronic spectral studies

Table 2.5 includes electronic spectral data of the ligands and complexes. The electronic spectra of H_3sal–dahp (**2.I**), H_3clsal–dahp (**2.II**) and H_3brsal–dahp (**2.III**) exhibit four UV absorption bands. Based on their extinction coefficients, these bands are interpreted as n→π* (317–329 nm), π→π* (254–256 and 277–279 nm) and φ→φ* (217–225 nm) transitions. The additional band for π→π* transition is possibly due to splitting of this transition. In complexes, the two π→π* bands collapse into one and appear at an average value (259–264 nm) while n→π* band appears at nearly same position. In addition, all complexes exhibit a medium intensity band at 413–431 nm due to ligand to metal charge transfer (LMCT) transition from the phenolate oxygen atom to an empty d–orbital of the molybdenum. As Mo^{VI}–complexes have $4d^0$ configuration, d→d band is not expected.

Table 2.5.

Electronic spectral data of ligands and complexes.

Compounds	Solvents	λ_{max}(nm)/ ε(litre mol^{-1} cm^{-1})
H_3sal–dahp	MeOH	217 (2.8×10^4), 256 (1.3×10^4), 279 (4.6×10^3), 317 (4.5×10^3)
H_3clsal–dahp	MeOH	223 (5×10^4), 256 (8.2×10^3), 277 (1.9×10^3), 327 (2.8×10^3)
H_3brsal–dahp	MeOH	225 (7.2×10^4), 254 (2.5×10^4), 279 (6.6×10^3), 329 (8.4×10^3)
$[Mo^{VI}O_2(sal–dahp)(H_2O)]$	DMSO	263 (3.8×10^4), 321 (7.7×10^3), 414 (0.3×10^3)
$[Mo^{VI}O_2(clsal–dahp)(H_2O)]$	DMSO	264 (2.6×10^4), 328 (9×10^3), 415 (0.3×10^3)
$[Mo^{VI}O_2(brsal– dahp)(H_2O)]$	DMSO	263 (4.7×10^4), 329 (1.5×10^4), 413 (0.4×10^3)

$[Mo^{VI}O_2(sal–dahp)(py)]$	DMSO	263 (2.6×10^4), 321 (7.5×10^3), 430 (0.5×10^3)
$[Mo^{VI}O_2(clsal–dahp)(py)]$	DMSO	260 (2.1×10^4), 329(6.8×10^3), 430 (0.5×10^3)
$[Mo^{VI}O_2(brsal–dahp)(py)]$	DMSO	259 (2.1×10^4), 329 (6.2×10^3), 431 (0.5×10^3)

2.3.6. ^{1}H and ^{13}C NMR studies

The coordinating modes of H_3sal–dahp (**2.I**), H_3clsal–dahp (**2.II**) and H_3brsal–dahp (**2.III**) were also confirmed by comparing their ^{1}H NMR spectral patterns with the corresponding complexes. The relevant spectral data are collected in Table 2.6. Fig. 2.6 reproduces ^{1}H NMR spectra of a representative ligand and its complexes. All the ligands show two signals at δ = 13.56 (br, 2H) and 5.24 (br, 1H) ppm due to the phenolic and alcoholic OH, respectively. Absence of signal due to alcoholic OH in the complexes is in conformity with the coordination of the alcoholic oxygen to the molybdenum while the existence of phenolic signal integrating to one proton indicates the involvement of one of the phenolic oxygen in coordination after proton replacement. Similarly, the appearance of two signals due to azomethine proton (each equivalent to 1H) with a coordination–induced shifts [$\Delta\delta$= [δ(complex) – δ(free ligand)] of 0.25 ppm in complexes demonstrates the coordination of only one of the azomethine groups to molybdenum. Appearance of two signals of equal intensity for azomethine groups rules out the possibility of dynamic equilibrium between free and coordinated nitrogen functions in solution. The –CH proton is also affected and appears at $\Delta\delta$= 0.62 ppm towards down field than observed in free ligands. Similarly, the $–CH_2$ group that forms five members ring upon coordination of alcoholic oxygen to the molybdenum also show a significant downfield shift. Signals due to aromatic protons and other CH_2 group appear in the expected regions in spectra of the ligands as well as of the complexes, with slight shifts in their positions.

Table 2.6.

^{1}H NMR chemical shifts [δ in ppm] of ligands and complexes recorded in DMSO–D_6.

Compounds[a, b]	–OH (phenolic)	–OH (alcoholic)	–CH=N–
2.I	13.56 (br, 2H)	5.24 (br, 1H)	8.54 (s, 2H)
2.II	13.56 (br, 2H)	5.24 (br, 1H)	8.54 (s, 2H)
2.III	13.56 (br, 2H)	5.24 (br, 1H)	8.54 (s, 2H)
2.1 (**Δδ**)	13.45 (br, 1H)		8.54 (s, 1H), 8.79 (s, 1H) (0.25)
2.2 (**Δδ**)	13.45 (br, 1H)		8.54 (s, 1H), 8.79 (s, 1H) (0.25)
2.3 (**Δδ**)	13.45 (br, 1H)		8.54 (s, 1H), 8.79 (s, 1H) (0.25)
2.4 (**Δδ**)	13.45 (br, 1H)		8.54 (s, 1H), 8.79 (s, 1H) (0.25)
2.5 (**Δδ**)	13.45 (br, 1H)		8.54 (s, 1H), 8.79 (s, 1H) (0.25)
2.6 (**Δδ**)	13.45 (br, 1H)		8.54 (s, 1H), 8.79 (s, 1H) (0.25)

Compounds[a, b]	Aliphatic protons –CH	–CH_2	Aromatic protons
2.I	4.03 (m, 1H)	3.77 (dd, 2H), 3.56 (m, 2H)	7.47–6.90 (m, 8H)
2.II	4.03 (m, 1H)	3.77 (dd, 2H), 3.56 (m, 2H)	7.47–6.90 (m, 8H)
2.III	4.03 (m, 1H)	3.77 (dd, 2H), 3.56 (m, 2H)	7.47–6.90 (m, 8H)
2.1 (**Δδ**)	4.65 (m, 1H) (0.62)	4.29 (dd, 2H), 3.88 (m, 2H)	7.65–6.90 (m, 8H)
2.2 (**Δδ**)	4.65 (m, 1H) (0.62)	4.29 (dd, 2H), 3.88 (m, 2H)	7.65–6.90 (m, 8H)
2.3 (**Δδ**)	4.65 (m, 1H) (0.62)	4.29 (dd, 2H), 3.88 (m, 2H)	7.65–6.90 (m, 8H)
2.4 (**Δδ**)	4.65 (m, 1H) (0.62)	4.29 (dd, 2H), 3.88 (m, 2H)	7.65–6.90 (m, 8H)
2.5 (**Δδ**)	4.65 (m, 1H) (0.62)	4.29 (dd, 2H), 3.88 (m, 2H)	7.65–6.90 (m, 8H)
2.6 (**Δδ**)	4.65 (m, 1H) (0.62)	4.29 (dd, 2H), 3.88 (m, 2H)	7.65–6.90 (m, 8H)

[a]Letters given in parentheses indicate the signal structure: s = singlet, dd = doublet of doublet, q = quartet, m = multiplet, br = broad (unresolved). [b]Coordination induced shifts $\Delta\delta$= [δ(complex) – δ(free ligand)].

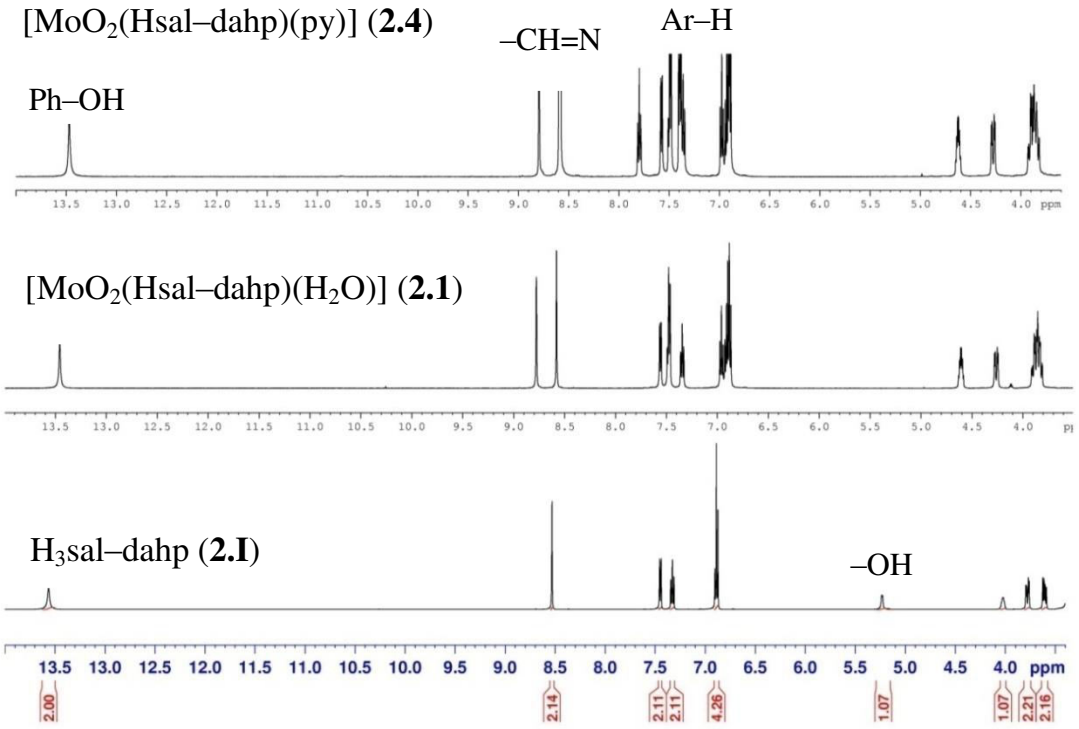

Figure 2.6. ^{1}H NMR spectra of H_3sal–dahp (**2.I**), [MoO_2(Hsal–dahp)(H_2O)] (**2.1**) and [MoO_2(Hsal–dahp)(py)](**2.4**).

The ^{13}C NMR spectra of ligands and complexes also provide useful information for the elucidation of the structures of the complexes. Spectra of a representative ligand H_3sal–dahp (**2.I**) and its complexes **2.1** and **2.4** are presented in Fig.2.7 while Table 2.7 provides entire spectral data. Assignments of the peaks are based on the intensity patterns of the chemical shift and on the coordination–induced shifts ($\Delta\delta$) of the signals for carbon atoms in the vicinity of the coordinating atoms [140]. All the ligands display 9 signals corresponding to the 17 carbon atoms due to the presence of a centre of symmetry. As expected, 17 signals were observed for complexes **2.1**–**2.3** and 20 for pyridine analogues due to asymmetry generated after coordination of the ligands to the molybdenum. A large coordination–induced shift of the signal for the carbon atom bearing alcoholic oxygen (C9) atom demonstrates coordination of the alcoholic oxygen to the molybdenum. All

ligands display single signal each for azomethine (C1 and C11) and the phenolate carbon atoms. Appearance of two distinct signals each due to azomethine (C1 and C11) and the phenolate carbons (C3 and C13) against single signal each for these carbons in the ligands suggest the involvement of only one set of the azomethine nitrogen and the phenolate oxygen atoms in coordination. Again these signals suggest no possibility of dynamic equilibrium in coordinated and free functional groups. Three distinct signals appear in the δ = 134.7–150.0 ppm region in complexes **2.4**–**2.6** due to coordinated pyridine. A considerable separation ($\delta_{C8} - \delta_{C10}$ = 2.1–2.4 ppm) in the signals due to methylene carbons (C8 and C10) has also been noticed due to the involvement of C8 in the ring formation. Thus, ^{1}H and ^{13}C NMR data confirm the IR and UV/Vis evidence.

Table 2.7.

^{13}C NMR spectral data of ligand and complexes

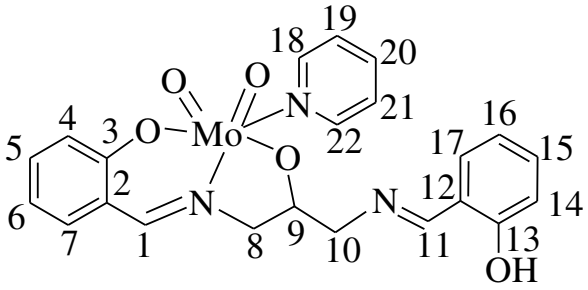

Compounds	C1, C11	C3, C13	C9	C8, C10
2.I	161.3	167.5	69.8	63.2
2.II	160.5	166.4	69.5	62.9
2.III	161.0	166.3	69.5	62.8
2.1 (Δδ)	160.7, 161.4	164.2, 167.5	80.0 (10.2)	60.9, 63.0
2.2 (Δδ)	160.2, 160.7	163.8, 166.7	80.5 (11.0)	61.2, 63.6
2.3 (Δδ)	160.7, 161.2	163.8, 166.6	80.5 (11.0)	61.2, 63.6
2.4 (Δδ)	161.0, 162.0	164.7, 168	80.5 (10.7)	61.4, 63.5
2.5 (Δδ)	160.2, 160.8	163.9, 166.7	80.5 (11.0)	61.2, 63.6
2.6 (Δδ)	160.3, 160.7	163.4, 166.2	80.1 (10.6)	60.7, 63.1

Compounds	C2, C12,	C4–C7, C14–C17	C18–C22
2.I	132.7	117, 132, 118, 119,	
2.II	132.5	119, 131, 120, 122,	
2.III	135.2	109, 133, 119, 120	
2.1	133, 134	118.6, 131.7, 119.4, 120.9,	
		118.5, 132.4, 119.2, 116.5	
2.2	133, 134	119, 131, 120, 122,	
		121, 132.6, 122.5, 123	
2.3	136, 137	109, 133, 119, 120,	
		110, 135, 122, 123	
2.4	134, 135	119.1, 132, 119.9, 121,	150.0,136.6, 124.4
		119, 133, 119.7, 117	
2.5	133, 134.7	119, 131, 121, 122,	150.0,136.6, 124.4
		120, 132.6, 122.5, 123	
2.6	135.6, 137	109, 133.5, 119, 121,	149.6, 136.2, 124.0
		109.8, 135, 120.3, 122.7	

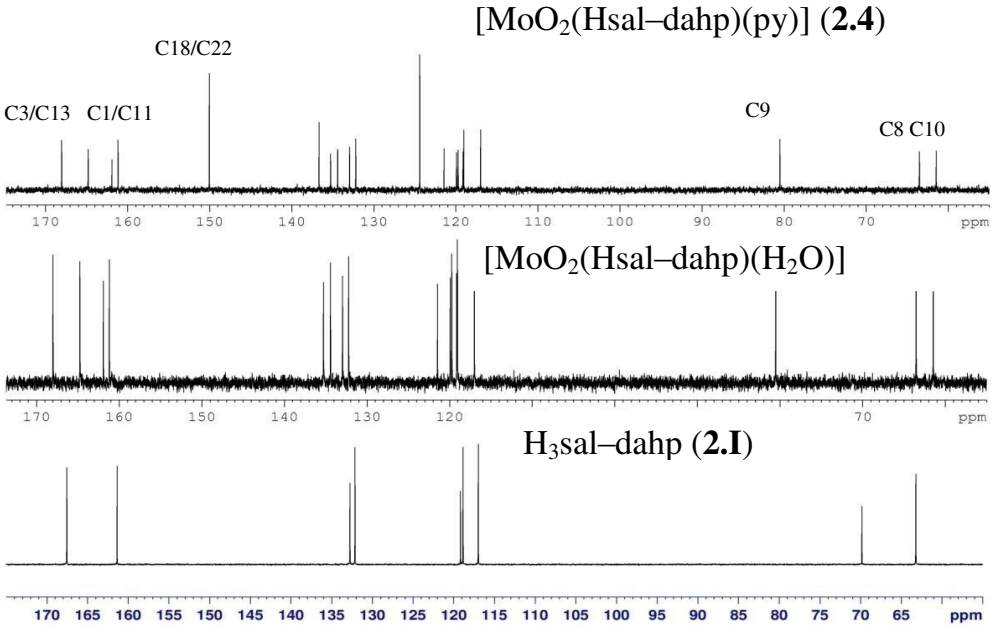

Figure 2.7. ^{13}C NMR spectra of H_3sal–dahp (**2.I**), [MoO_2(Hsal–dahp)(H_2O)] (**2.1**) and [MoO_2(Hsal–dahp)(py)](**2.4**).

2.3.7. Reactivity of dioxidomolybdenum(VI) complexes with H_2O_2

It is known that dioxidomolybdenum(VI) complexes react with H_2O_2 to give the corresponding $[Mo^{VI}O(O_2)]^{2+}$ complexes. To support the reaction mechanism, we tried to isolate such peroxido complexes in the solid state but failed due to insolubility of the corresponding dioxido complexes in methanol/ ethanol while difficulty in isolating peroxidomolybdenum(VI) complexes from solvent like DMSO. However, the generation of such species has been established in DMSO by electronic absorption spectroscopy. In a typical reaction, 15 mL of ca. 10^{-3} M solution of $[MoO_2(Hclsal–dahp)(H_2O)]$ (**2.2**) was treated with one drop portion of 30% aqueous H_2O_2 (0.253 g, 2.3 mmol) dissolved in 5 mL of DMSO and the resultant spectroscopic changes are presented in Fig. 2.8 (b). The weak and broad charge transfer band appearing at 415 nm slowly increases in intensity along with broadening and shifting to 425 nm. Similar titration with dilute solution of complex causes small shift of 328 nm band to 333 nm along with only marginal change in intensity while 264 nm band increases its intensity considerably and finally disappears; Fig. 2.8 (a). These changes indicate the interaction of $[MoO_2(Hclsal–dahp)(H_2O)]$ (**2.2**) with H_2O_2 and the plausible formation of $[Mo^{VI}O(O_2)(Hclsal–dahp)]$ in DMSO (Eq. 2.3). Similar changes have also been noted for other complexes; Figs. 2.8 (c) and 2.8 (d) (only 380–500 nm region shown).

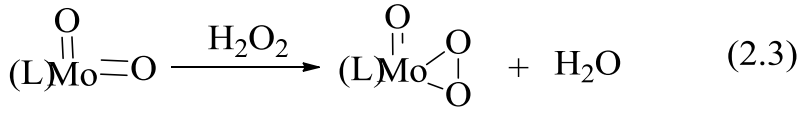

(2.3)

(L = ligand)

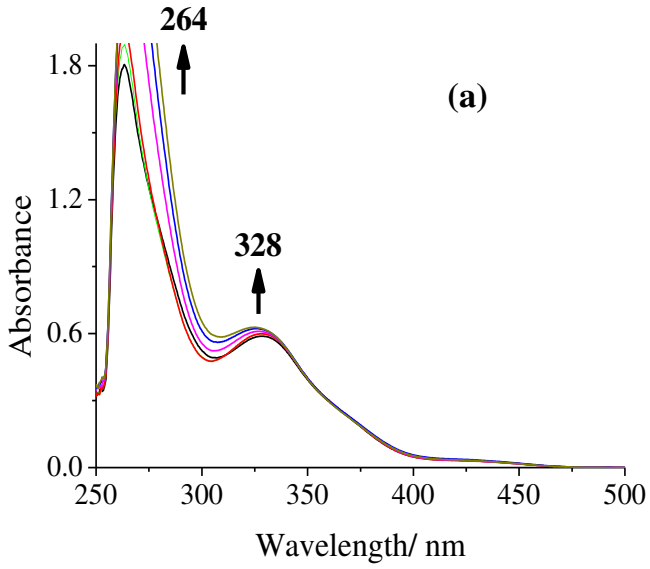

Figure 2.8 (a) The spectra were recorded after successive addition of one drop portion of 30% H_2O_2 (0.351 g, 3.1 mmol) dissolved in 5 mL (2.06 M) DMSO to 20 mL of 6.7×10^{-5} M solution of [MoO_2(Hclsal–dahp)(H_2O)] (**2.2**).

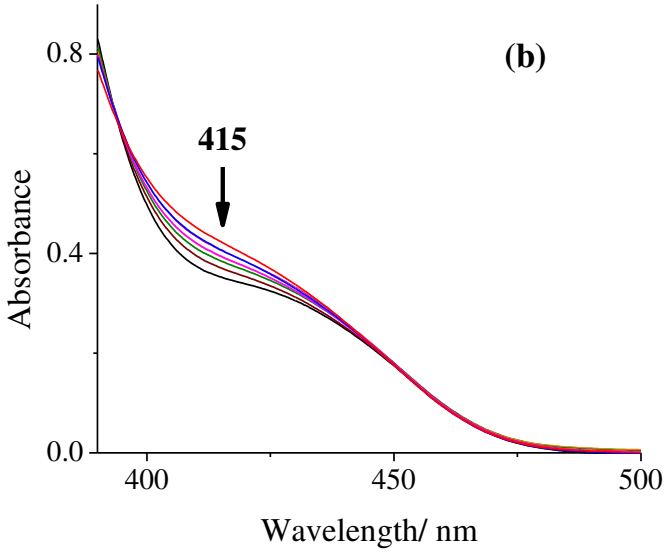

Figure 2.8 (b) The spectra were recorded after successive addition of one drop portion of 30% H_2O_2 (0.253 g, 2.3 mmol) dissolved in 5 mL (1.48 M) DMSO to 15 mL of 10^{-3} M solution of [MoO_2(Hclsal–dahp)(H_2O)] (**2.2**).

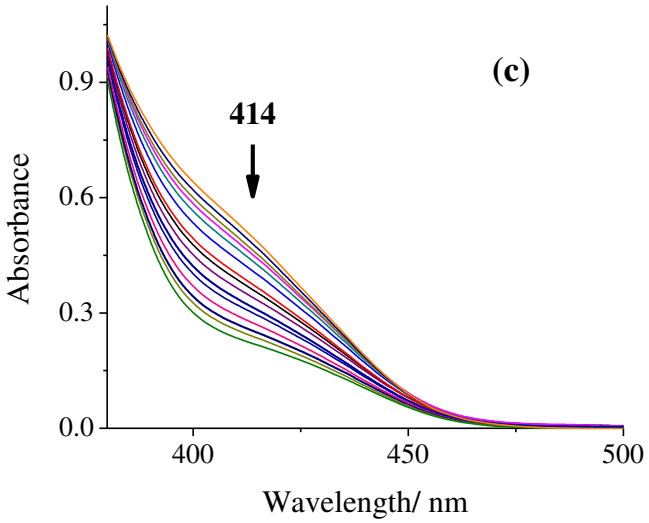

Figure 2.8 (c) The spectra were recorded after successive addition of one drop portion of 30% H_2O_2 (0.237 g, 2.10 mmol) dissolved in 5 mL (1.37 M) DMSO to 15 mL of 10^{-3} M solution of [MoO_2(Hsal–dahp)(H_2O)] (**2.1**).

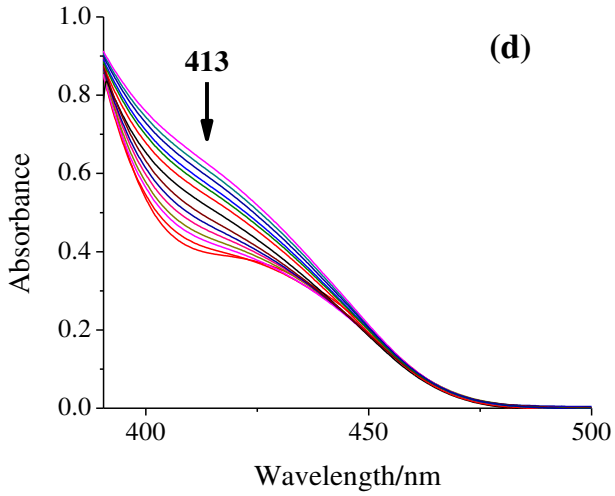

Figure 2.8 (d) The spectra were recorded after successive addition of one drop portion of 30% H_2O_2 (0.273 g, 2.4 mmol) dissolved in 5 mL (1.60 M) DMSO to 15 mL of 10^{-3} M solution of [MoO_2(Hbrsal–dahp)(H_2O)] (**2.3**).

2.3.8. Catalytic activity studies

2.3.8.1. Oxidative bromination of styrene

The oxidative bromination of styrene using **2.1**, **2.2** and **2.3** as catalyst precursors in the presence of KBr, 70% aqueous $HClO_4$ and 30 % aqueous H_2O_2 under a bi–phasic (CH_2Cl_2–H_2O) system gave mainly three major products, namely, 1,2–dibromo–1–phenylethane, 2–bromo–1–phenylethane–1–ol and 1–phenylethane–1,2–diol (Scheme 2.3) along with some minor products like benzaldehyde, styrene epoxide, benzoic acid and 4–bromostyrene but their overall percentage is extremely low of the total of the main products. The obtained main products were confirmed by ^1H NMR spectroscopy as well as GC–MS after their separations and are same as reported using vanadium complexes as catalysts [141–143].

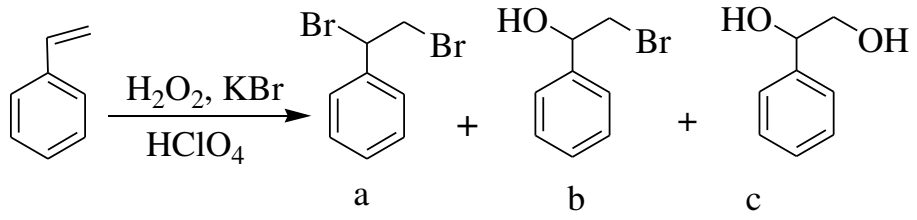

Scheme 2.3. Main products obtained by oxidative bromination of styrene: (a) 1,2–dibromo–1–phenylethane (dibromide), (b) 2–bromo–1–phenylethane–1–ol (a bromohydrin) and (c) 1–phenylethane–1,2–diol.

The reaction conditions were optimized for: i) the maximum oxidative bromination of styrene, irrespective of the selectivity of products and ii) for the maximum formation of 2–bromo–1–phenylethane–1–ol, considering different parameters like amounts of catalyst, H_2O_2, KBr and $HClO_4$ using [$Mo^{VI}O_2$(Hsal–dahp)(H_2O)] (**2.1**) as a representative catalyst precursor. Thus, for 10 mmol of styrene (1.04 g), three different amounts of catalyst (0.001, 0.0015 and 0.002 g), 30 % aqueous H_2O_2 (10, 20 and 30 mmol), KBr (20, 30 and 40 mmol) and $HClO_4$ (20, 30 and 40 mmol, added in four equal portions to the reaction mixture, first portion at t = 0 and other three portions after every

15 min intervals) were taken in dichloromethane–water (40 mL, v/v) mixture and the reaction was carried out at room temperature. Acid (here $HClO_4$) was found to be essential to carry out catalytic bromination. Its way of addition to the reaction mixture controls the stability of the substrate while its amount has great influence on the conversion and selectivity of products. The complexes slowly decompose during the reaction; decomposition is slowed down, if $HClO_4$ is successively added in four portions during 1 h of reaction time.

Table 2.8 summarizes all the conditions considered and the corresponding percentage of oxidative bromination of styrene along with the selectivity of different reaction products. It is clear from the data presented in table that conversions are competitive, 97–99%, in most reaction conditions. However, the selectivity of products differs on varying the reagents. The best suited conditions (entry no. 9 of Table 2.8) for the maximum oxidative bromination of styrene with 98% conversion are: catalyst (0.001g), 30 % aqueous H_2O_2 (2.27 g, 20 mmol), KBr (2.38 g, 20 mmol) and $HClO_4$ (4.29 g, 30 mmol) in dichloromethane–water (40 mL, v/v) mixture). Under these conditions the selectivity of different major products follows the order: phenylethane–1,2–diol (67%) > 1,2–dibromo–1–phenylethane (21%) > 2–bromo–1–phenylethane–1–ol (3%). Using 0.001 g of catalyst and considering the substrate to different reagents in the molar ratio of 1:2 (entry no 8 of Table 2.8) gave highest selectivity of 2–bromo–1–phenylethane–1–ol (34%) with no formation of 1,2–dibromo–1–phenylethane amongst all the conditions applied. Increasing the amounts of KBr as well as acid results in the formation of increased dibromo product at the expense of monobromo one while increasing oxidant improves the formation of mainly phenylethane–1,2–diol. Under the optimized conditions for the maximum conversion of styrene, other catalysts i.e. **2.2** and **2.3** exhibit similar catalytic activity along with similar selectivity of different products (entry no. 10 and 11, and Fig. 2.9 and 2.10). Negative controls under conditions presented in entry no. 12 and 13 of Table 2.8 resulted in 44 and 60 % conversion, respectively and formation of only two products was observed.

Table 2.8.

Conversion of styrene (1.04 g, 10 mmol), TOF and product selectivity using $[Mo^{VI}O_2(Hsal–dahp)(H_2O)]$ (**2.1**) as a catalyst precursor in 1 h of reaction time under different reaction conditions.

Entry No.	KBr [g (mmol)]	H_2O_2 [g (mmol)]	$HClO_4$ [g (mmol)]	Catalyst [g (mmol)]
1.	3.57 (30)	3.39 (30)	5.72 (40)	0.001 (2.2×10^{-3})
2	3.57 (30)	3.39 (30)	5.72 (40)	0.0015(3.4×10^{-3})
3	3.57 (30)	3.405 (30)	5.72 (40)	0.002 (4.5×10^{-3})
4	3.57 (30)	2.27 (20)	5.72 (40)	0.001 (2.2×10^{-3})
5	3.57 (30)	4.52 (40)	5.72 (40)	0.001 (2.2×10^{-3})
6	2.38 (20)	2.27 (20)	5.72 (40)	0.001 (2.2×10^{-3})
7	4.76 (40)	2.27 (20)	5.72 (40)	0.001 (2.2×10^{-3})
8	2.38 (20)	2.27 (20)	2.86 (20)	0.001 (2.2×10^{-3})
9	2.38 (20)	2.27 (20)	4.29 (30)	0.001 (2.2×10^{-3})
10[a]	2.38 (20)	2.27 (20)	4.29 (30)	0.001 (1.9×10^{-3})
11[b]	2.38 (20)	2.27 (20)	4.29 (30)	0.001 (1.6×10^{-3})
12	2.38 (20)	2.27 (20)	2.86 (20)	blank
13	2.38 (20)	2.27 (20)	4.29 (30)	blank

Entry No.	Conv. [%]	TOF [h^{-1}]	Mono Bromo	Dibromo	Diol	Other product
1.	98	4454	0.1	39.9	52	8
2	98	2882	0.2	27.4	63.4	9
3	99	2200	0.4	26	67.6	6
4	97	4409	15	9.2	69.8	6
5	98	4454	0.6	21.4	66	12
6	98	4454	26	28	41	5
7	99	4500	0.3	32	55.7	12

8	97	4409	34	0	61	5
9	98	4454	3	21	67	9
10[a]	98	5157	1	27	63	9
11[b]	97	6062	2	15	72	11
12	44	–	45	0	52	3
13	60	–	39	0	58	3

[a]Data for $[Mo^{VI}O_2(clsal–dahp)(H_2O)]$.

[b]Data for $[Mo^{VI}O_2(brsal–dahp)(H_2O)]$.

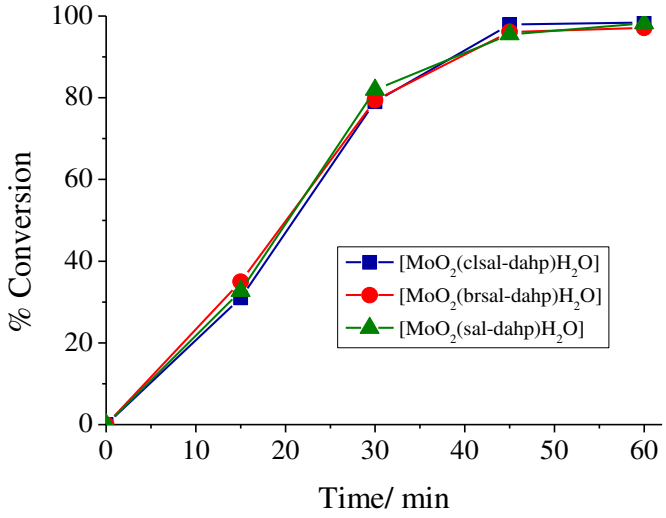

Figure 2.9. Effect of different catalysts on the oxidative bromination of styrene.

The oxidative bromination of styrene and the selectivity of different reaction products for catalysts **2.1**, **2.2** and **2.3** under the optimized reaction conditions (see entry no. 9, 10 and 11 of Table 2.8) have also been analyzed as a function of time and are presented in Fig. 2.10 (b, c and d). The formation of all three products starts with the conversion of styrene and follows very similar patterns with the elapse of time. Thus the selectivity of 46–55 % of 1–phenylethane–1,2–diol at t = 15 min improves with time and reaches 63–72 % at the end of 1 h while that of 2–bromo–1–phenylethane–1–ol (bromohydrin) starts with 42–50% at t = 15 min and goes down to 1–3% at the end of

reaction. The formation of 1,2–dibromo–1–phenylethane is nearly zero in the beginning but slowly improves with time and reaches 15–27%. It seems that formation of 1–phenylethane–1,2–diol occurs at the expense of mono bromo derivative (see scheme 2.4). Under the conditions presented in entry no. 8, the selectivity of the formation of two products at t = 15 min follows the order: 2–bromo–1–phenylethane–1–ol (61%) > 1–phenylethane–1,2–diol (33%) but it becomes reverse and follows the order: 1–phenylethane–1,2–diol 61% > 2–bromo–1–phenylethane–1–ol (34%) at the end of 1 h (Fig.2.10 (a)).

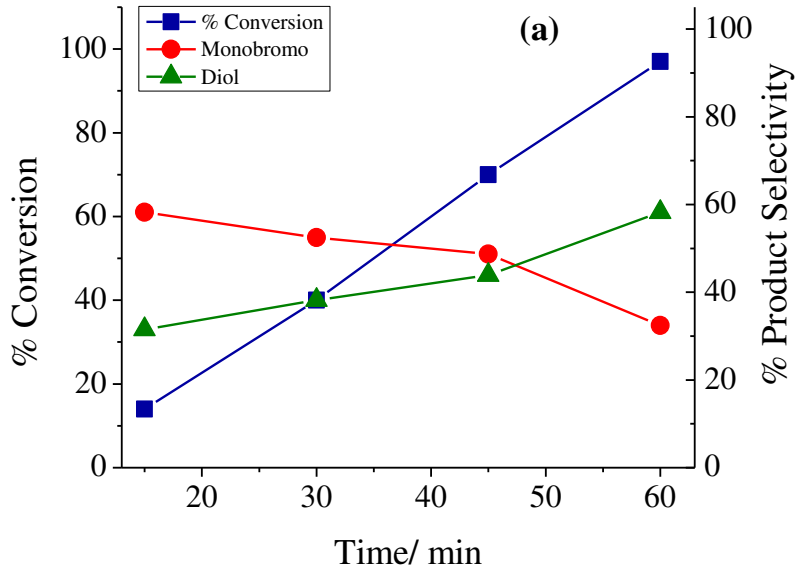

Figure 2.10. (a) Plots showing percentage conversion of styrene and the selectivity of the formation of different reaction products as a function of time. Reaction conditions: styrene (1.04 g, 10 mmol), [$Mo^{VI}O_2$(Hsal–dahp)(H_2O)] (**2.1**) (0.001g), 30 % aqueous H_2O_2 (2.27g, 20 mmol), KBr (2.38 g, 20 mmol) and 70 % aqueous $HClO_4$ (2.86 g, 20 mmol).

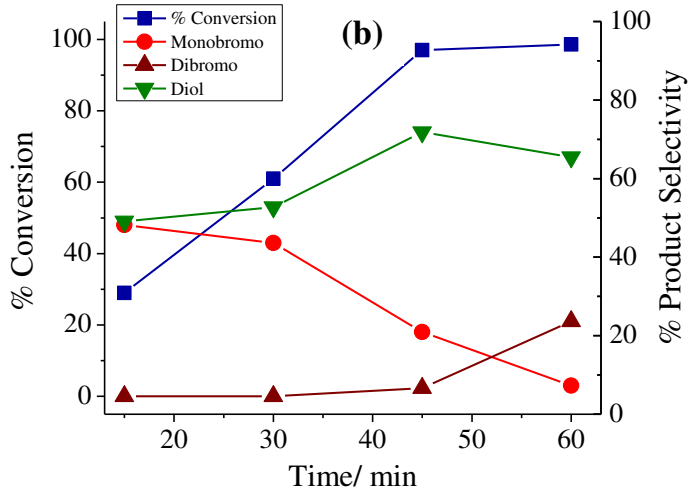

Figure 2.10. (b) Plots showing percentage conversion of styrene and the selectivity of the formation of different reaction products as a function of time. Reaction conditions: styrene (1.04 g,10 mmol), [$Mo^{VI}O_2$(Hsal–dahp)(H_2O)] (**2.1**) (0.001g), 30 % aqueous H_2O_2 (2.27 g, 20 mmol), KBr (2.38 g, 20 mmol) and 70 % aqueous $HClO_4$ (4.29 g, 30 mmol).

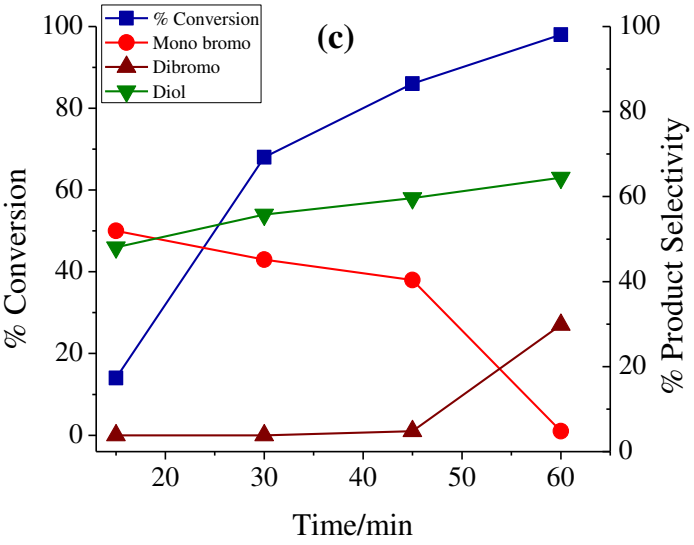

Figure 2.10. (c) Plots showing percentage conversion of styrene and the selectivity of the formation of different reaction products as a function of time. Reaction conditions are similar to Fig. 2.10(b) taking [$Mo^{VI}O_2$(Hclsal–dahp)(H_2O)] (**2.2**) as catalyst.

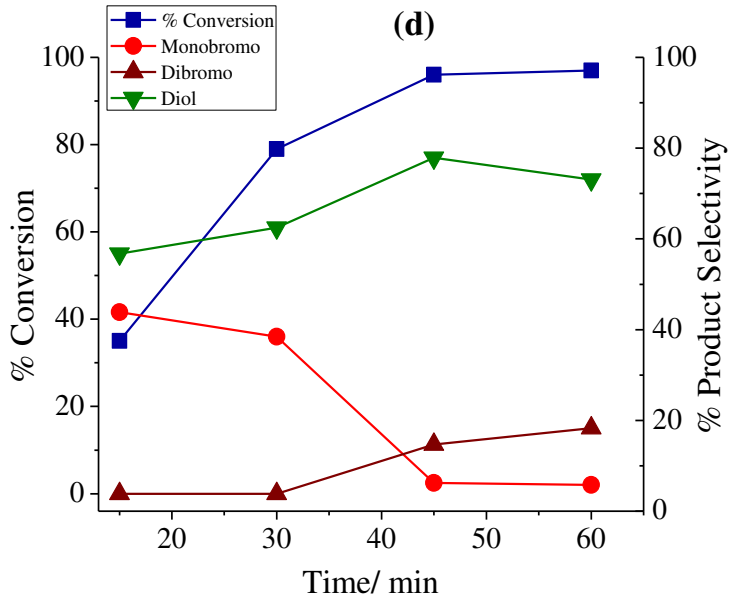

Figure 2.10. (d) Plots showing percentage conversion of styrene and the selectivity of the formation of different reaction products as a function of time under reaction conditions similar to (b) taking $[Mo^{VI}O_2(Hbrsal–dahp)(H_2O)]$ (**2.3**) as catalyst.

As observed in vanadium complexes [129–131], catalytically generated HOBr and/or Br^+, Br_2, Br^{3-}, by the reaction of molybdenum complexes with KBr in the presence of H_2O_2 and $HClO_4$, react with styrene to give bromonium ion as an intermediate. The nucleophile Br^- as well as H_2O both may attack on the α–carbon of the intermediate to give 1,2–dibromo–1–phenylethane and 2–bromo–1–phenylethane–1–ol, respectively (Scheme 2.4). The formation of dibromo product in most cases at later stage is possibly due the presence of less amount of brominating reagent generated initially. The nucleophile H_2O may further attack on the α–carbon of 2–bromo–1–phenylethane–1–ol to give 1–phenylethane–1,2–diol. All these justify the formation of 1–phenylethane–1,2–diol in highest yield. Oxidative bromination of styrene has mainly been reported by vanadium complexes. However, catalytic potential shown by molybdenum complexes for the oxidative bromination of styrene reported here compares well with those shown by vanadium complexes [143].

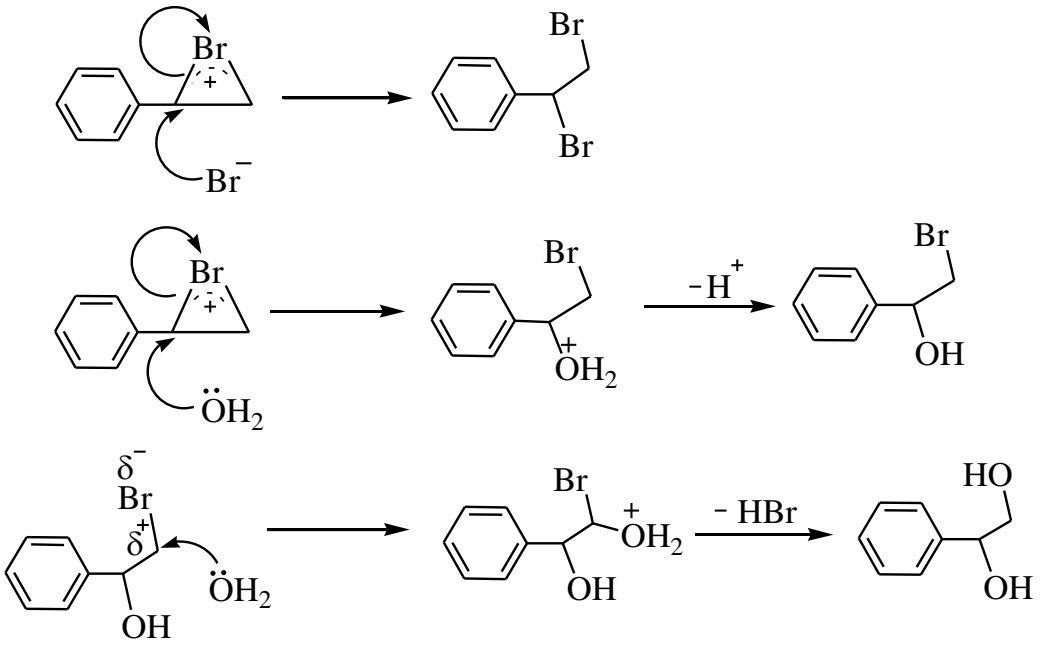

Scheme 2.4. Mechanism of action of HOBr on styrene.

2.3.8.2.. Oxidation of methyl phenyl sulfide

The sulfur atom of the organic sulfide is electron rich and undergoes electrophilic oxidation catalyzed by several molybdenum oxotransferases [144,145]. Chakravarthy *et al.* have proposed possible mechanism of the catalytic sulfoxidation of methyl phenyl sulfide [61]. Such oxidation of methyl phenyl sulfide was tested using complexes **2.1**, **2.2** and **2.3** as catalyst and corresponding sulfoxide as well as sulfone was obtained as shown in Scheme 2.5. Sulfoxides and sulfone, the oxidation product of sulfides, are useful precursors for biologically and chemically important compounds [146,147]. Sulfoxides have been used as ligands in asymmetric catalysis [148] and as oxotransfer reagents [149] and sulfones have been employed for stabilizing radicals [150] and anions, [151] and acting as cationic synthons [152].

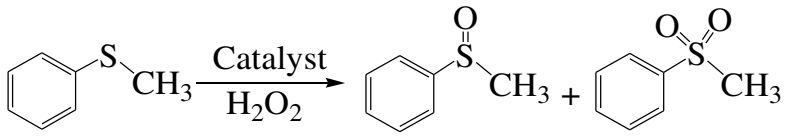

Scheme 2.5. Oxidation products of methyl phenyl sulfide with H_2O_2.

Again, $[Mo^{VI}O_2(Hsal–dahp)(H_2O)]$ (**2.1**) was taken as a representative catalyst and various parameters were optimized to get the maximum oxidation of methyl phenyl sulfide. Thus for 10 mmol (1.24 g) of methyl phenyl sulfide, the amount of catalyst (0.001 g, 0.00015 g and 0.002 g), 30% aqueous H_2O_2 (10, 20 and 30 mmol) and volume of acetonitrile (5, 7 and 10mL) were varied and the reaction was carried out at room temperature. The conversions obtained with all these conditions, plotted as a function of time, are presented in Fig. 2.11 (a, b and c). Table 2.9 summarizes all conditions and conversion obtained under particular condition. The optimized conditions for highest catalytic activity with 98% conversion of methyl phenyl sulfide were concluded as: methyl phenyl sulfide (1.24 g, 10 mmol), catalyst **2.1** (0.0015 g), 30% aqueous H_2O_2 (2.27 g, 20 mmol) and CH_3CN (5 mL).

The percent conversion of methyl phenyl sulfide under the optimized reaction conditions and the selectivity of reaction products as a function of time are shown in Fig. 2.11(d). It is clear from the plot that both the products start to form with the conversion of methyl phenyl sulfide. However, the initial selectivity of 76 % for methyl phenyl sulfoxide at 38 % conversion of methyl phenyl sulfide in the first half an hour starts to decrease and reaches 66.8 % after 2 h of reaction time. Thus, initially formed sulfoxide partly reacts with H_2O_2 present in the reaction mixture to give sulfone.

Table 2.9.

Conversion of methyl phenyl sulfide (1.24 g, 10 mmol) using [MoO_2(sal–dahp)(H_2O)] (**2.1**) as catalyst in 2 h of reaction time under different reaction conditions.

Entry No.	Catalyst [g (mmol)]	H_2O_2[g(mmol)]	CH_3CN [mL]	Conv. [%]
1	0.0015 (3.3×10^{-3})	1.14 (10)	5	37
2	0.0015 (3.3×10^{-3})	2.27 (20)	5	98
3	0.0015 (3.3×10^{-3})	3.39 (30)	5	99
4	0.0015 (3.3×10^{-3})	2.27 (20)	7	78
5	0.0015 (3.3×10^{-3})	2.27 (20)	10	25
6	0.0010 (2.2×10^{-3})	2.27 (20)	05	52
7	0.0020 (4.4×10^{-3})	2.27 (20)	05	99

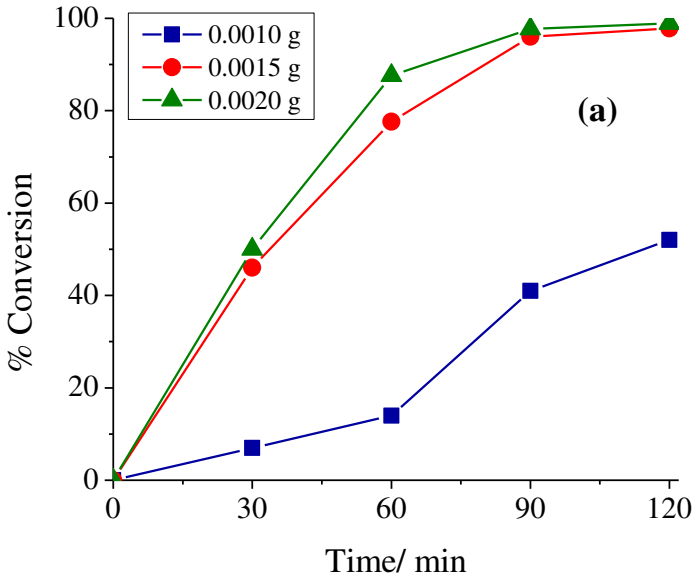

Figure 2.11. (a) Effect of catalyst amount on the oxidation of methyl phenyl sulfide. Reaction conditions: methyl phenyl sulfide (1.24 g, 10 mmol), 30 % H_2O_2 (2.27 g, 20 mmol) and acetonitrile (5 mL).

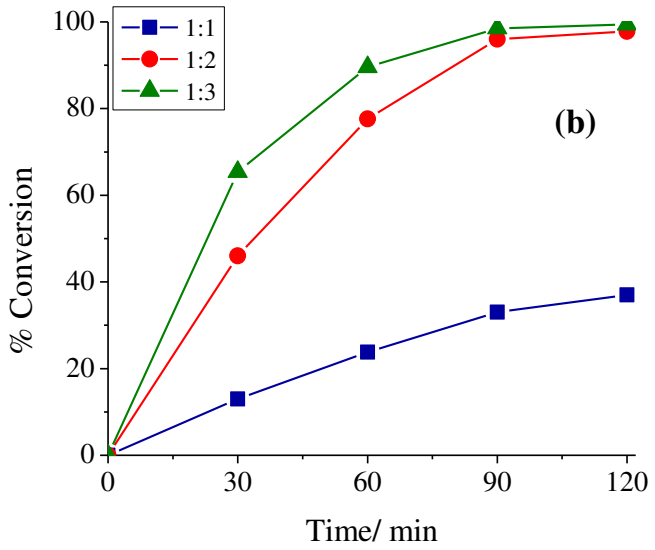

Figure 2.11. (b) Effect of oxidant amount on the oxidation of methyl phenyl sulfide. Reaction conditions: methyl phenyl sulfide (1.24 g, 10 mmol), catalyst (0.0015 g) and acetonitrile (5 mL)**.**

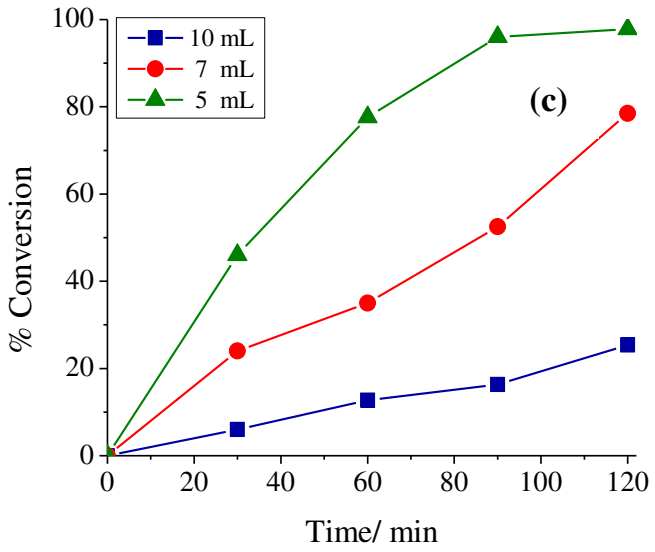

Figure 2.11. (c) Effect of solvent amount on the oxidation of methyl phenyl sulfide. Reaction conditions: methyl phenyl sulfide (1.24 g, 10 mmol), catalyst (0.0015 g) and 30 % H_2O_2 (2.27 g, 20 mmol).

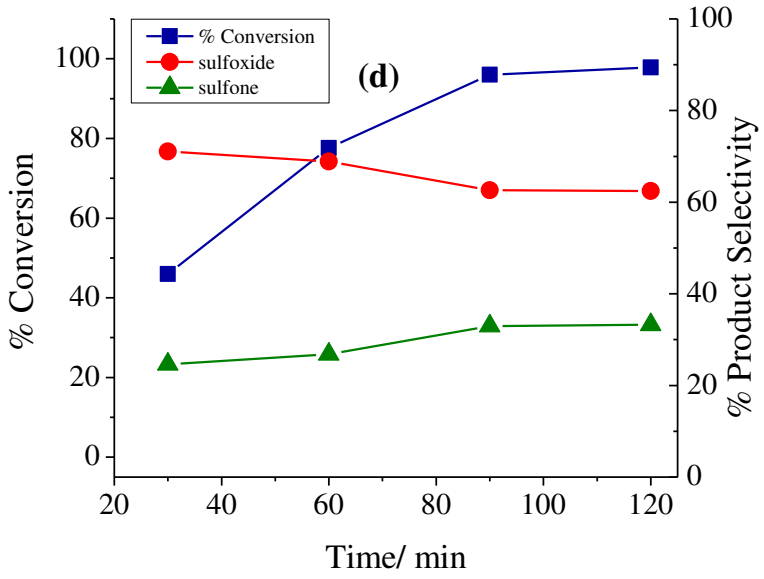

Figure 2.11. (d) Plot showing percentage conversion of methyl phenyl sulfide and the selectivity of the formation of methyl phenyl sulfoxide and methyl phenyl sulfone as a function of time under optimized conditions using [MoO_2(Hsal–dahp)(H_2O)] (**2.1**) as catalyst.

Other catalysts [MoO_2(Hclsal–dahp)(H_2O)] (**2.2**) and [MoO_2(Hbrsal–dahp)(H_2O)] (**2.3**), tested under the above optimized reaction conditions gave maxima of 97% and 96% conversion, respectively; Fig. 2.12. Thus, amongst the three complexes, the catalytic efficiency varies in the order: **2.1** > **2.2** > **2.3**. The selectivity of different products along with the conversion and turn over frequency for these catalysts are presented in Table 2.10. It is clear from the data presented in table that the selectivity of the formation of methyl phenyl sulfoxide is nearly same in all three cases but is always higher than methyl phenyl sulfone.

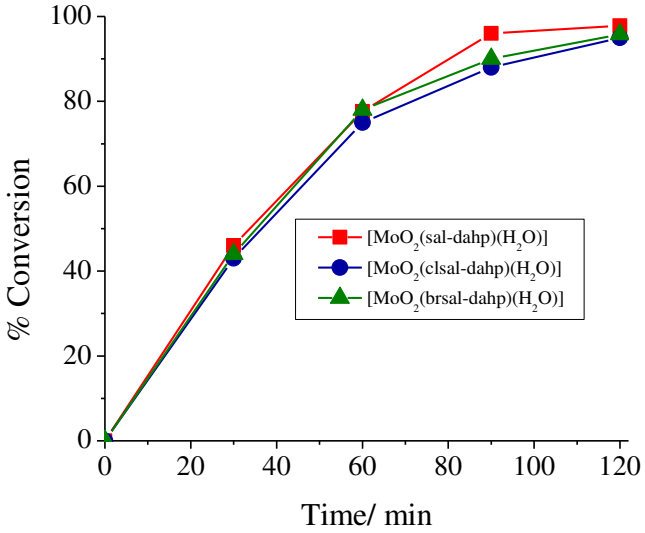

Figure 2.12. Effect of different catalysts on oxidation of methyl phenyl sulfide.

Table 2.10.

Oxidation of methyl phenyl sulfide, TOF and product selectivity using molybdenum complexes as catalyst.

Catalysts [g (mmol)]	TOF [h^{-1}][a]	Conv. [%]	Selectivity [%][b]	
			sulfoxide	sulfone
[MoO_2(Hsal–dahp)(H_2O)] [0.0015 (3.4×10^{-3})]	1441	98	66.8	33.2
[MoO_2(Hclsal–dahp)(H_2O)] [0.0015 (2.9×10^{-3})]	1672	97	68	32
[MoO_2(Hbrsal–dahp)(H_2O)] [0.0015 (2.5×10^{-3})]	1920	96	70	30
Blank reaction	–	20	79	21

[a]TOF values calculated at 2 h of reaction time.
[b]sulfoxide; methyl phenyl sulfoxide; sulfone: methyl phenyl sulfone.

The catalytic potential of these complexes in the oxidation of methyl phenyl sulfide are either better than or compare well with those reported using *cis*–[$Mo^{VI}O_2$]–

(ONO) complexes, where ONO stands for simple as well as chiral Schiff base ligands [61,128].

2.3.8.3. Oxidation of benzoin

The oxidation of benzoin has attracted attention of the researchers because one of its oxidized products, benzil, is a very useful intermediate for the synthesis of heterocyclic compounds and benzylic acid rearrangements [153]. The oxidation of benzoin, catalyzed by Mo^{VI}–O_2 complexes was carried out in refluxing methanol and the products mainly obtained were benzoic acid, benzaldehyde–dimethylacetal, methylbenzoate and benzil; Scheme 2.6.

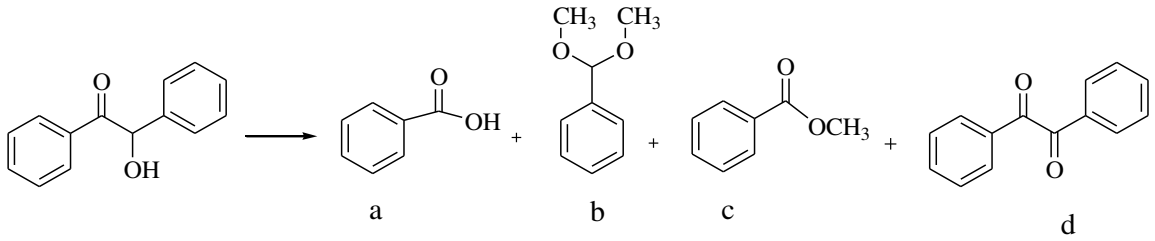

Scheme 2.6. Various oxidation products of benzoin. (a) benzoic acid, (b) benzaldehyde–dimethylacetal, (c) methylbenzoate and (d) benzil.

The reaction conditions were optimized using 5 mmol (1.06 g) of benzoin, varying the amount of catalyst (0.0005, 0.001 and 0.0015 g), 30 % aqueous H_2O_2 (10, 15 and 20 mmol) and volume of methanol (10, 15 and 20 mL). About 4 h was required to attain the equilibrium. Table 2.11 and Fig. 2.13 summarizes all conditions and conversion obtained under particular condition. From these experiments the best suited reaction conditions concluded for the maximum oxidation of benzoin are: $[MoO_2(Hsal–dahp)(H_2O)]$ (**2.1**) (0.0005 g), benzoin (1.06 g, 5 mmol) and 30% aqueous H_2O_2 (1.7 g, 15 mmol) and refluxing methanol (10 mL). Fig. 2.14 presents the selectivity of products along with the conversion of benzoin as a function of time under these conditions. It is clear from the plot that all products form with the conversion of benzoin. The highest selectivity of benzoic acid (*ca*. 54%) was observed in the first one hour. With the elapse of time its selectivity slowly decreases and finally becomes almost constant and reaches 40 % after

4 h. Similarly benzil starts with ca. 21% and reaches 15 %. The selectivity of benzaldehyde–dimethylacetal and methyl benzoate increases continuously from 4 to 13 % and 21 to 32 %, respectively in 4 h. Thus, with the maximum benzoin oxidation of 95 % after 4 h of reaction time, the selectivity of the reaction products varies in the order: benzoic acid (40) > methyl benzoate (32 %), >benzil (15%) >benzaldehyde–dimethylacetal (13 %).

Table 2.11.

Conversion of benzoin (1.06 g, 5 mmol) using $[MoO_2(Hsal–dahp)(H_2O)]$ (**2.1**) as catalyst in 4 h of reaction time under different reaction conditions.

Entry No.	Catalyst [g (mmol)]	H_2O_2[g (mmol)]	CH_3OH [mL]	Conv. [%]
1	0.0005 (1.1×10^{-3})	1.14 (10)	10	83
2	0.0005 (1.1×10^{-3})	1.71 (15)	10	95
3	0.0005 (1.1×10^{-3})	2.27 (20)	10	97
4	0.0005 (1.1×10^{-3})	1.71 (15)	15	88
5	0.0005 (1.1×10^{-3})	1.71 (15)	20	86
6	0.0010 (2.2×10^{-3})	1.71 (15)	10	96
7	0.0015 (3.4×10^{-3})	1.71 (15)	10	97

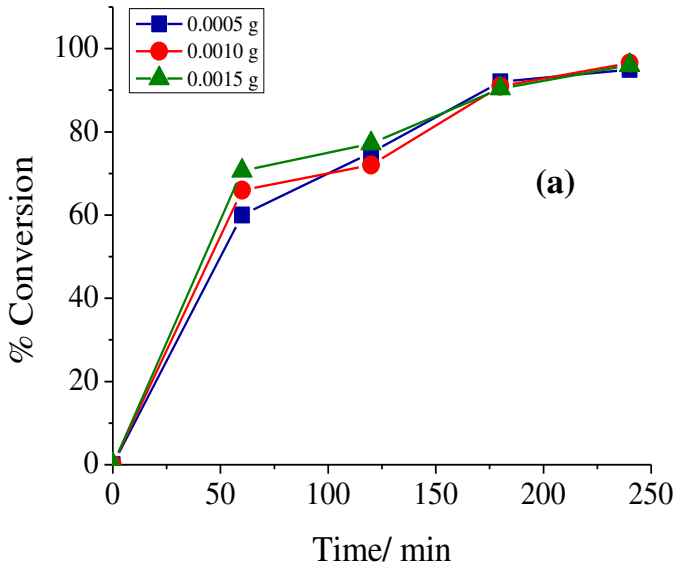

Figure 2.13. (a) Effect of catalyst amount on the oxidation of benzoin. Reaction conditions: benzoin (1.06 g, 5 mmol), 30 % H_2O_2 (1.7 g, 15 mmol) and methanol (10 mL).

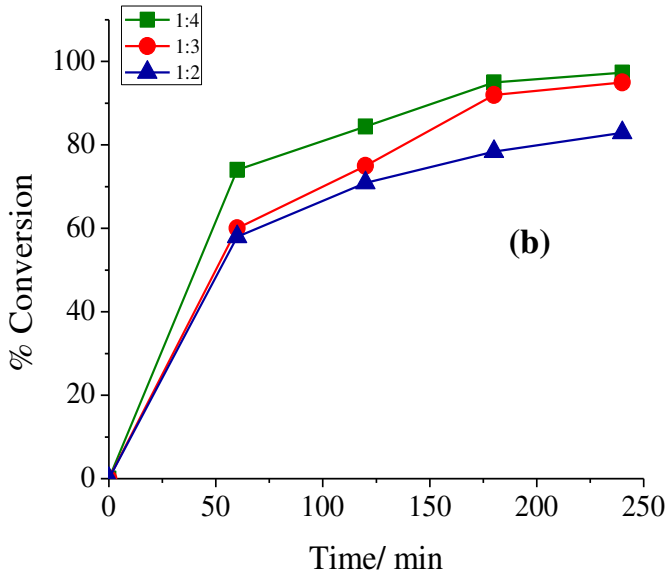

Figure 2.13. (b) Effect of oxidant amount on the oxidation of benzoin. Reaction conditions: benzoin (1.06 g, 5 mmol), catalyst amount (0.0005 g) and methanol (10 mL).

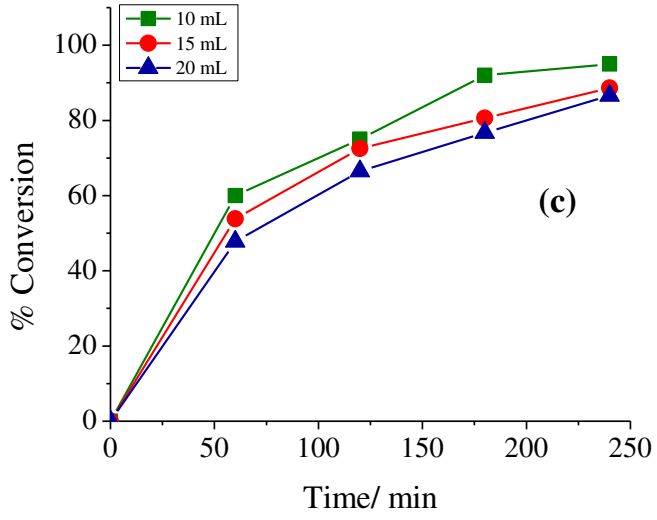

Figure 2.13. (c) Effect of solvent amount on the oxidation of benzoin. Reaction conditions: benzoin (1.06 g, 5 mmol), catalyst amount (0.0005 g) and 30% H_2O_2 (1.7 g, 15 mmol).

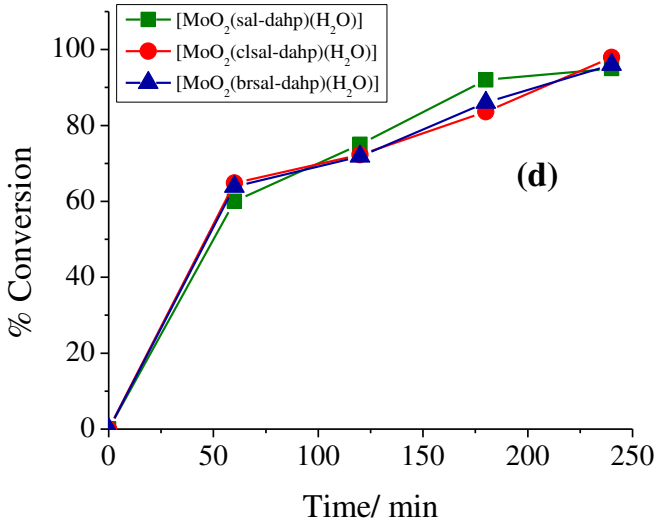

Figure 2.13. (d) Effect of various catalysts on the oxidation of benzoin. Reaction conditions: benzoin (1.06 g, 5 mmol), 30% H_2O_2 (1.7 gm, 15 mmol), catalyst amount (0.0005 g) and methanol (10 mL).

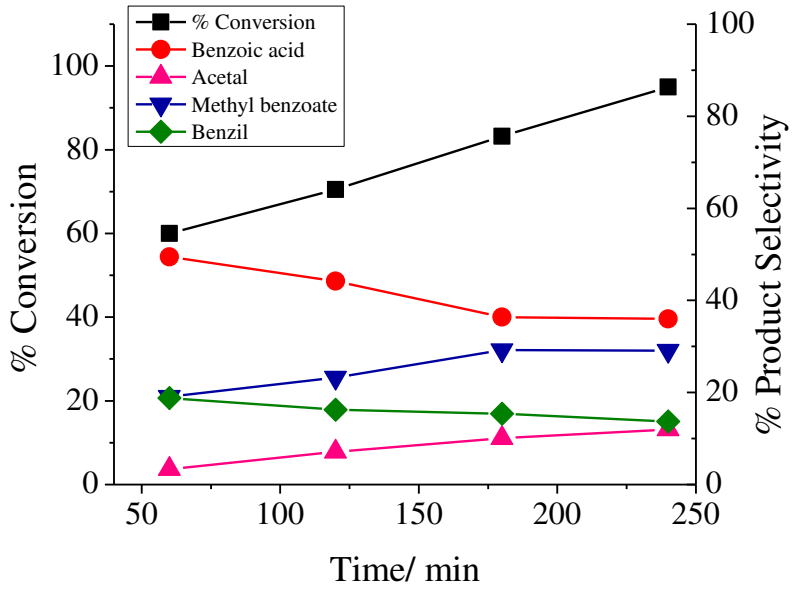

Figure 2.14. Profiles showing percentage conversion of benzoin and the selectivity of the formation of benzoic acid, benzaldehyde–dimethylacetal, methyl benzoate and benzil as a function of time. Reaction condition: benzoin (1.06 g, 5 mmol), H_2O_2 (1.7 g, 15 mmol), $[MoO_2(Hsal–dahp)H_2O]$ (**2.1**) (0.0005 g) and methanol (10 mL) at reflux temperature.

Under the above reaction conditions catalytic activity of other complexes for the oxidation of benzoin were also tested and details on the conversion of benzoin, turnover frequency and selectivity of the various products obtained at the end of 4 h of reaction are summarized in Table 2.12. As shown, all complexes show equally good catalytic activity with ca. 95% conversion of benzoin and substituent on the benzene ring has no influence on their activity. Similarly, selectivity of different products, though slightly differs for different complexes, essentially follows the same order for all. Catalytic potential of these complexes for the oxidation of benzoin are much better than the one obtained by polymer anchored $[Mo^{VI}O_2(salphen)]$ catalyst but the later one is more selective to benzyl [123].

Table 2.12.

Effect of different catalysts on the oxidation of benzoin, TOF and product selectivity.

Catalyst [g (mmol)]	TOF [h^{-1}][a]	Conv. [%]	Selectivity [%][b]			
			a	b	c	d
$[MoO_2(Hsal–dahp)(H_2O)]$ [0.0005 (1.1×10^{-3})]	1080	95	40	13	32	15
$[MoO_2(Hclsal–dahp)(H_2O)]$ [0.0005 (0.97×10^{-3})]	1213	97	49	10	30	11
$[MoO_2(Hbrsal–dahp)(H_2O)]$ [0.0005 (0.83×10^{-3})]	1446	96	41	11	30	18

[a]TOF values calculated at 4 h of reaction time.

[b]See scheme 6 for details of products.

2.4. Conclusions

The dioxidomolybdenum(VI) complexes with dibasic tridentate ligands are mostly known to exist either as five coordinated monomeric $[Mo^{VI}O_2L]$ [50,135], five coordinated oligomeric $[Mo^{VI}O_2L]^n$ with [Mo=O→Mo] [136] structure or six coordinated $[Mo^{VI}O_2L(D)]$ [136] (D = coordinating solvent which is normally used to prepare the complex). Complexes reported here belongs to the latter category where ligands only behave as dibasic tridentate ONO donor and other functional groups are free from coordination. However, in–situ generated H_3clsal–dahp in methanolic solution on reaction with $[Mo^{VI}O_2(acac)_2]$ in DMSO gave $[Mo^{VI}O_2(clsal–hdap)(DMSO)]_4[Mo_8O_{26}]\cdot 6DMSO$ (**2.7**) where non–coordinated azomethine nitrogen hydrolyzes giving free protonated amine group; the $[Mo_8O_{26}]^{4–}$ anion is stabilized through hydrogen bonding with $[Mo^{VI}O_2(clsal–hdap)(DMSO)]^+$ cation. The dioxidomolybdenum(VI) complexes $[Mo^{VI}O_2(Hsal–dahp)(H_2O)]$ (**2.1**), $[Mo^{VI}O_2(Hclsal–dahp)(H_2O)]$ (**2.2**) and $[Mo^{VI}O_2(Hbrsal–dahp)(H_2O)]$ (**2.3**) present good functional

models of haloperoxidases in that they catalyze the oxidative bromination of styrene, giving 1, 2–dibromo–1–phenyl–ethane, 1–phenylethane–1, 2–diol and 2–bromo–1–phenylethane–1–ol. These complexes are also good catalyst precursors for the oxidation of methyl phenyl sulphide, an activity shown by molybdenum oxotransferases, and benzoin.

CHAPTER 3

Synthesis, characterization, reactivity and catalytic activity of dioxidomolybdenum(VI) complexes derived from tribasic ONS donor ligands

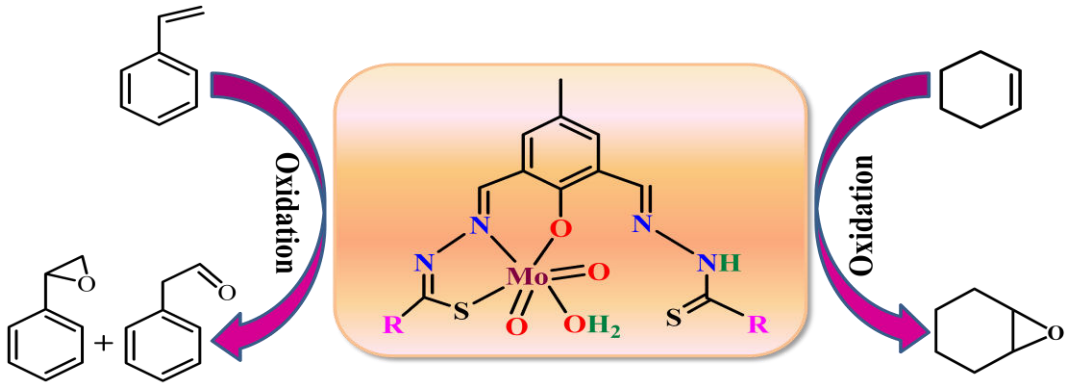

R = -$SCH_2C_6H_5$: $[MoO_2\{Hdfmp\text{-}(sbdt)_2\}H_2O]$ (1)
R = -SCH_3 : $[MoO_2\{Hdfmp\text{-}(smdt)_2\}H_2O]$ (2)
R = -NH_2 : $[MoO_2\{Hdfmp\text{-}(tsc)_2\}H_2O]$ (3)

The matter of this chapter is published in the journal "Polyhedron"

3.1. Introduction

Molybdenum–containing enzymes hold key positions both in biochemical cycles of carbon, nitrogen and sulfur and in the metabolism of every organism [154]. The oxygen atom transfer (OAT) between competent centers as a fundamental reaction in chemistry and biology, has been extensively investigated in past decades [155, 156]. Molybdenum enzymes catalyze a number of such reactions. Oxotransferases containing oxido–(dioxide-) molybdenum units: These oxotrnasferases can also contain the sulfido and/or sulfido + oxido molybdenum unit; see, e.g., the xanthine oxidase family [157]. In most biological systems, molybdenum containing enzymes, such as sulfite oxidase, dimethyl sulfoxide reductase, and nitrate reductase, catalyze oxygen atom transfer reactions at the mononuclear oxidomolybdenum active centers [30, 157(a)], wherein XO/X functions as donor/acceptor and the oxidation state of molybdenum atom changes by two units (Eq. 3.1).

$$Mo^{VI}O_2L_n + X \rightleftharpoons Mo^{IV}OL_n + XO \qquad (3.1)$$

Molybdenum complexes are known for their catalytic applications in the oxidation [64, 107–116, 119–120, 123, 125–126] and oxidative bromination of organic substrates [50, 87, 124, 158], and oxidation of sulfides [37, 61, 127–128]. Catalytic efficiency of these catalysts, e.g. oxidation of organic compounds, has been found to be improved using co–catalyst $NaHCO_3$ in presence of H_2O_2 as terminal oxidant [159–162]. It has been presumed that this is due to efficient formation of oxidoperoxidomolybdenum(VI) intermediate during catalytic reaction.

Synthetic strategies for *cis*–$[Mo^{VI}O_2]^{2+}$ complexes of O and N donor ligands have extensively been reported in the literature [39, 50, 87, 158] in comparison to O, N and S donor ligands [65, 163, 164]. Ligands derived from 2,6–diformyl–4–methylphenol and *S*–benzyldithiocarbazate, *S*–methyldithiocarbazate, and thiosemicarbazide are tribasic pentadenate O, N and S donor ligands (Scheme 3.1) but non–participation of second

azomethine and thiol groups of second Schiff base moiety may results in tridentate behavior of these. However, the non–participated arm may involve in intermolecular π–bonding/ hydrogen bonding leading to supramolecular arrangement. Therefore, we report herein synthesis and characterization of new *cis*–$[Mo^{VI}O_2]^{2+}$ complexes of these ligands. Their catalytic potentials, in presence of co–catalyst $NaHCO_3$ are demonstrated by studying the oxidation of styrene and cyclohexene.

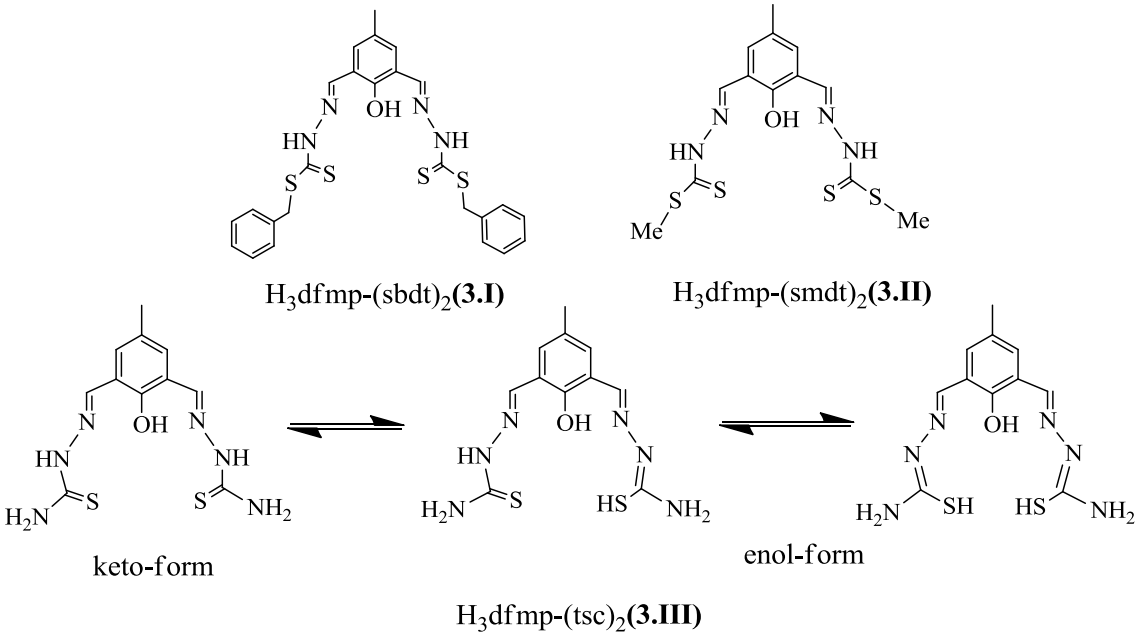

Scheme 3.1. Structure of the ligands designated by **3.I**, **3.II** and **3.III** used in this work. Keto–enol tautomerism is shown in only one of the ligands.

3.2. Experimental section

3.2.1. Materials and methods

Cyclohexene, methyl iodide (Himedia, India) and benzyl chloride (S.D. fine chemicals, India) were used as obtained. 2, 6–diformyl–4–methylphenol [165], *S*–

benzyldithiocarbazate [166] and *S*–methyldithiocarbazate [167] were prepared according to the methods reported in the literature. Details of other chemicals are given in chapter 2.

3.2.2. Instrumentation and Characterization Procedures

Details of instrumentation and characterization procedures are presented in chapter 2.

3.2.3. Preparations

3.2.3.1. Preparations of H_3dfmp(sbdt)$_2$ (3.I), H_3dfmp(smdt)$_2$ (3.II) and H_3dfmp(tsc)$_2$ (3.III)

The ligands H_3dfmp(sbdt)$_2$ (**3.I**), H_3dfmp(smdt)$_2$ (**3.II**) and H_3dfmp(tsc)$_2$ (**3.III**) were prepared by a general procedure; the preparation of H_3dfmp(sbdt)$_2$ is described here. A solution of 2,6–diformyl–4–methylphenol (1.64 g, 10 mmol) dissolved in methanol (30 ml) was added to a solution of *S*–benzyldithiocarbazate (3.966 g, 20 mmol) dissolved in methanol (10 ml). The obtained reaction mixture was refluxed on a water bath for 4 h. During this period a yellow solid slowly separated out. This was filtered, washed with methanol followed by petroleum ether and dried over silica gel under vacuum.

Data for H_3dfmp(sbdt)$_2$ (3.I): Yield: 4.93 g (94%). Anal. Calc. for $C_{25}H_{24}N_4S_4O$ (524): C, 57.24; H, 4.62; N, 10.69; S, 24.40. Found: C, 56.92; H, 4.56; N, 10.58; S, 24.36%.

Data for H_3dfmp(smdt)$_2$ (3.II): Yield: 3.49 g (93.8%). Anal. Calc. for $C_{13}H_{16}N_4S_4O$ (372): C, 41.93; H, 4.33; N, 15.06; S, 34.38. Found: C, 41.52; H, 4.16; N, 15.18; S, 34.26%.

Data for H_3dfmp(tsc)$_2$ (3.III): Yield: 2.99 g (96.5%). Anal. Calc. for $C_{11}H_{14}N_6S_2O$ (310): C, 42.57; H, 4.55; N, 27.08; S, 20.66. Found: C, 42.72; H, 4.46; N, 27.19; S, 20.56%.

3.2.3.2. Preparation of $[Mo^{VI}O_2\{Hdfmp(sbdt)_2\}(H_2O)]$ (3.1)

A solution of $[Mo^{VI}O_2(acac)_2]$ (0.66 g, 2 mmol) dissolved in 10 ml of methanol was added to a stirred solution of $H_3dfmp(sbdt)_2$ (1.048 g, 2 mmol) in methanol (20 ml) and the obtained reaction mixture was stirred at room temperature where upon a yellow solid started to form. After 2 h of stirring, the separated solid was filtered, washed with methanol and dried in a vacuum desiccator over silica gel. Yield: 1.15 g (85.8%). Anal. Calc. for $C_{25}H_{24}N_4S_4O_4Mo$ (668.7): C, 44.91; H, 3.62; N, 8.38; S, 19.18. Found: C, 44.63; H, 3.56; N, 8.54; S, 19.26%. Crystals of $[Mo^{VI}O_2\{Hdfmp(sbdt)_2\}(MeOH)]\cdot 2MeOH$ (**3.1a**·2MeOH) suitable for X–ray analysis were grown by slow evaporation of a solution of (**3.1**) in methanol.

3.2.3.3. Preparation of $[Mo^{VI}O_2\{Hdfmp(smdt)_2\}(H_2O)]$ (3.2)

Complex **3.2** was prepared from $[Mo^{VI}O_2(acac)_2]$ (0.66 g, 2 mmol) and $H_3dfmp(smdt)_2$ (0.744, 2 mmol) in methanol by the method outlined for **3.1**. The separated yellow solid was filtered, washed with cold methanol and dried in a vacuum desiccator over silica gel. Yield: 0.890 g (86.4%). Anal. Calc. for $C_{13}H_{16}N_4S_4O_4Mo$ (516.4): C, 30.23; H, 3.12; N, 10.85; S, 24.83 %. Found: C, 30.28; H, 3.36; N, 10.50; S, 24.96%. Crystals of $[Mo^{VI}O_2\{Hdfmp(smdt)_2\}(DMSO)]\cdot DMSO$ (**3.2a**·DMSO) suitable for X–ray analysis were grown by slow evaporation of a solution of **3.2** in DMSO.

3.2.3.4. Preparation of $[Mo^{VI}O_2\{Hdfmp(tsc)_2\}(H_2O)]$ (3.3)

Complex **3.3** was prepared from $[Mo^{VI}O_2(acac)_2]$ (0.66 g, 2 mmol) and $H_3dfmp(tsc)_2$ (0.620 g, 2 mmol) in methanol following the method described for **3.1**. After 2 h of stirring, the separated yellow solid was filtered, washed with cold methanol and dried in a vacuum desiccator over silica gel. Yield: 0.772 g (85.0%). Anal. Calc. for $C_{11}H_{14}N_6S_2O_4Mo$ (454.33): C, 29.08; H, 3.11; N, 18.50; S, 14.11. Found: C, 29.19; H, 3.28; N, 18.48; S, 14.26%. Crystals of $[Mo^{VI}O_2\{Hdfmp(tsc)_2\}(MeOH)]\cdot MeOH$

(**3.3a**·MeOH) suitable for X–ray analysis were grown by slow evaporation of a solution of **3.3** in methanol.

3.2.4. X–Ray crystal structure determination

Three–dimensional X–ray data were collected on a Bruker Kappa Apex CCD diffractometer at low temperature for **3.1a** and **3.2a**, and room temperature for **3.3a** by the ϕ–ω scan method. Reflections were measured from a hemisphere of data collected from frames each of them covering 0.3º in ω. Of the 117594 for **3.1a**, 51408 for **3.2a** and 41327 for **3.3a** reflections measured, all were corrected for Lorentz and polarization effects and for absorption by multi–scan methods based on symmetry–equivalent and repeated reflections, 7162, 6643 and 5942, respectively, independent reflections exceeded the significance level ($|F|/\sigma|F|$) > 4.0. Complex scattering factors were taken from the program package SHELXTL [134]. The structures were solved by direct methods and refined by full matrix least–squares on F^2. Hydrogen atoms were located in difference Fourier map and left to refine freely in **3.1a**, except to C(1M), C(2M), C(3M) and C(16). Hydrogen atom of O (3M) was located in difference Fourier map and fixed to oxygen atom in **3.1a**. In other structures, hydrogen atoms were included in calculation positions and refined in the riding mode, except to C(3), N(4), C(5), N(8), C(11), C(16), C(18), C(21) and C(24) in **3.2a** and O(1M), C(2), N(3), C(4), N(5), N(6), C(6) and C(9) in **3.3a**, which were located in difference Fourier map and left to refine freely. Refinements were done with allowance for thermal anisotropy of all non–hydrogen atoms. The crystal of **3.2a** presents a disorder on the second DMSO coordinated molecule present in the asymmetric unit. This disorder has been refined and two atomic sites for one sulfur atom has been observed and refined with the anisotropic atomic displacement parameters in each case. Unfortunately, hydrogen atoms for this disordered DMSO molecule have not been located. The site occupancy factor was 0.70240 for S (10A). Further details of the crystal structure determination are given in Table 3.1. A final difference Fourier map showed no residual density outside: 0.865 and –0.794 e. Å^{-3} for **3.1a**, 2.401 and –1.268 e.Å^{-3} for **3.2a** and 1.733 and –1.362 e.Å^{-3} for **3.3a**. A weighting scheme w = 1/[σ^2(F_o^2) +

$(0.053000\ P)^2 + 0.922900\ P]$ for **3.1a**, $w = 1/[\sigma^2(F_o^2) + (0.078300\ P)^2 + 8.261801\ P]$ for **3.2a** and $w = 1/[\sigma^2(F_o^2) + (0.019700\ P)^2 + 3.996000\ P]$ for **3.3a**, where $P = (|F_o|^2 + 2|F_c|^2)/3$, were used in the latter stages of refinement.

Table 3.1.

Crystal data and structure refinement for $[Mo^{VI}O_2\{Hdfmp(sbdt)_2\}(MeOH)]\cdot 2MeOH$ (**3.1a**·2MeOH) $[Mo^{VI}O_2\{Hdfmp(smdt)_2\}(DMSO)]\cdot DMSO$ (**3.2a**·DMSO) and for $[Mo^{VI}O_2\{Hdfmp(tsc)_2\}(MeOH)]\cdot MeOH$ (**3.3a**·MeOH).

	3.1a·2MeOH	**3.2a**·DMSO	**3.3a**·MeOH
Formula	$C_{28}H_{34}MoN_4O_6S_4$	$C_{34}H_{52}Mo_2N_8O_{10}S_{12}$	$C_{13}H_{20}MoN_6O_5S_2$
Formula mass	746.77	1309.44	500.41
T, *K*	100(2)	100(2)	293(2)
Wavelength, Å	0.71073	0.71073	0.71073
Crystal system	Triclinic	Monoclinic	Monoclinic
Space group	$P\bar{1}$	$P2_1/n$	$P2_1/n$
a/Å	11.6267(8)	24.045(5)	11.0943(13)
b/Å	12.4104(8)	7.324(5)	15.5237(18)
c/Å	13.6600(8)	29.729(5)	11.5641(13)
α/°	104.841(2)	90	90
β/°	96.344(3)	92.849(5)	96.510(5)
γ/°	114.661(3)	90	90
V/Å^3	1677.65(19)	5229(4)	1978.8(4)
Z	2	4	4
F_{000}	768	2672	1016
D_{calc}/g cm^{-3}	1.478	1.663	1.680
μ/mm^{-1}	0.685	1.017	0.911
θ/(°)	1.59 to 28.91	1.70 to 24.41	2.21 to 33.75
R_{int}	0.0609	0.0776	0.0343

Crystal size/ mm^3	0.46 × 0.19 × 0.16	0.225 × 0.125 × 0.200	0.23 × 0.19 × 0.16
Goodness–of–fit on F^2	1.080	1.086	1.058
$R_1[I>2\sigma(I)]$ [a]	0.0334	0.0454	0.0394
wR_2 (all data) [b]	0.1011	0.1436	0.0848
Largest differences peak and hole ($e Å^{-3}$)	0.865 and –0.794	2.401 and –1.268	1.733 and –1.362

[a] $R_1 = \Sigma \| |F_o| - |F_c| \| / \Sigma |F_o|$. [b] $wR_2 = \{\Sigma[w(|F_o|^2 - |F_c|^2)^2] / \Sigma[w(F_o^4)]\}^{1/2}$

3.2.5. Catalytic activity studies

3.2.5.1. Oxidation of styrene

In a typical reaction, styrene (0.52 g, 5 mmol), aqueous 30% H_2O_2 (2.27 g, 20 mmol), $NaHCO_3$ (0.168 g, 2 mmol) and catalyst (0.0005 g) were dissolved in acetonitrile (5 mL) and the temperature of the reaction mixture was set to 60 °C. The reaction was monitored by withdrawing small aliquots of the reaction mixture at every 30 min and analyzing them quantitatively by gas chromatography. The identities of the products were confirmed by GC–MS. The effects of various parameters, such as amount of oxidant, amount of sodium bicarbonate, catalyst, temperature and solvent were studied to see their effect on the conversion and selectivity of the reaction products.

3.2.5.2. Oxidation of cyclohexene

Aqueous 30% H_2O_2 (2.27 g, 20 mmol), cyclohexene (0.41 g, 5 mmol), $NaHCO_3$ (0.168 g, 2 mmol) and catalyst (0.0005 g) were mixed in CH_3CN (5 mL) and the reaction mixture was heated at 60 °C with continuous stirring in an oil bath for ca. 2.5 h. The reaction was monitored by withdrawing small aliquots of the reaction mixture at every 30 min and analyzing them quantitatively by gas chromatography. The identities of the products were confirmed as mentioned above. The effects of various parameters, such as

amounts of oxidant, amount of sodium bicarbonate, catalyst, temperature and solvent were studied to see their effect on the conversion and selectivity of the reaction products.

3.3. Results and discussion

3.3.1. Synthesis and characterization of complexes

The dioxidomolybdenum(VI) precursor $[Mo^{VI}O_2(acac)_2]$ reacts with the ligands $H_3dfmp(sbdt)_2$ (**3.I**), $H_3dfmp(smdt)_2$ (**3.II**) and $H_3dfmp(tsc)_2$ (**3.III**) (*c.f.* Scheme 3.1) in methanol to give dioxidomolybdenum(VI) complexes $[Mo^{VI}O_2\{Hdfmp(sbdt)_2\}(H_2O)$(**3.1**), $[Mo^{VI}O_2\{Hdfmp(smdt)_2\}(H_2O)]$ (**3.2**) and $[Mo^{VI}O_2\{Hdfmp(tsc)_2\}(H_2O)]$ (**3.3**), respectively [Eq. (3.2) taking (**3.I**) as a representative example].

$$[Mo^{VI}O_2(acac)_2] + H_3dfmp(sbdt)_2 + H_2O \rightarrow [Mo^{VI}O_2\{Hdfmp(sbdt)_2\}(H_2O)] + 2Hacac \quad (3.2)$$

All these complexes are soluble in methanol, ethanol and dichloromethane. In these complexes the sixth coordination site is occupied by water, however, complexes **3.1**, **3.2** and **3.3** could be isolated as MeOH, DMSO or MeOH coordinated, respectively on crystallizing them in respective solvent. Scheme 3.2 provides idealized structures of the complexes, which are based on the spectroscopic (IR, UV/Vis, ^1H and ^{13}C NMR) data, elemental analyses and X–ray diffraction studies of $[Mo^{VI}O_2\{Hdfmp(sbdt)_2\}(MeOH)]\cdot 2MeOH$ (**3.1a**·2MeOH), $[Mo^{VI}O_2\{Hdfmp(smdt)_2\}(DMSO)]\cdot DMSO$ (**3.2a**·DMSO) and $[Mo^{VI}O_2\{Hdfmp(tsc)_2\}(MeOH)]\cdot MeOH$ (**3.3a**·MeOH).

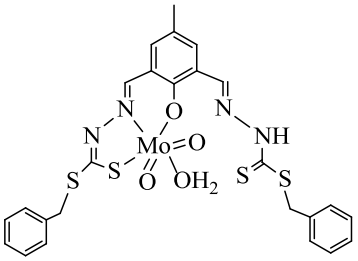

$[MoO_2\{Hdfmp\text{-}(sbdt)_2\}(H_2O)]$ (**3.1**)

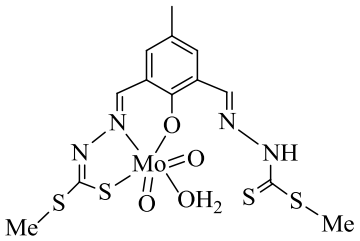

$[MoO_2\{Hdfmp\text{-}(smdt)_2\}(H_2O)]$ (**3.2**)

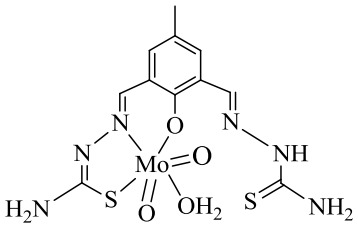

$[MoO_2\{Hdfmp\text{-}(tsc)_2\}(H_2O)]$ (**3.3**)

Scheme 3.2. Proposed structures of complexes.

3.3.2. Thermal studies

Thermal stability of monomeric complexes **3.1**, **3.2** and **3.3** has been studied under an oxygen atmosphere. These complexes lose mass roughly equal to one water molecule in the temperature range 100–160 °C, indicating the presence of coordinated water. The anhydrous complexes on further increasing the temperature decompose exothermically in two/ three overlapping steps and form MoO_3 at ca. 650 ^oC (for **3.1**: Found: 21.5; Calc.: 21.5%), ca. 520 ^oC (for **3.2**: Found: 26.3; Calc.: 27.9%) and at ca. 480 ^oC (for **3.3**: Found: 30.8; Calc.: 31.7%) as the final product.

3.3.3. Structure descriptions

ORTEP diagrams of $[Mo^{VI}O_2\{Hdfmp(sbdt)_2\}(MeOH)]\cdot 2MeOH$ (**3.1a**·2MeOH), $[Mo^{VI}O_2\{Hdfmp(smdt)_2\}(DMSO)]\cdot DMSO$ (**3.2a**·DMSO) and $[Mo^{VI}O_2\{Hdfmp(tsc)_2\}(MeOH)]\cdot MeOH$ (**3.3a**·MeOH) are shown in Figs. 3.1, 3.2 and 3.3, respectively. Figs. 3.4, 3.5 and 3.6 present the intermolecular π–π interactions. Selected bond distances and angles are given in Table 3.2. These complexes adopt a six–

coordinated structure in a distorted octahedral geometry. In the complexes, the phenolic oxygen, enthiolate sulfur and the azomethine nitrogen atoms of the ligands coordinate to the molybdenum while other set of sulfur and azomethine nitrogen atoms of the ligands do not participate in coordination. One methanol molecule in **3.1a**·2MeOH, one DMSO molecule in **3.2a**·DMSO and one methanol molecule in **3.3a**·MeOH and two oxido groups complete the coordination sphere. Two methanol molecules in **3.1a**·2MeOH, other DMSO molecule in **3.2a**·DMSO and one methanol molecule in **3.3a**·MeOH are present in the crystal packing. One of the coordinated molecules of DMSO presents a disorder on sulphur atom. Two atomic sites have been observed for the first DMSO molecule [site occupancy factor for S (10A) is 0.70240].

The asymmetric unit of complex **3.2a**·DMSO contains two complexes $[Mo^{VI}O_2\{Hdfmp(smdt)_2\}(DMSO)]$ and two DMSO molecules. In complex **3.2a**·DMSO, the lateral chains of the two complexes interact by π–π interactions. In π–π interactions the major contributions to the interaction energy come from the electrostatic and van der Waals components [168], but geometrical requirements are necessary for attractive electrostatic interactions dominate over the repulsive. Steric requirements, derived from coordination sphere around Mo, prevent π–π interactions between the phenol rings. In the solid state the complexes form an antiparallel dimer through π–π interactions, between C=S bonds and phenol rings and between the C=N bonds of two complexes (see Fig. 3.5). The distances between centroids are: $d_{c1–c2}$ = 3.863 Å [c1 (C8–N3), c2 (C24–N7)], $d_{c3–c4}$ = 3.991 Å [c3 (C9–S3), c4 (C14–C15–C16–C17–C18–C19)] $d_{c5–c6}$ = 3.933 Å [c5 (C25–S7), c6 (C1–C2–C3–C4–C5–C6). In **3.1a**·2MeOH, a weak π–π interactions appear only between C=N bonds, $d_{c1–c2}$ = 3.737 Å [c1 (C9J–N2J), c2 (C9A–N2A)], but it keep the antiparallel placement (Fig. 3.4). In compound **3.3a**·MeOH, similar π–π interactions are present in the crystal packing, but in this case the interactions occur between C=N bonds and phenol rings in an antiparallel placement. The distance between centroids are: $d_{c1–c2}$ = 3.329 Å [c1 (C2F–N4F), c2 (C3A–C4A–C5A–C6A–C7A–C8A)], $d_{c3–c4}$ = 3.329 Å

[c3 (C2A–N4A), c4 (C3F–C4F–C5F–C6F–C7F–C8F)] (see Fig. 3.6). Intermolecular hydrogen bonds are present in the crystal packing in the three structures (see Table 3.3).

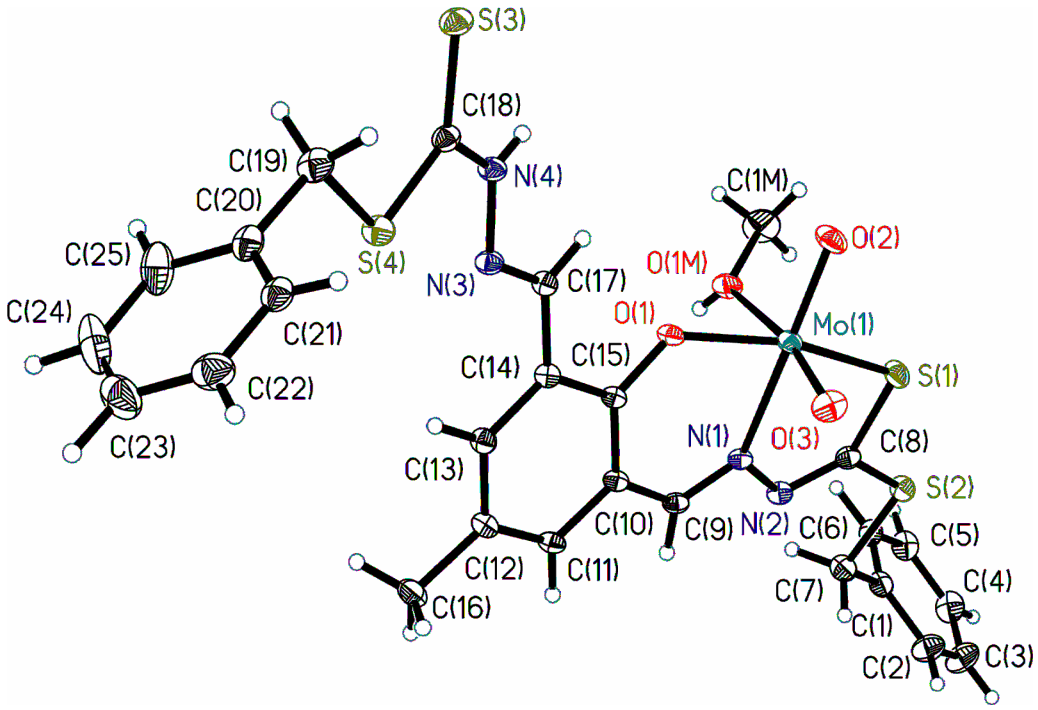

Figure 3.1. ORTEP plot of complex $[Mo^{VI}O_2\{Hdfmp(sbdt)_2\}(MeOH)]\cdot 2MeOH$ (**3.1a**·2MeOH). All the non–hydrogen atoms are presented by their 30% probability ellipsoids. Hydrogen atoms are omitted for clarity.

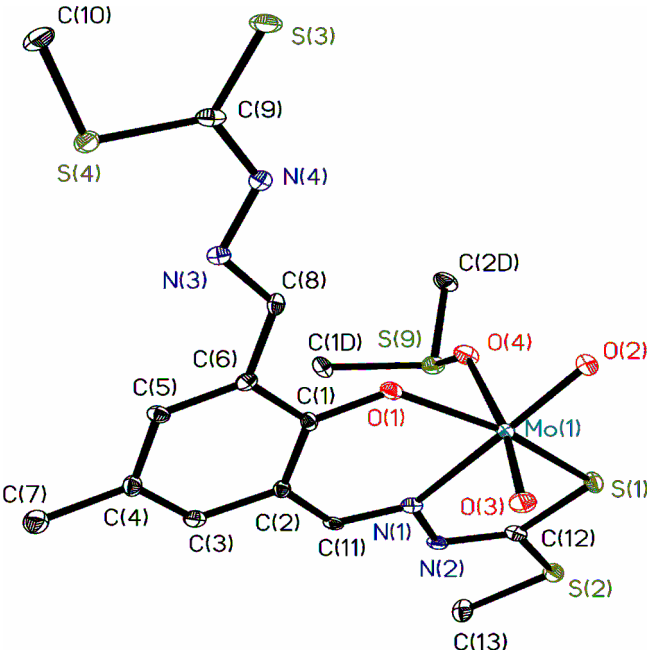

Figure 3.2. ORTEP plot of complex $[Mo^{VI}O_2\{Hdfmp(smdt)_2\}(DMSO)]\cdot DMSO$ (**3.2a**·DMSO). All the non–hydrogen atoms are presented by their 30% probability ellipsoids. Hydrogen atoms and solvent DMSO are omitted for clarity.

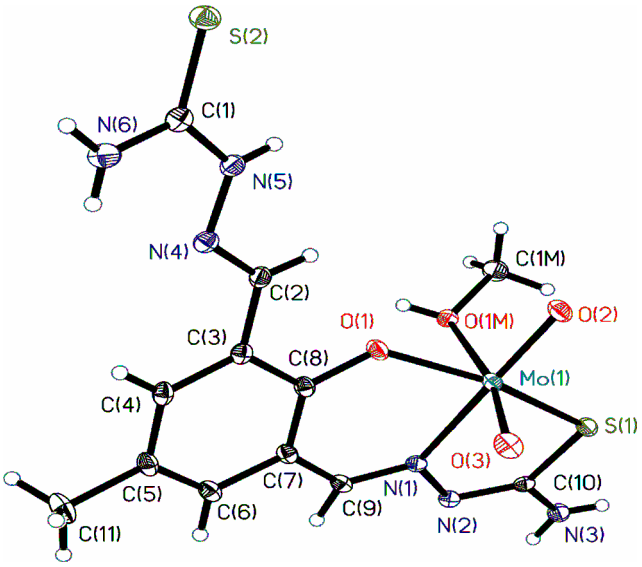

Figure 3.3. ORTEP plot of complex $[Mo^{VI}O_2\{Hdfmp(tsc)_2\}(MeOH)]\cdot MeOH$ (**3.3a**·MeOH). All the non–hydrogen atoms are presented by their 30% probability ellipsoids.

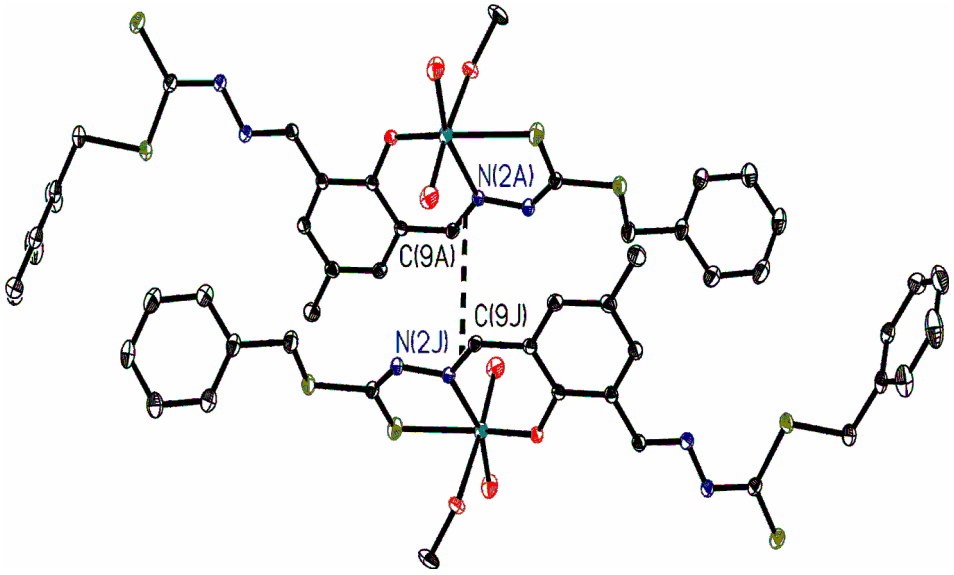

Figure 3.4. Intermolecular π–π interactions in **3.1a**·2MeOH. Dashed lines link the centres of the π clouds involving in each interaction.

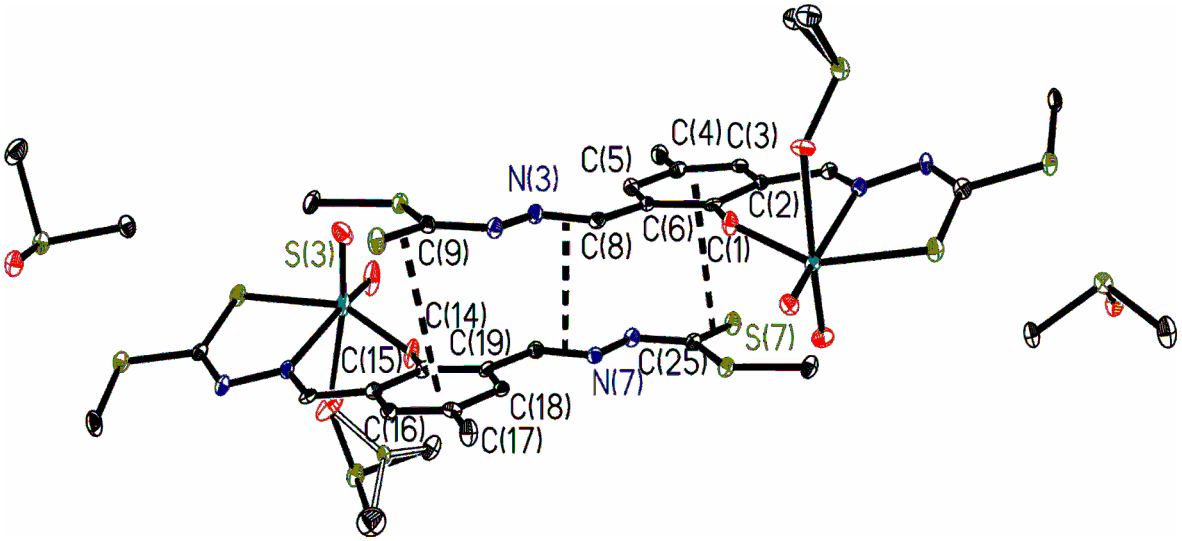

Figure 3.5. Intermolecular π–π interactions in **3.2a**·DMSO. Dashed lines link the centres of the π clouds involving in each interaction.

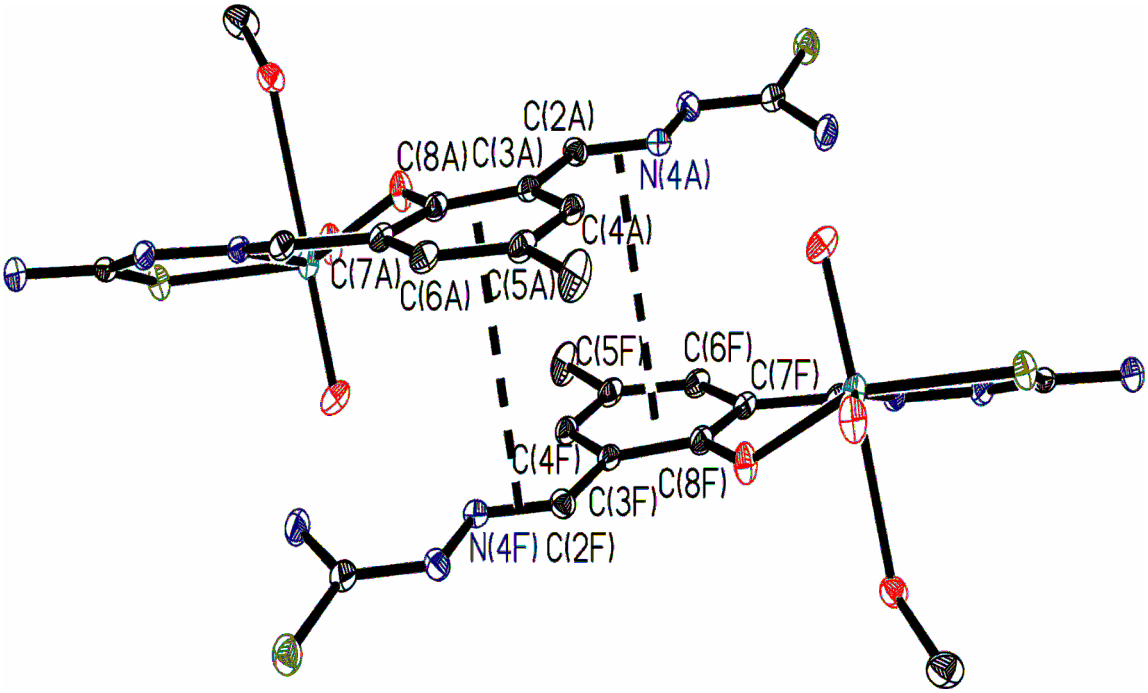

Figure 3.6. Intermolecular π–π interactions in **3.3a**·MeOH. Dashed lines link the centres of the π clouds involving in each interaction.

Table 3.2.

Bond lengths [Å] and angles [°] for $[Mo^{VI}O_2\{Hdfmp(sbdt)_2\}(MeOH)]\cdot 2MeOH$ (**3.1a**·2MeOH), $[Mo^{VI}O_2\{Hdfmp(smdt)_2\}(DMSO)]\cdot DMSO$ (**3.2a**·DMSO) and $[Mo^{VI}O_2\{Hdfmp(tsc)_2\}(MeOH)]\cdot MeOH$ (**3.3a**·MeOH).

Bond lengths	**3.1a**·2MeOH	**3.2a**·DMSO	**3.3a**·MeOH
Mo(1)–O(1)	1.9357(15)	1.938(4)	1.9333(17)
Mo(1)–O(2)	1.7088(17)	1.708(4)	1.7022(17)
Mo(1)–O(3)	1.6895(18)	1.687(4)	1.7061(18)
Mo(1)–O(1M)	2.2644(19)	Mo(1)–O(4) 2.247(4)	2.3112(18)
Mo(1)–N(1)	2.2664(17)	2.272(4)	2.2848(18)
Mo(1)–S(1)	2.4440(6)	2.4475(15)	2.4137(6)
Mo(2)–O(5)		1.944(4)	
Mo(2)–O(6)		1.683(5)	
Mo(2)–O(7)		1.699(4)	
Mo(2)–O(8)		2.297(5)	
Mo(2)–N(5)		2.254(5)	
Mo(1)–S(5)		2.4566(15)	

Bond angles	**3.1a**·2MeOH	**3.2a**·DMSO	**3.3a**·MeOH
O(3)–Mo(1)–O(2)	106.07(9)	104.49(19)	105.69(9)
O(3)–Mo(1)–O(1)	98.46(8)	98.27(18)	97.94(8)
O(2)–Mo(1)–O(1)	105.17(8)	105.82(16)	106.30(8)
O(3)–Mo(1)–O(1M)	168.11(8)	O(3)–Mo(1)–O(4) 170.43(16)	167.44(8)
O(2)–Mo(1)–O(1M)	85.82(9)	O(2)–Mo(1)–O(4) 85.08(16)	86.51(8)
O(1)–Mo(1)–O(1M)	77.99(7)	O(1)–Mo(1)–O(4) 78.44(16)	75.28(7)
O(3)–Mo(1)–N(1)	90.55(8)	89.53(18)	90.08(8)
O(2)–Mo(1)–N(1)	160.68(8)	162.74(17)	161.24(8)
O(1)–Mo(1)–N(1)	81.44(6)	81.55(15)	80.88(7)

O(1M)–Mo(1)–N(1)	77.74(7)	N(1)–Mo(1)–O(4) 81.12(15)	78.49(6)
O(3)–Mo(1)–S(1)	97.66(7)	98.00(14)	100.70(7)
O(2)–Mo(1)–S(1)	91.60(6)	91.96(13)	90.83(6)
O(1)–Mo(1)–S(1)	152.41(5)	151.95(12)	150.16(5)
O(1M)–Mo(1)–S(1)	81.65(5)	O(4)–Mo(1)–S(1) 81.77(11)	81.76(5)
N(1)–Mo(1)–S(1)	76.16(5)	75.89(12)	76.03(5)
O(6)–Mo(2)–O(7)		104.8(2)	
O(6)–Mo(2)–O(5)		97.84(19)	
O(7)–Mo(2)–O(5)		105.26(18)	
O(6)–Mo(2)–N(5)		93.13(19)	
O(7)–Mo(2)–N(5)		159.7(2)	
O(5)–Mo(2)–N(5)		81.08(16)	
O(6)–Mo(2)–O(8)		168.96(19)	
O(7)–Mo(2)–O(8)		85.1(2)	
O(5)–Mo(2)–O(8)		83.93(18)	
N(5)–Mo(2)–O(8)		76.33(17)	
O(6)–Mo(2)–S(5)		96.72(15)	
O(7)–Mo(2)–S(5)		92.21(15)	
O(5)–Mo(2)–S(5)		153.48(14)	
N(5)–Mo(2)–S(5)		76.10(12)	
O(8)–Mo(2)–S(5)		77.75(12)	

Table 3.3.

Hydrogen bonds for $[Mo^{VI}O_2\{Hdfmp(sbdt)_2\}(MeOH)]\cdot 2MeOH$ (**3.1a**·2MeOH), $[Mo^{VI}O_2\{Hdfmp(smdt)_2\}\cdot DMSO]\cdot DMSO$ (**3.2**) and $[Mo^{VI}O_2\{Hdfmp(tsc)_2\}\cdot MeOH]\cdot MeOH$ (**3.3**).

D–H...A	d(D–H)	d(H...A)	d(D...A)	<(DHA)
N(4)–H(4N)...O(9)#1	0.79(6)	2.08(6)	2.843(6)	162(6)
N(8)–H(8N)...O(10)#2	0.77(6)	2.05(6)	2.806(6)	165(6)
N(8)–H(8N)...S(12)#2	0.77(6)	3.02(6)	3.775(5)	168(6)
O(1M)–H(1M)...O(1W)#3	0.78(3)	1.86(4)	2.629(3)	174(4)
O(1W)–H(1W)...N(2)#4	0.82	1.98	2.783(3)	165.6
N(3)–H(3NB)...S(2)#5	0.77(3)	2.65(3)	3.419(2)	176(2)
N(3)–H(3NA)...O(2)#6	0.82(3)	2.44(3)	3.050(3)	133(3)
N(5)–H(5N)...S(2)#7	0.83(3)	2.73(3)	3.494(2)	154(3)
N(6)–H(6NB)...O(3)#8	0.80(3)	2.32(3)	3.066(3)	155(3)
O(1M)–H(1M)...O(3M)	0.69(4)	1.94(4)	2.625(3)	175(4)
O(3M)–H(3M)...S(3)#9	0.82	2.57	3.274(2)	143.9
N(4)–H(4N)...O(2M)	0.77(3)	2.03(3)	2.801(3)	170(3)

Symmetry transformations used to generate equivalent atoms (#1 and #2 correspond to **3.2**, #3, #4, #5, #6, #7 and #8 correspond to **3.3**)

#1 –x+1/2,y–1/2,–z+3/2 #2 –x+3/2,y+1/2,–z+3/2 #3 –x+1,–y,–z #4 x–1,y,z

#5 –x+3/2,y+1/2,–z+1/2 #6 x+1/2,–y+1/2,z–1/2 #7 –x+1,–y,–z+1 #8 –x+2,–y,–z+1, #9 x,y,z+1

3.3.4. IR spectral studies

A partial list of IR spectral data of ligands and complexes is presented in Table 3.4. The IR spectra of ligands exhibit a sharp band due to ν(C=N) (azomethine) stretch at 1609–1616 cm^{-1}, though there are two azomethine groups present in the ligands. All complexes retain its position with slight deviations along with the appearance of a new band at considerably lower wave number indicating the coordination of only one of the azomethine nitrogen atoms to the molybdenum. The appearance of a strong band between 1030–1038 cm^{-1} due to the ν(C=S) indicates the thione (thiocarbonyl) nature of the uncoordinated ligands which is further supported by the absence of an IR band at ca. 2500 cm^{-1} for ν(SH) and the presence of a band at ca. 3100 cm^{-1} for ν(NH) of the hydrazide moiety [169]. Again all the complexes retain the positions of these bands with slight deviations but the appearance of a new band at 679–697 cm^{-1} due to the ν(C–S) stretch suggests the thioenolisation of one of the C=S groups and coordination of the enethiolate sulfur to molybdenum. A new band at 965–998 cm^{-1} arising out due to thioenolization and formation of –N=N– group has also been observed. The presence of several medium intensity bands between 2800 and 2500 cm^{-1} in the ligands as well as in complexes suggest the existence of C–H stretching due to $–CH_2$. In addition, these complexes display two sharp bands at 923–945 and 892–910 cm^{-1} due to the ν_{asym}(O=Mo=O) and ν_{sym}(O=Mo=O) streching modes, respectively due to the presence of *cis*–[$Mo^{VI}O_2$] moiety [136].

Table 3.4.

IR spectral data [in cm^{-1}] of compounds

Compounds	ν(C=S)	ν(C=N)	ν(N–N)	ν(C–S)	ν(O=Mo=O)[a]
H_3dfmp(sbdt)$_2$	1030	1609			
[$Mo^{VI}O_2${Hdfmp(sbdt)$_2$}(H_2O)]	1026	1606, 1560	972	697	945, 910
H_3dfmp(smdt)$_2$	1023	1616			
[$Mo^{VI}O_2${Hdfmp(smdt)$_2$}(H_2O)]	1027	1606, 1559	998	680	945, 906
H_3dfmp(tsc)$_2$	1038	1611			
[$Mo^{VI}O_2${Hdfmp(tsc)$_2$}(H_2O)]	1068	1618, 1570	994	679	923, 892

[a] Asymmetric and symmetric ν(O=Mo=O) values.

3.3.5. Electronic spectral studies

The electronic spectra of ligands could only be recorded in DMSO due to their insolubility in other solvents while spectra of complexes were recorded in methanol successfully. Table 3.5 presents electronic spectral data of the ligands and complexes. The electronic spectra of H_3dfmp(sbdt)$_2$ (**3.I**), H_3dfmp(smdt)$_2$ (**3.II**) and H_3dfmp(tsc)$_2$ (**3.III**) exhibit two sets of UV/vis absorption bands possibly due to the presence of asymmetry in two sets of coordination sites. Based on their extinction coefficients, these bands are interpreted as n→π* (365–367 and 401–405 nm) and π→π* (329 and 245 nm). The region below this did not show any band in DMSO solvent. However, electronic spectra of metal complexes recorded in methanol exhibit bands in the lower region as well. As one site of the each ligand (i.e. azomethine N and thioenolic S) is not involved in coordination as confirmed by X–ray crystal studies e.g. for complexes **3.2** and **3.3** (vide supra), these complexes exhibit two sets of intra ligand electronic spectral transitions i.e. due to free as well as coordinated portions of ligands and thus show complexity in the

UV region (Table 3.5); the band due to φ→φ* (207–209 nm) also become visible in the complexes. In addition, all complexes exhibit a medium intensity band at 430–435 nm due to ligand to metal charge transfer (LMCT) transition from the phenolate oxygen atom to an empty d–orbital of the molybdenum. As Mo^{VI} –complexes have $4d^0$ configuration, d→d band is not expected.

Table 3.5.

Electronic spectral data of ligands and complexes.

Compound	Solvent	λ_{max} /nm (ε/ $M^{-1}cm^{-1}$)
H_3dfmp(sbdt)$_2$ (**3.I**)	DMSO	329 (4×10^4), 345 (4.5×10^4), 367 (4×10^4), 405 (3.2×10^4)
[$Mo^{VI}O_2${Hdfmp(sbdt)$_2$}(H_2O)](**3.1**)	MeOH	209 (8×10^4), 282 (2.8×10^4), 326 (6.3×10^4), 339 (6.9×10^4), 376 (4×10^4), 401 (2.8×10^4), 435 (7.3×10^3)
H_3dfmp(smdt)$_2$ (**3.II**)	DMSO	329 (3.3×10^4), 345 (3.7×10^4), 365 (3.2×10^4), 401 (2.6×10^4)
[$Mo^{VI}O_2${Hdfmp(smdt)$_2$}(H_2O)] (**3.2**)	MeOH	208 (3×10^4), 280 (1.4×10^4), 325 (3.4×10^4), 337 (3.7×10^4), 375 (2×10^4), 399 (1.3×10^4), 435 (2.9×10^3)
H_3dfmp(tsc)$_2$ (**3.III**)	DMSO	315 (4.9×10^4), 328 (4.2×10^4), 369 (2.7×10^4), 387 (2×10^4)
[$Mo^{VI}O_2${Hdfmp(tsc)$_2$}(H_2O)] (**3.3**)	MeOH	207 (1.2×10^4), 238 (8.6×10^4), 312 (1.5×10^4), 351 (1×10^4), 384 (5.6×10^3), 430 (1.7×10^3)

3.3.6. ^{1}H and ^{13}C NMR studies

The coordinating modes of H_3dfmp(sbdt)$_2$ (**3.I**), H_3dfmp(smdt)$_2$ (**3.II**) and H_3dfmp(tsc)$_2$ (**3.III**) were also confirmed by comparing their ^{1}H NMR spectral patterns with the corresponding complexes. The relevant spectral data are collected in Table 3.6. Fig. 3.7 reproduces ^{1}H NMR spectra of a representative ligand **3.II** and its complex. All the ligands show two signals at δ = 11.52–13.50 (br, 2H) and 9.56–10.81 (br, 1H) ppm corresponding to the NH and phenolic OH, respectively. Absence of signal due to phenolic OH in the complexes confirms coordination of the phenolic oxygen to the molybdenum. The existence of a NH signal equivalent to 1H indicates that only one of the NH protons is involved in tautomerization with C=S moiety which then coordinates with molybdenum after proton replacement while other C=S remains free. Similarly, the appearance of two signals due to azomethine proton (each equivalent to 1H) in complexes with a coordination–induced shifts [$\Delta\delta$ = [δ(complex) – δ(free ligand)] of 0.08 –0.51 ppm in complexes demonstrates the coordination of only one of the azomethine N atoms to molybdenum. Further, equal intensity for these two azomethine protons signals rules out the possibility of dynamic equilibrium between free and coordinated nitrogen atoms in solution. Signals due to aromatic protons and aliphatic protons appear in the expected regions in the spectra of the ligands as well as of the complexes with slight shifts in their positions.

Table 3.6.

^{1}H NMR chemical shifts [δ in ppm] of ligands and complexes recorded in DMSO–d_6.

Compounds[a]	–NH	–OH	–CH=N–	$–CH_2$	$–CH_3$	Aromatic protons
3.I	13.48 (br, 2H)	10.75 (br,1H)	8.50 (s, 2H)	4.51 (s, 4H)	2.25(s, 3H)	7.51 (s, 2H), 7.26–7.44 (m, 10H)
3.1	13.30 (br, 1H)		9.01 (s, 1H), 8.62 (s, 1H)	4.52 (s, 2H), 4.44 (s, 2H)	2.35(s, 3H)	7.91 (s, 1H), 7.80 (s, 1H), 7.10–7.63 (m, 10H)
3.II	13.50 (br, 2H)	10.81 (br, 1H)	8.52 (s, 2H)		2.57 (s, 6H), 2.30 (s, 3H)	7.57 (s, 2H)
3.2	13.28 (br, 1H)		8.90 (s, 1H), 8.60 (s, 1H)		2.60 (s, 3H), 2.52 (s, 3H), 2.33 (s, 3H)	7.78 (s, 1H), 7.70 (s, 1H)
3.III	11.52 (br, 2H)	9.56 (br, 1H)	8.32 (s, 2H)		2.25 (s, 3H)	7.59 (s, 2H), 8.08(d, 4H)
3.3	11.41 (br, 1H)		8.40 (s, 1H), 8.38 (s, 1H)		2.35 (s, 3H)	7.40 (s, 1H),7.90 (s, 1H) 8.19 (s, 2H), 7.20 (s, 2H)

[a] Letters given in parentheses indicate the signal structure: s = singlet, m = multiplet, br = broad (unresolved).

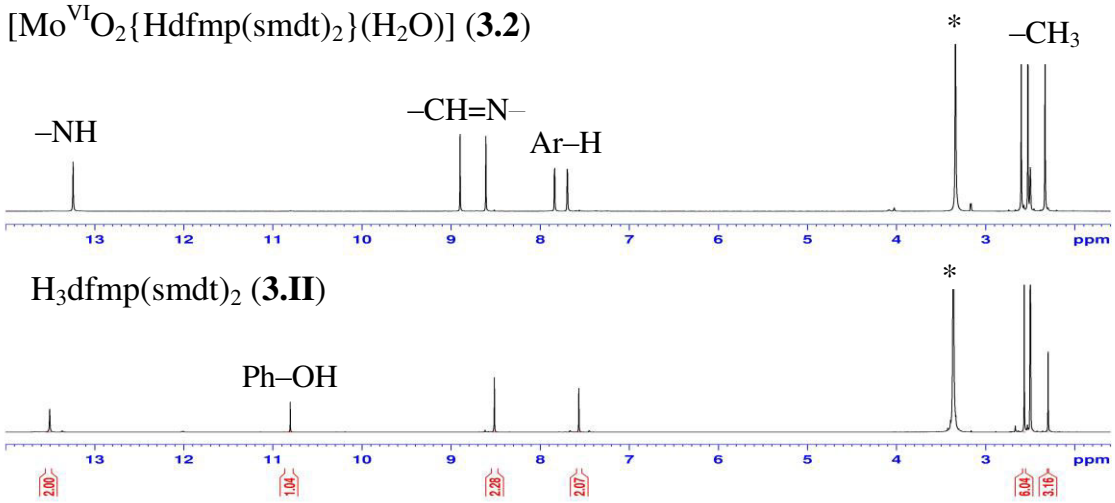

Figure 3.7. ^{1}H NMR spectra of H_3dfmp(smdt)$_2$ (**3.II**) and complex [Mo^{VI}O$_2${Hdfmp(smdt)$_2$}(H$_2$O)] (**3.2**)

The ^{13}C NMR spectra of a representative ligand H_3dfmp(smdt)$_2$ (**3.II**) and its complex **3.2** are presented in Fig. 3.8 while Table 3.7 provides entire spectral data. Assignments of the peaks are based on the intensity patterns of the chemical shift and on the coordination–induced shifts ($\Delta\delta$) of the signals for carbon atoms in the vicinity of the coordinating atoms [140]. These assignments also provide useful information for the elucidation of the structures of the complexes. Ligands **3.I**, **3.II** and **3.III** display 12, 8 and 7 signals corresponding to the 24, 16 and 14 carbon atoms, respectively due to the presence of a centre of symmetry. A maximum of 21, 13 and 11 signals were observed for complexes **3.1**, **3.2** and **3.3**, respectively due to asymmetry generated after coordination of the ligands to the molybdenum. All ligands display single signal each for azomethine (C8 and C9) and the thiolate (C10 and C11) carbon atoms. Appearance of two distinct signals each due to azomethine (C8 and C9) and the thiolate carbons (C10 and C11) with good coordination–induced shifts ($\Delta\delta$) against single signal each for these carbons in the ligands suggest the involvement of only one set of the azomethine nitrogen and the thiolate sulfur atoms in coordination. Complexes **3.1** and **3.2** shows two signals

each for $–CH_2$ and $–CH_3$ carbons due to asymmetry in the structure against single signal each for these carbons in the corresponding ligand.

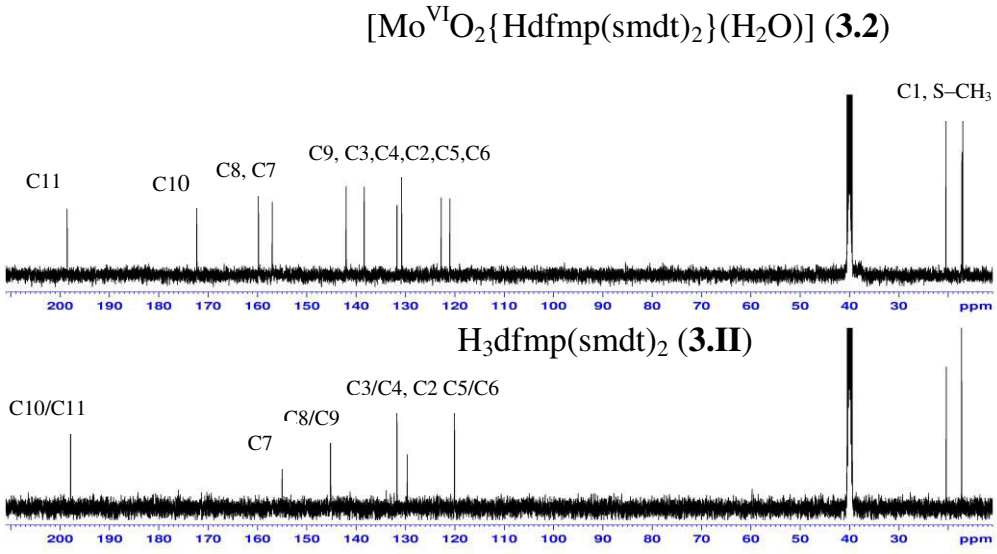

Figure 3.8. ^{13}C NMR spectra of $H_3dfmp(smdt)_2$ (**3.II**) and complex $[Mo^{VI}O_2\{Hdfmp(smdt)_2\}(H_2O)]$ (**3.2**)

Table 3.7.

^{13}C NMR spectral data of ligand and complexes

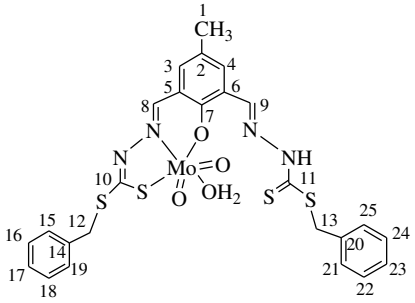

Compounds	C1	C2	C3/C4	C5/C6	C7	C8/C9
3.I	20.3	129.7	131.7	119.9	155.0	145.5
3.1 ($\Delta\delta$)	20.4	129.7	137.3, 130.5	122.6, 121.0	157.1(2.1)	160.0, 142.5 (14.5)
3.II [a]	20.4	129.6	131.7	120.1	155.0	145.2
3.2 [b] ($\Delta\delta$)	20.4	130.8	138.4, 131.7	122.7, 121.0	157.0(2.0)	159.8, 142.0 (14.6)
3.III	20.3	129.3	130.9	121.2	153.2	141.8
3.3 ($\Delta\delta$)	20.3	130.0	135.5, 130.3	122.9, 122.0	150.9(–2.3)	155.9, 138.3 (14.1)

Compounds	C10/C11	C12/C13	C14/C20	C15–C19,C21–C25
3.I	195.9	38.2	137.0	128.9, 129.4, 127.7
3.1 ($\Delta\delta$)	170.9, 196.6 (–25)	37.8, 38.0	137.4, 138.5	128.9, 129.7, 127.7, 130.9, 131.7, 127.8
3.II [a]	197.8		–	–
3.2 [b]($\Delta\delta$)	172.3, 198.5 (–25.5)		–	–
3.III	178.2	–	–	–
3.3 ($\Delta\delta$)	166.6, 178.3 (–11.6)	–	–	–

[a] Methyl carbons of **3.II** appear at 17.3 ppm.

[b] Methyl carbons of **3.2** appear at 17.0 and 17.2 ppm.

3.3.7. Catalytic activity studies

3.3.7.1. Oxidation of styrene

Oxidation of styrene catalyzed by vanadium complexes have been extensively studied where H_2O_2 has been used as oxidant [170]. At least five oxidation products have been obtained using polymer–anchored catalysts PS–[$V^{IV}O$(sal–ohyba)·DMF] [124] and PS–K[$V^{V}O(O_2)$(L)] [L = 2–(2–pyridyl)benzimidazole and 2–(3–pyridyl)benzimidazole] [171]. Oxidation of styrene, catalyzed by dioxidomolybdenum(VI) complexes using aqueous 30% H_2O_2 as oxidant did not proceed. However, addition of $NaHCO_3$ activated the catalytic oxidation process and gave two products namely, styrene oxide and phenyl acetaldehyde (Scheme 3.3). Such $NaHCO_3$ assisted oxidation of styrene has been reported in the literature [159–162].

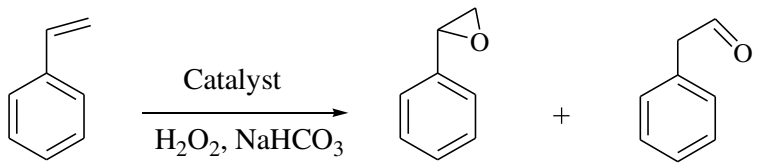

Scheme 3.3. $NaHCO_3$ activated oxidation products of styrene using H_2O_2 as oxidant.

We have selected [MoO_2{Hdfmp$(tsc)_2$}(H_2O)] (**3.3**) as a representative catalyst and optimized the reaction conditions for the maximum oxidation of styrene by studying five different parameters viz. the effect of amounts of oxidant (moles of H_2O_2 per mole of styrene), catalyst (amount of catalyst per mole of styrene), $NaHCO_3$ and solvent, and temperature of the reaction mixture in detail. The effect of oxidant was studied considering styrene: aqueous 30% H_2O_2 molar ratios of 1:2, 1:3 and 1:4, where the mixture of styrene (0.520 g, 5 mmol), catalyst (0.0005 g), $NaHCO_3$ (0.168 g, 2 mmol) and oxidant was taken in 5 ml of CH_3CN and the reaction was carried out at 60 ^oC. As illustrated in entries no. 1, 6 and 7 of Table 3.8, the percent conversion of styrene improved from 27% to 97% on increasing the styrene : oxidant ratio from 1:2 to 1:4 through 82% for 1:3, suggesting that 1:4 (styrene : H_2O_2) molar ratio is sufficient enough

to perform the reaction with good conversion. Similarly, for three different amounts viz. 0.0005, 0.0010 and 0.0015 g of catalyst at styrene to H_2O_2 molar ratio of 1:4 under above reaction conditions, 0.0005 g catalyst gave 97% conversion while 0.001 and 0.0015 g catalyst improved the conversion only slightly (98%) (entries no. 1, 2 and 3 of Table 3.8). The amount of $NaHCO_3$ has played significant role on the conversion of styrene and best conversion was obtained with 2 mmol of $NaHCO_3$ (entries no. 1, 4 and 5 in Table 3.8). In the absence of $NaHCO_3$ there was no conversion of substrate. Amongst three different temperatures of 40, 50 and 60 $^{\circ}$C for the fixed operating condition of styrene (0.52 g, 5 mmol), H_2O_2 (2.27 g, 20 mmol), $[MoO_2\{Hdfmp(tsc)_2\}(H_2O)]$ (**3.3**) (0.0005 g), $NaHCO_3$ (0.168, 2 mmol) and MeCN (5 ml), running the reaction at 60 $^{\circ}$C gave much better conversion (entries no. 1, 10 and 11 of Table 3.8). Only the time required in achieving the maximum conversion was reduced on carrying out the reaction at 80 $^{\circ}$C. Variation in the volume of CH_3CN (5, 10 and 15 ml) was also studied (entries no. 1, 8 and 9 of Table 3.8) and it was observed that 5 ml of CH_3CN was sufficient enough to get good transformation of styrene while running the reaction at 60 ^{o}C under above reaction conditions. Thus, all reaction conditions as concluded above (i.e. styrene (0.52 g, 5 mmol), H_2O_2 (2.27 g, 20 mmol), $[MoO_2\{Hdfmp(tsc)_2\}(H_2O)]$ (**3.3**) (0.0005 g), $NaHCO_3$ (0.168, 2 mmol), MeCN (5 ml) and reaction temperature 60 ^{o}C) were considered essential and applied for the maximum transformation of styrene into a mixture of oxidation products. Fig. 3.9 and Table 3.8 summarize all the conditions and conversions obtained under a particular set of conditions.

Table 3.8.

Conversion of styrene (0.520 g, 5 mmol) using $[Mo^{VI}O_2\{Hdfmp(tsc)_2\}(H_2O)]$ (**3.1**) as catalyst in 2 h of reaction time under different reaction conditions.

Entry No.	Catalyst [g (mmol)]	H_2O_2 [g (mmol)]	$NaHCO_3$ [g (mmol)]	CH_3CN [mL]	Temp. (^oC)	Conv. [%]
1	0.0005 (1.1×10^{-3})	2.27 (20)	0.168 (2)	5	60	97
2	0.0010 (2.2×10^{-3})	2.27 (20)	0.168 (2)	5	60	98
3	0.0015 (3.3×10^{-3})	2.27 (20)	0.168 (2)	5	60	98
4	0.0005 (1.1×10^{-3})	2.27 (20)	0.084 (1)	5	60	67
5	0.0005 (1.1×10^{-3})	2.27 (20)	0.252 (3)	5	60	99
6	0.0005 (1.1×10^{-3})	1.14 (10)	0.168 (2)	5	60	27
7	0.0005 (1.1×10^{-3})	1.69 (15)	0.168 (2)	5	60	82
8	0.0005 (1.1×10^{-3})	2.27 (20)	0.168 (2)	7	60	44
9	0.0005 (1.1×10^{-3})	2.27 (20)	0.168 (2)	10	60	20
10	0.0005 (1.1×10^{-3})	2.27 (20)	0.168 (2)	5	50	75
11	0.0005 (1.1×10^{-3})	2.27 (20)	0.168 (2)	5	40	33

The conversion of styrene and the selectivity of different reaction products using $[MoO_2\{Hdfmp(tsc)_2\}(H_2O)]$ (**3.3**) as catalyst under the optimized reaction conditions (entry no. 1 of Table 3.8) have been analyzed as a function of time and are presented in Fig. 3.10 and Table 3.9. Thus, under the optimized reaction conditions, the selectivity of the two oxidation products varies in the order: styrene oxide (92%) > phenyl acetaldehyde (8%). Complexes **3.1** and **3.2** also follow same order of the selectivity of products with only slightly different turn over frequencies. Blank reaction (i.e. in absence of catalyst while using H_2O_2 and $NaHCO_3$) under above reaction conditions gave 32% conversion. The reaction also carried out at room temperature under same conditions in

presence of $NaHCO_3$ only and it gave 11% conversion of styrene. All these suggest the enhancement of catalytic ability of complexes using H_2O_2 in presence of $NaHCO_3$.

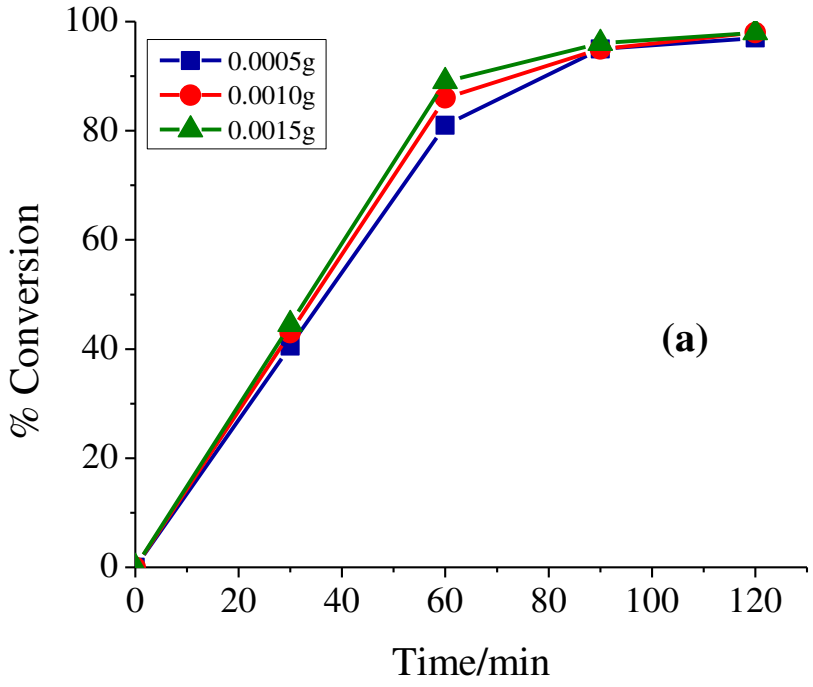

Figure 3.9. (a) Effect of catalyst amount on the oxidation of styrene. Reaction conditions: styrene (0.520 g, 5 mmol), 30 % H_2O_2 (2.27 g, 20 mmol), $NaHCO_3$ (0.168 g, 2 mmol), temperature (60 ^oC and acetonitrile (5 ml).

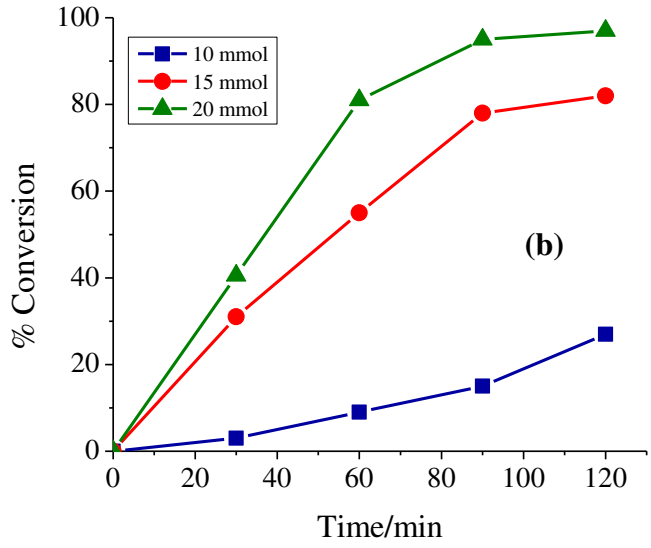

Figure 3.9. (b) Effect of oxidant amount on the oxidation of styrene. Reaction conditions: styrene (0.520 g, 5 mmol), catalyst (0.0005 g), $NaHCO_3$ (0.168 g, 2 mmol), temperature (60 ^oC) and acetonitrile (5 ml).

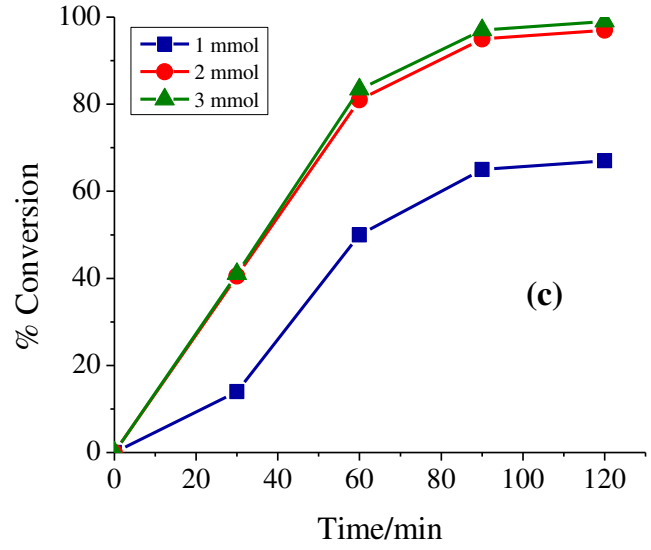

Figure 3.9. (c) Effect of $NaHCO_3$ amount on the oxidation of styrene. Reaction conditions: styrene (0.520 g, 5 mmol), catalyst (0.0005 g), 30 % H_2O_2 (2.27 g, 20 mmol), temperature (60 ^oC) and acetonitrile (5 ml).

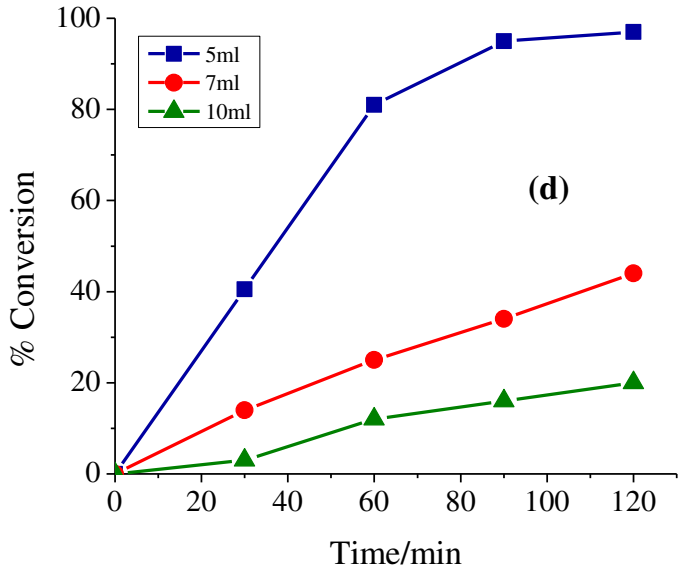

Figure 3.9. (d) Effect of solvent amount on the oxidation of styrene. Reaction conditions: styrene (0.520 g, 5 mmol), 30 % H_2O_2 (2.27 g, 20 mmol), $NaHCO_3$ (0.168 g, 2 mmol), catalyst (0.0005 g) and temperature (60 ^oC).

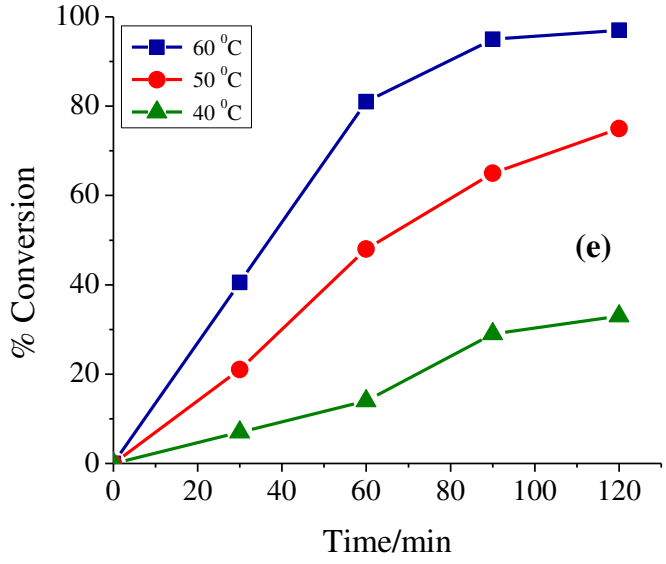

Figure 3.9. (e) Effect of temperature on the oxidation of styrene. Reaction conditions: styrene (0.520 g, 5 mmol), 30 % H_2O_2 (2.27 g, 20 mmol), $NaHCO_3$ (0.168 g, 2 mmol), catalyst (0.0005 g) and acetonitrile (5 ml).

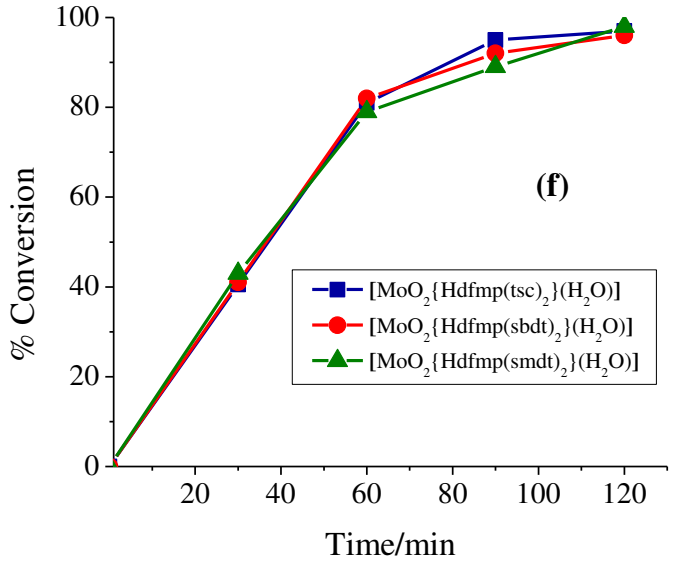

Figure 3.9. (f) Plot showing conversion of oxidation of styrene using different metal complexes.

Table 3.9.

Oxidation of styrene, TOF and product selectivity using molybdenum complexes as catalyst.

Catalyst (g, mol%)	TOF [h^{-1}][a]	Conv. [%]	Selectivity [%][b]	
			phac	so
$[Mo^{VI}O_2\{Hdfmp(sbdt)_2\}(H_2O)]$ (0.0005g, 0.015)	3243	96	7	93
$[Mo^{VI}O_2\{Hdfmp(smdt)_2\}(H_2O)]$ (0.0005g, 0.019)	2552	98	6.7	93.3
$[Mo^{VI}O_2\{Hdfmp(tsc)_2\}(H_2O)]$ (0.0005g, 0.022)	2204	97	8	92
Blank reaction	–	32	4	96

[a] TOF values calculated at 2 h of reaction time.

[b] so: styrene oxide; phac: phenyl acetaldehyde.

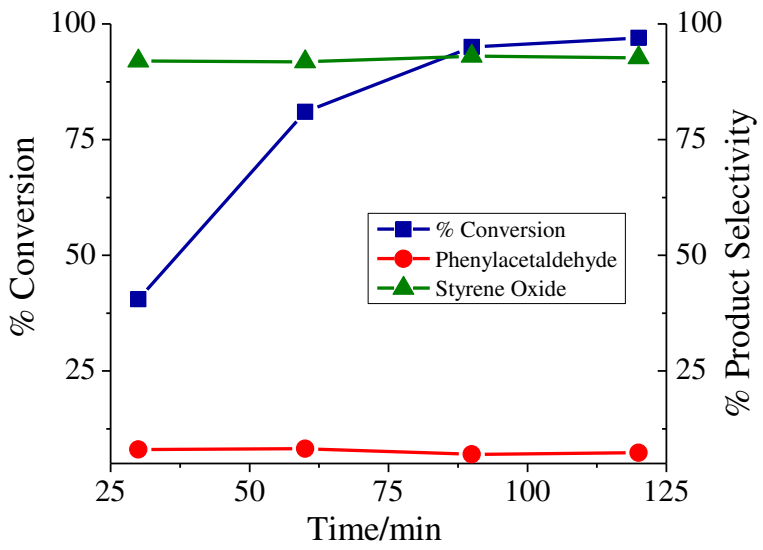

Figure 3.10. Profiles showing conversion and selectivity of products as a function of time.

3.3.7.2. Oxidation of cyclohexene

Complex $[Mo^{VI}O_2\{Hdfmp(tsc)_2\}(H_2O)]$ (**3.3**) was also used as a representative catalyst to study oxidation of cyclohexene by H_2O_2 and $NaHCO_3$ was found necessary to assist the catalytic activity. As shown in Scheme 3.4 it gave only cyclohexene oxide selectively.

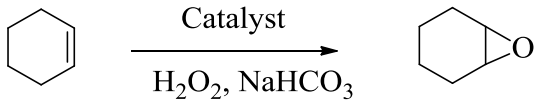

Scheme 3.4. $NaHCO_3$ activated oxidation product of cyclohexene using H_2O_2 as oxidant.

In order to achieve optimum reaction conditions, three different cyclohexene to aqueous 30% H_2O_2 molar ratios viz. 1:2, 1:4 and 1:6 were considered for the fixed amount of cyclohexene (0.41 g, 5 mmol), $NaHCO_3$ (0.168 g, 2 mmol) and catalyst

(0.0005 g) in 5 ml of MeCN and reaction was carried out at 60 ^{o}C. As presented in entries no. 1, 6 and 7 of Table 3.10 and Fig. 3.11 (a), a maximum of 22% conversion was obtained at a cyclohexene to H_2O_2 molar ratio of 1:2 in 2.5 h of reaction time. This conversion reached 96% on increasing this ratio to 1:4 while 1:6 ratio has shown only marginal improvement (98%) in the conversion. Under the operating conditions as fixed above i.e. cyclohexene (0.41 g, 10 mmol), 30% H_2O_2 (2.27 g, 20 mmol), $NaHCO_3$ (0.168 g, 2 mmol) in 5 ml of MeCN, the effect of catalyst considering three different amounts viz. 0.0005, 0.0010 and 0.0015 g as a function of time was studied and results are illustrated in Fig. 3.11 (b) (also see entries no. 1, 2 and 3 of Table 3.10). It is clear from the plot that 0.0005 g catalyst was the best one to obtain a maximum of 96% conversion of cyclohexene as 0.001 and 0.0015 g catalysts showed only marginal improvement in conversion. We have also optimized the amount of $NaHCO_3$ (entries no. 1, 4 and 5), the amount of solvent (acetonitrile, entries no. 1, 8 and 9) and temperature (entries no. 1, 10 and 11) of the reaction and found that 2 mmol of $NaHCO_3$, 5 ml of solvent and 60°C reaction temperature were sufficient enough to obtained 96% conversion under above reaction conditions. Table 3.10 and Fig. 3.11 summarize all the conditions and conversions obtained under a particular set of conditions. No conversion of substrate in the absence of $NaHCO_3$ was obtained. Blank reaction (i.e. in absence of catalyst while using H_2O_2 and $NaHCO_3$) under above reaction conditions gave 36% conversion. Oxidation reaction of cyclohexene under same conditions at room temperature, gave only 22% conversion.

Table 3.10.

Conversion of cyclohexene (0.410 g, 5 mmol) using $[Mo^{VI}O_2\{Hdfmp(tsc)_2\}(H_2O)]$ (**3.1**) as catalyst in 2.5 h of reaction time under different reaction conditions.

Entry No.	Catalyst [g (mmol)]	H_2O_2 [g (mmol)]	$NaHCO_3$ [g (mmol)]	CH_3CN [mL]	Temp. (^{0}C)	Conv. [%]
1	0.0005 (1.1×10^{-3})	2.27 (20)	0.168 (2)	5	60	96
2	0.0010 (2.2×10^{-3})	2.27 (20)	0.168 (2)	5	60	99
3	0.0015 (3.3×10^{-3})	2.27 (20)	0.168 (2)	5	60	99
4	0.0005 (1.1×10^{-3})	2.27 (20)	0.084 (1)	5	60	73
5	0.0005 (1.1×10^{-3})	2.27 (20)	0.252 (3)	5	60	99
6	0.0005 (1.1×10^{-3})	1.14 (10)	0.168 (2)	5	60	22
7	0.0005 (1.1×10^{-3})	3.39 (30)	0.168 (2)	5	60	98
8	0.0005 (1.1×10^{-3})	2.27 (20)	0.168 (2)	7	60	39
9	0.0005 (1.1×10^{-3})	2.27 (20)	0.168 (2)	10	60	20
10	0.0005 (1.1×10^{-3})	2.27 (20)	0.168 (2)	5	50	74
11	0.0005 (1.1×10^{-3})	2.27 (20)	0.168 (2)	5	40	38

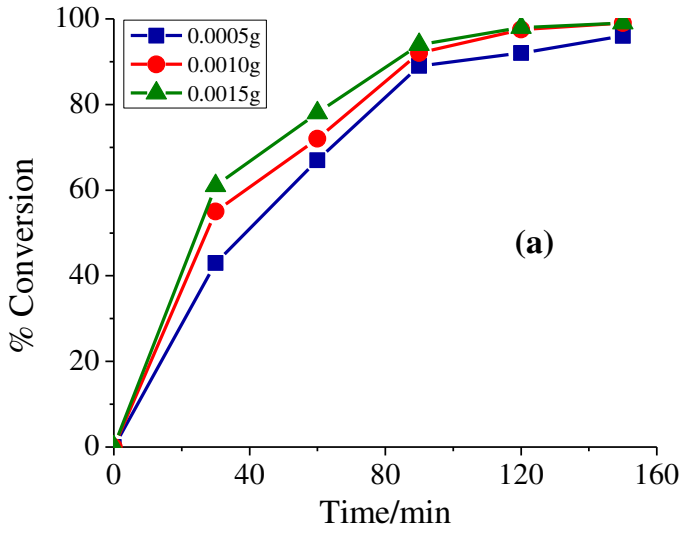

Figure 3.11. (a) Effect of catalyst amount on the oxidation of cyclohexene. Reaction conditions: cyclohexene (0.410 g, 5 mmol), 30 % H_2O_2 (2.27 g, 20 mmol), $NaHCO_3$ (0.168 g, 2 mmol), temperature (60 ^{o}C) and acetonitrile (5 ml).

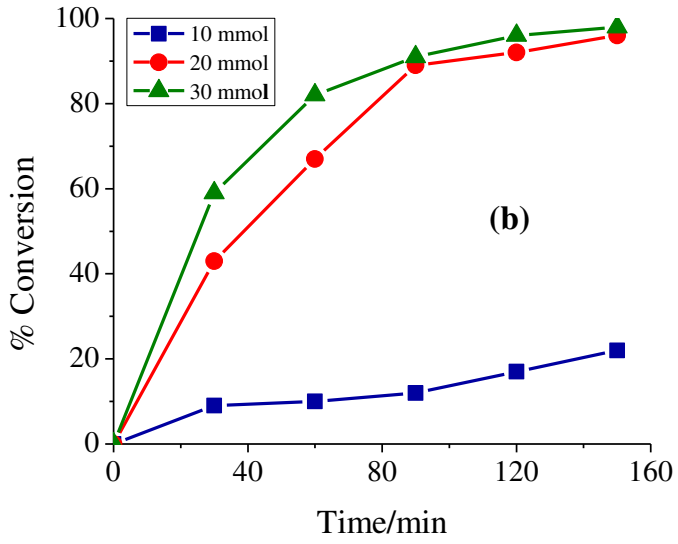

Figure 3.11. (b) Effect of oxidant amount on the oxidation of cyclohexene. Reaction conditions: cyclohexene (0.410 g, 5 mmol), catalyst (0.0005 g), $NaHCO_3$ (0.168 g, 2 mmol), temperature (60 ^oC) and acetonitrile (5 ml).

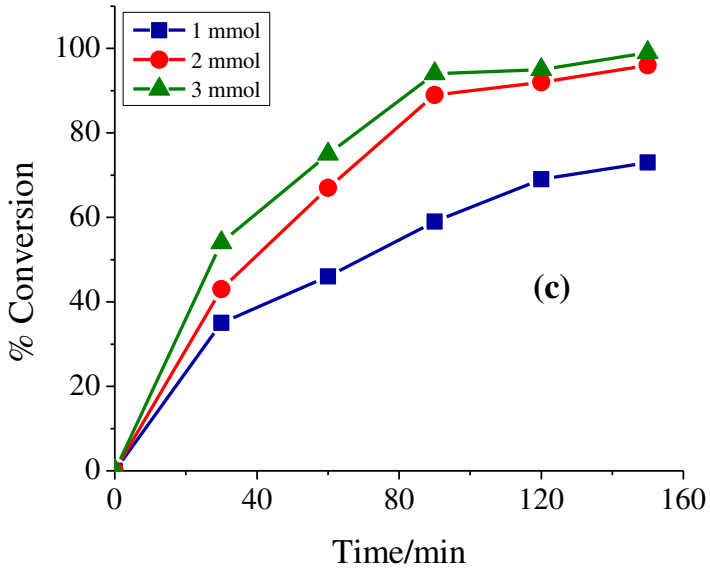

Figure 3.11. (c) Effect of $NaHCO_3$ amount on the oxidation of cyclohexene. Reaction conditions: cyclohexene (0.410 g, 5 mmol), catalyst (0.0005 g), 30 % H_2O_2 (2.27 g, 20 mmol), temperature (60 ^oC) and acetonitrile (5 ml).

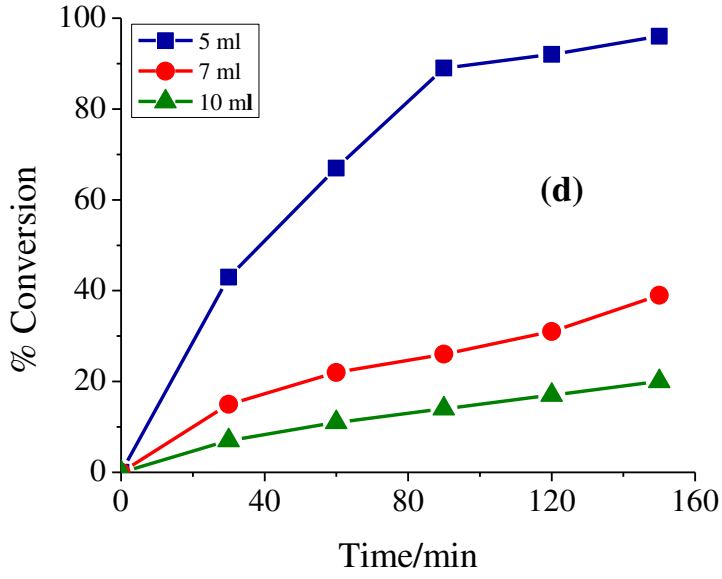

Figure 3.11. (d) Effect of solvent amount on the oxidation of cyclohexene. Reaction conditions: cyclohexene (0.410 g, 5 mmol), 30 % H_2O_2 (2.27 g, 20 mmol), $NaHCO_3$ (0.168 g, 2 mmol), catalyst (0.0005 g) and temperature (60 ^oC)

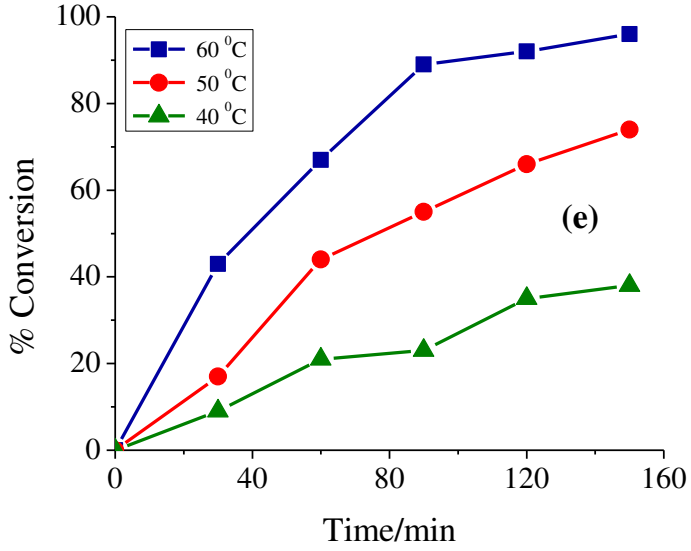

Figure 3.11. (e) Effect of temperature on the oxidation of cyclohexene. Reaction conditions: cyclohexene (0.410 g, 5 mmol), 30 % H_2O_2 (2.27 g, 20 mmol), $NaHCO_3$ (0.168 g, 2mmol), catalyst (0.0005 g) and acetonitrile (5 ml).

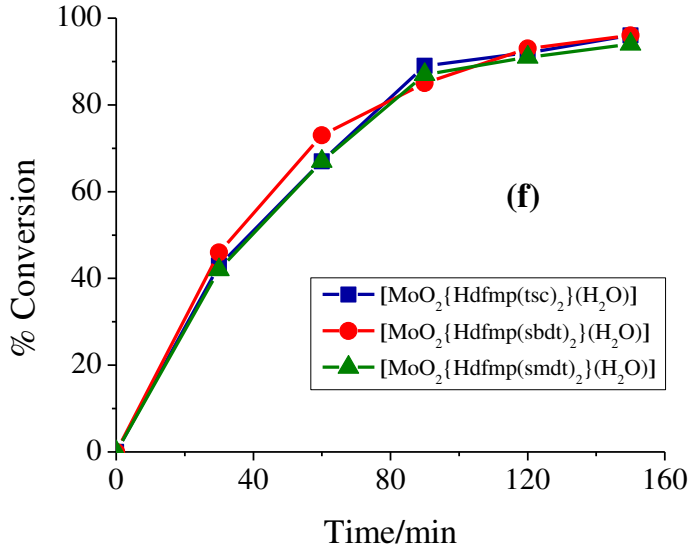

Figure 3.11. (f) Plot showing conversion of cyclohexene using different metal complexes.

Table 3.11.

Oxidation of cyclohexene, TOF and selectivity cyclohexene oxide using different dioxidomolybdenum(VI) complexes as catalyst

Catalyst (g, mol %)	TOF [h^{-1}][a]	% Conv.	% Selectivity
[$Mo^{VI}O_2${Hdfmp$(sbdt)_2$}(H_2O)] (0.0005g, 0.015)	2594	96	100
[$Mo^{VI}O_2${Hdfmp$(smdt)_2$}(H_2O)] (0.0005g, 0.019)	1958	94	100
[$Mo^{VI}O_2${Hdfmp$(tsc)_2$}(H_2O)] (0.0005g, 0.022)	1745	96	100
Blank reaction	–	36	100

[a] TOF values calculated at 2.5 h of reaction time.

3.3.8. Reactivity of dioxidomolybdenum(VI) complexes and possible mechanism for catalytic oxidation of substrates.

As observed earlier, dioxidomolybdenum(VI) complexes react with H_2O_2 to give the corresponding $[Mo^{VI}O(O_2)]^{2+}$ complexes [172]. The generation of such species has been also established in methanol by electronic absorption spectroscopy. In a typical reaction, 20 mL of 2×10^{-5} M solution of $[Mo^{VI}O_2\{Hdfmp(smdt)_2\}(H_2O)]$ (**3.2**) was treated with one drop portion of 30% aqueous H_2O_2 (0.825 g, 7.3 mmol) dissolved in 5 mL of methanol and the resultant spectroscopic changes are presented in Fig. 3.12 (a). Thus 325, 375 and 399 nm bands shift to 322, 380 and 394 nm, respectively along with only marginal change in the intensity while 208 and 280 nm bands (not shown in figure) increase their intensity considerably and finally disappear. The broad charge transfer band appearing at 435 nm slowly decreases in intensity (Fig. 3.12 (b)) along with further broadening and finally disappears upon carrying out similar titration with concentrate solution (*ca.* 10^{-4} M) of complex **3.2**. These changes indicate the interaction of $[Mo^{VI}O_2\{Hdfmp(smdt)_2\}(H_2O)]$ (**3.2**) with H_2O_2 and the plausible formation of $[Mo^{VI}O(O_2)\{Hdfmp(smdt)_2\}(H_2O)]$ (**3.2**) in methanol; Eq. (3.4). Similar changes have also been noted for other complexes; Fig. 3.12(c) and 3.12(d).

$$[Mo^{VI}O_2\{Hdfmp(smdt)_2\}(H_2O)] + H_2O_2 \rightarrow [Mo^{VI}O(O_2)\{Hdfmp(smdt)_2\}(H_2O)] + H_2O \quad (3.4)$$

To understand the combine effect of $NaHCO_3$ and H_2O_2 on $[Mo^{VI}O_2\{Hdfmp(smdt)_2\}(H_2O)]$ (**3.2**) during catalytic action, a mixture of $NaHCO_3$ (0.025g, 0.30 mmol) and 30% H_2O_2 (0.146 g, 1.3 mmol) dissolved in 5 mL of methanol was treated with 20 mL of 2×10^{-5} M solution of $[Mo^{VI}O_2\{Hdfmp(smdt)_2\}(H_2O)]$ (**3.2**). The spectral changes recorded are presented in Fig. 3.13. Surprisingly, very similar spectral changes could be obtained, as exhibited by H_2O_2 alone, after adding only few drops of a mixture of $NaHCO_3$ and H_2O_2 and thus, hinting the quick formation of oxidoperoxido species. It has been reported that $NaHCO_3$ reacts with H_2O_2 instantly and

produces HCO_4^- (peroxymonocarbonate) [159–162]. This species reacts with dioxidomolybdenum(VI) complex to give oxidoperoxidomolybdenum(VI) intermediate more rapidly as compared to H_2O_2 alone via another plausible intermediate formation, as suggested by Bhattacharya and others [159, 160] as shown in Scheme 3.5.

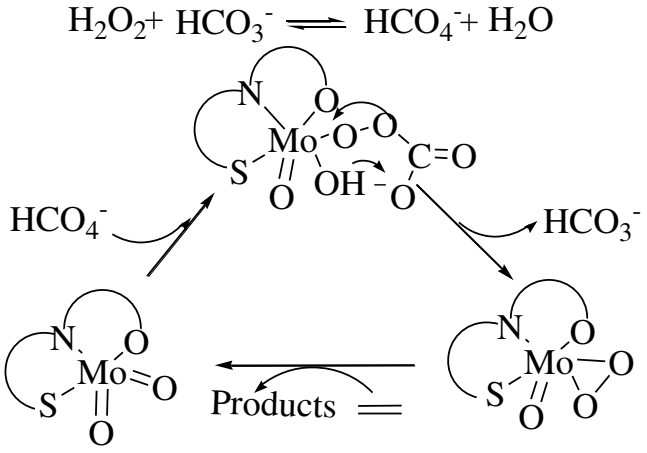

Scheme 3.5. Proposed catalytic mechanism for the oxidation of alkenes.

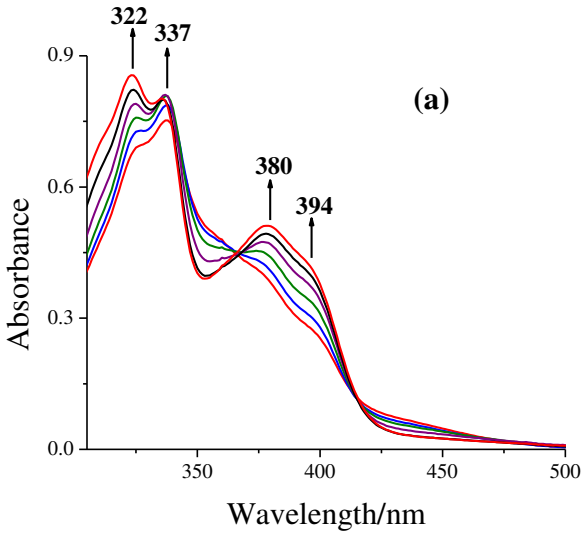

Figure 3.12. (a) The spectra were recorded after successive addition of one drop portion of 30% H_2O_2 (0.825 g, 7.3 mmol) dissolved in 5 mL of MeOH (final concentration of H_2O_2 = 1.46 M) to 20 mL of 2 × 10^{-5} M solution of [$Mo^{VI}O_2${Hdfmp(smdt)$_2$}(H_2O)] (**3.2**).

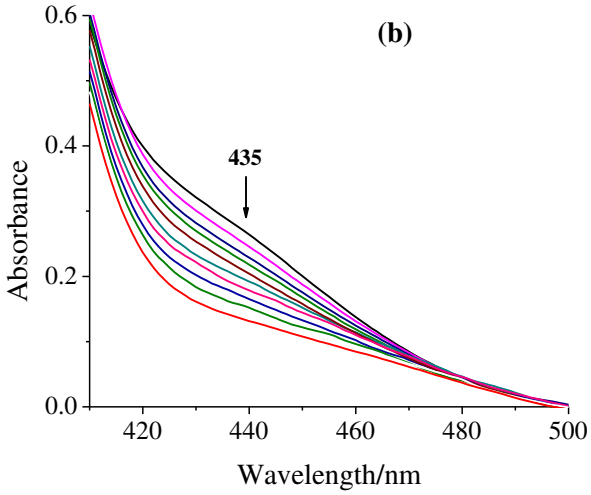

Figure 3.12. (b) The spectra were recorded after successive addition of one drop portion of 30% H_2O_2 (0.565 g, 5 mmol) dissolved in 5 mL of MeOH (final concentration of H_2O_2 = 0.97 M) to 20 mL of 10^{-4} M solution of [$Mo^{VI}O_2${Hdfmp(smdt)$_2$}(H_2O)] (**3.2**).

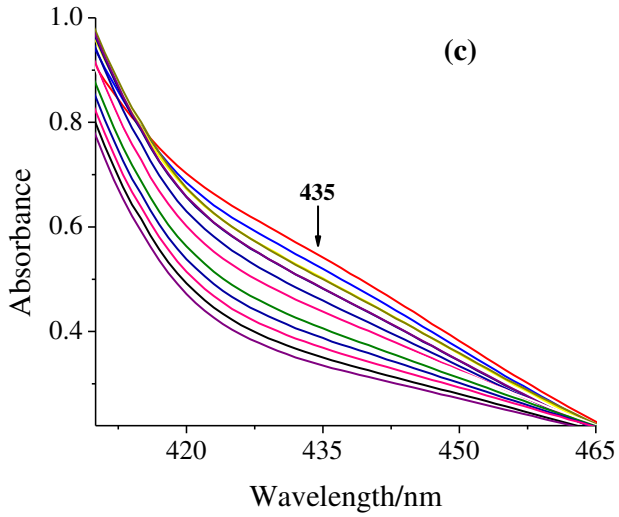

Figure 3.12. (c) The spectra were recorded after successive addition of one drop portion of 30% H_2O_2 (0.715 g, 6.3 mmol) dissolved in 5 mL of MeOH (final concentration of H_2O_2 = 1.25 M) to 20 of mL of 1.2 × 10^{-4} M solution of [$Mo^{VI}O_2${Hdfmp(sbdt)$_2$}(H_2O)] (**3.1**).

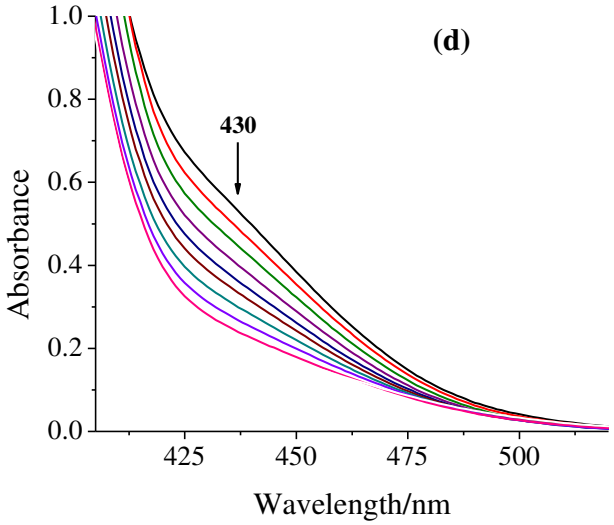

Figure 3.12. (d) The spectra were recorded after successive addition of one drop portion of 30% H_2O_2 (0.450 g, 4.0 mmol) dissolved in 5 mL of MeOH (final concentration of H_2O_2 = 0.79 M) to 20 mL of 1.7 × 10^{-4} M solution of [$Mo^{VI}O_2${Hdfmp(tsc)$_2$}(H_2O)] (**3.3**).

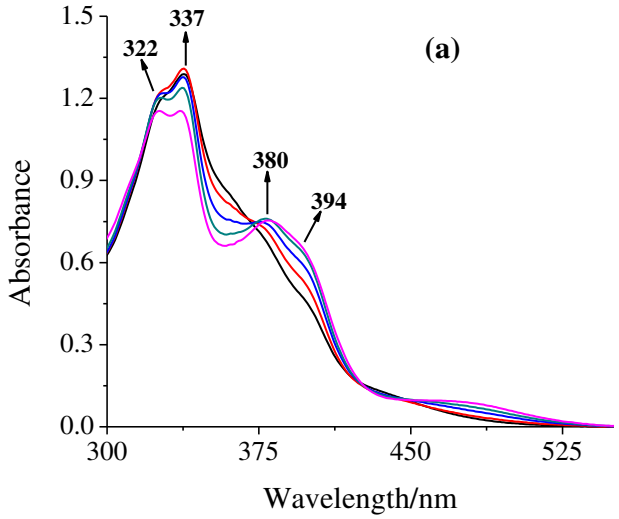

Figure 3.13. (a) The spectra were recorded after successive addition of one drop portion of mixture of $NaHCO_3$ (0.025g, 0.30 mmol) and 30% H_2O_2 (0.146 g, 1.3 mmol) dissolved in 5 mL of MeOH to 20 mL of 2 × 10^{-5} M solution of $[Mo^{VI}O_2\{Hdfmp(smdt)_2\}(H_2O)]$ (**3.2**).

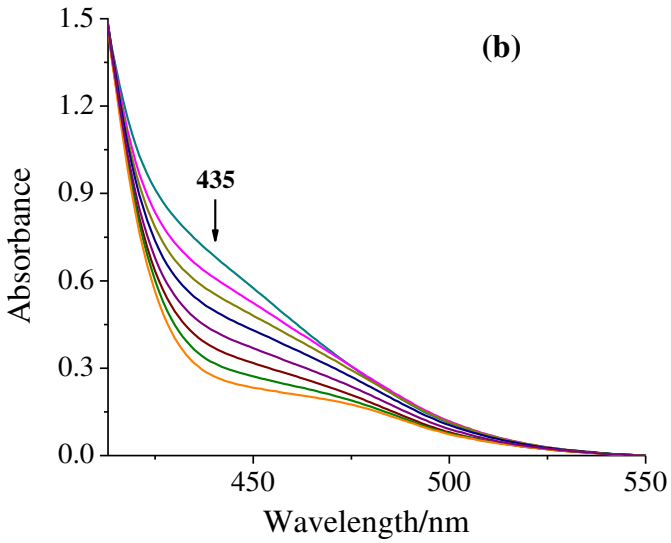

Figure 3.13. (b) The spectra were recorded after successive addition of one drop portion of mixture of $NaHCO_3$ (0.020 g, 0.24 mmol) and 30% H_2O_2 (0.073 g, 0.65 mmol) dissolved in 5 mL of MeOH to 20 mL of 10^{-4} M solution of $[Mo^{VI}O_2\{Hdfmp(smdt)_2\}(H_2O)]$ (**3.2**).

3.4. Conclusions

The dioxidomolybdenum(VI) complexes $[Mo^{VI}O_2\{Hdfmp(sbdt)_2\}(H_2O)]$ (**3.1**), $[Mo^{VI}O_2\{Hdfmp(smdt)_2\}H_2O]$ (**3.2**) and $[Mo^{VI}O_2\{Hdfmp(tsc)_2\}H_2O]$ (**3.3**) have been prepared from potential tribasic pentadentate ligands $H_3dfmp(sbdt)_2$ (**3.I**), $H_3dfmp(smdt)_2$ (**3.II**) and $H_3dfmp(tsc)_2$ (**3.III**), respectively but they behave as dibasic tridente and other set of the coordinating atoms remain free. In the solid state, the asymmetric unit of $[Mo^{VI}O_2\{Hdfmp(smdt)_2\}(DMSO)]\cdot DMSO$ (**3.2a**·DMSO) contains two complexes and form an antiparallel dimer through π–π interactions, between C=S bonds and phenol rings and between the C=N bonds. Similar π–π interactions are also present in the crystal packing of $[Mo^{VI}O_2\{Hdfmp(tsc)_2\}(MeOH)]\cdot MeOH$ (**3.3a**·MeOH), but here the interactions occur between C=N bonds and phenol rings in an antiparallel disposition while in **3.1a**·2MeOH these interactions appear only between C=N bonds.

Complexes $[Mo^{VI}O_2\{Hdfmp(sbdt)_2\}H_2O]$ (**3.1**), $[Mo^{VI}O_2\{Hdfmp(smdt)_2\}H_2O]$ (**3.2**) and $[Mo^{VI}O_2\{Hdfmp(tsc)_2\}H_2O]$ (**3.3)** are good catalyst precursors for the oxidation of styrene and cyclohexene. In the presence of sodium bicarbonate, oxidation of styrene using 30 % H_2O_2 as oxidant gave styrene oxide as a major (ca. 92%) and as a phenylacetaldehyde minor (ca. 8%) product under optimized reaction conditions. Oxidation of cyclohexene gave cyclohexene oxide selectively. No conversion of substrates in the absence of $NaHCO_3$ was obtained and thus demonstrates the importance of $NaHCO_3$ for such catalysts. These complexes upon treatment with $NaHCO_3$ and H_2O_2 in methanol instantly generate oxidoperoxido species in solution which is considered to be the intermediate species responsible for the transfer of oxygen to the substrates during catalytic oxidation.

CHAPTER 4

Oxidation of secondary alcohols by conventional and microwave-assisted methods using molybdenum complexes of ONO donor ligands

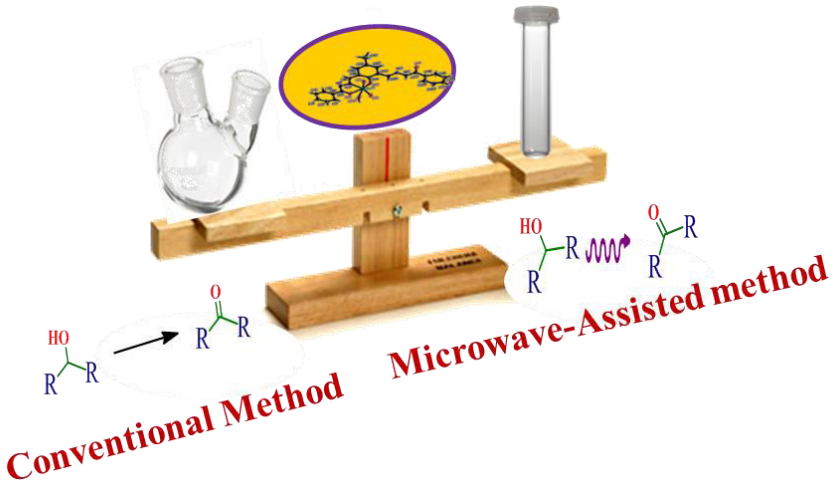

The matter of this chapter is published in the journal "New Journal of Chemistry"

4.1. Introduction

The oxidation of volatile organic compounds e.g. secondary alcohols to respective carbonyl compounds as crucial precursors of drugs, dyes and fine chemicals have attracted much attention in chemical research during last few decades [173–175]. Recently, considerable efforts have been paid in investigating highly efficient catalytic processes for oxidation of alcohols [176,177]. Traditional oxidation reactions can be efficient and selective but they often involve the use of harmful oxidants, such as CrO_3, $KMnO_4$ etc. in the presence of halogenated/ non–halogenated solvents, which result in the generation of large amounts of waste. To minimize harmful wastes, the development of catalytic oxidation procedures that involve green oxidants, e.g. dioxygen or peroxides [H_2O_2, *tert*–butylhydroperoxide (TBHP)], is a matter of current interest and out of these H_2O_2 is widely used in liquid oxidation of organic compounds due to its clean and environment friendly nature [178,179]. Molybdenum compounds are considered to be very effective catalysts for the oxidation of organic compounds with TBHP and H_2O_2 [158,180]. A number of soluble molybdenum complexes bearing different ligands have been synthesized and employed as homogeneous catalysts for the epoxidation of alkenes [181,182]; molybdenum complexes catalyzed oxidation of alcohols are also reported in the literature [183,184].

The microwave irradiation is an alternate method compared to conventional liquid phase method and has widely been applied in syntheses of organic compounds [185–190]. Here, the energy is transferred directly to the reaction components resulting in shorter reaction time compared to conventional reactions [185] and cleaner reaction with a better yield and selectivity [191–192]. Addition of small amount of solvent to the reaction mixture generally improves efficiency of the catalyst due to its smooth and homogenous heating.

The hydrazones are relatively cheap and environmentally tolerable ligands, which are available commercially or can be synthesize through simple synthetic procedures [193–195]. The *cis*–$[Mo^{VI}O_2]^{2+}$ complexes of Schiff bases having ONO donor sites have drawn much attention due to their interesting catalytic properties [39, 50, 87, 158, 193].

Herein, we have selected ligands derived from 2,6–diformyl–4–methylphenol (dfmp) and aromatic hydrazides [benzoylhydrazide (bhz), isonicotinoylhydrazide (inh) and nicotinoylhydrazide (nah)] which are potential tribasic pentadenate O, N and O donors (Scheme 4.1) but they sometimes behave only as tridentate ONO due to non–participation of the potential coordination sites of one of the arms. Their new *cis*–$[Mo^{VI}O_2]^{2+}$ complexes, characterization and catalytic potential in the production of ketones by conventional liquid phase and microwave assisted peroxidative oxidation of secondary alcohols are reported.

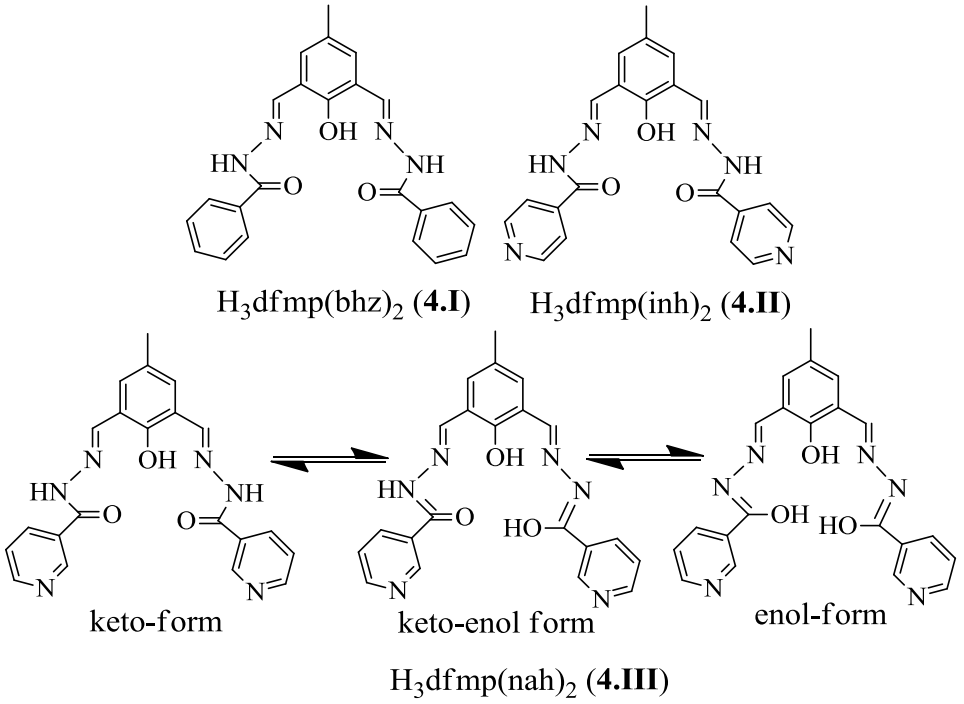

Scheme 4.1. Structures of the ligands designated by **4.I**, **4.II** and **4.III** used in this work.

4.2. Experimental Section

4.2.1. Materials and methods

Ethyl benzoate, hydrazine hydrate, isonicotinoylhydrazide (LobaChemie, Mumbai, India), nicotinic acid hydrazide (Acros organics, New Jersey, USA), 1–phenyl ethanol (Aldrich Chemicals Co., U.S.A.), 2–propanol (Thomas Baker, Mumbai, India) and 2–

butanol (Sisco research laboratory, Mumbai, India) were used as obtained. The ligands H_3dfmp(bhz)$_2$ (**4.I**), H_3dfmp(inh)$_2$ (**4.II**) and H_3dfmp(nah)$_2$ (**4.III**) were prepared according to the reported method [143]. Benzoyl hydrazide was prepared by the reaction of a twofold excess of hydrazine hydrate with ethyl benzoate in ethanol. Details of other chemicals are given in chapter 2

4.2.2. Instrumentation and characterization Procedures

Details of instrumentation and characterization procedures are presented in chapter 2.

4.2.3. Preparations

4.2.3.1. Preparation of [$Mo^{VI}O_2${Hdfmp(bhz)$_2$}(MeOH)] (4.1)

A solution of [$Mo^{VI}O_2$(acac)$_2$] (0.66 g, 2 mmol) dissolved in 10 ml of methanol was added to a stirred solution of H_3dfmp(bhz)$_2$ (**4.I**) (0.80 g, 2 mmol) in methanol (20 ml) and the obtained reaction mixture was stirred at room temperature whereupon an yellow solid started to form. After 3h of stirring, the separated solid was filtered, washed with cold methanol followed by petroleum ether and dried in a vacuum desiccator over silica gel. Yield: 1.03 g (92.0%). Anal. Calc. for $C_{24}H_{22}N_4O_6Mo$ (558.39): C, 51.62; H, 3.97; N, 10.03. Found: C, 51.93; H, 3.86; N, 10.24 %. X–ray diffraction quality crystals of **4.1** having formulation [$Mo^{VI}O_2${Hdfmp(bhz)$_2$}(H_2O)]·DMSO (**4.1a**) were grown by diffusing MeOH to a DMSO–water (95:5) solution of complex.

4.2.3.2. Preparation of [$Mo^{VI}O_2${Hdfmp(inh)$_2$}(MeOH)] (4.2)

Complex **4.2** was prepared from [$Mo^{VI}O_2$(acac)$_2$] (0.66 g, 2 mmol) and H_3dfmp(inh)$_2$(**4.II**) (0.804, 2 mmol) in methanol by the method used for **4.1**. The separated yellow solid was filtered, washed with cold methanol followed by petroleum ether and dried in a vacuum desiccator over silica gel. Yield: 1.02 g (91.0%). Anal. Calc. for $C_{22}H_{20}N_6O_6Mo$ (560.37): C, 47.15; H, 3.60; N, 15.00. Found: C, 47.68; H, 3.56; N, 15.20 %.

4.2.3.3. Preparation of $[Mo^{VI}O_2\{Hdfmp(nah)_2\}(MeOH)]$ (**4.3**)

Complex **4.3** was prepared from $[Mo^{VI}O_2(acac)_2]$ (0.66 g, 2 mmol) and $H_3dfmp(nah)_2$ (**4.III**) (0.804 g, 2 mmol) in methanol following the method described for **4.1**. After 3h of stirring, the separated yellow solid was filtered, washed with cold methanol followed by petroleum ether and dried in a vacuum desiccator over silica gel. Yield: 1.00 g (89.3%). Anal. Calc. for $C_{22}H_{20}N_6O_6Mo$ (560.37): C, 47.15; H, 3.60; N, 15.00. Found: C, 47.28; H, 3.68; N, 15.23 %. X–ray diffraction quality crystals of **4.3** having formulation $[Mo^{VI}O_2\{Hdfmp(nah)_2\}(MeOH)]\cdot DMSO$ (**4.3**·DMSO) were grown by diffusing MeOH to a DMSO solution of complex.

4.2.4. X–Ray crystal structure determination

Three–dimensional X–ray data were collected on a Bruker Kappa Apex CCD diffractometer at room temperature for **4.1a** and low temperature for **4.3**·DMSO by the ϕ–ω scan method. Reflections were measured from a hemisphere of data collected from frames each of them covering 0.3º in ω. Of the 18084 for **4.1a** and 17509 for **4.3**·DMSO reflections measured, all were corrected for Lorentz and polarization effects and for absorption by multi–scan methods based on symmetry–equivalent and repeated reflections, 4894 and 2699, respectively, independent reflections exceeded the significance level ($|F|/\sigma|F|$) > 4.0. Complex scattering factors were taken from the program package SHELXTL [134]. The structures were solved by direct methods and refined by full matrix least–squares on F^2. In **4.1a**, hydrogen atoms were located in the difference Fourier map and left to refine freely, except for C(2), C(5), C(15), C(22) and N(4), which were included in calculated positions and refined in the riding mode. Hydrogen atoms of O(1W), C(1S) and C(2S), were located in the difference Fourier map and fixed to the corresponding atoms. In **4.3**·DMSO, hydrogen atoms were included in calculation positions and refined in the riding mode, except for C(7), C(15) and N(5), which were located in the difference Fourier map and left to refine freely. Refinements were done with allowance for thermal anisotropy of all non–hydrogen atoms. Further details of the crystal structure determination are given in Table 4.1. A final difference

Fourier map showed no residual density outside: 0.504 and –0.825 e.Å^{-3} for **4.1a** and 1.167 and –1.259 e.Å^{-3} for **4.3**·DMSO. A weighting scheme w = 1/[$\sigma^2(F_o^2)$ + (0.068800 P)^2 + 0.282000 P] for **4.1a** and w = 1/[$\sigma^2(F_o^2)$ + (0.060200 P)^2 + 12.752000 P] for **4.3**·DMSO, where P = ($|F_o|^2$ + 2$|F_c|^2$)/3, were used in the latter stages of refinement. The crystal of **4.1a** presents important disorder on DMSO molecule. The disorder on DMSO molecule was solved and the atomic sites have been observed and refined with anisotropic atomic displacement parameters. The site occupancy factor was 0.88613 for S(1S). This disorder was refined using 43 restraints (SADI, SIMU and DELU restraints were used).

Table 4.1. Crystal data and structure refinement for [$Mo^{VI}O_2${Hdfmp(bhz)$_2$}(H_2O)]·DMSO (**4.1a**) and for [$Mo^{VI}O_2${Hdfmp(nah)$_2$}(MeOH)]·DMSO (**4.3**·DMSO).

	4.1a	**4.3**·DMSO
Formula	$C_{25}H_{26}MoN_4O_7S$	$C_{24}H_{26}MoN_6O_7S$
Formula mass	622.50	638.51
T, *K*	293(2)	100(2)
Wavelength, Å	0.71073	0.71073
Crystal system	Triclinic	Triclinic
Space group	P $\bar{1}$	P $\bar{1}$
a/Å	8.782(5)	7.3114(10)
b/Å	11.521(5)	13.174(2)
c/Å	14.083(5)	13.6623(19)
α/º	106.769(5)	98.512(7)
β/º	98.537(5)	91.457(6)
γ/º	91.636(5)	90.513(7)
V/Å^3	1345.3(11)	1300.9(3)
Z	2	2

F_{000}	636	652
D_{calc}/g cm^{-3}	1.537	1.630
μ/mm^{-1}	0.616	0.641
θ/ (º)	1.53 to 32.79	1.51 to 26.20
R_{int}	0.0386	0.1632
Crystal size/ mm^3	0.29 × 0.24 × 0.21	0.10 × 0.06 × 0.03
Goodness–of–fit on F^2	1.094	1.112
R_1 [a]	0.0460	0.0830
wR_2 (all data) [b]	0.1421	0.2258
Largest differences peak and hole (eÅ^{-3})	0.504 and –0.825	1.167 and –1.259

[a] $R_1 = \Sigma \left| \left| F_o \right| - \left| F_c \right| \right| / \Sigma \left| F_o \right|$. [b] $wR_2 = \{\Sigma[w(\left| \left| F_o \right|^2 - \left| F_c \right|^2 \right|)^2] / \Sigma[w(F_o^4)]\}^{1/2}$

4.2.5. Catalytic activity studies

4.2.5.1. Oxidation of secondary alcohols with aqueous H_2O_2

4.2.5.1.1. Conventional liquid phase method

Oxidation reactions were carried out in a 50 mL round–bottom flasks equipped with a reflux condenser. Under typical conditions, secondary alcohol 5 mmol {1–phenyl ethanol (0.610 g), 2– propanol (0.300 g) or 2– butanol (0.370 g)}, aqueous 30% H_2O_2 (1.69 g, 15 mmol), additive (0.250 g) and catalyst (0.002 g) were dissolved in acetonitrile (5 mL) and the obtained solution was stirred for a particular time depending upon the substrate using magnetic stirrer. The desired reaction temperature (typically 80 ^oC) was maintained using an oil bath. The reaction was monitored by withdrawing small aliquots of the reaction mixture at definite time interval, extracting with hexane and analyzing quantitatively by gas chromatograph. The identities of the products were confirmed by GC–MS.

4.2.5.1.2. Microwave–assisted method

Anton Paar Monowave 300 Microwave synthesis reactor equipped with IR sensing probe to control the reaction temperature was used to carry out all catalytic reactions. Non–thermal effects were not studied as the instrument does not permit to work below 40 ^{o}C. The oxidation of secondary alcohols was carried out in a sealed Pyrex tube under focused microwave irradiation under the reaction conditions pre–fixed for conventional liquid phase method in the minimum amount of solvent. The reaction mixture was irradiated (25 W) along with stirring for 30–120 min (depending up on the substrate) at 80 ^{o}C. After cooling the reaction mixture to room temperature, it was extracted with hexane and analyzed by GC and GC–MS.

4.3. Results and discussion

4.3.1. Synthesis and characterization of complexes

Scheme 4.2 provides idealized structures of the complexes, which are based on the spectroscopic (IR, UV/Vis, ^{1}H and ^{13}C NMR) data, elemental analyses and X–ray diffraction studies of $[Mo^{VI}O_2\{Hdfmp(bhz)_2\}(H_2O)]\cdot DMSO$ (**4.1a**) and $[Mo^{VI}O_2\{Hdfmp(nah)_2\}(MeOH)]\cdot DMSO$ (**4.3**·DMSO).

The dioxidomolybdenum(VI) precursor $[Mo^{VI}O_2(acac)_2]$ reacts with the ligands $H_3dfmp(bhz)_2$ (**4.I**), $H_3dfmp(inh)_2$ (**4.II**) and $H_3dfmp(nah)_2$ (**4.III**) (*c.f.* Scheme 4.1) in methanol to give dioxidomolybdenum(VI) complexes $[Mo^{VI}O_2\{Hdfmp(bhz)_2\}(MeOH)]$ (**4.1**), $[Mo^{VI}O_2\{Hdfmp(inh)_2\}(MeOH)]$ (**4.2**) and $[Mo^{VI}O_2\{Hdfmp(nah)_2\}(MeOH)]$ (**4.3**), respectively. The ligands coordinate via the dianionic (ONO(2−)) enolate–tautomeric moiety, while other potential coordination sites remain free. [Eq. (4.1) taking **4.I** as a representative example].

$$[Mo^{VI}O_2(acac)_2] + H_3dfmp(bhz)_2 + MeOH \rightarrow [Mo^{VI}O_2\{Hdfmp(bhz)_2\}(MeOH)] + 2Hacac \quad (4.1)$$

All these complexes are soluble in methanol, ethanol and acetonitrile. In these complexes, the sixth coordination site is occupied by methanol.

4.3.2. Thermal studies

The thermal stability of monomeric complexes **4.1**, **4.2** and **4.3** has been studied under an oxygen atmosphere. These complexes lose mass roughly equal to one methanol molecule in the temperature range 100–140 °C, indicating the presence of coordinated methanol. On further increasing the temperature the solvent free complexes decompose exothermically in two/ three overlapping steps and form MoO_3 as a final product. The observed MoO_3 contents of 25.7 % at ca. 510 ^oC for **4.1**, 25.0 % at 470 ^oC for **4.2** and 24.7 % at 475 ^oC for **4.3** match closely with the calculated values of 25.9, 25.8 and 25.8 %, respectively.

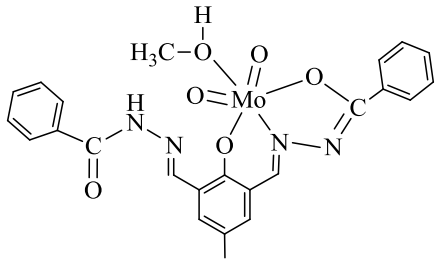

$[MoO_2\{Hdfmp(bhz)_2\}(MeOH)]$ (**4.1**)

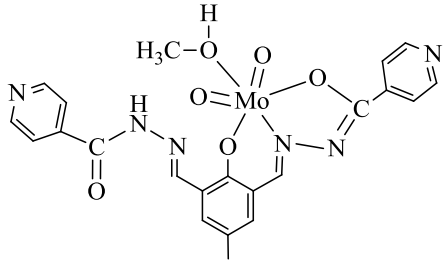

$[MoO_2\{Hdfmp(inh)_2\}(MeOH)]$ (**4.2**)

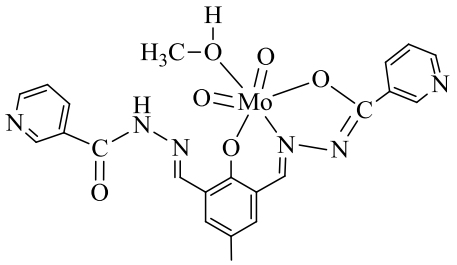

$[MoO_2\{Hdfmp(nah)_2\}(MeOH)]$ (**4.3**)

Scheme 4.2. Structure of metal complexes.

4.3.3. Structure descriptions

The ORTEP diagrams of complexes **4.1a** and **4.3**·DMSO are shown in Figs. 4.1 and 4.2, respectively. Fig. 4.3 presents the intermolecular π–π interactions. Selected bond distances and angles are given in Table 4.2. These complexes adopt a six–coordinated

structure in a distorted octahedral geometry. In the complexes, the phenolic oxygen, hydrazide oxygen and the azomethine nitrogen atoms of the ligands coordinate to the molybdenum while other set of hydrazide oxygen and azomethine nitrogen atoms of the ligands do not participate in coordination, as in other similar compounds [143]. One water molecule in **4.1a**, one methanol molecule in **4.3**·DMSO and two oxido groups complete the coordination sphere. One DMSO molecule in **4.1a** and other DMSO molecule in **4.3**·DMSO are present in the crystal packing. The DMSO molecule of **4.1a** presents a disorder on sulphur atom. Two atomic sites have been observed for the first DMSO molecule [site occupancy factor for S(1S) is 0.88613].

In complex **4.1a**, the phenyl groups of the coordinated set of two complexes interact by π–π interactions. The steric requirements, derived from coordination sphere around Mo, prevent π–π interactions between the phenol rings (see Fig. 4.3). The distances between centroids are: d_{c1-c2} = 3.727 Å [c1(C1G–C2G–C3G–C4G–C5G–C6G), c2 (C1K–C2K–C3K–C4K–C5K–C6K)]. Intermolecular hydrogen bonds are present in the crystal packing in these structures (see Table 4.3).

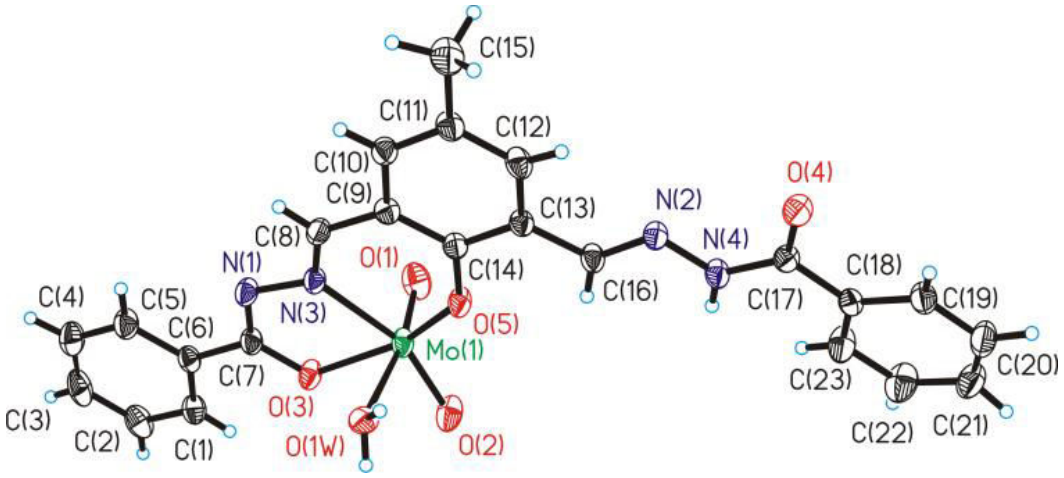

Figure 4.1. ORTEP plot of complex **4.1a**. All the non–hydrogen atoms are presented by their 30% probability ellipsoids. DMSO is omitted for clarity.

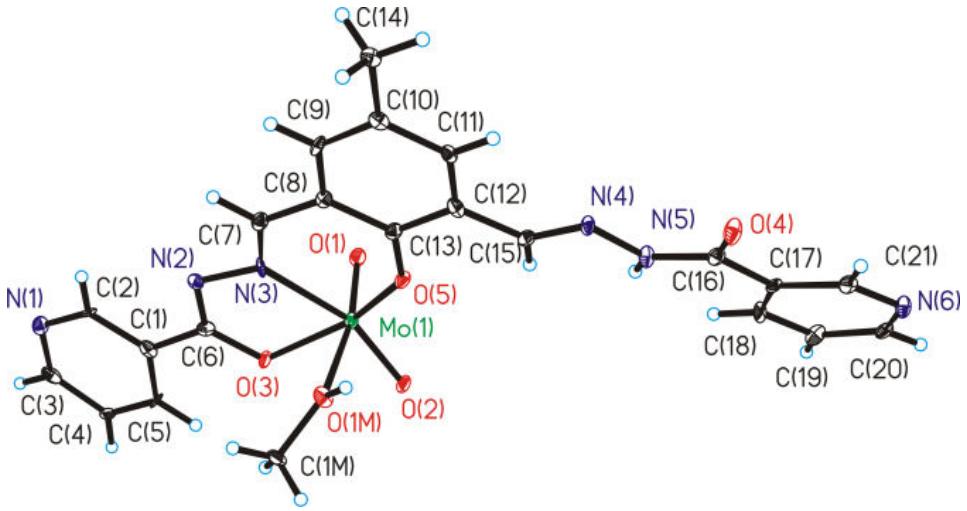

Figure 4.2. ORTEP plot of complex **4.3**·DMSO. All the non–hydrogen atoms are presented by their 30% probability ellipsoids. DMSO is omitted for clarity.

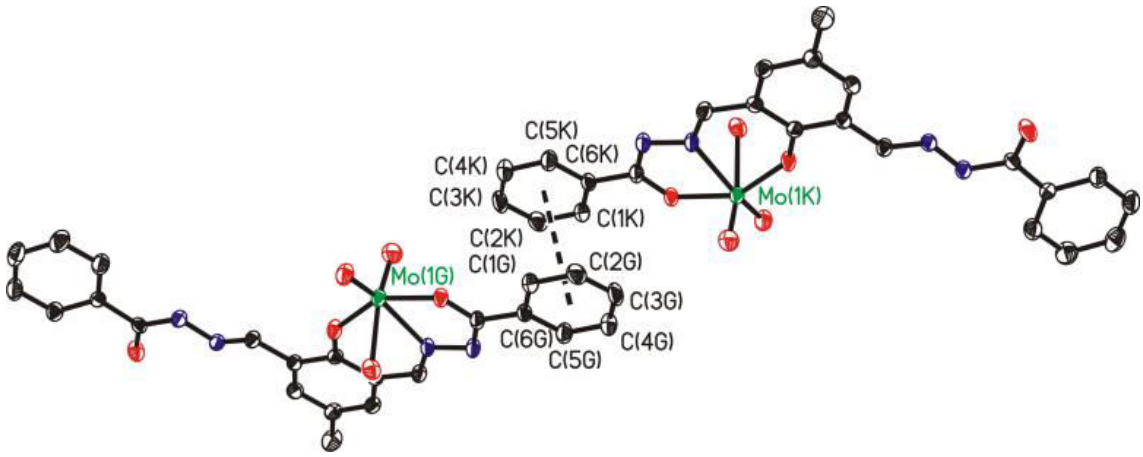

Figure 4.3. Intermolecular π–π interactions in **4.1a**. Dashed lines link the centres of the π clouds involving in each interaction.

Table 4.2.

Bond lengths [Å] and angles [°] for **4.1a** and **4.3**·DMSO

Bond lengths **4.1a**		Bond lengths **4.3**·DMSO	
Mo(1)–O(1)	1.689(3)		1.704(7)
Mo(1)–O(2)	1.697(3)		1.705(7)
Mo(1)–O(3)	2.008(2)		1.999(6)
Mo(1)–O(5)	1.922(2)		1.900(7)
Mo(1)–O(1W)	2.338(3)	Mo(1)–O(1M)	2.288(7)
Mo(1)–N(3)	2.239(3)		2.234(9)

Bond angles **1a**		Bond angles **3**·DMSO	
O(1)–Mo(1)–O(2)	105.73(16)		105.8(4)
O(1)–Mo(1)–O(5)	99.23(14)		100.2(3)
O(2)–Mo(1)–O(5)	104.24(11)		103.9(3)
O(1)–Mo(1)–O(3)	95.82(13)		95.6(3)
O(2)–Mo(1)–O(3)	96.37(11)		96.4(3)
O(5)–Mo(1)–O(3)	149.99(11)		149.6(3)
O(1)–Mo(1)–N(3)	94.05(13)		91.8(3)
O(2)–Mo(1)–N(3)	157.96(13)		160.0(3)
O(5)–Mo(1)–N(3)	81.55(10)		81.6(3)
O(3)–Mo(1)–N(3)	71.57(10)		72.1(3)
O(1)–Mo(1)–O(1W)	169.45(12)	O(1)–Mo(1)–O(1M)	167.9(3)
O(2)–Mo(1)–O(1W)	84.30(13)	O(2)–Mo(1)–O(1M)	86.1(3)
O(5)–Mo(1)–O(1W)	81.07(11)	O(5)–Mo(1)–O(1M)	77.9(3)
O(3)–Mo(1)–O(1W)	79.52(10)	O(3)–Mo(1)–O(1M)	81.2(3)
N(3)–Mo(1)–O(1W)	75.52(10)	N(3)–Mo(1)–O(1M)	76.1(3)

Table 4.3.
Hydrogen bonds for complex **4.1a** [Å and °].

D–H...A	d(D–H)	d(H...A)	d(D...A)	<(DHA)
O(1W)–H(1WB)...O(4)#1	0.87	1.86	2.726(4)	173.5
O(1W)–H(1WA)...O(4)#2	0.84	2.28	2.919(3)	132.8
O(1W)–H(1WA)...N(2)#2	0.84	2.27	3.047(4)	154.6
N(4)–H(4N)...O(1S)	0.86	2.04	2.864(4)	159.9

Symmetry transformations used to generate equivalent atoms: #1 –x+2,–y+1,–z+1 #2 x–1,y,z

4.3.4. IR spectral studies

A partial list of IR spectral data of ligands and complexes are presented in Table 4.4. Though, there are two azomethine, ketonic and NH groups present in all the ligands, they exhibit single band for each. The IR spectra of the ligands exhibit ν(NH) and ν(C=O) at 3021–3064 and 1645–1665 cm^{-1}, respectively. These bands indicate their ketonic nature in the solid state (*cf.* Scheme 4.1). All the complexes retain the positions of these bands with slight deviations along with the appearance of a new band at 1246–1259 cm^{-1} due to the ν(C–O) stretch. This observation suggests the enolization of one of the ketonic groups and replacement of H by the metal ion while the presence of a ketonic band suggests that all the ligands have at least one ketonic group free from coordination. Recently reported DFT calculations on vanadium complexes with these ligands have suggested the mixing of the enolic ν(C–O) stretch with a number of δ(CH) and δ(NH) bending modes [143]. Similarly, all complexes exhibit two azomethine stretches; one at nearly same position to that of respective ligand while other one at lower wave number (1571–1617 cm^{-1}). This shows the coordination of only one of the azomethine nitrogen to the metal ion. The presence of several medium intensity bands between 2800 and 2500 cm^{-1} in the ligands as well as in complexes suggest the existence of C–H stretching bands due to $–CH_2$. In addition, these complexes display two sharp bands at 933–944 and 914–

920 cm^{-1} due to the ν_{asym}(O=Mo=O) and ν_{sym}(O=Mo=O) streching modes, respectively due to the presence of *cis*–[$Mo^{VI}O_2$] moiety [136].

Table 4.4.

IR spectral data [in cm^{-1}] of compounds

Compounds	ν(NH)	ν(C=O)	ν(C=N)	ν(C–O)	ν(O=Mo=O)[a]
H_3dfmp(bhz)$_2$	3050	1665	1619		
[$Mo^{VI}O_2${Hdfmp(bhz)$_2$}(MeOH)]	3064	1651	1571,1616	1259	933, 914
H_3dfmp(inh)$_2$	3030	1655	1618		
[$Mo^{VI}O_2${Hdfmp(inh)$_2$}(MeOH)]	3021	1663	1577,1615	1246	944, 920
H_3dfmp(nah)$_2$	3050	1645	1616		
[$Mo^{VI}O_2${Hdfmp(nah)$_2$}(MeOH)]	3040	1652	1594,1617	1254	935, 920

[a]Asymmetric and symmetric ν(O=Mo=O) values.

4.3.5. Electronic spectral studies

The electronic absorption spectra of ligands and metal complexes were recorded in methanol successfully. Table 4.5 presents absorption maxima of the ligands and complexes with their extinction coefficients. The electronic spectra of ligands **4.I**, **4.II** and **4.III** exhibit three spectral bands at 427–453, 363–364, 300–303 and 201–218 nm [143]. Based on their extinction coefficients, these bands are interpreted as split n→π* (first two bands), π→π* and φ→φ* transitions, respectively. All these bands are present in complexes with slight variations. In addition, all complexes exhibit a medium intensity band at 430–450 nm due to ligand to metal charge transfer (LMCT) transition from the phenolate oxygen atom to an empty d–orbital of the molybdenum and n→π* (imine type) transitions [196,197]. As Mo^{VI}–complexes have $4d^0$ configuration, the d→d band is not expected.

Table 4.5.

Electronic spectral data of ligands and complexes recorded in methanol

Compound	λ_{max} /nm (ε/ $M^{-1}cm^{-1}$)
H_3dfmp(bhz)$_2$	203(5.0×10^3), 300(7.0×10^3), 363(2.5×10^3), 427(4.0×10^2)
[$Mo^{VI}O_2${Hdfmp(bhz)$_2$}(MeOH)]	299(2.5×10^4), 358(9.0×10^3), 430(5.2×10^3)
H_3dfmp(inh)$_2$	201(2.5×10^4), 303(3.4×10^4), 364(1.7×10^4), 453(2.8×10^3)
[$Mo^{VI}O_2${Hdfmp(inh)$_2$}(MeOH)]	304(1.8×10^4), 360(1.3×10^4), 450(5.4×10^3)
H_3dfmp(nah)$_2$	218(1.1×10^4), 300(2.0×10^4), 363(8.7×10^3), 453(1.2×10^3)
[$Mo^{VI}O_2${Hdfmp(nah)$_2$}(MeOH)]	300(3.0×10^4), 360(1.6×10^4), 446(6.1×10^3)

4.3.6. ^{1}H and ^{13}C NMR spectral studies

The ^{1}H NMR spectra of ligands and the corresponding complexes were recorded to confirm their coordinating modes. Table 4.6 provides ^{1}H NMR spectral data of ligands and complexes and Fig 4.4 presents representative ^{1}H NMR spectra of a ligand and the respective complex. The broad signal appearing at δ = 12.21–12.34 ppm, owing to the phenolic OH group, disappears in the spectra of the complexes due to coordination of the phenolic oxygen to the molybdenum. The appearance of two signals due to azomethine proton (each equivalent to 1H) in complexes, one at nearly same position as of ligand and other at significantly down field with a coordination–induced shifts [$\Delta\delta$= [δ(complex)–δ(free ligand)] of 0.21–0.35 ppm demonstrates the coordination of only one of the azomethine nitrogen atom. Similarly, signal equivalent to two protons due to the –NH– remains at nearly same position with one equivalent of proton, supports the enolization of only one of the NH groups and consequent replacement of H by the metal ion. Aromatic and aliphatic protons appear in the expected regions in spectra of the ligands as well as of

the complexes, with slight shifts in their positions. The entire spectral data confirms the coordination of ligands as dianionic (ONO(2−)) only.

Table 4.6.

^{1}H NMR chemical shifts[a] [δ in ppm] of ligands and complexes recorded in DMSO–d_6.

Compounds	–CH=N–	Aromatic H	
4.I	8.73(s, 2H)	7.57(m, 6H), 7.64(m, 2H), 7.95(d, 4H)	
4.1 ($\Delta\delta$)	8.94(s, 1H), 8.82(s,1H) (0.21)	7.59(m, 4H), 7.65(m, 3H), 8.02(d, 5H)	
4.II	8.74(s, 2H)	7.61(s, 2H), 7.86(d, 4H), 8.81(b, 4H)	
4.2 ($\Delta\delta$)	9.02(s, 1H), 8.81(s,1H) (0.28)	7.63(s, 1H), 7.88(d, 4H), 7.97(s, 1H), 8.79(b, 4H)	
4.III	8.75 (s, 2H)	7.69(d, 4H), 8.34(s, 2H), 8.82(s, 2H), 9.28(s, 2H)	
4.3 ($\Delta\delta$)	9.10(s, 1H), 8.80(s,1H) (0.35)	7.56(s, 2H), 7.58(s, 1H), 7.97(s, 1H), 8.32(m, 2H), 8.77(d, 3H), 8.98(s, 1H)	
Compounds	–OH	–NH	–CH_3
4.I	12.34(s, 1H)	12.15(s, 2H)	2.31(s, 3H)
4.1 ($\Delta\delta$)	– 	12.03(s, 1H) (–0.12)	2.36(s,3H) (0.05)
4.II	12.21(s, 1H)	12.43(s. 2H)	2.39(s,3H)
4.2 ($\Delta\delta$)	– 	12.21(s, 1H) (–0.22)	2.37(s, 3H) (–0.02)
4.III	12.21(s, 1H)	12.42(s, 2H)	2.37(s, 3H)
4.3 ($\Delta\delta$)	– 	12.15(s, 1H) (–0.27)	2.36(s, 3H) (–0.01)

[a]Letters given in parentheses indicate the signal structure: s = singlet, m = multiplet, d = doublet, br = broad (unresolved).

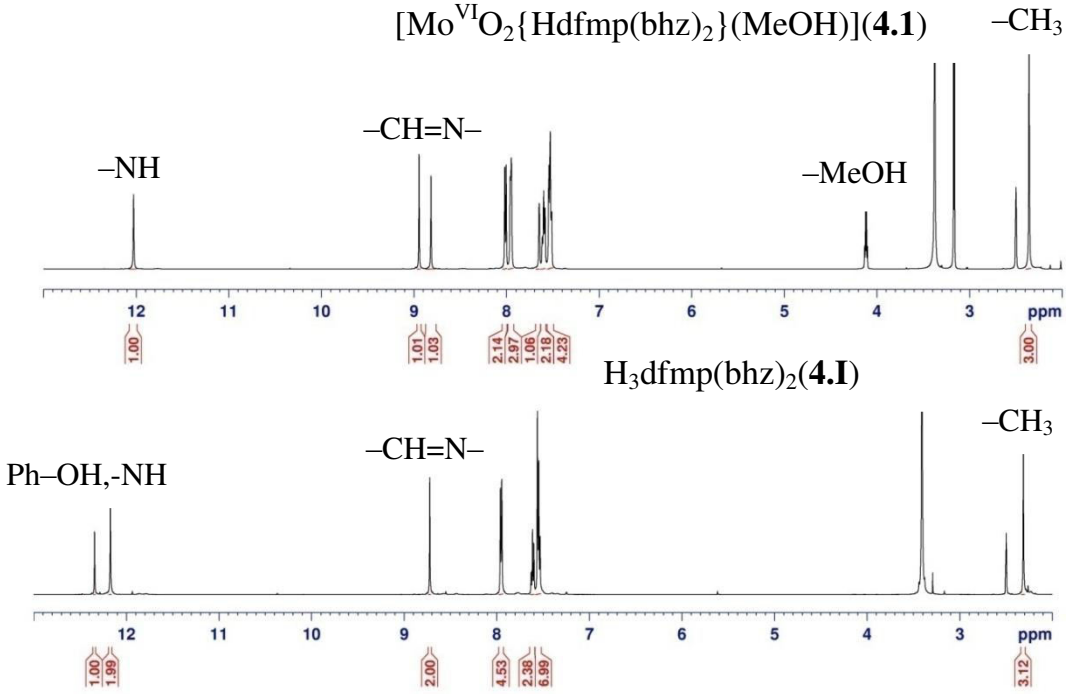

Figure 4.4. ^{1}H NMR spectra of H_3dfmp(bhz)$_2$ (**4.I**), and [Mo^{VI}O$_2${Hdfmp(bhz)$_2$}(MeOH)] (**4.1**).

The ^{13}C NMR spectra of a representative ligand **4.I** and its complex **4.1** are presented in Fig. 4.5 while Table 4.7 provides entire spectral data. Ligands **4.I**, **4.II** and **4.III** display 11, 10 and 12 signals corresponding to the 23, 21 and 21 carbon atoms, respectively due to the presence of a centre of symmetry. A total of 18, 16 and 20 signals were observed for complexes **4.1**, **4.2** and **4.3**, respectively due to asymmetry generated after coordination of the ligands to the molybdenum. All ligands display single signal each for azomethine (C8 and C9) and the enolate (C10 and C11) carbon atoms. Appearance of two distinct signals each due to azomethine (C8 and C9) and the enolate carbons (C10 and C11) with significant coordination–induced shifts ($\Delta\delta$) against one of the signal each for these two different carbons of the ligands suggest the involvement of

only one set of the azomethine nitrogen and the enolate oxygen atoms in coordination. In addition, these complexes show one signal each for coordinated MeOH. Assignments of the peaks are based on the chemical shift obtained for various carbons and on the coordination–induced shifts ($\Delta\delta$) of the signals for carbon atoms in the vicinity of the coordinating atoms [140]. These data supplement the inference obtained from IR studies.

Table 4.7.

^{13}C NMR spectral data of ligand and complexes

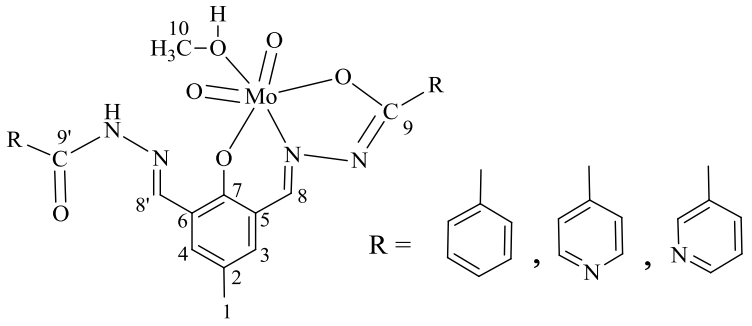

Compounds	C1	C2	C3/C4	C5/C6	C7	C8/C8'
4.I	20.38	129.03	132.47	120.37	155.18	146.63
4.1 (Δδ)	19.94	130.70	132.14	120.92	142.23 (–12.95)	163.01, 136.34 (16.38)
4.II	20.35	128.91	131.32	120.17	155.37	147.73
4.2 (Δδ)	20.35	131.36	131.98	121.22	156.34 (0.97)	163.20, 143.52 (15.47)
4.III	20.32	129.07	131.18	120.14	155.25	147.32
4.3 (Δδ)	20.35	131.37	131.69	121.27	156.55 (1.3)	162.11, 143.32 (14.79)

Compounds	C9/C9'	C10	R
4.I	163.48		133.35, 130.88, 128.73, 128.15
4.1 (Δδ)	168.90, 155.98 (5.42)	48.63	128.88, 133.20, 129.83, 131.85, 127.69, 128.04, 128.50, 123.92
4.II	161.94		140.41, 150.85, 123.25
4.2 (Δδ)	167.32, 158.41 (5.38)	48.70	138.20, 140.46, 152.02, 152.58, 129.42, 125.80
4.III	162.11		128.86, 148.99, 124.18, 152.88, 136.02
4.3 (Δδ)	167.84, 157.12 (5.73)	48.52	124.48, 126.51, 152.8, 149.07, 123.52, 124.08, 149.25, 135.95, 152.95, 137.16

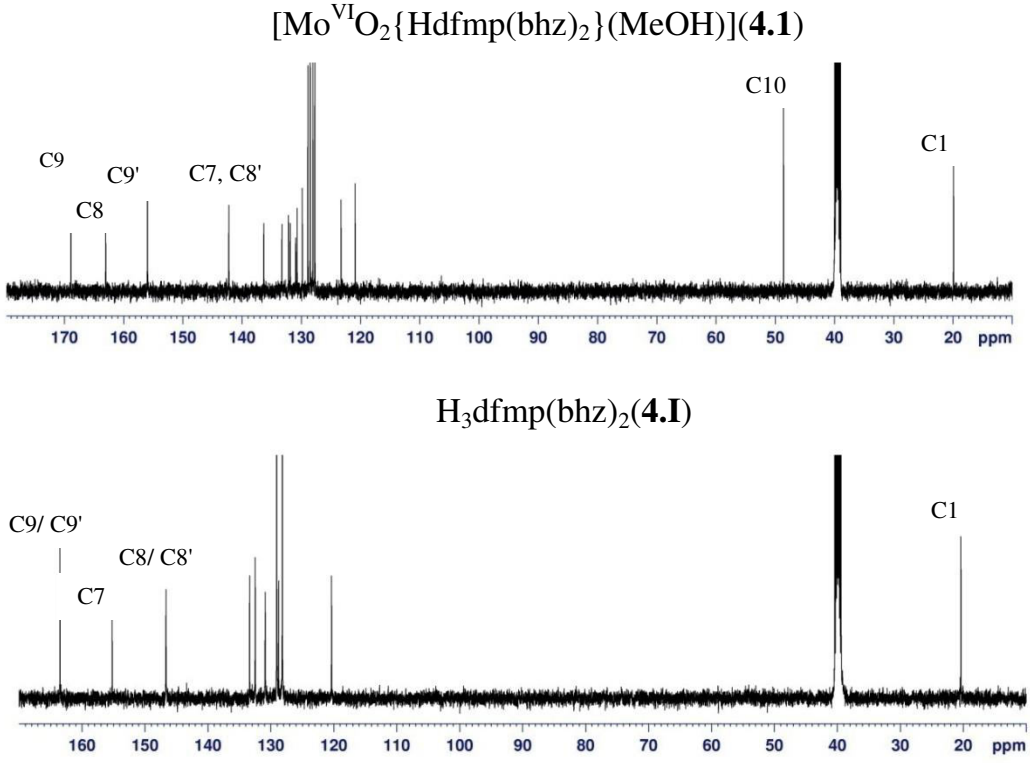

Figure 4.5. ^{13}C NMR spectra of $H_3dfmp(bhz)_2$ (**4.I**) and complex $[Mo^{VI}O_2\{Hdfmp(bhz)_2\}(MeOH)]$ (**4.1**).

4.3.7. Catalytic activity studies

4.3.7.1. Conventional liquid phase method for the oxidation of secondary alcohols

Oxidation of alcohols catalyzed by molybdenum (VI) complexes has been studied using TBHP as well as H_2O_2 as an oxidant [158,180]. All new molybdenum complexes reported here have ability to catalyze secondary alcohols *viz.* 1–phenyl ethanol, 2–butanol and 2–propanol to acetophenone, 2–butanone and acetone, respectively (Scheme 4.3), with remarkable yield as well as turn over frequency.

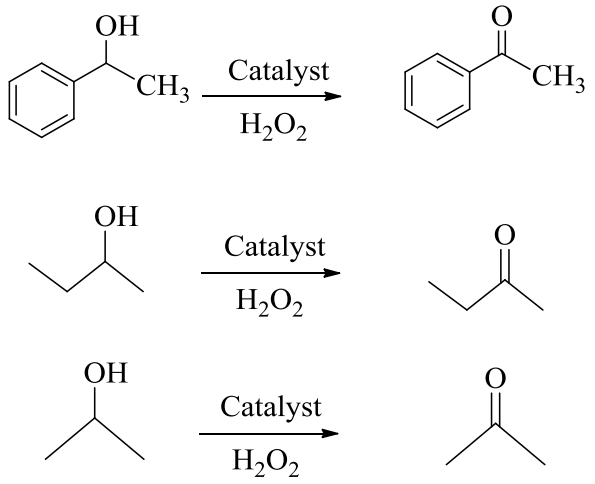

Scheme 4.3. Oxidation of secondary alcohols.

We have selected **4.1** as a representative catalyst and 1–phenyl ethanol as a representative secondary alcohol and optimized reaction conditions for the maximum oxidation of 1–phenyl ethanol by studying four different reaction parameters *viz.* the effect of amounts of catalyst, oxidant, solvent and temperature of the reaction mixture in detail. The effect of amount of catalyst was studied considering three different amounts: 0.001, 0.002 and 0.003 g of catalyst for 1–phenyl ethanol (0.610 g, 5 mmol) and aqueous 30% H_2O_2 (1.70 g, 15 mmol) in 5 ml of CH_3CN and the reaction was carried out at 80 ^oC. As illustrated in entries no. 1, 2 and 3 of Table 4.8, the percent conversion of 1–phenyl ethanol improved from 77% to 91% on increasing the amount of catalyst, from 0.001 g to 0.002 g, while 0.003 g catalyst improved the conversion only 3%, suggesting that 0.002 g of catalyst is sufficient enough to perform the reaction with good conversion. Similarly, three different molar ratios of 1–phenyl ethanol to H_2O_2were considered under above conditions (entries no. 4 and 5 of Table 4.8) and out of these 1:3 was the suitable one for the maximum conversion. Amongst three different temperatures of 60, 70 and 80 ^oC (entries no. 1, 8 and 9 of Table 4.8) for the fixed operating conditions of 1–phenyl ethanol (0.610 g, 5 mmol), H_2O_2 (1.70 g, 15mmol), **4.1** (0.002 g) and CH_3CN (5 ml), running the

reaction at 80 ^{o}C gave much better conversion. Variation in the volume of CH_3CN (5, 10 and 15 ml) was also studied (entries no. 1, 6 and 7 of Table 4.8) and it was observed that 5 ml of CH_3CN was sufficient enough to get good transformation of 1–phenyl ethanol. Thus, all reaction conditions as concluded above for 5 mmol 1–phenyl ethanol [i.e. H_2O_2 (1.70 g, 15mmol), **4.1** (0.002 g), CH_3CN (5 ml) and reaction temperature 80 ^{o}C] were considered essential and applied for the maximum transformation of 91% with 66 TOF of 1–phenyl ethanol into oxidation product. About 20 h was required to attain the equilibrium. Fig. 4.6 and Table 4.8 summarize all the conditions and conversions obtained under a particular set of conditions.

Table 4.8.

Conversion of 1–phenyl ethanol (0.61 g, 5 mmol), using **4.1** as catalyst precursor in 20 h of reaction time under different reaction conditions

Entry No.	Catalyst [g (mmol)]	H_2O_2 [g (mmol)]	CH_3CN [mL]	Temp.[^{o}C]	Conversion [%]
1	0.001 (1.8×10^{-3})	1.70 (15)	5	80	77
2	0.002 (3.5×10^{-3})	1.70 (15)	5	80	91
3	0.003 (5.3×10^{-3})	1.70 (15)	5	80	94
4	0.002 (3.5×10^{-3})	1.14 (10)	5	80	71
5	0.002 (3.5×10^{-3})	2.27 (20)	5	80	94
6	0.002 (3.5×10^{-3})	1.70 (15)	10	80	84
7	0.002 (3.5×10^{-3})	1.70 (15)	15	80	81
8	0.002 (3.5×10^{-3})	1.70 (15)	5	70	80
9	0.002 (3.5×10^{-3})	1.70 (15)	5	60	69

Under the optimized reaction conditions other catalysts precursors have also been tested and their catalytic potentials are equally good. The oxidation of other two alcohols, 2–butanol and 2–propanol using catalysts **4.1**, **4.2** and **4.3** under above optimized reaction

conditions gave 86–87% conversion in 8h with TOF of ca. 150 and 90–94% conversion in 6 h with TOF of ca. 210.

The addition of N–based additive like NEt_3 [179], accelerates the reaction with equally good conversion and reduces the equilibrium attainment time from 20h to 8 h, 8h to 3h and 6h to 2h for the substrate 1–phenyl ethanol, 2–butanol and 2–propanol, respectively.

Blank reaction (i.e. in absence of catalyst) under above reaction conditions gave 28% conversion for 1–phenylethanol, 32% conversion for 2–butanol and 38% conversion for 2–propanol.

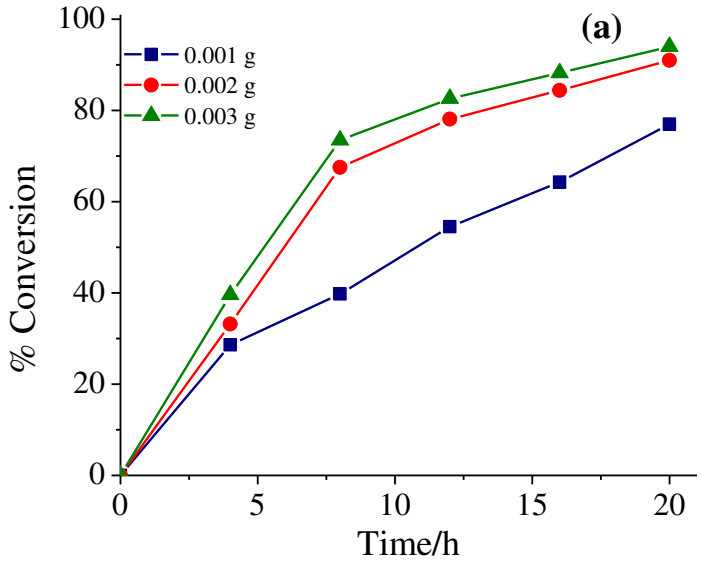

Figure 4.6. (a) Effect of catalyst amount on the oxidation of 5 mmol of 1–phenyl ethanol. Other reaction conditions: 30 % H_2O_2 (1.70g, 15 mmol), temperature (80 ^oC) and acetonitrile (5 ml).

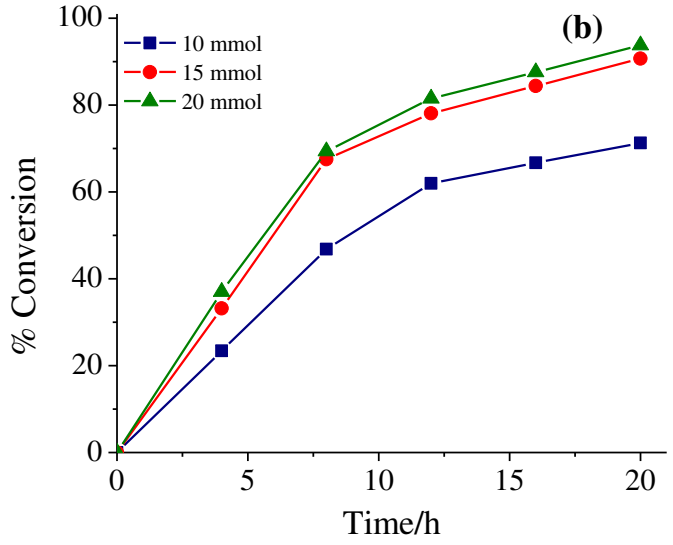

Figure 4.6. (b) Effect of oxidant amount on the oxidation of 5 mmol of 1–phenyl ethanol. Other reaction conditions: catalyst (0.002 g), temperature (80 ^{o}C) and acetonitrile (5 ml).

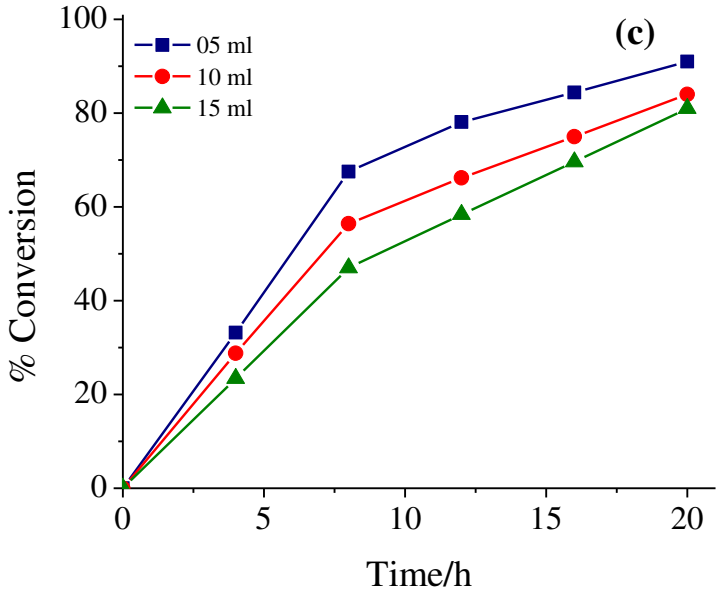

Figure 4.6. (c) Effect of solvent amount on the oxidation of 5 mmol of 1–phenyl ethanol. Other reaction conditions: catalyst (0.002 g), 30 % H_2O_2 (1.70 g, 15 mmol) and temperature (80 ^{o}C)

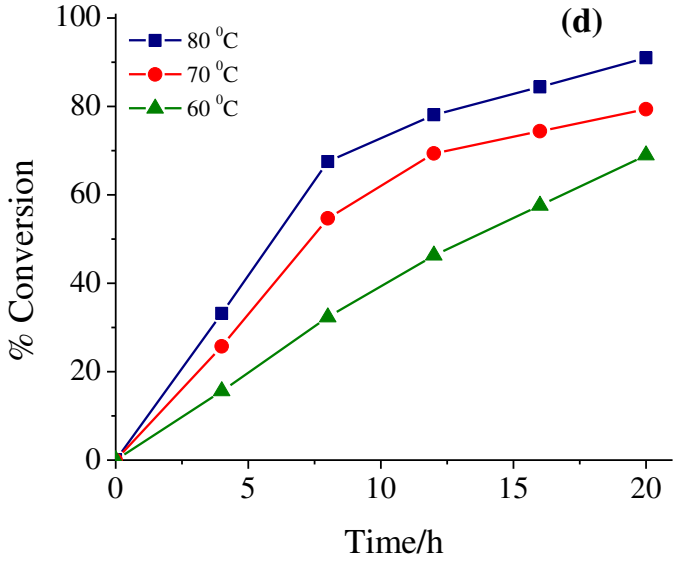

Figure 4.6. (d) Effect of temperature variation on the oxidation of 5 mmol of 1–phenyl ethanol. Other reaction conditions: catalyst (0.002 g), 30 % H_2O_2 (1.70 g, 15 mmol) and acetonitrile (5 ml).

4.3.7.2. Microwave assisted oxidation of secondary alcohols

Oxidation of secondary alcohols, catalyzed by copper complexes, by Microwave–assisted method has been reported in the literature [179,198]. Complexes **4.1**, **4.2** and **4.3** were also tested as catalyst precursor for the oxidation of 1–phenylethanol to acetophenone using aqueous 30 % H_2O_2 as oxidizing agent, under typical conditions of 80 °C in acetonitrile with low power (25 W) microwave irradiation (MW) for 30–120 min reaction time. The catalytic reactions in microwave were carried out under the same optimized reaction conditions as concluded for conventional method and the obtained results are summarized in Table 4.9 and compared with the results obtained by conventional method. It is clear from the data of table that reaction completes within 2 h compared to 20 h by conventional method. This time was further reduced to 1 h when additive NEt_3 (0.250 g) was used. Under the same reaction conditions other secondary

alcohols, 2–butanol and 2–propanol were also tested and similar proportionate reduction in reaction time was noted (Table 4.9). Apart from the respective ketone, GC and GC–MS analyses of the final reaction mixtures show no traces of by–product except the unreacted substrate. Thus, catalytic efficiency as well as selectivity of catalysts by microwave assisted method is comparable to conventional liquid phase oxidation method.

Control experiments (blank tests) were also carried out using microwave irradiation method and obtained conversions are 17% for 1–phenylethanol, 31% for 2–butanol and 23% for 2–propanol under the same experimental conditions.

Table 4.9.

Oxidation of alcohols by both conventional and microwave assisted method using molybdenum complexes as catalyst.

	Conventional method			
	Without additive		With additive [a]	
Catalyst	Conv. %	Time (h)	Conv. %	Time (h)
1– phenyl ethanol				
4.1	91	20	90	8
4.2	93	20	93	8
4.3	92	20	93	8
2–butanol				
4.1	86	8	91	3
4.2	87	8	92	3
4.3	87	8	95	3
2–propanol				
4.1	94	6	95	2
4.2	92	6	93	2
4.3	90	6	94	2

	Microwave method			
	Without additive		With additive [a]	
Catalyst	Conv. %	Time (h)	Conv. %	Time (h)
1– phenyl ethanol				
4.1	82	2	91	1
4.2	77	2	94	1
4.3	80	2	93	1
2–butanol				
4.1	81	1	91	0.5
4.2	85	1	92	0.5
4.3	84	1	89	0.5
2–propanol				
4.1	92	1	93	0.5
4.2	89	1	94	0.5
4.3	90	1	94	0.5

[a]additive NEt_3 (0.250 g)

4.3.8. Reactivity of dioxidomolybdenum(VI) complexes and possible mechanism for catalytic oxidation of substrates.

As observed earlier, the dioxidomolybdenum(VI) complexes react with H_2O_2 to give the corresponding $[Mo^{VI}O(O_2)]^{2+}$ complexes [172]. The generation of such species has been established here in methanol by electronic absorption spectroscopy. In a typical reaction, 20 mL of 2.6×10^{-5} M solution of **4.1** was treated drop wise with a solution prepared by dissolving 30% aqueous H_2O_2 (0.715 g, 6.3 mmol) in 5 mL of methanol and the resultant spectroscopic changes are presented in Fig. 4.7. Thus 358 nm band shifts to 363 nm along with only marginal change in the intensity while the 299 nm band increases its intensity considerably and finally disappears. The broad charge transfer band appearing at 430 nm slowly decreases in intensity (Fig. 4.7(a)) along with further broadening and finally disappears. Simultaneously, a new shoulder band appears at ca.

380 nm. These changes indicate the interaction of **4.1** with H_2O_2 and the plausible formation of $[Mo^{VI}O(O_2)\{Hdfmp(bhz)_2\}(MeOH)]$ (**4.1**) in methanol; Eq. 4.2. Similar spectral changes have also been noted for other complexes; Fig. 4.7 (b and c). Thus, the reaction of H_2O_2 with complexes during catalytic reaction is likely to proceed through the $[Mo^{VI}O(O_2)]^{2+}$ intermediate which may transfer oxygen to the substrates during the catalytic oxidation.

$$[Mo^{VI}O_2\{Hdfmp(bhz)_2\}(MeOH)] + H_2O_2 \rightarrow [Mo^{VI}O(O_2)\{Hdfmp(bhz)_2\}(MeOH)] + H_2O \qquad (4.2)$$

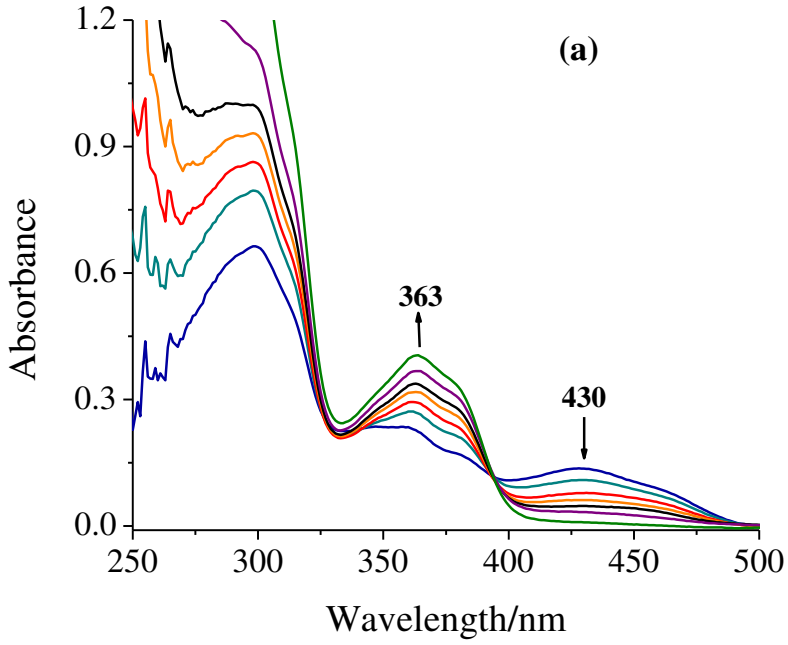

Figure 4.7. (a) The spectra were recorded after successive addition of one drop portion of H_2O_2 [30% H_2O_2 (0.715 g, 6.3 mmol) dissolved in 5 mL of MeOH; final concentration of H_2O_2 = 1.26 M)] to 20 mL of 2.6×10^{-5} M solution of $[Mo^{VI}O_2\{Hdfmp(bhz)_2\}(MeOH)]$ (**4.1**).

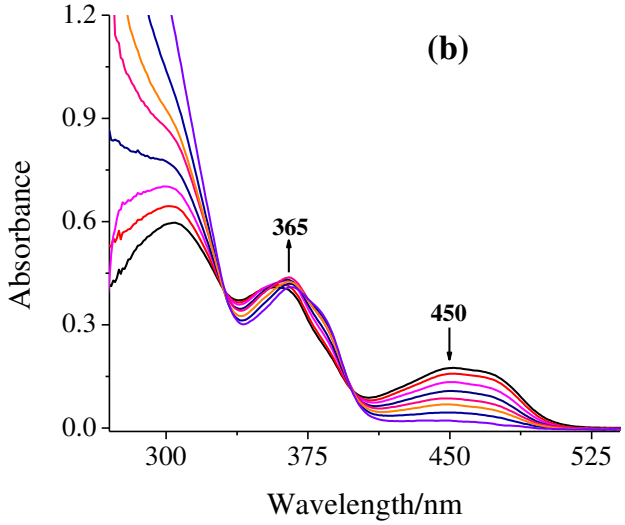

Figure 4.7. (b) The spectra were recorded after successive addition of one drop portion of H_2O_2 [30% H_2O_2 (0.910 g, 8.0 mmol) dissolved in 5 mL of MeOH; final concentration of H_2O_2 = 1.60 M)] to 20 mL of 3.2×10^{-5} M solution of [$Mo^{VI}O_2${Hdfmp(inh)$_2$}(MeOH)] (**4.2**).

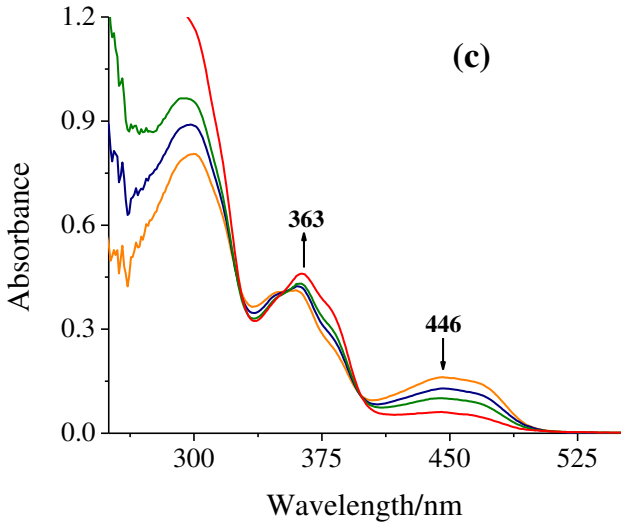

Figure 4.7. (c) The spectra were recorded after successive addition of one drop portion of H_2O_2 [30% H_2O_2 (0.845 g, 7.5 mmol) dissolved in 5 mL of MeOH; final concentration of H_2O_2 = 1.48 M] to 20 of mL of 2.4×10^{-5} M solution of [$Mo^{VI}O_2${Hdfmp(nah)$_2$}(MeOH)] (**4.3**).

4.4. Conclusions

The dioxidomolybdenum(VI) complexes $[Mo^{VI}O_2\{Hdfmp(bhz)_2\}(MeOH)]$ (**4.1**), $[Mo^{VI}O_2\{Hdfmp(inh)_2\}(MeOH)]$ (**4.2**) and $[Mo^{VI}O_2\{Hdfmp(nah)_2\}(MeOH)]$ (**4.3**) have been prepared from potential tribasic pentadentate $O(NO)_2$ type ligands $H_3dfmp(bhz)_2$ (**4.I**), $H_3dfmp(inh)_2$ (**4.II**) and $H_3dfmp(nah)_2$ (**4.III**), respectively but they behave as dibasic tridentate and other coordinating atoms remain free. All these complexes have fully been characterized by employing various spectroscopic techniques and two of them by single crystal X–ray study. The single crystal X–ray analysis of complexes **4.1** and **4.3** confirms the coordination of the ligands in the dianionic (ONO^{2-}) enolate–tautomeric form leaving one of the hydrazide moieties non–coordinated.

These complexes are good catalyst precursors for the oxidation of secondary alcohols, 1–phenylethaol, 2–butanol and 2–propanol in acetonitrile. In the presence of 30 % H_2O_2 as oxidant these secondary alcohols gave corresponding ketones with high yield ca. 90–95% under optimized reaction conditions. Microwave assisted catalytic oxidation technique reduces time considerably and also shows equally good conversion. In fact, this technique emerges out as a highly time efficient system over conventional liquid phase oxidation method. Addition of N–based additive assists both catalytic systems in reducing time without posing any side effect on the oxidation of secondary alcohols. The $[Mo^{VI}O_2]^{2+}$ complexes upon treatment H_2O_2 in methanol instantly generate $[Mo^{VI}O(O_2)]^{2+}$species in solution which is considered to be the intermediate species responsible for the transfer of oxygen to the substrates during catalytic oxidation.

CHAPTER 5

Oxidative bromination of monoterpene (thymol) using dioxidomolybdenum(VI) complexes ofhydrazones of 8-formyl-7-hydroxy-4-methylcoumarin

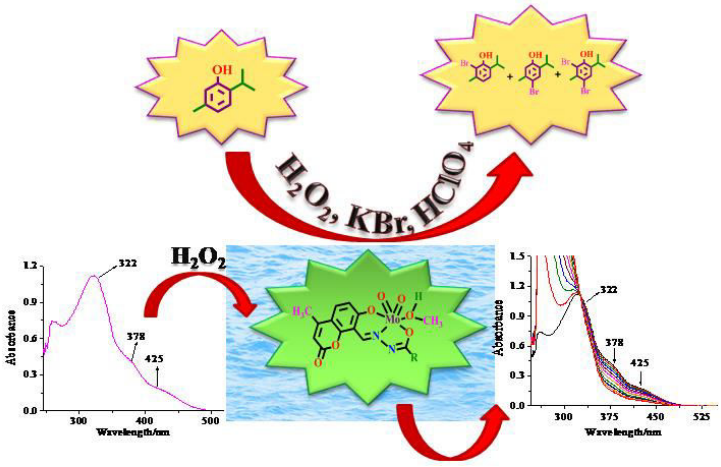

The matter of this chapter is accepted in the journal "Polyhedron"

5.1. Introduction

Terpenes are extremely miscellaneous division of natural products from which numerous commercial compounds are derived. Their potential therapeutic properties in pharmaceutical (like anticancer, anti–microbial and anti–inflammatory), uses in sanitary, cosmetic, agricultural and food industries, and making flavor and fragrance related compounds further show their importance [199]. Particularly monoterpenes represent a cheap and most abundant source of chiral substances that can be transformed into valuable bioactive compounds [200]. The most common thyme oil (thymus vulgaris) contains 20–54% thymol [201] which is an antiseptic and is the main active constituent of various mouthwashes and has also been found to be effective against various fungi. Thymol is a pretty atypical terpene; and thymol is achiral.

Coumarins are oxygen containing heterocyclic compounds, which show their significance in the territory of natural products and synthetic organic chemistry [202]. Coumarin and its derivatives have been a subject of several investigations due to their miscellaneous biological activities [203, 204], interesting photophysical, photochemical and metal binding properties. It has been found that the coordination of coumarin moiety to metal preserves or even boosts its biological activity [204, 205].They can also provoke modification in cell growth, development of intracellular communication mechanisms. Many coumarins are selective coronary vasodilators and possess radioactive properties [206].

The hydrazones are relatively cheap and environmentally endurable ligands, which can be synthesize through simple synthetic procedures [53, 87, 207]. Hydrazone moieties are the most important pharmacophoric cores of several anti–inflammatory, antinociceptive, and antiplatelet drugs [208]. Their *cis*–$[Mo^{VI}O_2]^{2+}$ complexes have shown interesting antibacterial [53] and catalytic activities [207]. Catalytic activities of *cis*–$[Mo^{VI}O_2]^{2+}$ complexes of other ONO donor ligands have also been well documented in the literature [39, 50, 87,158].

The aim of the present work is to synthesize and characterize new *cis*–$[Mo^{VI}O_2]^{2+}$ complexes with newly synthesized hydrazones of 8–formyl–7–hydroxy–4–methylcoumarin (Scheme 5.1) and use them as catalyst precursor towards the oxidative bromination of monoterpene (thymol). Brominated compounds, widely distributed in nature, are used in different fields like agrochemicals and pharmaceuticals. They also act as intermediates in various organic transformations [209, 210]. A few examples of the oxidative bromination of thymol are reported in the literature [211–214].

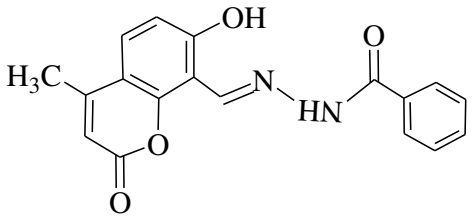

H_2fhmc-bhz (**5.I**)

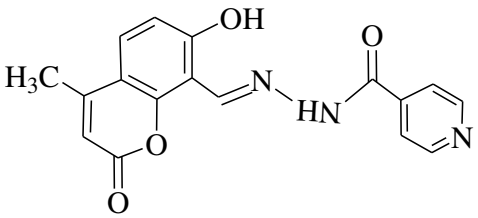

H_2fhmc-inh (**5.II**)

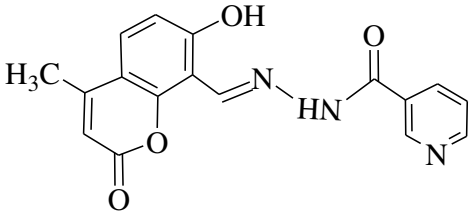

H_2fhmc-nah (**5.III**)

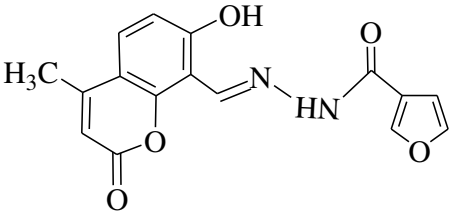

H_2fhmc-fah (**5.IV**)

Scheme 5.1. Structure of the ligands designated by **5.I, 5.II, 5.III** and **5.IV** used in this work.

5.2. Experimental Section

5.2.1. Materials and methods

Furoyl hydrazide, (Aldrich Chemicals Co., U.S.A.), thymol (Himedia), were used as obtained. 8–formyl–7–hydroxy–4–methylcoumarin [215] was prepared according to methods reported in the literature. Details of other chemicals are presented in chapter 2 and 4.

5.2.2. Instrumentation and characterization Procedures

Details of instrumentation and characterization procedures are presented in chapter 2.

5.2.3. Preparations

5.2.3.1. Preparations of H_2fhmc–bhz (5.I), H_2fhmc–inh (5.II) H_2fhmc–nah (5.III) and H_2fhmc–fah (5.IV)

All ligands were prepared using a general procedure. A representative preparation is presented here. A solution of 8–formyl–7–hydroxy–4–methylcoumarin (2.04 g, 10mmol) in methanol (20 ml) was mixed to a filtered solution of benzoyl hydrazide (1.36 g, 10mmol) in methanol (20 ml) with stirring and the obtained reaction mixture was refluxed on a water bath for 4h. The resulted solid was filtered after cooling, washed with methanol and dried over silica gel under vacuum.

H_2fhmc–bhz (5.I): Yield: 2.50 g (77.6%). Anal. Calc. for $C_{18}H_{14}N_2O_4$ (322.30): C, 67.07; H, 4.38; N, 8.69. Found: C, 67.19; H, 4.32; N, 8.72%.

H_2fhmc–inh (5.II): Yield: 2.45 g (75.8%).Anal. Calc. for $C_{17}H_{13}N_3O_4$ (323.30): C, 63.16; H, 4.05; N, 13.00. Found: C, 63.08; H, 4.15; N, 13.12%.

H_2fhmc–nah (5.III): Yield: 2.47 g (76.4%). Anal. Calc. for $C_{17}H_{13}N_3O_4$ (323.30): C, 63.16; H, 4.05; N, 13.00. Found: C, 63.10; H, 4.11; N, 13.09%.

H_2fhmc–fah (IV): Yield: 2.39 g (76.6%). Anal. Calc. for $C_{16}H_{12}N_2O_5$ (312.28): C, 61.54; H, 3.87; N, 8.97. Found: C, 61.60; H, 3.85; N, 9.00%.

5.2.3.2. Preparation of [$Mo^{VI}O_2$(fhmc–bhz)(MeOH)] (5.1)

A solution of [$Mo^{VI}O_2(acac)_2$] (0.66 g, 2 mmol) dissolved in 5 ml of methanol was added to a stirred solution of H_2fhmc–bhz (0.64 g, 2 mmol) in methanol (10 ml) and the obtained reaction mixture was stirred at room temperature whereupon an yellow solid started to form. After 3 h of stirring, the separated solid was filtered, washed with cold methanol followed by petroleum ether and dried in a vacuum desiccator over silica gel. Yield: 0.910 g (94.7%). Anal. Calc. for $C_{19}H_{16}N_2O_7Mo$ (480.30): C, 47.51; H, 3.36; N, 5.83%. Found: C, 47.45; H, 3.28; N, 5.89%.X–ray diffraction quality crystals for [$Mo^{VI}O_2$(Hfhmc–bhz)(DMSO)] (**5.1a**) were grown by slow evaporation of a solution of **5.1** in DMSO.

5.2.3.3. Preparations of [$Mo^{VI}O_2$(fhmc–inh)(MeOH)] (5.2), [$Mo^{VI}O_2$(fhmc–nah)(MeOH)](5.3) and [$Mo^{VI}O_2$(fhmc–fah)(MeOH)] (5.4)

These complexes were prepared similarly by the reaction of 2 mmol of [$Mo^{VI}O_2(acac)_2$] and 2 mmol of ligand, H_2fhmc–inh (**5.II**) H_2fhmc–nah (**5.III**) or H_2fhmc–fah (**5.IV**).

[$Mo^{VI}O_2$(fhmc–inh)(MeOH)] (5.2): Yield: 0.920 g (95.6%). Anal. Calc.for $C_{18}H_{15}N_3O_7Mo$ (481.29): C, 44.92; H, 3.14; N, 8.73 %. Found: C, 44.85; H, 3.18; N, 8.80 %.

[$Mo^{VI}O_2$(fhmc–nah)(MeOH)] (5.3): Yield: 0.936 g (97.3%). Anal. Calc.for $C_{18}H_{15}N_3O_7Mo$ (481.29): C, 44.92; H, 3.14; N, 8.73 %. Found: C, 44.90; H, 3.10; N, 8.78 %.

[$Mo^{VI}O_2$(fhmc–fah)(MeOH)] (5.4): Yield: 0.900 g (95.7%).Anal. Calc.for $C_{17}H_{14}N_2O_8Mo$ (470.26): C, 43.42; H, 3.00; N, 5.96%. Found: C, 43.48; H, 2.96; N, 5.89%.

5.2.4. X–Ray crystal structure determination

Three–dimensional X–ray data were collected on a Bruker Kappa Apex CCD diffractometer at room temperature for **5.1a** by the ϕ–ωscan method. Reflections were measured from a hemisphere of data collected from frames, each of them covering 0.3º in ω. 14540 reflections measured were corrected for Lorentz and polarization effects and for absorption by multi–scan methods based on symmetry–equivalent and repeated reflections. Of them, 3113 independent reflections exceeded the significance level ($|F|/\sigma|F|$) > 4.0. After data collection, in each case an empirical absorption correction (SADABS) [216] was applied, and the structure was solved by direct methods and refined by full matrix least–squares on F^2 data using SHELX suite of programs [217]. Hydrogen atoms were included in calculation position and refined in the riding mode, except for C(2), C(9), C(10), C(11) and C(14), which were located in difference Fourier map and left to refine freely. Refinements were done with allowance for thermal anisotropy of all non–hydrogen atoms. A final difference Fourier map showed no residual density in the crystal: 0.496 and –0.727e.Å^{-3}. A weighting scheme w = $1/[\sigma^2(F_o^2) + (0.066000\ P)^2 + 0.015900\ P]$, was used in the latter stages of refinement. Further details of the crystal structure determination are given in Table 5.1.

Table 5.1.

Crystal data and structure refinement for the complexes $[Mo^{VI}O_2(fhmc–bhz)(DMSO)]$ (**5.1a**).

	5.1a
Formula	$C_{20}\ H_{18}\ Mo\ N_2\ O_7\ S$
Formula mass	526.36
T, *K*	293
Wavelength, Å	0.71073
Crystal system	Triclinic
Space group	P $\bar{1}$
a/Å	8.7732(3)
b/Å	8.9318(3)
c/Å	13.2399(5)
α/°	86.631(2)
β/°	88.075(2)
γ/°	86.938(2)
V/Å^3	1033.73(6)
Z	2
F_{000}	532
D_{calc}/g cm^{-3}	1.691
μ/mm^{-1}	0.782
θ/ (°)	1.54 to 25.57
R_{int}	0.0401
Crystal size/ mm^3	0.22 x 0.21 x 0.18
Goodness–of–fit on F^2	1.105
$R_1[I>2\sigma(I)]$ [a]	0.0386
wR_2 (all data) [b]	0.1138
Largest differences peak and hole (eÅ^{-3})	0.496 and –0.727

[a] $R_1 = \Sigma \left| \left| F_o \right| - \left| F_c \right| \right| / \Sigma \left| F_o \right|$. [b] $wR_2 = \{\Sigma[w(\left| \left| F_o \right|^2 - \left| F_c \right|^2 \right|)^2] / \Sigma[w(F_o^2)^2]\}^{1/2}$

5.2.5. Catalytic oxidative bromination of thymol

Thymol (1.50 g, 10 mmol), 30 % aqueous H_2O_2 (3.39g, 30 mmol), 70% $HClO_4$ (5.72 g, 40 mmol) and KBr (3.57 g, 30mmol) were taken in water (20 mL) at room temperature. After adding catalyst (0.002g) to the above reaction mixture, it was stirred and the obtained oxidized products were analyzed quantitatively by gas chromatography. The obtained main products were confirmed by ^{1}H NMR spectroscopy as well as GC–MS after their separations and their quantifications were made on the basis of the relative peak area of the respective product.

5.3. Results and discussion

5.3.1. Synthesis and characterization of complexes

The reaction between equimolar amounts of $[Mo^{VI}O_2(acac)_2]$ and H_2fhmc–bhz (**5.I**), H_2fhmc–inh (**5.II**), H_2fhmc–nah (**5.III**) or H_2fhmc–fah (**5.IV**)in methanol results in the formation of *cis*–$[Mo^{VI}O_2]^{2+}$complexes, $[Mo^{VI}O_2$(fhmc–bhz)(MeOH)] (**5.1**), $[Mo^{VI}O_2$(fhmc–inh)(MeOH)] (**5.2**) $[Mo^{VI}O_2$(fhmc–nah)(MeOH)] (**5.3**) and $[Mo^{VI}O_2$(fhmc–fah)(MeOH)] (**5.4**), respectively. The sixth coordination site is occupied by methanol in these complexes. [Eq. (5.1) taking **5.I** as a representative example].

$[Mo^{VI}O_2(acac)_2]$ + H_2fhmc–bhz + MeOH →

$[Mo^{VI}O_2$(fhmc–bhz)(MeOH)] + 2Hacac (5.1)

Idealized structures of the complexes are shown in Scheme 5.2 which are based on the spectroscopic (IR, UV/Vis, ^{1}H and ^{13}C NMR) data, elemental analyses and X–ray diffraction study of $[Mo^{VI}O_2$(fhmc–bhz)(DMSO)] (**5.1a**). All these complexes are soluble in DMF and DMSO and partially soluble in methanol and acetonitrile.

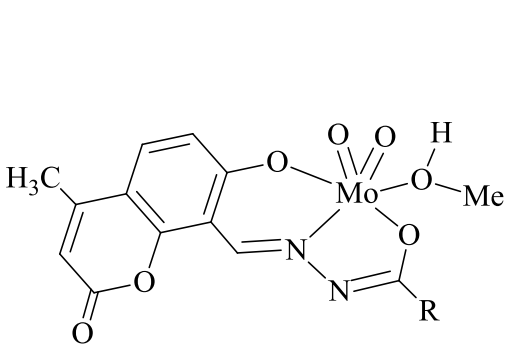

R	Complex
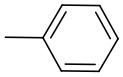	$[Mo^{VI}O_2(fhmc\text{-}bhz)(MeOH)]$ (**5.1**)
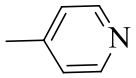	$[Mo^{VI}O_2(fhmc\text{-}inh)(MeOH)]$ (**5.2**)
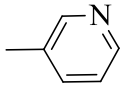	$[Mo^{VI}O_2(fhmc\text{-}nah)(MeOH)]$ (**5.3**)
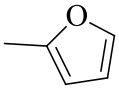	$[Mo^{VI}O_2(fhmc\text{-}fah)(MeOH)]$ (**5.4**)

Scheme 5.2. Proposed structure of *cis*–$[Mo^{VI}O_2]^{2+}$complexes.

5.3.2. Thermal studies

Thermal stability of monomeric complexes **5.1, 5.2, 5.3** and **5.4** has been studied under an oxygen atmosphere. These complexes lose mass roughly equal to one methanol molecule in the temperature range 100–170 °C, indicating the presence of a coordinated methanol. On further increasing the temperature the solvent free complexes decompose exothermically in two/ three overlapping steps and form MoO_3 as final product. The observed MoO_3 contents of 29.2 % at ca. 615°C for **5.1,** 29.0 % at 440°C for **5.2**, 28.9 % at 440°C for **5.3** and 29.7 % at 490 °C for **5.4** match closely with the calculated values of 30.0, 29.9, 29.9 and 30.6 %, respectively.

5.3.3. Structure descriptions

ORTEP diagram for the complex $[Mo^{VI}O_2(Hfhmc–bhz)(DMSO)]$ (**5.1a**) is shown in Fig.5.1. Selected bond distances and angles are given in Table 5.2.In compound **5.1a**, one complex is present in the asymmetric unit. The $O_{hydroxy}$ of methylcoumarin group, N_{azo} and $O_{benzoylhydrazide}$ atoms of the ligand, which acts as ONO tridentate, and two oxido groups coordinate to molybdenum centre. The equatorial plane is formed for these three atoms of the ligand and one of the terminal oxygen atoms. The molybdenum atom is

displaced toward the apical oxido ligand from the equatorial plane by 0.3003 Å, with respect to the plane O3–O4–O5–N1 (mean deviation from plane 0.0402(15) Å) One DMSO molecule completes the coordination sphere of a distorted octahedral geometry. The O=Mo=O angle is 105.90(16)ºand Mo=O distances are 1.696(3) Å and 1.695(3) Å. The Mo–O–S angle and Mo–O distance for Mo–DMSO are 126.37(18)°(average of two angles of disordered sulphur atoms) and 2.286(3)Å, respectively, similar to other examples in literature [218,219].

The presence of intermolecular forces between the rings of methylcoumarin group and phenyl ring of benzoylhydrazide group determine the crystal packing. The distances between π cloud around carbon atom, C6, and the centroids of phenyl rings are: $d_{C6–c1}$ = 3.510 Å [(C6A), c1 (C13B–C14B–C15B–C16B–C17B–C18B) and repeated for other carbon–centroids].

Table 5.2.

Bond lengths [Å] and angles [°] for [$Mo^{VI}O_2$(fhmc–bhz)(DMSO)] (**5.1a**).

Bond lengths	**5.1a**
Mo(1)–O(3)	1.937(3)
Mo(1)–O(4)	1.999(3)
Mo(1)–O(5)	1.696(3)
Mo(1)–O(6)	1.695(3)
Mo(1)–O(1S)	2.286(3)
Mo(1)–N(1)	2.243(3)
N(1)–C(11)	1.294(5)
N(1)–N(2)	1.396(4)
N(2)–C(12)	1.313(5)

Angles	**5.1a**
O(6)–Mo(1)–O(5)	105.90(16)
O(6)–Mo(1)–O(3)	97.81(13)
O(5)–Mo(1)–O(3)	103.21(13)
O(6)–Mo(1)–O(4)	95.43(13)
O(5)–Mo(1)–O(4)	97.65(13)
O(3)–Mo(1)–O(4)	151.10(12)
O(6)–Mo(1)–N(1)	94.25(14)
O(5)–Mo(1)–N(1)	158.32(13)
O(3)–Mo(1)–N(1)	81.39(11)
O(4)–Mo(1)–N(1)	72.08(11)
O(6)–Mo(1)–O(1S)	167.83(13)
O(5)–Mo(1)–O(1S)	86.06(13)
O(3)–Mo(1)–O(1S)	81.23(11)
O(4)–Mo(1)–O(1S)	80.47(10)
N(1)–Mo(1)–O(1S)	73.60(11)
S(1A)–O(1S)–Mo(1)	125.34(17)
S(1B)–O(1S)–Mo(1)	127.4(2)

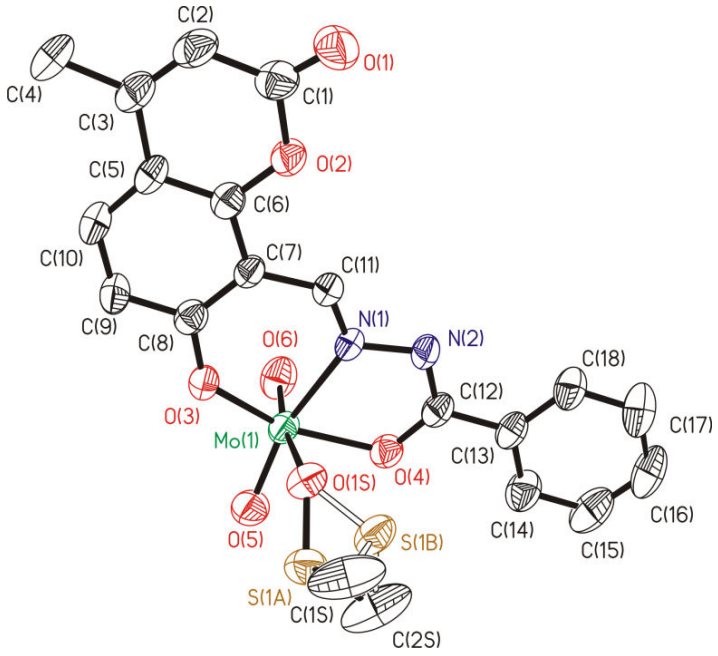

Figure 5.1. ORTEP plot of [$Mo^{VI}O_2$(fhmc–bhz)(DMSO)] (**5.1a**). All the non–hydrogen atoms are presented by their 50% probability ellipsoids. Hydrogen atoms are omitted for clarity.

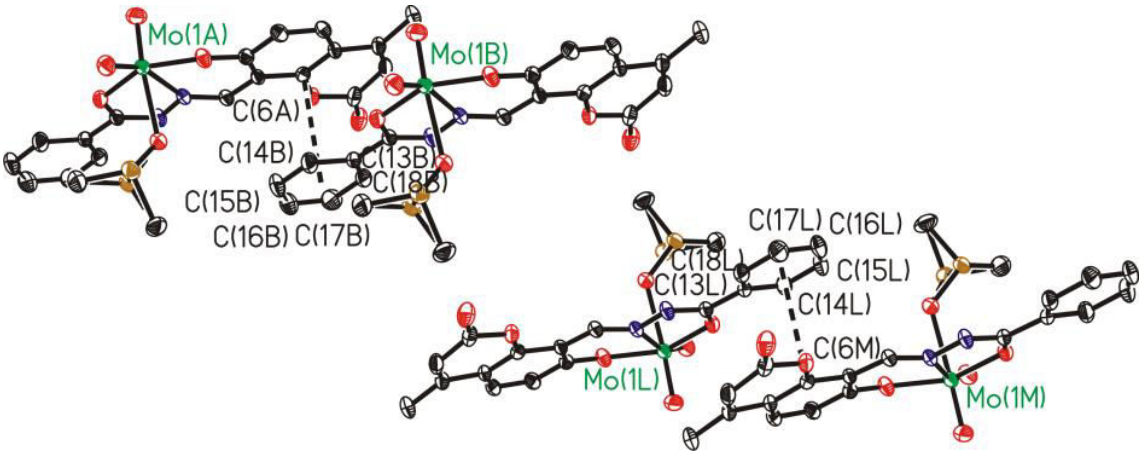

Figure 5.2.π–π–stacking interactions between π clouds around of C6 of 4–methylcoumarin group with centroid on phenyl group of the other framework in [$Mo^{VI}O_2$(fhmc–bhz)(DMSO)] (**5.1a**).

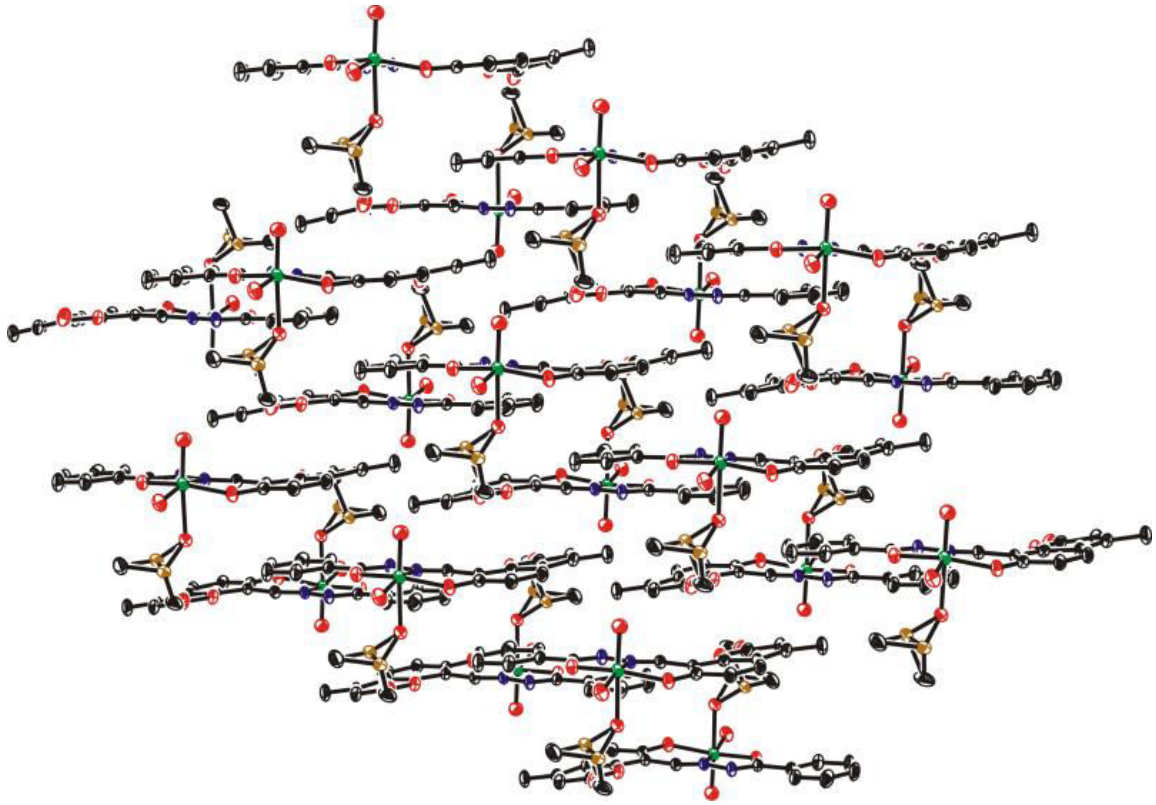

Figure5.3. Crystal packing of [$Mo^{VI}O_2$(fhmc–bhz)(DMSO)] (**5.1a**). Layer structure linked by π–π–stacking interactions (see Fig.5.2).

5.3.4. IR spectral studies

Table 5.3 reveals a partial list of the IR spectral data. The IR spectra of the ligands H_2fhmc–bhz (**5.I**), H_2fhmc–inh (**5.II**), H_2fhmc–nah (**5.III**) or H_2fhmc–fah (**5.IV**) show four characteristic bands at 3053–3060, 1705–1716, 1673–1678, and 1586–1588 cm^{-1} due to υ(NH), $\upsilon(C{=}O)_{pyrone/hydrazide}$ and υ(C=N) stretches, respectively [169], which show their ketonic behavior in the solid state. Appearance of a new band at 1179–1200 cm^{-1} due to the υ(C–O) stretch and the absence of a υ(NH) band in all the complexes suggests the enolization of the ketonic group and replacement of H by the metal ion. A band at ca.1703–1717cm^{-1} due to the ketonic group of the pyrone moiety is still present in all the complexes. A very sharp band appearing at 1543–1551 cm^{-1} in complexes confirms the

coordination of the azomethine nitrogen atom. This lower wavenumber band occurs due to the donation of electron density from the nitrogen atom to an empty d–orbital of the metal ion. A band appearing at 1066–1074 cm^{-1} due to υ(N–N) in ligands is also affected by the coordination of the nitrogen atom and shifts to a higher wavenumber in complexes. The presence of several medium intensity bands between 2500 and 2800 cm^{-1} in the ligands as well as in complexes suggest the existence of C–H stretching bands due to $–CH_2$.The $[MoO_2]^{2+}$complexes are well characterized by two prominent peaks at 936–945 and 906–920 cm^{-1}, which are assigned to υ_{asym}(O=Mo=O) and υ_{sym}(O=Mo=O) modes, respectively due to the *cis*–$[MoO_2]$ structure [136].

Table 5.3.

IR spectral data [in cm^{-1}] of compounds.

Compounds	ν(NH)	$\nu(C=O)_{pyrone/hydrazide}$	ν(C=N)	ν(C–O)	ν(O=Mo=O)[a]
H_2fhmc–bhz	3060	1705, 1673	1586		
H_2fhmc–inh	3058	1710, 1678	1588		
H_2fhmc–nah	3056	1713, 1676	1586		
H_2fhmc–fah	3053	1716, 1674	1587		
$[Mo^{VI}O_2$(fhmc–bhz)(MeOH)]		1703, 1624	1551	1182	938, 906
$[Mo^{VI}O_2$(fhmc–inh)(MeOH)]		1707, 1621	1547	1179	945, 915
$[Mo^{VI}O_2$(fhmc–nah)(MeOH)]		1711, 1616	1551	1200	936, 906
$[Mo^{VI}O_2$(fhmc–fah)(MeOH)]		1717, 1611	1543	1180	938, 920

[a]Asymmetric and symmetric ν(O=Mo=O) values.

5.3.5. UV–Vis spectral studies

Table 5.4 presents absorption maxima of ligands and complexes with their extinction coefficients. The UV–Vis spectra of ligands and $[Mo^{VI}O_2]^{2+}$complexes were recorded in DMSO. All ligands exhibit three very similar spectral bands at 380–388, 314–317 and 267–272 nm. Based on their extinction coefficient values, these bands explicate as n→π* (first two bands) and π→π* transitions, respectively. All these bands

are also present in complexes with slight variations. In addition, all complexes exhibit a medium intensity band at 425–431 nm due to the ligand to metal charge transfer (LMCT) transition from the phenolate oxygen atom to an empty d–orbital of the molybdenum. As $[Mo^{VI}O_2]^{2+}$complexes have $4d^0$ configuration, d→d band is not expected.

Table 5.4.

UV–Vis spectral data of ligands and complexes recorded in methanol.

Compound	λ_{max} /nm (ε/ M^{-1} cm^{-1})
H_2fhmc–bhz (**5.I**)	272 (1.8×10^4), 317 (3.1×10^4), 380 (7.6×10^3)
H_2fhmc–inh(**5.II**)	268 (8.8×10^3), 317 (2.3×10^4), 382 (3.2×10^3)
H_2fhmc–nah (**5.III**)	267 (7.8×10^3), 314 (2.4×10^4), 381 (2.1×10^3)
H_2fhmc–fah (**5.IV**)	270 (9.5×10^3), 317 (2.6×10^4), 388 (5.7×10^3)
$[Mo^{VI}O_2$(fhmc–bhz)(MeOH)] (**5.1**)	261 (1.8×10^4), 322 (2.8×10^4), 378 (1.0×10^4), 425 (4.3×10^3)
$[Mo^{VI}O_2$(fhmc–inh)(MeOH)] (**5.2**)	259 (1.2×10^4), 318 (2.3×10^4), 382 (6.1×10^3), 430 (2.4×10^3)
$[Mo^{VI}O_2$(fhmc–nah)(MeOH)] (**5.3**)	261 (1.3×10^4), 318 (2.9×10^4), 380 (6.0×10^3), 431 (2.7×10^3)
$[Mo^{VI}O_2$(fhmc–fah)(MeOH)] (**5.4**)	267 (1.4×10^4), 317 (3.3×10^4), 379 (7.2×10^3), 430 (3.0×10^3)

5.3.6. ^{1}H and ^{13}C NMR studies

The ^{1}H NMR spectral data of ligands and complexes are collected in Table 5.5**.** The spectral data confirm their coordinating modes. The ^{1}H NMR spectra of a representative ligand H_2fhmc–nah (**III**) and its complex is shown in Fig. 5.3.The ligands show two broad signals at δ = 12.61–12.74 ppm and 12.41–12.57 ppm owing to the phenolic –OH and –NH, respectively. These signals disappear in the spectra of complexes due to coordination of the phenolate oxygen and enolate oxygen after replacing H by the metal ion. A signal due to azomethine proton (equivalent to 1H) in ligands illustrates a notable downfield shifts in complexes with a coordination–induced

shifts [$\Delta\delta$= [δ(complex) – δ(free ligand)] of 0.06–0.14 ppm, confirming the coordination of the azomethine nitrogen atom. The aromatic and aliphatic protons appear in the expected regions in spectra of ligands as well as of complexes, with slight shifts in their positions.

Table 5.5.

^{1}H NMR chemical shifts [a] [δ in ppm] of ligands and complexes recorded in DMSO–d_6.

Compounds[a]	–CH=N–	Aromatic H	–OH	–NH	$–CH_3$
5.I	9.06	6.18 (d, 1H), 6.88 (t, 1H), 7.54 (t, 2H),7.61 (t, 2H), 7.94 (t, 2H)	12.74	12.41	2.35
5.1(Δδ)	9.14(0.08)	6.34 (s, 1H), 6.97 (d, 1H), 7.51 (t, 2H), 7.59 (t, 1H), 7.89 (d, 1H), 8.03 (d, 2H)	–	–	2.42
5.II	9.07	6.22 (s, 1H), 6.91 (d, 1H), 7.66 (d, 1H), 7.85 (d, 2H), 8.81 (s, 2H)	12.63	12.57	2.36
5.2(Δδ)	9.21(0.14)	6.34 (s, 1H), 6.99 (d, 1H), 7.93 (s, 3H), 8.77 (s, 2H)	–	–	2.43
5.III	9.11	6.22 (s, 1H), 6.92 (d, 1H), 7.66 (s, 1H), 7.68 (d, 1H), 8.28 (d, 1H), 8.79 (s, 1H), 9.07 (s, 1H)	12.61	12.55	2.37
5.3(Δδ)	9.18(0.07)	6.35 (s, 1H), 6.99 (d, 1H), 7.57 (s, 1H), 7.91 (d, 1H), 8.35 (d, 2H), 8.78 (s,1H)	–	–	2.50
5.IV	9.07	6.26 (s, 1H), 6.73 (s, 1H), 6.75 (d, 1H), 7.35 (s, 1H), 7.70 (d, 1H), 8.00 (s,1H)	12.66	12.51	2.40
5.4(Δδ)	9.13(0.06)	6.34 (s, 1H), 6.73 (s, 1H), 6.97 (d, 1H), 7.27 (d, 1H), 7.88 (d, 1H), 7.98 (s, 1H)	–	–	2.40

[a]Letters given in parentheses indicate the signal structure: s = singlet, d = doublet.

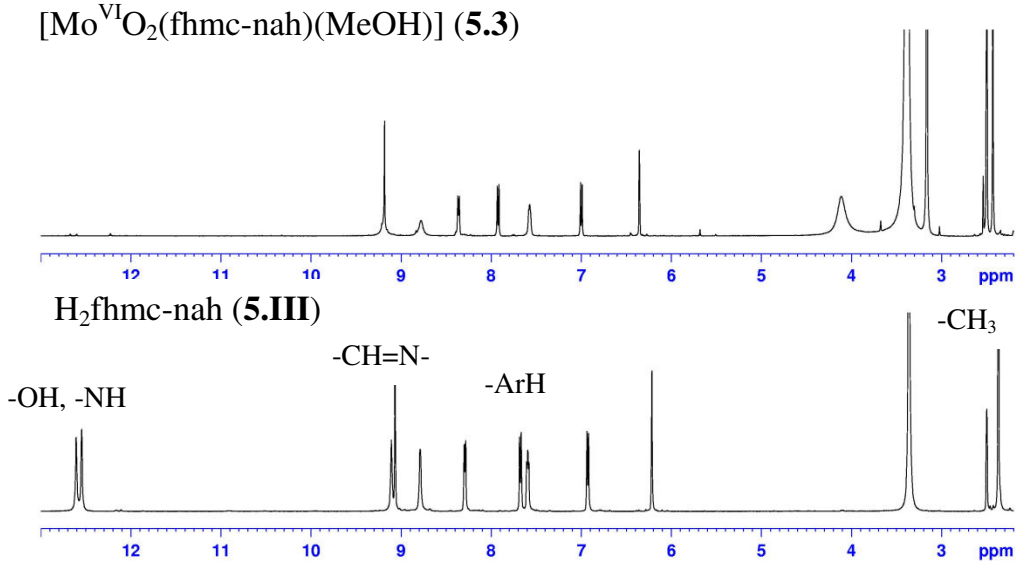

Figure5.4. ^{1}H NMR spectra of H_2fhmc–nah (**5.III**) and [$Mo^{VI}O_2$(fhmc–nah)(MeOH)] (**5.3**).

Table 5.6 provides ^{13}C NMR spectral data of ligands and their corresponding dioxidomolybdenum (VI) complexes whereas Fig.5.5 presents spectra of a representative ligand H_2fhmc–nah (**5.III**) and its complex **5.3**. The peaks are assigned again on the basis of the coordination–induced shifts ($\Delta\delta$) of the signals for carbon atoms in the vicinity of the coordinating atoms [140].These assignments also provide useful information for the elucidation of the structures of the complexes. Ligands **5.I**, **5.II, 5.III** and **5.IV**display 16, 15, 17 and 16 signals corresponding to the 18, 17, 17 and 16 carbon atoms, respectively. A total of 17, 16, 18 and 17signals were observed for complexes **5.1**, **5.2**, **5.3** and **5.4**, respectively after coordination of ligands to the molybdenum. A large coordination induced shift of the signals for the carbon atoms associated with the phenolic oxygen (C1), the azomethine nitrogen (C11) and the enolic oxygen (C12)

confirms the coordination of these functionalities to the molybdenum ion. In addition, these complexes show one signal each for coordinated MeOH at ca. 48.80–49.10 ppm.

Table 5.6.

^{13}C NMR spectral data of ligand and complexes.

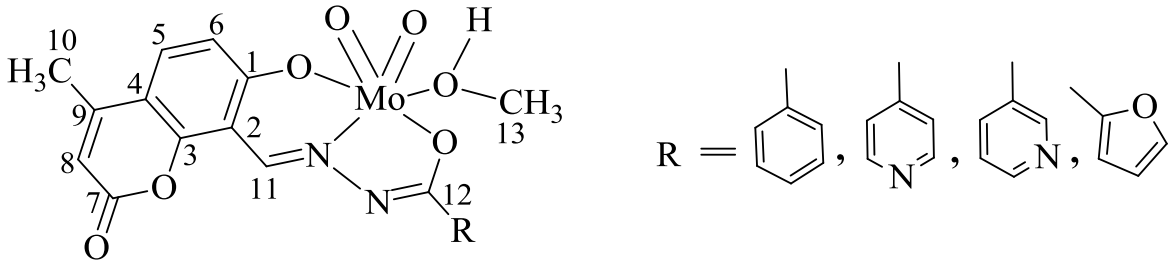

Compounds	C1	C2–C9	C10
5.I	159.71	113.90, 152.90, 106.11,128.48, 112.25, 161.56, 111.20,154.28	18.80
5.1 ($\Delta\delta$)	154.12 (–5.59)	113.89, 132.81, 106.23, 128.65, 112.00, 154.21, 108.65, 149.30	18.84
5.II	159.66	113.96, 151.04, 105.82, 128.91 112.33, 161.46, 111.29, 154.32	18.83
5.2 ($\Delta\delta$)	152.75 (–6.91)	115.92, 136.24, 108.79, 127.12, 113.28, 154.90, 112.43, 149.56	19.30
5.III	159.64	113.94, 153.24, 105.88, 128.41, 112.34, 161.54, 111.23, 154.34	18.77
5.3 ($\Delta\delta$)	154.11 (–5.53)	115.93, 149.35, 108.55, 131.60, 113.96, 159.28, 112.05, 153.06	18.81
5.IV	154.44	114.10, 146.28, 111.24, 114.21 112.90, 159.77, 112.39, 153.00	18.91
5.4 ($\Delta\delta$)	152.18 (–2.26)	117.38, 147.79, 113,27, 131.35, 115.94, 159.37, 114.01, 149.03	18.89

Compounds	C11	C12	C13	R
5.I	143.97	162.90	–	132.83, 128.16, 129.16, 132.53
5.1	162.40	169.65	48.80	129.95, 115.93, 129.36, 131.36
(Δδ)	(18.43)	(6.75)		
5.II	145.21	161.59	–	139.58, 121.90, 153.04
5.2	162.13	168.19	48.90	128.50, 122.76, 132.43
(Δδ)	(16.92)	(6.60)		
5.III	144.70	161.65		135.89, 128.81, 124.24, 149.12,153.02
5.3	162.40	168.06	49.05	126.20, 136.15, 124.53, 150.14
(Δδ)	(17.70)	(6.41)		
5.IV	144.20	161.50	–	128.17, 113.87, 106.09, 116.18
5.4	162.23	168.35	49.10	147.06, 108.71, 112.16, 144.58
(Δδ)	(18.03)	(6.85)		

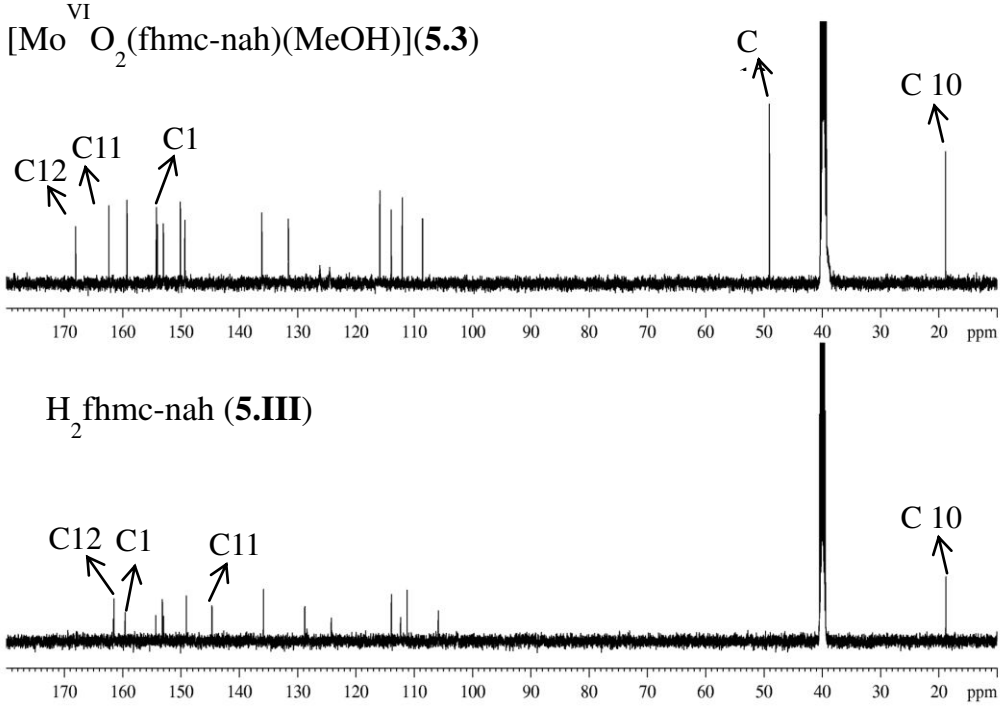

Figure 5.5. ^{13}C NMR spectra of H_2fhmc–nah (**5.III**) and [$Mo^{VI}O_2$(fhmc–nah)(MeOH)] (**5.3**).

5.3.7. Oxidative bromination of thymol

Scheme 5.3 presents the oxidative bromination of thymol, using **5.1**, **5.2**, **5.3** and **5.4** as catalyst precursors in the presence of KBr, 70% aqueous $HClO_4$ and 30 % aqueous H_2O_2 under an aqueous system. The bromination of thymol mainly gives two isomers, 2–bromothymol as minor and 4–bromothymol as major product due to steric hindrance at the *ortho* position. On further bromination of 4–bromothymol it gives 2,4–dibromothymol. Consequently, the reaction has been investigated by changing different parameters that may affect the rate of thymol bromination and the selectivity of products.

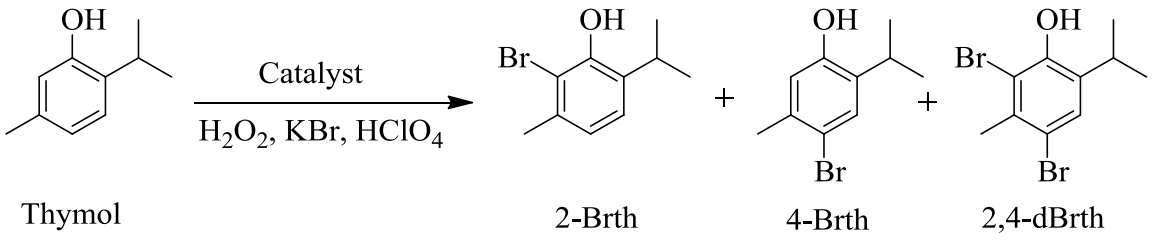

Scheme 5.3. Products of the oxidative bromination of thymol. 2–Brth = 2–bromothymol, 4–Brth = 4–bromothymol, 2,4–dBrth = 2,4–dibromothymol.

Reaction conditions were optimized for considering different parameters like amounts of catalyst, 30% aqueous H_2O_2, KBr and $HClO_4$ using [$Mo^{VI}O_2$(fhmc–bhz)(MeOH)] (**5.1**) as a representative catalyst precursor. Thus, for 10 mmol of thymol (1.50 g), three different amounts of catalyst (0.001, 0.002 and 0.003 g), 30 % aqueous H_2O_2 (10, 20 and 30 mmol), KBr (10, 20 and 30 mmol) and 70% $HClO_4$ (10, 20, 30 and 40 mmol, added in four equal portions to the reaction mixture, first portion at t = 0 and other three portions after every 30 min intervals) were taken in 20 mL water and the reaction was carried out at room temperature. The $HClO_4$ was found to be crucial to bring out catalytic bromination and its amount has great influence on the conversion and selectivity of products. The complexes slowly decompose during the reaction; decomposition is slowed down, if $HClO_4$ is successively added in four equal portions during 2 h of reaction time.

Table 5.7 presents all the conditions considered and the corresponding percentage of oxidative bromination of thymol along with the selectivity of different reaction products. It is clear from the data shown in table that the conversions and the selectivity of products differ on varying the reagents. However, the best appropriate reaction conditions (entry no. 10 of Table 5.7) for the maximum oxidative bromination of thymol with 94% conversion are: catalyst (0.002g), H_2O_2 (3.39 g, 30 mmol), KBr (3.57 g, 30 mmol) and $HClO_4$ (5.72 g, 40 mmol) in 20 mL water. Under these conditions the selectivity of different major products follows the order: 2,4–dibromothymol (84.6%) >

2–bromothymol (8.4%) > 4–bromothymol (7%). Using 0.002 g of catalyst and considering the substrate to different reagents in the molar ratio presented in entry no 15 of Table 5.7 gave highest selectivity (85.3%) of 4–bromothymol amongst all the conditions applied. Increasing the amounts of KBr or acid results in the formation of more 2,4–dibromothymol product at the expense of 4–bromoproduct.Under the optimized conditions for the maximum conversion of thymol, other catalysts i.e. **5.2**, **5.3** and **5.4** exhibit similar catalytic activity along with similar selectivity of different products (entry no 11, 12 and 13). Blank reaction i.e without catalyst, under same conditions (entry no. 16 of Table 5.7) resulted in 54% conversion. These complexes enhance conversion of thymol and alter the products yield.

Table 5.7.

Conversion of thymol (1.50g, 10 mmol), TOF and product selectivity using $[Mo^{VI}O_2(fhmc–bhz)(MeOH)]$ (**5.1**) as a catalyst precursor in 2 h of reaction time under different reaction conditions.

Entry No.	KBr[g(mmol)]	H_2O_2[g(mmol)]	$HClO_4$[g(mmol)]	Catalyst [g (mmol)]
1.	1.19 (10)	1.13 (10)	1.43 (10)	$0.001(2.0 \times 10^{-3})$
2.	1.19 (10)	1.13 (10)	1.43 (10)	$0.002(4.1 \times 10^{-3})$
3	1.19 (10)	1.13 (10)	1.43 (10)	$0.003(6.2 \times 10^{-3})$
4	1.19 (10)	2.27 (20)	1.43 (10)	$0.002(4.1 \times 10^{-3})$
5	1.19 (10)	3.39 (30)	1.43 (10)	$0.002(4.1 \times 10^{-3})$
6	2.38 (20)	3.39 (30)	1.43 (10)	$0.002(4.1 \times 10^{-3})$
7	3.57 (30)	3.39 (30)	1.43 (10)	$0.002(4.1 \times 10^{-3})$
8	3.57 (30)	3.39 (30)	2.86 (20)	$0.002(4.1 \times 10^{-3})$
9	3.57 (30)	3.39 (30)	4.29 (30)	$0.002(4.1 \times 10^{-3})$
10	3.57 (30)	3.39 (30)	5.72 (40)	$0.002(4.1 \times 10^{-3})$
11[a]	3.57 (30)	3.39 (30)	5.72 (40)	$0.002(4.1 \times 10^{-3})$
12[b]	3.57 (30)	3.39 (30)	5.72 (40)	$0.002(4.1 \times 10^{-3})$

13 [c]	3.57 (30)	3.39 (30)	5.72 (40)	0.002(4.1×10^{-3})
14	2.38 (20)	2.27 (20)	2.86 (20)	0.002(4.1×10^{-3})
15	2.38 (20)	2.27 (20)	4.29 (30)	0.002(4.1×10^{-3})
16	3.57 (30)	3.39 (30)	5.72 (40)	blank

Entry No.	Conv. [%]	TOF [h^{-1}]	2–Brth	4–Brth	2,4–dBrth
1.	14	171	15.3	84.7	0
2	24	293	14.7	83.3	1
3	27	330	16.2	83.8	2
4	37	451	12.7	85	2.3
5	45	549	13.3	84.3	2.4
6	62	750	8.5	57	34.5
7	71	872	9.2	52	38.8
8	79	956	4.2	32.3	63.5
9	86	1048	4.0	18.7	77.3
10	94	1146	8.4	7	84.6
11 [a]	99	1207	8.3	8	83.7
12 [b]	98	1195	6.3	5.4	88.3
13 [c]	97	1155	6.5	4.2	89.3
14	60	731	12.5	82.2	5.3
15	73	890	12.6	85.3	2.1
16	54	–	20.7	26	53.3

[a][$Mo^{VI}O_2$(fhmc–inh)(MeOH)] (**5.2**),[b][$Mo^{VI}O_2$(fhmc–nah)(MeOH)] (**5.3**)

[c][$Mo^{VI}O_2$(fhmc–fah)(MeOH)] (**5.4**)

The oxidative bromination of thymol and the selectivity of different reaction products for catalyst **5.1** under the optimized reaction conditions (see Table 5.8) have also been studied in different solvents. Though, conversion of thymol is almost same in all solvents, the selectivity of products varies. In H_2O,H_2O/CH_2Cl_2 and $H_2O/CHCl_3$, all three products were obtained and the selectivity followed the order: 2,4–dibromothymol > 2–bromothymol > 4–bromothymol, whereas H_2O/MeOH and H_2O/MeCN systems gave

only two products; 2,4–dibromothymol being a major one and 2–bromothymol a minor. With all three products in H_2O/hexane, the selectivity follows the order: 2,4–dibromothymol (77.7%) > 4–bromothymol (17.6%) >2–bromothymol (4.7%).

Table 5.8.

Solvents effect on the selectivity of product.

Solvents	Conversion [%]	2–Brth	4–Brth	2,4–dBrth
H_2O	94	8.4	7	84.6
H_2O/CH_2Cl_2	99	9.1	1.3	89.6
$H_2O/CHCl_3$	99	13.2	3.4	86.4
H_2O/MeOH	99	13.6	–	86.4
H_2O/MeCN	99	13.3	–	86.7
H_2O/Hexane	97	4.7	17.6	77.7

5.3.8. Reactivity of dioxidomolybdenum(VI) complexes and possible mechanism for catalytic oxidation of substrate.

As reported earlier, dioxidomolybdenum(VI) complexes react with H_2O_2 to give the corresponding $[Mo^{VI}O(O_2)]^{2+}$ complexes [172]. Such species has been generated in DMSO and monitored by UV–vis spectroscopy. In a typical reaction, 20 mL of 4.0×10^{-5} M solution of $[Mo^{VI}O_2$(fhmc–bhz)(MeOH)](**5.1**) was treated with a drop wise solution prepared by dissolving 30% aqueous H_2O_2 (0.904 g, 8.0mmol) in 5 mL of DMSO and the observed spectroscopic changes are depicted in Fig. 5.6(a). The intensity of the bands at 322 and 261nm considerably increases and finally disappears. The broad charge transfer band appearing at 425 nm slowly decreases in intensity [Fig.5.6(a)] along with broadening and finally vanishes. Simultaneously, a band at ca. 378 nm also decreases in intensity and disappears. These changes in spectra occur due to the interaction of H_2O_2 with the complex and plausible formation of $[Mo^{VI}O(O_2)$(fhmc–bhz)] in DMSO. Similar spectral changes have also been noted for other complexes; Figs.5.6(b–d).

In the model vanadium complex system studied in bi–phasic system for oxidative bromination, initially the intermediate oxidoperoxidovanadium(V) derivative forms in the presence of H_2O_2 which oxidizes Br^- to $HOBr/Br_2$. This intermediate enters into organic phase where the bromination of appropriate organic substrates takes place [141, 214]. During this process acid probably promotes the protonation of the peroxide intermediate. A similar mechanism may also be proposed here.

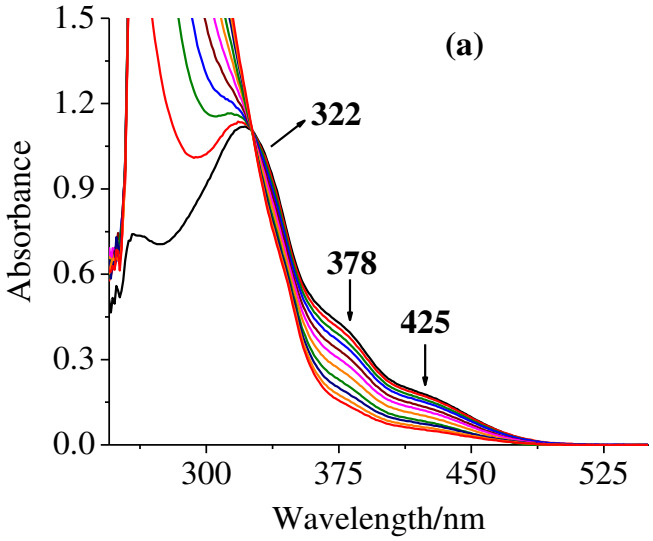

Figure 5.6. (a) The spectra were recorded after successive addition of one drop portion of H_2O_2 [30% H_2O_2 (0.904 g, 8.0 mmol) dissolved in 5 mL of DMSO; final concentration of H_2O_2 = 1.59 M)] to 20 mL of 4.0×10^{-5} M solution of $[Mo^{VI}O_2(fhmc–bhz)(MeOH)]$ (**5.1**).

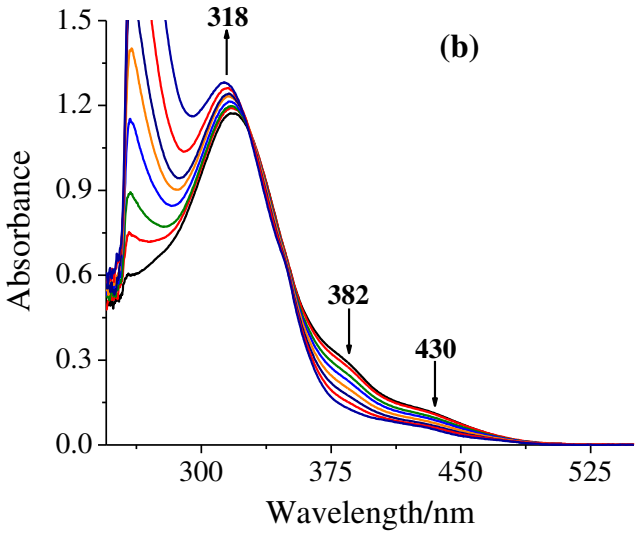

Figure 5.6. (b) The spectra were recorded after successive addition of one drop portion of H_2O_2 [30% H_2O_2 (0.990 g, 8.8 mmol) dissolved in 5 mL of DMSO; final concentration of H_2O_2 = 1.74 M)] to 20 mL of 5×10^{-5} M solution of [$Mo^{VI}O_2$(fhmc–inh)(MeOH)] (**5.2**).

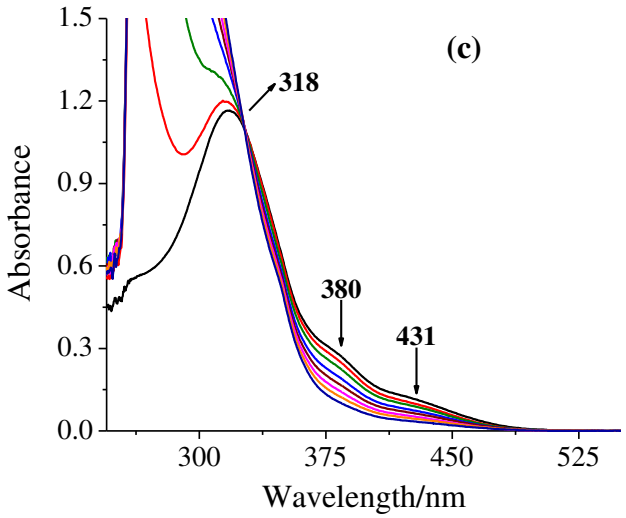

Figure 5.6. (c) The spectra were recorded after successive addition of one drop portion of H_2O_2 [30% H_2O_2 (0.825 g, 7.3 mmol) dissolved in 5 mL of DMSO; final concentration of H_2O_2 = 1.45 M] to 20 of mL of 4×10^{-5} M solution of [$Mo^{VI}O_2$(fhmc–nah)(MeOH)] (**5.3**).

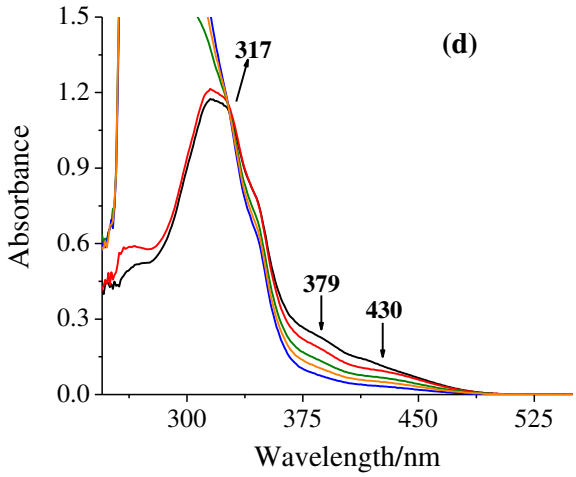

Figure 5.6. (d) The spectra were recorded after successive addition of one drop portion of H_2O_2 [30% H_2O_2 (0.938 g, 8.3 mmol) dissolved in 5 mL of DMSO; final concentration of H_2O_2 = 1.65 M] to 20 of mL of 3.5 × 10^{-5} M solution of [$Mo^{VI}O_2$(fhmc–fah)(MeOH)] (**5.4**).

5.4. Conclusions

The dioxidomolybdenum(VI) complexes [$Mo^{VI}O_2$(fhmc–bhz)(MeOH)] (**5.1**), [$Mo^{VI}O_2$(fhmc–inh)(MeOH)] (**5.2**) [$Mo^{VI}O_2$(fhmc–nah)(MeOH)] (**5.3**) and [$Mo^{VI}O_2$(fhmc–fah)(MeOH)] (**5.4**) have been prepared from tridentate ONO type ligands H_2fhmc–bhz (**5.I**), H_2fhmc–inh (**5.II**), H_2fhmc–nah (**5.III**) and H_2fhmc–fah (**5.IV**), respectively and characterized. These complexes are good catalyst precursors for the oxidative bromination of thymol in the presence of green oxidant 30 % H_2O_2, $HClO_4$ and bromide ion, therefore acting as functional models of vanadium dependent haloperoxidases; though molybdenum complexes do not have coordination atmosphere like [$VO(O^-)(OH)_2$] histidine present in vanadium complexes. [$Mo^{VI}O_2$]$^{2+}$ complexes upon treatment with H_2O_2 instantly generates [$Mo^{VI}O(O_2)$]$^{2+}$species which ultimately oxidizes Br^- to HOBr/ Br_2 in the presence of acid. This species brominates the thymol and give corresponding brominating products in high yield of ca. 94–99 under optimized % reaction conditions. The conversion of thymol is generally same in different solvents but the number of products and their selectivity are solvent dependent.

SUMMARY AND CONCLUSIONS

Synthesis of new dioxidomolybdenum(VI) complexes, their characterization and catalytic aspects for various organic transformations in homogenous environment have been reported in this thesis. To accomplish this goal the tribasic pentadentate Schiff bases H_3sal-dahp (**2.I**), H_3clsal-dahp(**2.II**) and H_3brsal-dahp(**2.III**) derived from 1,3-diamino-2-hydroxypropane and salicylaldehyde, 5-chlorosalicylaldehyde and 5-bromosalicylaldehyde, form dioxidomolybdenum(VI) complexes by the reaction of $[Mo^{VI}O_2(acac)_2]$ with in methanol at reflux conditions. These complexes catalyze the oxidative bromination of styrene in the presence of KBr, $HClO_4$ and H_2O_2 in biphasic aqueous/ CH_2Cl_2 solution yields 1, 2-dibromo-1-phenyl-ethane, 1-phenylethane-1, 2-diol and 2-bromo-1-phenylethane-1-ol, therefore they act as functional models of vanadium dependent haloperoxidases. It has also been demonstrated that complexes are catalyst precursors for the oxidation of methyl phenyl sulfide and benzoin.

The binucleating hydrazones [H_3dfmp(sbdt)$_2$ (**3.I**), H_3dfmp(smdt)$_2$ (**3.II**) and H_3dfmp(tsc)$_2$ (**3.III**) [derived from the condensation of 2,6-diformyl-4-methylphenol (dfmp) with *S*-benzyldithiocarbazate (sbdt), *S*-methyldithiocarbazate (smdt) and thiosemicarbazide (tsc)] results mononuclear dioxidomolybdenum(VI) complexes. All these complexes are characterized in the solid state and in solution namely by elemental analyses, spectroscopic techniques (IR, electronic, ^{1}H and ^{13}C NMR) and thermogravmetric analyses. Structures of these complexes also confirmed by single crystal X-ray study reveal that only one set of azomethine nitrogen, enthiolate sulfur and phenolate oxygen atoms of the ligands are coordinated to the molybdenum. These molybdenum complexes catalyze the oxidation of styrene and cyclohexene using 30 % H_2O_2 as oxidant in the presence of sodium bicarbonate. Styrene under optimized reaction conditions gave two reaction products namely, styrene oxide as a major and phenylacetaldehyde as a minor product. Oxidation of cyclohexene gave cyclohexene oxide selectively.

In addition the synthesis of dioxidomolybdenum(VI) complexes derived from the ligand [H_3dfmp(inh)$_2$ (**4.I**), H_3dfmp(nah)$_2$ (**4.II**) and H_3dfmp(bhz)$_2$ (**4.III**); inh = isonicotinoylhydrazide, nah = nicotinoylhydrazide and bhz = benzoylhydrazide] have been described. Single crystal X-ray analysis of complexes confirms the coordination of the ligand in the dianionic (ONO^{2-}) enolate-tautomeric form and one of the

hydrazido moieties remains non-coordinated. Oxidation of secondary alcohols: 1-phenyl ethanol, 2-propanol and 2-butanol, catalyzed by these molybdenum complexes, using conventional liquid phase and microwave-assisted methods in the presence of 30 % H_2O_2 as an oxidant have been tested. The effects of various factors, such as temperature and amounts of catalyst, H_2O_2 and solvent have been investigated. These alcohols under the optimized reaction conditions gave high yields of the respective ketone. Addition of an N-based additive reduces the reaction time considerably. Amongst the two methods studied, the microwave technique proves to be a time efficient system.

At the end haloperoxidases mimicking property of dioxidomolybdenum(VI) complexes $[Mo^{VI}O_2(fhmc\text{-}bhz)(MeOH)]$, $[Mo^{VI}O_2(fhmc\text{-}inh)(MeOH)]$, $[Mo^{VI}O_2(fhmc\text{-}nah)(MeOH)]$ and $[Mo^{VI}O_2(fhmc\text{-}fah)(MeOH)]$ has been described. These metal complexes have been tested against oxidative bromination of monoterpene (thymol) to yield 2-bromothymol, 4-bromothymol and 2,4-dibromothymol using H_2O_2 as an oxidant. The effects of various factors, such as amounts of catalyst, oxidant, KBr, $HClO_4$ and different solvents have beenconsidered to optimize the reaction conditions for the maximum brominated products.

Thus, synthesis, characterization, reactivity and catalytic activities of dioxidomolybenum(VI) complexes presented in the thesis contribute considerably to the existing knowledge.

REFERENCES

1. B.H. Davis, in G. Ertl, H. Knözinger and J. Weitkamp (Eds.), "Handbook of Heterogeneous Catalysis", Vol. 1, VCH, Weinheim, 1997.

2. I. Horiuti and M. Polanyi, "Exchange reactions of hydrogen on metallic catalysts", *Trans. Faraday Soc.*, **30** (1934) 1164–1172.

3. H.S. Taylor, "A theory of the catalytic surface", *Proc. R. Soc. A*., **108** (1925) 105–111.

4. A.J. van Peski, "Synthetic oil by catalytic polymerization of cracked gasoline hydrocarbons", 1937, US Pat. 2067030 19370105.

5. F. Schick and E. Emilius, "Catalytic cracking of heavy hydrocarbons", 1937, US Pat. 2097989 19371102.

6. F.A. Cotton, G. Wilkinson, C.A. Murillo and M. Bochmann, "Advanced Inorganic Chemistry", John Wiley & Sons, Inc. 6th Edition, 1999, p.1270.

7. E.B. Andrews, "Cobalt–molybdenum desulfurization catalyst", *Proc. Chem. Eng. Group Soc. Chem. Ind.*, (1963) 1396–1400.

8. W.J. Hendriks, J.C. Vlugter and H.I. Waterman, "Catalytic desulfurization of crude oil", *Brennstoff–Chemie*, **42** (1961) 1–11.

9. D.R. Armstrong, R. Fortune and P.G. Perkins, "A molecular orbital investigation of the wacker process for the oxidation of ethylene to acetaldehyde", *J. Catal.*, **45** (1976) 339–348.

10. B.R. James and M. Kastner, "Reactions of ethylene with rhodium(III) chloride, Catalytic oxidation of ethylene to acetaldehyde in aqueous hydrochloric acid solutions containing pentachloroaquorhodate(III)", *Canadian J. Chem.*, **50** (1972) 1698–1707.

11. P.B. Weisz and V.J. Frilette, "Intracrystalline and molecular–shape–selective catalysis by zeolite salts", *J. Phy. Chem.*, **64** (1960) 382–383.

12. P.B. Weisz, W.O. Haag and P.G. Rodewald, "Catalytic production of high–grade fuel (gasoline) from biomass compounds by shape–selective catalysis", *Science*, **206** (1979) 57–58.

13. M. Boudart, "Catalysis by supported metals", *Adv. Catal.*, **20** (1969) 153–166.

14. S.H. Oh and C.C. Eickel, "Influence of metal particle size and support on the catalytic properties of supported rhodium: carbon monoxide–oxygen and carbon monoxide–nitric oxide reactions", *J. Catal.*, **128** (1991) 526–536.

15. K.I. Jagel and F.G. Dwyer, "Hydro–carbon monoxide oxidation catalysts for vehicle exhaust emission control", *Proc. – Am. Petro. Inst., Div. Refining*, **51** (1971) 169–185.

16. G.H. Meguerian and C.R. Lang, "Nitric oxide/nitrogen dioxide reduction catalysts for vehicle emission control", *Proc. – Am. Petro. Inst., Div. Refining*, **51** (1971) 186–206.

17. O. Norbert, "DESONOX Process for Flue Gas Cleaning", *Catal. Today*, **16** (1993) 247–261.

18. J.A. Sullivan, J. Cunningham, M.A. Morris and K. Keneavey, "Conditions in which Cu–ZSM–5 out performs supported vanadia catalysts in SCR of NO, by NH_3", *Appl. Catal. B: Environ.*, **7** (1995) 137–151.

19. J. James and R.H.R. Julian, "The development of supported vanadia catalysts for the combined catalytic removal of the oxides of nitrogen and of chlorinated hydrocarbons from flue gases", *Catal. Today*, **35** (1997) 97–105.

20. S. Blumrich and B. Engler, "The DESONOX/REDOX–process for flue gas cleaning. A flue gas purification process for the simultaneous removal of NO, and SO_2 resp. CO and UHC", *Catal. Today*, **17** (1993) 301–310.

21. "The 12 Principle of Green Chemistry", United States Environmental Protection Agency". http://www.epa.gov/greenchemistry/pubs/principles.html. Retrieved on 2006–07–31.

22. Y.H. Chang, P.M. Chan, Y.F. Tsai, G.H. Lee, and H.F. Hsu, "Catalytic Reduction of Hydrazine to Ammonia by a Mononuclear Iron(II) Complex on a Tris(thiolato)phosphine Platform", *Inorg. Chem.,* **53** (2014) 664−666.

23. W.C. Chu, C.C. Wu, and H.F. Hsu, "Catalytic Reduction of Hydrazine to Ammonia by a Vanadium Thiolate Complex", Inorg. *Chem.,* **5** (2006) 3164−3166.

24. J.J. Boruah, D. Kalita, S.P. Das, S. Paul, and N.S. Islam, "Polymer−Anchored Peroxo Compounds of Vanadium(V) and Molybdenum(VI): Synthesis, Stability, and Their Activities with Alkaline Phosphatase and Catalase", *Inorg. Chem.,* **50** (2011) 8046–8062.

25. F. Saleem, G.K. Rao, G. Mukherjee and A.K. Singh, "Half sandwich

ruthenium(II) complexes of click generated 1,2,3–triazole based organo–sulfur/selenium ligands: structural and donor site dependent catalytic oxidation and transfer hydrogenation aspects", *Organometallics*, **32** (2013) 3595–3603.

26. G.K. Rao, A. Kumar, S. Kumar, U.B. Dupare and A.K. Singh, "Palladacycles of thioethers catalyzing Suzuki Miyaura C–C coupling: generation and catalytic activity of nanoparticles", *Organometallics*, **32** (2013) 2452–2458.

27. H. Joshi, K.N. Sharma, A.K. Sharma, O. Prakash and A.K. Singh, "Graphine oxide grafted with $Pd_{17}Se_{15}$ nano particles generated from single source precursor as recyclable and efficient catalyst for C–O coupling in O–arylation at room temperature", *Chem. Commun.,* **49** (2013) 7483–7485.

28. H. Bortels, "Molybdenum as a catalyst in the biogical fixation of nitrogen", *Arch. Mikrobiol*., **1** (1930) 333–342.

29. C. Andreini, I. Bertini, G. Cavallaro, G.L. Holliday and J.M. Thornton, "Metal ions in biological catalysis: from enzyme databases to general principles", *JBIC,* **13** (2008) 1205–1218.

30. R. Hille, "The mononuclear molybdenum enzymes", *Chem. Rev.,* **96** (1996) 2757–2816.

31. G. Schwarz, R.R. Mendel and M.W. Ribbe, "Molybdenum cofactors, enzymes and pathways", *Nature,* **460** (2009) 839–847.

32. K.V. Rajagopalan and J.L. Johnson, "The pterin molybdenum cofactors", *J. Biol. Chem.,* **267** (1992) 10199–10202.

33. R.C. Weast, "CRC Handbook of Chemistry and Physics*",* CRC Press, 61st edn., 1981, Boca Raton, FL.

34. P. Patnaik, "Handbook of Inorganic Chemicals", The McGraw–Hill Companies, United States of America 2003.

35. F.J. Arnaiz, R. Aguado, J. Sanz–Aparicio and M. Martinez–Ripoll, "Addition compounds of dichlorodioxomolybdenum(VI) from hydrochloric acid solutions of molybdenum trioxide. Crystal structure of dichlorodioxo diaquamolybdenum(VI) bis(2,5,8–trioxanonane)", *Polyhedron,***13** (1994) 2745–2749.

36. R. Sanz and M.R. Pedrosa, "Applications of dioxomolybdenum(VI) complexes to organic synthesis", *Curr. Org. Synth.,* **6** (2009) 239–263.

37. K. Jeyakumar and D.K. Chand, "Application of molybdenum(VI) dichloride dioxide (MoO_2C1_2) in organic transformations", *J. Chem. Sci.,***121** (2009) 111–123.

38. F.E. Kühn, A.D. Lopes, A.M. Santos, E. Herdtweek, J.J. Haider, C.C. Romão and A.G. Santos, "Lewis base adducts of bis–(halogeno) dioxomolybdenum(VI): syntheses, structures, and catalytic applications", *J Mol. Catal. A: Chem.,* **151** (2000) 147–160.

39. R.D. Chakravarthy and D.K. Chand, "Synthesis, structure and application of cis–dioxomolybdenum(VI)–(ONO) type complexes", *J Chem. Sci.,* **123** (2011) 187–199.

40. R.K. Grasselli, "Advances and future trends in selective oxidation and ammoxidation catalysis", *Catal. Today,* **49** (1999) 141–153.

41. M. Herbert, F. Montilla, A. Galindo, R. Moyano, A. Pastorand E. Àlvarez, "Influence of *N*–donor bases and the solvent in oxodiperoxomolybdenum catalysed olefin epoxidation with hydrogen peroxide in ionic liquids", *Dalton Trans.,***40** (2011) 5210–5219.

42. M. Herbert, F. Montilla, E. Àlvarez, and A. Galindo, "New insights into the mechanism of oxodiperoxomolybdenum catalysed olefin epoxidation and the crystal structures of several oxo–peroxo molybdenum complexes", *Dalton Trans.,* **41** (2012) 6942–6956.

43. M. Herbert, F. Montilla and A. Galindo, "Olefin epoxidation in solvent less conditions and a polar media catalysed by specialised oxodiperoxomolybdenum complexes", *J Mol. Catal. A: Chem.,* **338** (2011) 111–120.

44. M.E. Judmaier, C.H. Sala, F. Belaj, M. Volpe and N.C. Mösch–Zanetti, "Dimeric μ–oxo bridged molybdenum(VI) dioxo complexes as catalysts in the epoxidation of internal and terminal alkenes", *New J. Chem.,* **37** (2013) 2139–2149.

45. P. Traar, J.A. Schachner, B. Stanje, F. Belaj and N.C. Mösch–Zanetti, "Dioxomolybdenum(VI) complexes with naphtholate–oxazoline ligands in catalytic epoxidation of olefins", *J Mol. Catal. A: Chem.,* **385** (2014) 54–60.

46. K.J. Ivin and J.C. Mol, "Olefin metathesis polymerization", Academic Press, London 1997.

47. J. Belgacem, J. Kress and J.A. Osborn, "On the Allylic Rearrangements in Metal Oxo Complexes: Mechanistic and Catalytic Studies on $MoO_2(allyloxo)_2(CH_3CN)_2$ and analogous Complexes", *J. Am. Chem. Soc*., **114** (1992) 1501–1502.

48. R.D. Chakravarthy, V. Ramkumar and D.K. Chand, "A molybdenum based metallomicellar catalyst for controlled and selective sulfoxidation reactions in aqueous medium", *Green Chem.,* **16** (2014) 2190–2196.

49. J.J. Boruah, S.P. Das, S.R. Ankireddy, S.R. Gogoi and N.S. Islam, "Merrifield resin supported peroxomolybdenum(VI) compounds: recoverable heterogeneous catalysts for the efficient, selective and mild oxidation of organic sulfides with H_2O_2", *Green Chem.*, **15** (2013) 2944–2959.

50. J.J. Boruah, S.P. Das, R. Borah, S.R. Gogoi and N.S. Islam, "Polymer–anchored peroxo compounds of molybdenum and tungsten as efficient and versatile catalysts for mild oxidative bromination", *Polyhedron,* **52** (2013) 246–254.

51. G.C. Tucci, J.P. Donahue and R.H. Holm, "Comparative kinetics of oxo transfer to substrate mediated by bis(dithiolene)dioxomolybdenum and −tungsten Complexes", *Inorg. Chem.,* **37** (1998) 1602–1608.

52. M.A. Hussein, T.S. Guan, R.A. Haque, M.B.K. Ahamed and A.M.S.A. Majid, "Synthesis and characterization of thiosemicarbazonato molybdenum(VI) complexes: *In vitro* DNA binding, cleavage, and antitumor activities", *Polyhedron,* **85** (2015) 93–100.

53. S. Pasayat, S.P. Dash, Saswati , P.K. Majhi, Y.P. Patil, M. Nethaji, H.R. Dash, S. Das and R. Dinda, "Mixed–ligand aroylhydrazone complexes of molybdenum: Synthesis, structure and biological activity", *Polyhedron*, **38** (2012) 198–204.

54. S.K. Sridhar, M. Saravanan and A. Ramesh, "Synthesis and antibacterial screening of hydrazones, Schiff and Mannich bases of isatin derivatives", *Eur. J. Med. Chem.*, **36** (2001) 615–625.

55. S.N. Pandeya, D. Sriram, G. Nath and E. De Clercq, "Synthesis, antibacterial, antifungal and anti–HIV activities of Schiff and Mannich bases derived from isatin derivatives and N–[4–(4'–chlorophenyl)thiazol–2–yl] thiosemicarbazide," *Eur. J. Pharm. Sci.* **9** (1999) 25–31.

56. R. Mladenova, M. Ignatova, N. Manolova, T.S. Petrova and I. Rashkov, "Preparation, characterization and biological activity of Schiff base compounds derived from 8–hydroxyquinoline–2–carboxaldehyde and Jeffamines ED", *Eur. Polym. J.* **38** (2002) 989–999.

57. Y. Wong, D.K.P. Ng and H.K. Lee, "New Chloro, μ–Oxo, and Alkyl Derivatives of Dioxomolybdenum(VI) and Tungsten(VI) Complexes Chelated with N_2O Tridentate Ligands: Synthesis and Catalytic Activities toward Olefin Epoxidation", *Inorg. Chem.* **41** (2002) 5276–5285.

58. A. Lehtonen and R. Sillanpää, "Dioxomolybdenum(VI) complexes with tri– and tetradentate aminobis(phenolate s) ", *Polyhedron*, **24** (2005) 257–265.

59. S. Gupta, S. Pal, A.K. Barik, S. Roy, A. Hazra, T.N. Mandal, R.J. Butcher and S.K. Kar, "Molybdenum(VI) complexes of a few pyrimidine derived ligands and the study of metal mediated C=N bond cleavage resulting in ligand transformation during complex formation", *Polyhedron*, **28** (2009) 711–720.

60. Y.Wong, L.H. Tong, J.R. Dilworth, D.K.P. Ng and H.K. Lee, "New dioxo–molybdenum(VI) and –tungsten(VI) complexes with *N*–capped tripodal N_2O_2 tetradentate ligands: Synthesis, structures and catalytic activities towards olefin epoxidation", *Dalton Trans.*, **39** (2010) 4602–4611.

61. R.D. Chakravarthy, K. Suresh, V. Ramkumar and D.K. Chand, "New chiral molybdenum complex catalyzed sulfide oxidation with hydrogen peroxide", *Inorg. Chim. Acta*, **376** (2011) 57–63.

62. P. Neves, S. Gago, S.S. Balula, A.D. Lopes, A.A. Valente, L. Cunha–Silva, F.A. Almeida Paz, M. Pillinger, J. Rocha, C.M. Silva and I.S. Gonçalves, "Synthesis and Catalytic Properties of Molybdenum(VI) Complexes with Tris(3,5–dimethyl–1–pyrazolyl)methane", *Inorg. Chem.,* **50** (2011) 3490–3500.

63. F. Madeira, S. Barroso, S. Namorado, P.M. Reis, B. Royo and A.M. Martins, "Epoxidation of *cis*–cyclooctene using diamine bis(phenolate) vanadium, molybdenum and tungsten complexes as catalysts", *Inorg. Chim. Acta*, **383** (2012) 152–156.

64. M.E. Judmaier, C. Holzer, M. Volpe and N.C. Mösch–Zanetti, "Molybdenum(VI) dioxocomplexes employing schiff base ligands with an intramolecular donor for highly selective olefin epoxidation", *Inorg. Chem.*, **51** (2012) 9956–9966.

65. M. Chakraborty, S. Roychowdhury, N.R. Pramanik, T.K. Raychaudhuri, T. K.Mondal, S. Kundu, M.G.B. Drew, S. Ghosh andS.S. Mandal, "Synthesis, characterization, crystal structure and density functional theory (DFT) calculations of dioxomolybdenum (VI) complexes of an ONS donor ligand derived from benzoylacetone and S–benzyl dithiocarbazate", *Polyhedron*, **50** (2013) 602–611.

66. S.K. Kurapati, S. Maloth and S. Pal, "Complexes of *cis*–dioxomolybdenum(VI) with unsymmetrical tripodal NO_3–donor ligands: Synthesis, characterization and catalytic applications", *Inorg. Chim. Acta*, **430** (2015) 66–73.

67. C.P. Rao, A. Sreedhara, P.V. Rao, M.B. Verghese, K. Rissanen, E. Kolehmainen, N.K. Lokanath, M.A. Sridhar and J.S. Prasad, "Syntheses, structure, reactivity and species recognition studies of oxo–vanadium(V) and molybdenum(VI) complexes", *J. Chem. Soc*., *Dalton Trans*., (1998) 2383–2393.

68. A. Mukhopadhyay, A. Karkamkar, E. Kolehmainen and C.P. Rao, "Transition metal–saccharide chemistry: synthesis, characterization and solution stability studies of cis–dioxomolybdenum saccharide complexes", *Carbohydrate Research,* **311** (1998) 147–154.

69. A.K. Sah, C.P. Rao, P.K. Saarenketo, E.K. Wegelius, E. Kolehmainen and K. Rissanen, "First Crystallographic Investigation of Complexes of *cis*–VO_2^+, *cis*–MoO_2^{2+}, and *trans*–UO_2^{2+}Species with Schiff–Base Molecules Derived from 4,6–*O*–Ethylidene– β–D–glucopyranosylamine", *Eur. J. Inorg. Chem.,* (2001) 2773–2781.

70. M.R. Maddani, and K.P. Prabhu, "Dioxomolybdenum reagents in organic synthesis: utility of redox capability to design reduction and oxidation", *J. Indian Inst. Sci.,* **90** (2010) 287–297.

71. J. Kollar, "Catalytic epoxidation of olefinically unsaturated compounds by using organic hydroperoxides as epoxidizing agents", US3350422.

72. M.N. Sheng and J.G. Zajacek, "Epoxides", 1968, GB1136923.

73. K.B. Sharpless, and R.C. Michaelson, "High stereo− and regioselectivities in the transition metal catalyzed epoxidations of olefinic alcohols by tert−butyl hydroperoxide", *J Am. Chem. Soc.,* **95** (1973) 6136–6137.

74. A.U. Barlan, A. Basak and H. Yamamoto, "Enantioselective oxidation of olefins catalyzed by a chiral bishydroxamic acid complex of molybdenum", *Angew. Chem. Int. Ed.,* **45** (2006) 5849–5852.

75. A. Schmidt, N. Grover, T.K. Zimmermann, L. Graser, M. Cokoja, A. Pöthig and F.E. Kühn, "Synthesis and characterization of novel cyclopentadienyl molybdenumimidazo[1,5–a]pyridine–3–ylidene complexes and their application in olefin epoxidation catalysis", *J. Catal.,***319** (2014) 119–126.

76. M.M. Javadi, M. Moghadam, I.M. Baltork, S. Tangestaninejad, V. Mirkhani, H. Kargar and M.N. Tahir, "Oxidation of alkenes and sulfides catalyzed by a new binuclear molybdenum bis–oxazoline complex", *Polyhedron,* **72** (2014) 19–26.

77. R. Mayilmurugan, P. Traar, J.A. Schachner, M. Volpe, and N.C. Mösch–Zanetti, "Dioxidomolybdenum(VI) complexes containing ligands with the bipyrrolidine backbone as efficient catalysts for olefin epoxidation", *Eur. J. Inorg. Chem.* 2013, 3664–3670.

78. S. Maignien, S.A. Mohand and J. Muzart, "A practical molybdenum–catalyzed oxidation of alcohols by sodium percarbonate", *Synlett,* (1996) 439–440.

79. K. Jeyakumar and D.K. Chand, "Aerobic oxidation of benzyl alcohols by Mo^{VI} compounds", *Appl. Organometal. Chem.,* **20** (2006) 840–844.

80. D.K. Chand and R.D. Chakravarthy, "Molybdenum oxide chloride" in *The Handbook of Reagents for Organic Synthesis: Catalytic Oxidation Reagents,* P. L. Fuchs, John Wiley & Sons, Ltd, England, 1st edn., 2013, pp 407–410.

81. A.V. Biradar, M.K. Dongare and S.B. Umbarkar, "Selective oxidation of aromatic primary alcohols to aldehydes using molybdenum acetylide oxo–peroxo complex as catalyst", *Tetrahedron Letters,* **50** (2009) 2885–2888.

82. N. Gharah, S. Chakraborty, A.K. Mukherjee and R. Bhattacharyya, "Oxoperoxo molybdenum(VI)− and tungsten(VI) complexes with 1−(2′−hydroxyphenyl) ethanone oxime: Synthesis, structure and catalytic uses in the oxidation of olefins, alcohols, sulfides and amines using H_2O_2 as a terminal oxidant", *Inorg. Chim. Acta*, **362** (2009) 1089–1100.

83. K. Jeyakumar and D.K. Chand, "Selective oxidation of sulfides to sulfoxides and sulfones at room temperature using H_2O_2 and a Mo(VI) salt as catalyst", *Tetrahedron Lett.,* **47** (2006) 4573–4576.

84. C. A. Gamelas, T. Lourenco, A. Pontes da Costa, A.L. Simplicio, B. Royo and C.C. Romao, "Selective and mild oxidation of sulfides to sulfoxides or sulfones using H_2O_2 and $Cp'Mo(CO)_3C1$ as catalysts", *Tetrahedron Lett.,* **49** (2008) 4708–4712.

85. W. Zhu, H. Li, Q.Q. Gu, P. Wu, G. Zhu, Y. Yan and G. Chen, "Kinetics and mechanism for oxidative desulfurization of fuels catalyzed by peroxo–molybdenum amino acid complexes in water–immiscible ionic liquids", *J Mol. Catal. A: Chem.,* **336** (2011) 16–22.

86. K. Jeyakumar and D.K. Chand, "Molybdenum(VI) dichloride dioxide catalyzed conversion of β–hydroxycarbonyls to α–bromo 1,3–dicarbonyls by N–bromosuccinimide", *Synthesis,* (2009) 306–310.

87. S. Pasayat, S.P. Dash, S. Roy, R. Dinda, S. Dhaka, M.R. Maurya, W. Kaminsky, Y.P. Patil and M. Nethaji, "Synthesis, structural studies and catalytic activity of dioxidomolybdenum(VI) complexes with aroylhydrazones of naphthol–derivative", *Polyhedron*, **67** (2014) 1–10.

88. H. Yang, H. Wang and C. Zhu, "Enantioselective pinacol coupling of aryl aldehydes catalyzed by chiral salan–Mo(IV) complexes", *J. Org. Chem.,***72** (2007) 10029–10034.

89. R. Sanz, R. Aguado, M.R. Pedrosa and F.J. Arnaiz, "Simple and selective oxidation of thiols to disulfides with dimethylsulfoxide catalyzed by dichlorodioxomolybdenum(VI)", *Synthesis,* (2002) 856–858.

90. K. Jeyakumar and D.K. Chand, "Ring opening reactions of epoxides catalyzed by molybdenum(VI) dichloride dioxide", *Synthesis,* (2008) 807–819.

91. P. Costa, P.M. Reis, C. Gamelas, C.C. Romão and B. Royo, "Dioxo–molybdenum(VI) and −tungsten(VI) BINOL and alkoxide complexes: Synthesis and catalysis in sulfoxidation, olefin epoxidation and hydrosilylation of carbonyl groups", *Inorg. Chim. Acta*, **361** (2008) 1915–1921.

92. M. Abrantes, I.S. Gonçalves, M. Pillinger, C. Vurchio, F.M. Cordero and A. Brandi, "Molybdenum oxide/bipyridine hybrid material $\{[MoO_3(bipy)][MoO_3(H_2O)]\}_n$ as catalyst for the oxidation of secondary amines to nitrones", *Tetrahedron Lett.,* **52** (2011) 7079–7082.

93. A.V. Biradar, T.V. Kotbagi, M.K. Dongare and S.B. Umbarkar, "Selective N–oxidation of aromatic amines to nitroso derivatives using a molybdenum acetylide oxo–peroxo complex as catalyst", *Tetrahedron Lett.,* **49** (2008) 3616–3619.

94. S. Das, T. Bhowmick, T. Punniyamurthy, D. Dey, J. Nath and M.K. Chaudhuri, "Molybdenum(VI)–peroxo complex catalyzed oxidation of alkylbenzenes with hydrogen peroxide", *Tetrahedron Lett*. **44** (2003) 4915–4917.

95. E.I. Stiefel, "Molybdenum bolsters the bioinorganic brigade", *Science,* **272** (1996) 1599–1600.

96. M.M. Abu–omar, A. Loaiza and N. Hontzeas, "Reaction mechanisms of mononuclear non–heme iron oxygenases", *Chem. Rev.,* **105** (2005) 2227–2252.

97. C.A. McAuliffe, F.P. Mc Cullough, M.J. Parrott, C.A. Rice, B.J. Sayle and W. Levanson, "The chemistry of molybdenum and tungsten. part 7.l oxomolybdenum(V) and oxotungsten(V) complexes of neutral aromatic Schiff base ligands", *J. Chem. Soc. Dalton Trans.,* (1977) 1762–1766.

98. R.H. Holm, "The biologically relevant oxygen atoms transfer chemistry of molybdenum: From synthetic analog systems to enzymes", *Coord. Chem. Rev.,* **100** (1990) 183–221.

99. J.T. Spence, "Modeling the molybdenum centers of the molybdenum hydroxylases", *Coord. Chem. Rev.,* **48** (1983) 59–82.

100. A. Thapper, A. Behrens, J. Fryxelius, M.H. Johansson, F. Prestopino, M. Czaun, D. Rehder and E. Nordlander, "Synthesis and characterization of molybdenum oxo complexes of two tripodal ligands: reactivity studies of a functional model for molybdenum oxotransferases", *Dalton Trans.,* **21** (2005) 3566–3571.

101. R. Hahn, W.A. Herrmann, G.R.J. Artens and M. Kleine, "Biologically relevant metal coordination compounds: $Mo^{VI}O_2$ and nickel(II) complexes with tridentate aromatic schiff bases", *Polyhedron,***14** (1995) 2953–2960.

102. J. Liimatainen, A. Lehtonen and R. Sillanpaa, "Cis–Dioxomolybdenum(VI) complexes with tridentate and tetradentate Schiff base ligands. Preparation, structures and inhibition of aerial oxidation of aldehydes", *Polyhedron,* **19** (2000) 1133–1138.

103. U. Sandbhor, S. Padhye and E. Sinn, "Cis di–oxomolybdenum(VI) complexes with a tridentate ONO donor ligand; synthesis, X–ray crystal structure, spectroscopic properties and oxotransfer chemistry", *Transition Met. Chem.,* **27** (2002) 681–685.

104. M. Cindric, N. Strukan, V. Vrdoljak and B. Kamenar, "A series of molybdenum(VI) complexes with tridentate schiff base ligands", *Z. Anorg, Allg. Chem.* **628** (2002) 2113–2117.

105. H. Arzoumanian, G. Agrifoglio, H. Krentzien and M. Capparelli, "Arylalkane oxidation by dioxo [4,4/−di (tert−butyI)−2,2'−bipyridyl] molybdenum (VI)complexes", *J. Chem. Soc. Chem. Commun.,* (1995) 655–656.

106. H. Arzoumanian, L. Maurino and G. Agrifoglio, "Thiocyanatodioxomolybdenum(VI) complexes as efficient oxidizing agents", *J. Mol. Catal. A: Chem.* **117** (1997) 471–478.

107. M.M. Farahani, F. Farzaneh and M. Ghandi, "Synthesis of tetradentate N_4 Schiff base dioxomolybdenum (VI) complex within MCM–41 as selective catalyst for epoxidation of olefins", *Catal. Commun.,* **8** (2007) 6–10.

108. M.M. Farahani, F. Farzaneh and M. Ghandi, "Synthesis and characterization of molybdenum complexes with bidentate Schiff base ligands within nano reactors of MCM–41 as epoxidation catalysts", *J. Mol. Catal. A: Chem.,* **248** (2006) 53–60.

109. K. Ambroziak, R. Pelech, E. Milchert, T. Dziembowska and Z. Rozwadowski, "New dioxomolybdenum(VI) complexes of tetradentate Schiff base as catalysts for epoxidation of olefins", *J. Mol. Catal. A: Chem.,* **211** (2004) 9–16.

110. Y. Sui, X. Zeng, X. Fang, X. Fu, Y. Xiao, L. Chen, M. Li and S.J. Cheng, "Syntheses, structure, redox and catalytic epoxidation properties of dioxomolybdenum(VI) complexes with Schiff base ligands derived from tris(hydroxymethyl)amino methane", *J. Mol. Catal. A: Chem.*, **270** (2007) 61–67**.**

111. J. Zhao, X. Zhou, A.M. Santos, E. Herdtweck, C.C. Romao and F.E. Kühn, "Molybdenum(VI) cis–dioxo complexes bearing sugar derived chiral Schiff–base ligands: synthesis, characterization, and catalytic applications", *Dalton Trans.,* (2003) 3736–3742.

112. X. Zhou, J. Zhao, A.M. Santos and F.E. Kühn, "Molybdenum(VI) cis –Dioxo Complexes with Chiral Schiff Base Ligands: Synthesis, Characterization, and Catalytic Applications", *Naturforschung*, **59** (2004) 1223–1228.

113. J.M. Sobczak and J.J. Ziólkowski, "Molybdenum complex–catalysed epoxidation of unsaturated fatty acids by organic hydroperoxides", *Appl. Catal. A,* **248** (2003) 261–268.

114. M. Bagherzadeh, R. Latifi, L. Tahsini, V. Amani, A. Ellern and L.K. Woo, "Synthesis, characterization and crystal structure of a dioxomolybdenum(VI) complex with a N,O type bidentate Schiff base ligand as a catalyst for homogeneous oxidation of olefins", *Polyhedron,* **28** (2009) 2517–2521.

115. A. Rezaeifard, I. Sheikhshoaie, N. Monadi and M. Alipour, "Synthesis, characterization and pronounced epoxidation activity of cis–dioxomolybdenum(VI) tridentate Schiff base complexes using tert–butyl hydroperoxide", *Polyhedron,* **29** (2010) 2703–2709.

116. J. Pisk, D. Agustin, V. Vrdoljak and R. Poli, "Epoxidation Processes by Pyridoxal Dioxomolybdenum(VI) (Pre)Catalysts Without Organic Solvent", *Adv. Synth. Catal.,* **353** (2011) 2910–2914.

117. J. Pisk, B. Prugovečki, D. Matković–Čalogović, R. Poli, D. Agustin and V. Vrdoljak, "Charged dioxomolybdenum(VI) complexes with pyridoxal thiosemicarbazone ligands as molybdenum(V) precursors in oxygen atom transfer process and epoxidation (pre)catalysts", *Polyhedron,* **33** (2012) 441–449.

118. K.C. Gupta and A.K. Sutar, "Catalytic activities of Schiff base transition metal complexes", *Coord. Chem. Rev.,* **252** (2008) 1420–1450.

119. X. Lei and N. Chelamalla, "Dioxomolybdenum(VI) complexes with linear and tripodal tetradenate ligands: Synthesis, structures and their use as olefin epoxidation catalysts", *Polyhedron,* **49** (2013) 244–251.

120. M.R. Maurya, "Catalytic applications of polymer–supported molybdenum complexes in organic transformations" *Curr. Org. Chem.,* **16** (2012) 73–88.

121. K.I. Smith, L.L. Borer and M.M. Olmstead, "Vanadium(IV) and vanadium(V) complexes of salicyladimine ligands", *Inorg. Chem.,* **42** (2003) 7410–7415.

122. M.R. Maurya, M. Bisht, N. Chaudhary, F. Avecilla, U. Kumar and H.F. Hsu, "Synthesis, structural characterization, encapsulation in zeolite Y and catalytic activity of an oxidovanadium(V) complex with a tribasic pentadentate ligand", *Polyhedron,* **54** (2013) 180–188.

123. R.K. Bhatia and G.N. Rao, "Oxidation of benzoin with anchored vanadyl and molybdenyl catalysts", *J. Mol. Catal. A: Chem.,* **121** (1997) 171–178.

124. M.R. Maurya, U. Kumar and P. Manikandan, "Polymer supported vanadium and molybdenum complexes as potential catalysts for the oxidation and oxidative bromination of organic substrates", *Dalton Trans.,* (2006) 3561–3575.

125. M.R. Maurya, A. Arya, P. Adão and J.C. Pessoa, "Immobilisation of oxovanadium(IV), dioxomolybdenum(VI) and copper(II) complexes on polymers for the oxidation of styrene, cyclohexene and ethylbenzene", *Appl. Catal. A: Gen.,* **351** (2008) 239–252.

126. Z. Hu, X. Fu and Y. Li, "Olefin epoxidation catalyzed by Schiff base molybdenum (VI) complexes immobilized onto zirconium poly (styrene–phenylvinylphosphonate)–phosphate", *Inorg. Chem. Commun.,* **14** (2011) 497–501.

127. M. Bagherzadeh, M.M. Haghdoost, M. Amini and P.G. Derakhshandeh, "Molybdenum oxo–peroxo complex: A very fast catalyst for oxidation and reduction of sulfur–based compounds", *Catal.Commun.,* **23** (2012) 14–19.

128. I. Sheikhshoaie, A. Rezaeifard, N. Monadi and S. Kaafi, "A novel tridentate Schiff base dioxo–molybdenum(VI) complex: Synthesis, crystal structure and catalytic performance in green oxidation of sulfides by urea hydrogen peroxide", *Polyhedron,* **28** (2009) 733–738.

129. A. Butler, M.J. Clague and G.E. Meister, "Vanadium peroxide complexes", *Chem. Rev.,* **94** (1994) 625–638.

130. C.J. Schneider, J.E. Penner–Hahn and V.L. Pecoraro, "Elucidating the protonation site of vanadium peroxide complexes and the implications for biomimetic catalysis", *J. Am. Chem. Soc.,* **130** (2008) 2712–2713.

131. P. Adao, J.C. Pessoa, R.T. Henriques, M.L. Kuznetsov, F. Avecilla, M.R. Maurya, U. Kumar and I. Correia, "Synthesis, characterization, and application of vanadium−salan complexes in oxygen transfer reactions", *Inorg. Chem.,* **48** (2009) 3542–3561.

132. G.J.J. Chen, J.W. McDonald and W.E. Newton, "Synthesis of Mo(IV) and Mo(V) complexes using oxo abstraction by phosphines. Mechanistic implications", *Inorg. Chem.,* **15** (1976) 2612–2615.

133. M.R. Maurya, M. Bisht and F. Avecilla, "Synthesis, characterisation and catalytic activities of vanadium complexes containing ONN donor ligand (E)–4–[(2–(dimethylamino)ethylimino]methyl–5–(hydroxymethyl)–2– methylpyridin–3–ol", *Indian J. Chem.,* **50A** (2011) 1562–1573.

134. G.M. Sheldrick, SHELXS–97: An integrated system for solving crystal structures from diffraction data, Revision 5.1, University of Göttingen, Germany, 1997.

135. R. Dinda, P. Sengupta, S. Ghosh and W.S. Sheldrick, "Synthesis, structure, and reactivity of a new mononuclear molybdenum(VI) complex resembling the active center of molybdenum oxotransferases", *Eur. J. Inorg. Chem.,* (2003) 363–369.

136. A. Syamal and M.R. Maurya, "Coordination chemistry of schiff base complexes of molybdenum", *Coord. Chem. Rev.,* **95** (1989) 183–238.

137. A.J. Bridgeman and G. Cavigliasso, "Electronic structure of the α and β isomers of $[Mo_8O_{26}]^{4-}$", *Inorg. Chem.,* **41** (2002) 3500–3507.

138. K.H. Tytko, J. Mehmke and S. Fischer, "Bonding and charge distribution in isopolyoxometalate ions and relevant oxides – a bond valence approach", *Struct. Bond.,* (Berlin) **93** (1999) 129–321**.**

139. M.R. Maurya, D.C. Antony, S. Gopinathan and C. Gopinathan, "Dioxomolybdenum(VI) complexes of new binucleating schiff bases derived from methylene–or dithio–bis(salicyclaldehyde) and various amines", *Polyhedron,* **12** (1993) 2731–2736.

140. A.D. Keramidas, A.B. Papaioannou, A. Vlahos, T.A. Kabanos, G. Bonas, A. Makriyannis, C.P. Rapropoulou and A. Terzis, "Model investigations for vanadium−protein interactions. synthetic, structural, and physical studies of vanadium(III) and oxovanadium(IV/V) complexes with amidate ligands", *Inorg. Chem.,* **35** (1996) 357–367.

141. V. Conte and B. Floris, "Vanadium catalyzed oxidation with hydrogen peroxide", *Inorg. Chim. Acta,* **363** (2010) 1935–1946.

142. V. Conte, A. Coletti, B. Floris, G. Licini and C. Zonta, "Mechanistic aspects of vanadium catalysed oxidations with peroxides", *Coord. Chem. Rev.,* **255** (2011) 2165–2177**.**

143. M.R. Maurya, C. Haldar, A. Kumar, M.L. Kuznetsov, F. Avecilla and J.C. Pessoa, "Vanadium complexes having $[VO]^{2+}$, $[VO]^{3+}$ and $[VO_2]^{+}$ cores with hydrazones of 2,6–diformyl–4–methylphenol: synthesis, characterization, reactivity, and catalytic potential", *Dalton Trans.,* **42** (2013) 11941–11962.

144. M.A. Anderson, A. Willets and S. Allenmark, "Asymmetric sulfoxidation catalyzed by a vanadium–containing bromoperoxidase", *J. Org. Chem.,* **62** (1997) 8455–8458.

145. H.B. ten Brink, H.E. Schoemaker and R. Wever, "Sulfoxidation mechanism of vanadium bromoperoxidase from *Ascophyllum nodosum*", *Eur. J. Biochem.,* **268** (2001) 132–138.

146. E. Clark, in: J.I. Kroschwitz, M. Howe–Grant (Eds.), Encyclopedia of Chemical Technology, vol. 23, fourth ed., Wiley, New York, 1997, pp. 134–146.

147. P.C.B. Page, Organosulfur Chemistry I and II, Springer, Berlin, 1999.

148. I. Fernandez and N. Khiar, "Recent developments in the synthesis and utilization of chiral sulfoxides", *Chem. Rev.,* **103** (2003) 3651–3705**.**

149. A.M. Khenkin and R. Neumann, "Oxygen transfer from sulfoxides: oxidation of alkylarenes catalyzed by a polyoxomolybdate, $[PMo_{12}O_{40}]^{3-}$", *J. Am. Chem. Soc.,* **124** (2002) 4198–4199.

150. L.A. Paquette, "The electrophilic and radical behavior of α–halosulfonyl systems", *Synlett.,* **1** (2001) 1–12.

151. C. Najera and J.M. Sansano, "Synthetic applications of functionalized sulfones as carbanionic reagents", *Recent Res. Dev. Org. Chem.,* **2** (1998) 637–683.

152. R. Chinchila and C. Najera, "Synthetic applications of sulfones as cationic reagents", *Recent Res. Dev. Org. Chem.,* **1** (1997) 437– 467.

153. G.B. Gill, in: G. Pattenden (Ed.), Comprehensive Organic Synthesis, Pergamon Press, New York, 1991, vol. 3, pp. 821–838.

154. E.I. Stiefel, "The biogeochemistry of molybdenum and tungsten", *Met. Ions Biol. Syst.,* **39** (2002) 1–29.

155. H. Dobbek, "Structural aspects of mononuclear Mo/W–enzymes", *Coord. Chem. Rev.,* **255** (2011) 1104–1116.

156. R.H. Holm, "Metal–centered oxygen atom transfer reactions", *Chem. Rev.,* **87** (1987), 1401–1449.

157. (a) A. Majumdar and S. Sarkar, "Bioinorganic chemistry of molybdenum and tungsten enzymes: A structural‑functional modeling approach", *Coord. Chem. Rev.,* **255** (2011) 1039–1054.
(b) R. Hille, T. Nishino and F. Bittner, "Molybdenum enzymes in higher organisms", *Coord. Chem. Rev.,* **255** (2011) 1179–1205.

158. M.R. Maurya, S. Dhaka and F. Avecilla, "Synthesis, characterization and catalytic activity of dioxidomolybdenum(VI) complexes of tribasic pentadentate ligands", *Polyhedron,* **67** (2014) 145–159.

159. S.K. Maiti, S. Dinda, S. Banerjee, A.K. Mukherjee and R. Bhattacharya, "Oxidoperoxidotungsten(VI) complexes with secondary hydroxamic acids: synthesis, structure and catalytic uses in highly efficient, selective and ecologically benign oxidation of olefins, alcohols, sulfides and amines with H_2O_2 as a terminal oxidant", *Eur. J. Inorg. Chem.,* (2008) 2038–2051.

160. M. Bagherzadeh, M. Amini, H. Parastar, M. Jalali–Heravi, A. Ellern and L.K. Woo, "Synthesis, X–ray structure and oxidation catalysis of a oxido–peroxido molybdenum(VI) complex with a tridentate Schiff base ligand", *Inorg. Chem. Commun.,* **20** (2012) 86–89.

161. B.S. Lane, M. Vogt, V.J. DeRose and K. Burgess, "Manganese–catalyzed epoxidations of alkenes in bicarbonate solutions", *J. Am. Chem. Soc.,* **124** (2002) 11946–11954.

162. D.E. Richardson, H. Yao, K.M. Frank and D.A. Bennett, "Equilibria, kinetics, and mechanism in the bicarbonate activation of hydrogen peroxide: oxidation of sulfides by peroxymonocarbonate", *J. Am. Chem. Soc.,* **122** (2000) 1729–1739.

163. V. Vrdoljak, J. Pisk, B. Prugovečki and D. Matković–Čalogović, "Novel dioxomolybdenum(VI) and oxomolybdenum(V) complexes with pyridoxal thiosemicarbazone ligands: Synthesis and structural characterisation", *Inorg. Chim. Acta,* **362** (2009) 4059–4064.

164. A. Rana, R. Dinda, P. Sengupta, S. Ghosh and L.R. Falvello, "Synthesis, characterisation and crystal structure of *cis*–dioxomolybdenum(VI) complexes of some potentially pentadentate but functionally tridentate (ONS) donor ligands", *Polyhedron,* **21** (2002) 1023–1030.

165. R.R. Gagne, C.L. Spiro, T.J. Smith, C.A. Hamann, W.R. Thies and A.D. Shiemke, "The synthesis, redox properties, and ligand binding of heterobinuclear transition–metal macrocyclic ligand complexes. Measurement of an apparent delocalization energy in a mixed–valent $cu^{I}cu^{II}$ complex", *J. Am. Chem. Soc.,* 103 (1981) 4073–4081.

166. M.A. Ali and M.T.H. Tarafder, "Metal complexes of sulphur and nitrogen–containing ligands: Complexes of s–benzyldithiocarbazate and a schiff base formed by its condensation with pyridine–2–carboxaldehyde", *J. Inorg. Nucl. Chem.,* **39** (1977) 1785–1791.

167. M. Das and S.E. Livingstone, "Metal chelates of dithiocarbazic acid and its derivatives. IX. Metal chelates of ten new schiff bases derived from S–methyldithiocarbazate", Inorg. Chim. Acta, 19 (1976) 5–10.

168. C.A. Hunter and J.K.M. Sanders, "The nature of pi–pi interactions" *J. Am. Chem. Soc.,* **112** (1990) 5525–5534.

169. M.R. Maurya, S. Khurana, Shailendra, A. Azam, W. Zhang and D. Rehder, "Synthesis, characterisation and antiamoebic studies of dioxovanadium(V) complexes containing ONS donor ligands derived from S–benzyldithiocarbazate", *Eur. J. Inorg. Chem.,* (2003) 1966–1973.

170. M.R. Maurya, A. Kumar and J.C. Pessoa, "Vanadium complexes immobilized on solid supports and their use as catalysts for oxidation and functionalization of alkanes and alkenes", *Coord. Chem. Rev.,* **255** (2011) 2315–2344.

171. M.R. Maurya, M. Kumar and U. Kumar, "Polymer–anchored vanadium(IV), molybdenum(VI) and copper(II) complexes of bidentate ligand as catalyst for the liquid phase oxidation of organic substrates", *J. Mol. Catal. A: Chem.,* **273** (2007) 133–143.

172. M.R. Maurya, N. Kumar and F. Avecilla, "Polymer and non–polymer–grafted dioxidomolybdenum(VI) complexes having ONO donor ligand and their catalytic activities for the oxidative bromination of organic substrates", *J. Mol. Catal. A: Chem.,* 392 (2014) 50–60.

173. G.J. ten Brink, I.W.C.E. Arends and R.A. Sheldon, "Green, catalytic oxidation of alcohols in water", *Science,* **287** (2000) 1636–1639.

174. P. Chaudhuri, M. Hess, T. Weyhermüller and K. Wieghardt, "Aerobic oxidation of primary alcohols by a new mononuclear Cu^{II} radical catalyst", *Angew. Chem., Int. Ed.,* **38** (1999) 1095–1098.

175. A. Dijkman, I.W.C.E. Arends and R.A. Sheldon, "Efficient ruthenium–TEMPO–catalysed aerobic oxidation of aliphatic alcohols into aldehydes and ketones", *Chem. Commun.,* (1999) 1591–1592.

176. I.E. Markó, P.R. Giles, M. Tsukazaki, S.M. Brown and C.J. Urch, "Copper catalyzed oxidation of alcohols to aldehydes and ketones: An efficient, aerobic alternative", *Science,* **274** (1996) 2044–2046.

177. I.E. Markó, P.R. Giles, M. Tsukazaki, I. Chellé–Regnaut, C.J. Urch and S.M. Brown, "Efficient, aerobic, ruthenium–catalyzed oxidation of alcohols into aldehydes and ketones", *J. Am. Chem. Soc.,* **119** (1997) 12661–12662.

178. Y.Y. Karabach, M.N. Kopylovich, K.T. Mahmudov and A.J.L. Pombeiro, "Microwave–assisted catalytic oxidation of alcohols to carbonyl compounds, in Advances in Organometallic Chemistry and Catalysis": The Silver/Gold Jubilee International Conference on Organometallic Chemistry Celebratory Book, ed. A. J. L. Pombeiro, Wiley, 2014, ch. 18, pp. 233–245.

179. R.R. Fernandes, J. Lasri, M.F.C. Guedes da Silva, J.A.L. da Silva, J.J.R. Frausto da Silva and A.J.L. Pombeiro, "Bis– and tris–pyridyl amino and imino thioether Cu and Fe complexes. Thermal and microwave–assisted peroxidative oxidations of 1– phenylethanol and cyclohexane in the presence of various N–based additives", *J. Mol. Catal. A: Chem.,* **351** (2011) 100–111.

180. K.A. Jorgensen, "Transition-metal-catalyzed epoxidations", *Chem. Rev.,* **89** (1989) 431–458.

181. R.M. Calvente, J.M. Campos–Martin and J.L.G. Fierro, "Effective homogeneous molybdenum catalyst for linear terminal alkenes epoxidation with organic hydroperoxide", *Catal. Commun.,* **3** (2002) 247–251.

182. W. Thiel, "Metal catalyzed oxidations. Part 5. Catalytic olefin epoxidation with seven–coordinate oxobisperoxo molybdenum complexes: a mechanistic Study", *J. Mol. Catal. A: Chem.,* **117** (1997) 449–454.

183. M. Araghi, A. Ghorbani and F.E. Yeganeh, "Efficient oxidation of alcohols with tert–butyl hydroperoxide catalyzed by $Mo(CO)_6$ supported on multiwall carbon nanotubes", *C. R. Chim.,* **16** (2013) 109–113.

184. S.K. Maiti, K.M.A. Malik and R. Bhattacharyya, "Oxoperoxo–molybdenum and –tungsten (VI) complexes: their synthesis, structure and catalytic uses in the peroxidic oxidation of alcohols to aldehydes and ketones", *Inorg. Chem. Commun.,* **7** (2004) 823–828.

185. B.L. Hayes, Microwave Synthesis, Chemistry at the Speed of Light, CEM Publishing, USA, 2002.

186. L. Bai and J.X. Wang, "Environmentally friendly suzuki aryl–aryl cross–coupling reaction", *Curr. Org. Chem.,* **9** (2005) 535–553.

187. M. Larhed, C. Moberg and A. Hallberg, "Microwave–accelerated homogeneous catalysis in organic chemistry", *Acc. Chem. Res.,* **35** (2002) 717–727.

188. V. Polshettiwar and R.S. Varma, "Microwave–assisted organic synthesis and transformations using benign reaction media", *Acc. Chem. Res.,* **41** (2008) 629–639.

189. J. Habermann, S. Ponzi and S.V. Ley, "Organic chemistry in ionic liquids using non–thermal energy–transfer processes", *Mini–Rev. Org.Chem.,* **2** (2005) 125–137.

190. S. Deshayes, M. Liagre, A. Loupy, J.L. Luche and A. Petit, "Microwave activation in phase transfer catalysis", *Tetrahedron,* **55** (1999), 10851–10870.

191. A. Lew, P.O. Krutzik, M.E. Hart and A.R. Chamberlin, "Increasing rates of reaction: microwave–assisted organic synthesis for combinatorial chemistry", *J. Comb. Chem.,* **4** (2002) 95–105.

192. P. Lidström, J. Tierney, B. Wathey and J. Westman, "Microwave assisted organic synthesis–a review", *Tetrahedron,* **57** (2001) 9225–9283.

193. P.A. Vigato and S. Tamburini, "The challenge of cyclic and acyclic schiff bases and related derivatives" *Coord. Chem. Rev.,* **248** (2004) 1717–2128.

194. M. Sutradhar, T.R. Barman, S. Ghosh and M.G.B. Drew "Synthesis and characterization of mixed–ligand complexes using a precursor mononuclear oxidovanadium(V) complex derived from a tridentate salicylhydrazone oxime ligand", *J. Mol. Struct.,* **1037** (2013), 276–282.

195. M. Sutradhar, T.R. Barman, J. Klanke, M.G.B. Drew and E. Rentschler, "A novel Cu(II) dimer containing oxime–hydrazone Schiff base ligands with an unusual mode of coordination: Study of magnetic, autoreduction and solution properties", *Polyhedron*, **53** (2013) 48–55.

196. D. Wang, M. Ebel, C. Schulzke, C. Grüning, S.K.S. Hazari and D. Rehder, "Vanadium(IV and V) complexes containing *SNO* (dithiocarbonylhydrazone; thiosemicarbazone) donor sets", *Eur. J. Inorg. Chem.,* (2001) 935–942.

197. J.C. Pessoa, M.J. Calhorda, I. Cavaco, I. Correia, M.T. Duarte, V. Felix, R.T. Henriques, M.F.M. Piedade and I. Tomaz, "Molecular modelling studies of N–salicylideneamino acidato complexes of oxovanadium(IV). Molecular and crystal structure of a new dinuclear LOV^{IV}–O–$V^{V}OL$ mixed valence complex", *J. Chem. Soc., Dalton Trans.,* (2002) 4407–4415.

198. A. Sabbatini, L.M.D.R.S. Martins, K.T. Mahmudov, M.N. Kopylovich, M.G.B. Drew, C. Pettinari and A.J.L. Pombeiro, "Microwave–assisted and solvent–free peroxidative oxidation of 1– phenylethanol to acetophenone with a Cu^{II}–TEMPO catalytic system *Catal. Commun.,* **48** (2014) 69–72.

199. P.K. Ajikumar, K. Tyo, S. Carlsen, O. Mucha, T.H. Phon and G. Stephanopoulos, "Terpenoids: opportunities for biosynthesis of natural product drugs using engineered microorganisms", *Mol. Pharmaceutics,* **5** (2008) 167–190.

200. C.C.C.R. de Carvalho and M.M.R. da Fonseca, "Biotransformation of terpenes", *Biotechnol. Adv.,* **24** (2006) 134–142.

201. M.S. Yusubo, L.A. Drygunov, A.V. Tkachev and V.V. Zhdankin, "Halomethoxylation of monoterpenes using (dichloroiodo)benzene", *Arkivoc IV,* (2005) 179–188.

202. S.A. Kotharkar, S.S. Bahekar and D.B. Shinde, "Chlorosulfonic acid–catalysed one–pot synthesis of coumarin", *Mendeleev Commun*., **16** (2006) 241–242.

203. G. Kokotos, V. Theodorou, C. Tzougraki, "Synthesis and in vitro cytotoxicity of aminocoumarin platinum(II) complexes", *Bioorg. Med. Chem. Lett.,* **7** (1997) 2165–2168.

204. A. Karaliota, O. Kretsi and C. Tzougraki, "Synthesis and characterization of a binuclear coumarin–3–carboxylate copper(II) complex", *J. Inorg. Biochem.,* **84** (2001) 33–37.

205. I. Kostova, I. Manolov, I. Nicolova, S. Konstantinov and M. Karaivanova, "New lanthanide complexes of 4–methyl–7–hydroxycoumarin and their pharmacological activity", *Eur. J. Med. Chem.,* **36** (2001) 339–347.

206. A.B. Dongmo, A.G.B. Azebaze, T.B. Nguelefack, B.M. Ouahouo, B. Sontia, M. Meyer, A.E. Nkengfack, A. Kamanyi and W. Vierling, "Vasodilator effect of the extracts and some coumarins from the stem bark of *Mammeaafricana* (Guttiferae)", *J. Ethnopharmacol.* **111** (2007) 329–334.

207. M.R. Maurya, S. Dhaka and F. Avecilla, "Oxidation of secondary alcohols by conventional and microwave–assisted methods using molybdenum complexes of ONO donor ligands", *New J. Chem.,* **39** (2015) 2130–2139.

208. A.C. Cunha, J.M. Figueiredo, J.L.M. Tributino, A.L.P. Miranda, H.C. Castro, R.B. Zingali, C.A.M. Fraga, M.C.B.V. Souza, V.F. Ferreira and E.J. Barreiro,

"Antiplatelet properties of novel N–substituted–phenyl–1,2,3–triazole–4–acylhydrazone derivatives", *Bioorg. Med. Chem.,* **11** (2003) 2051–2059.

209. S. S. Salih, "The antimicrobial activity of ethanol extract of *thymus vulgaris* on *salmonella typhi* in rabbits", *Br. J. Pharmacol. Toxicol.*, **3** (2012) 147–150.

210. (a) G.W. Gribble, "The diversity of naturally occurring organobromine compounds", *Chem. Soc. Rev.,* **28** (1999) 335–346.
(b) M. Liu, P.E. Hansen and X. Lin, "Bromophenols in marine algae and their bioactivities", *Mar. Drugs,* **9** (2011) 1273–1292.

211. D. Wischang, O. Brücher and J. Hartung, "Bromoperoxidases and functional enzyme mimics as catalysts for oxidative bromination—A sustainable synthetic approach", *Coord. Chem. Rev.,* **255** (2011) 2204–2217.

212. R. Kaur, M.P. Darokar, S.K. Chattopadhyay, V. Krishna and A. Ahmad, "Synthesis of halogenated derivatives of thymol and their antimicrobial activities", *Med. Chem. Res.,* **23** (2014) 2212–2217.

213. L. Getrey, T. Krieg, F. Hollmann, J. Schrader and D. Holtmann, "Enzymatic halogenation of the phenolic monoterpenes thymol and carvacrol with Chloroperoxidase", *Green Chem.,* **16** (2014) 1104–1108.

214. F. Sabuzi, E. Churakova, P. Galloni, R. Wever, F. Hollmann, B. Floris and V. Conte, "Thymol bromination: a comparison between enzymatic and chemical catalysis", *Eur. J. Inorg. Chem.,* (2015), DOI:10.1002/ejic.201500086.

215. K.S.S. Lamani, O. Kotresh, M.A. Phaniband and J.C. Kadakol, "Synthesis, characterization and antimicrobial properties of schiff bases derived from condensation of 8–Formyl–7–hydroxy–4–methylcoumarin and substituted triazole derivatives", *E–J. Chem.,* **6(S1)** (2009) S239–S246.

216. G.M. Sheldrick, *SADABS*, version 2.10, University of Göttingen, Germany (2004).

217. G. M. Sheldrick, "A short history of SHELX", *Acta Crystallogr. Sect. A,* **64** (2008) 112–122.

218. N.K. Ngan, K.M. Lo and C.S.R. Wong, "Synthesis, structure studies and electrochemistry of molybdenum(VI) Schiff base complexes in the presence of different donor solvent molecules", *Polyhedron,* **30** (2011) 2922–2932.

219. M.R. Maurya, L. Rana and F. Avecilla, "Catalytic oxidation of internal and terminal alkenes by oxidoperoxidomolybdenum(VI) and dioxidomolybdenum(VI) complexes", *Inorg. Chim. Acta,* **429** (2015) 138–147.